UNIVERSITY OF LIVERPOOL

Theoretical Study of Friction Induced Vibration in Frictional Systems

Thesis submitted in accordance with the requirements of the University of Liverpool for the degree of Doctor in Philosophy

By

Ningyu Liu

September 2020

To my family

Abstract

Friction induced vibration widely exists in mechanical systems. One typical example is the automobile brake noise that originates from the vibration of a brake system induced by the frictional contact between the rotating rotor and stationary pads. However, a thorough understanding of friction induced vibration in various mechanical systems has not been achieved yet and it remains a challenging research topic due to the immense complexity of this problem. Therefore the aim of the present thesis is to study the friction induced vibration in theoretical mechanical models in order to provide deeper understanding about the causes, the dynamic behaviours and the suppression of the friction-induced-vibration problem.

1. The dynamics of a mass-slider with in-plane and transverse springs and dampers in frictional contact with a spinning flexible disc in three different situations of spinning speed, i.e. constant deceleration, constant acceleration and constant speed, is studied. The in-plane motion of the slider causes time-varying normal force and bending moment on the disc, which can be seen as moving loads to excite the transverse vibration of the elastic disc. The transverse vibration of the disc will, in turn, influence the in-plane motion of the slider by affecting the magnitude of friction force through the varying normal force. Therefore the transverse vibration and the in-plane vibration of the slider are coupled. The numerical algorithm for the transient dynamic analysis of the system involving three different states of motion and non-smooth transitions among the states is proposed. Numerical simulation results show that distinct dynamic behaviours can be observed in the three situations of disc speed and two kinds of particular characteristics of differences are revealed. The significant effects of decelerating and accelerating disc rotation on the friction induced vibration of the system underlie the necessity

to take into account time-varying sliding velocity in the research of friction induced vibration.

2. The effects of tangential high-frequency harmonic excitation on the friction induced vibration in multi-degree-of-freedom systems that are coupled in the tangential and normal directions are theoretically investigated, in which a minimal two-degree-of-freedom system and a more complicated slider-on-disc system are considered. It is observed the tangential harmonic excitation with appropriate amplitude and frequency suppresses the friction induced vibration in the systems. The analytical method to determine the ranges of the amplitude and frequency of the harmonic excitation with which the friction-excited systems are stabilized is established. To verify the analytical results, a great amount of computational effort is also made to simulate the time responses of systems in various combinations of values of the amplitude and frequency, by which the parameter ranges where the friction induced vibration is suppressed can also be obtained. This research can provide theoretical guidance for the suppression of friction induced vibration in real mechanical systems by application of a tangential harmonic excitation.

3. The friction induced vibration of a five-degree-of-freedom mass-on-oscillating-belt model considering multiple types of nonlinearities is studied. The first type of nonlinearity in the system is the nonlinear contact stiffness, the second is the non-smooth behaviour including stick, slip and separation, and the third is the geometrical nonlinearity brought about by the moving-load feature of the mass slider on the rigid belt. Both the linear stability of the system and the nonlinear steady-state responses are investigated and rich dynamic behaviours of the system are revealed. The results of numerical study indicate the necessity of the transient dynamic analysis in the study of friction-induced-vibration problems as the linear stability analysis fails to detect the occurrence of self-excited vibration when two stable solutions coexist in the system. Additionally, the significant effects of each type of nonlinearity on the linear stability and nonlinear steady-state responses of the system are discovered, which underlie the necessity to take multiple types of nonlinearities into account in the research of friction induced vibration. The similar study is also conducted on a continuous slider-on-disc model.

4. A new pin-on-disc system with an L-mechanism to adjust the normal force is proposed and the friction induced stick-slip vibration of the system is theoretically studied. The Coulomb law of friction is utilized to model the friction force between the pin and disc. It is observed that the system is bi-stable at low disc speed and high normal preload, i.e., there is coexistence of a stable pure sliding solution and a stable stick-slip limit cycle for the pin, and the variable normal force can lead to the bifurcation and even chaotic behaviours of the responses in the system. Then the effect of non-uniform friction interface in which a sector of disc has a different set of friction property on the stick-slip vibration of the system is studied. It is found that with appropriate friction coefficients on the sector and an appropriate span angle of the sector, the range of disc speed and normal preload at which the stick-slip limit cycle exists will be greatly diminished. Therefore a potential approach to suppress the friction induced stick-slip vibration is provided.

Acknowledgements

I would like to pay my deepest and most sincere gratitude to my supervisor Professor Huajiang Ouyang, who is a professional, insightful and respectable scholar with caring character. He not only provided me with valuable guidance and help for me to advance my project and get through struggling times, but also instilled into me the passion and rigorous attitude towards research in the past four years.

Many thanks to my fellow PhD students and academic staff in the Dynamics and Control Group at the University of Liverpool for their advice and help in my research.

I would also love to thank my family and friends for their mental support and encouragement which helped me to settle in foreign environment and conduct my research cheerfully.

The joint scholarship of University of Liverpool and China Scholarship Council is also gratefully acknowledged, which provides me with financial support for my research and living expenses in the past four years.

Last but not the least, I would like to thank the city of Liverpool, which is such a vibrant and diverse city. I am very happy to spend four years studying and living here.

List of Publications

Journal papers:

1. **N. Liu**, H. Ouyang, Friction-induced vibration of a slider on an elastic disc spinning at variable speeds. *Nonlinear Dynamics* 98(1) (2019) 39-60.

2. **N. Liu**, H. Ouyang, Suppression of friction-induced-vibration in MDoF systems using tangential harmonic excitation. *Meccanica* 55 (2020) 1525–1542.

3. **N. Liu**, H. Ouyang, Friction-induced vibration considering multiple types of nonlinearities. *Nonlinear Dynamics* (2020). https://doi.org/10.1007/s11071-020-06055-x.

Conference papers:

1. **N. Liu**, H. Ouyang, Suppression of friction induced vibration of a pin-on-disc system by alternate friction interfaces. ICSV27, Annual Congress of International Institute of Acoustics and Vibration (IIAV), Prague.(The conference is postponed to July 2021).

Contents of Thesis

List of Figures

List of Tables

Nomenclature

A_b, A	the amplitudes of the tangential harmonic excitation on the slider in the two-degree-of-freedom friction model and on the slider in the slider-on-disc model in Chapter 5
a_0, b_0, c_0	the distance between the fixed point of the spring k_1 on the horizontal arm and the central axis, the distance between the fixed point of the spring k_2 at the back of the vertical plate and the central axis and both the distances between the fixed points of the spring k_2 and k_3 on the L-shape structure and the pivot, respectively, in the setup in Chapter 7
a, b, ρ, E, h, ν	the inner radius, the outer radius, the density of material, the Young's modulus, the thickness, the Poisson's ratio of the disc
c_1, c_2	the damping coefficients in the two-degree-of-freedom mass-on-belt model and the two-degree-of-freedom friction model in Chapter 3, or the damping coefficients on the slider in the two-degree-of-freedom model and the slider-on-disc model in Chapter 5, or the damping coefficients on the slider in the 5-DoF frictional model and the slider-on-disc model in Chapter 6, or the damping coefficients of rotation of the cylinder and the L-shape structure in Chapter 7
c, k	the damping coefficient and stiffness of the single-degree-of-freedom oscillator in Chapter 3
c_z, k_z	transverse damping coefficient and transverse spring stiffness of the mass slider in the model in Chapter 4
c_4, c_5, c_6	the horizontal and vertical damping coefficients on the belt in the 5-DoF frictional model in Chapter 6
F	the normal preload on the two-degree-of-freedom friction model in Chapter 3, or the two-degree-of-freedom model and slider-on-disc model in Chapter 5, or the 5-DoF frictional model and the slider-on-disc model in Chapter 6
$\mathbf{F}_\mathrm{T}$	vector of friction force
$\mathbf{F}_\mathrm{N}$	vector of normal force
F_f, F_T	the tangential friction force between contacting objects

F_{f1}, F_{f2}	the friction forces on two masses in the two-degree-of-freedom mass-on-belt model in Chapter 3
$\mathbf{F}_{\mathrm{con}}(\mathbf{x})$	the contact forces at the friction interface of the frictional system
$\mathbf{F}_{\mathrm{ext}}$	the external force applied on the friction system
I, c_φ, k_φ	the moment of inertia, in-plane damping coefficient and in-plane spring stiffness of the mass slider in the model in Chapter 4
J	the rotational inertia about the mass centre of the belt in the 5-DoF frictional model in Chapter 6
$J_{\mathrm{c}}, J_{\mathrm{L}}$	the rotational inertia of the cylinder and the L-shape structure, respectively, in the setup in Chapter 7
k_1, k_2	the stiffnesses in the two-degree-of-freedom mass-on-belt model or the stiffnesses of inclined springs in the two-degree-of-freedom friction model in Chapter 3, or the stiffnesses of inclined springs in the two-degree-of-freedom friction model and the stiffnesses of the horizontal and vertical springs in the slider-on-disc model in Chapter 5, or the stiffnesses of the horizontal and vertical springs on the slider in the 5-DoF frictional model and the slider-on-disc model in Chapter 6, or the stiffnesses of two linear springs in the setup in Chapter 7
k_3	the stiffness of vertical spring in the two-degree-of-freedom friction model in Chapter 3, or the stiffness of vertical spring in the two-degree-of-freedom friction model and the stiffness of the inclined spring in the slider-on-disc model in Chapter 5, or the stiffness of the inclined spring in the 5-DoF frictional model and the slider-on-disc model in Chapter 6, or the stiffness of one linear spring in the setup in Chapter 7
k_4, k_5, k_6	the stiffnesses of horizontal and vertical springs on the belt in the 5-DoF frictional model in Chapter 6
k_{nl}	the nonlinear contact stiffness in the 5-DoF frictional model or the slider-on-disc model in Chapter 6
l_1, l_2	the distances between the wheels and mass centre of the belt in the 5-DoF frictional model in Chapter 6 or the original lengths of two linear springs in the setup in Chapter 7
l_3	the original length of one linear spring in the setup in Chapter 7

m	the mass of the single-degree-of-freedom oscillator in Chapter 3, or the mass of the slider in the two-degree-of-freedom model in Chapter 3 and Chapter 5, or the mass of slider in the slider-on-disc models in Chapter 4, Chapter 5 and Chapter 6, or the mass of the belt in the 5-DoF frictional model in Chapter 6
M	the mass of the slider in the 5-DoF frictional model in Chapter 6
m_1, m_2	the masses in the two-degree-of-freedom mass-on-belt model in Chapter 3
$\mathbf{M}, \mathbf{C}, \mathbf{K}$	the mass matrix, damping matrix and stiffness matrix of a frictional system
N_0	the normal preload on the model in Chapter 4 or the setup in Chapter 7
N, F_{N}	the normal force between contacting objects
r_0	the radial distance of the mass slider from the disc centre in Chapter 4
t_{s}	the time at the onset of stick
u_0	the amplitude of the external excitation on the single-degree-of-freedom friction oscillator
v	the velocity of belt in the mass-on-belt models in this thesis
v_{r}	the relative velocity between contacting objects
$\mathbf{v}_{\mathrm{rel}}$	vector of relative velocity between contacting surfaces
v_{s}	the Stribeck velocity
v_{tol}	the tolerance velocity of the linear smooth function for the Coulomb's friction model
$w(r, \theta, t)$	the transverse displacement of an annular elastic thin plate
α_0	the negative slope of the friction force-relative velocity
α_1, α_2	the angles of inclination to the horizontal direction of inclined springs in the two-degree-of-freedom friction model in Chapter 3 or the two-degree-of-freedom friction model in Chapter 5
$\mu, \mu_0, \mu_1, \alpha$	the friction coefficient, the maximum value, the asymptotic value and the initial slope of the friction coefficient in Chapter 4
$\mu_{\mathrm{s}}, \mu_{\mathrm{k}}$	the coefficients of static friction and kinetic friction

σ	the smoothness factor for the hyperbolic tangent function to approximate the Coulomb's friction model
ω	the frequency of the external excitation on the single-degree-of-freedom friction oscillator in Chapter 3, or the frequency of the tangential harmonic excitation on the slider in the two-degree-of-freedom friction model and on the slider in the slider-on-disc model in Chapter 5
Ω	the spinning speed of disc
Ω_0, $t_{\max}$	the initial speed and the time duration of the deceleration process in the situation of decelerating disc in Chapter 4
Ω_1, a_{d}	the initial speed and the acceleration in the situation of accelerating disc in Chapter 4
Ω_{c}	the constant disc speed in Chapter 4

Chapter 1

Introduction

1.1 Background and motivations

Dry friction, which results from the relative motion of solids, plays a crucial, controlling role in a rich variety of mechanical systems as well as in everyday life. In many cases, friction acts as damping which develops between contact surfaces such as joints or connections to dissipate energy and weaken vibration. However, friction force can also cause self-excited vibration and lead to radiation of sound in various engineering applications and daily life. Examples of the vibration and sound which are generated by dry friction include string instrument music, rattling joints of robots, squealing windscreen wipers, stick-slip vibration of drill-strings, squeal noise of train wheels on sharp curved tracks, squeaking chalks on boards, some insect sounds, automobile brake noises, etc. [1,2]. Among them, automobile brake noise has been a major issue facing car manufacturers today, which may cause discomfort to passengers and be perceived as a quality problem, thereby increasing the warranty costs and impacting the brand reputations [3,4].

Due to the universality and importance of this problem, friction induced vibration has attracted great research interest and a considerable volume of literature has been produced of this subject on both theoretical studies and experimental studies. In terms of theoretical studies, theoretical mechanical models involving friction induced vibration that include low-degree-of-freedom lumped models, continuous models and finite element models were established for investigation. In terms of experimental studies, test rigs were specially designed to study the friction induced vibration in

specific mechanical systems. These studies enormously enhanced the understanding of this subject. Physical mechanisms for initiating friction induced vibration were uncovered, such as the stick-slip vibration, the sprag-slip instability, the mode-coupling instability, the frictional follower force, etc. Methods to predict the propensity of friction induced self-excited vibration and approaches to suppress the friction induced vibration were proposed. And the complex dynamic behaviours of the friction induced vibration such as bifurcations and chaotic behaviours of the dynamic responses were revealed.

However, the problem of friction induced vibration is not fully resolved yet and more research, especially from the theoretical perspective, needs to be done. The deficiencies in existing studies constitute the motivation for the research in this thesis. For example, a comprehensive study of the effects of multiple types of nonlinearities on friction induced vibration is yet to be done. Compared to the experimental study, the theoretical study is more advantageous in uncovering the basic mechanisms, predicting the dynamic behaviours unavailable in experiments and investigating the effects of parameters on the friction induced dynamics.

1.2 Aim and objectives

The aim of the present thesis is to study the friction induced vibration in theoretical mechanical models in order to provide deeper understanding about the causes, the dynamic behaviours and the suppression of the friction induced vibration in mechanical systems.

To achieve this aim, four objectives are established, which are,

(1) To build a theoretical mechanical model which consist of a mass-slider constrained by in-plane and transverse springs and dampers with an elastic disc clamped at the inner boundary and free in outer boundary in frictional contact, and to study the dynamics of the system in three different situations of spinning speed of disc, i.e. constant deceleration, constant acceleration and constant speed. The system responses under the decelerating and accelerating sliding motion are compared with the results under constant sliding speed to help reveal the effects of deceleration and acceleration on the friction induced dynamics of the system.

(2) To investigate the effects of tangential harmonic excitation on the friction induced vibration in two multi-degree-of-freedom (MDoF) systems that are coupled in the tangential and normal directions, i.e., a two-degree-of-freedom lumped model and a more complicated slider-on-disc model. The analytical method to determine the effective ranges of the amplitude and frequency of the harmonic excitation for the suppression of the friction induced vibration of the systems is established, and the analytical results are verified by the results obtained from a large number of simulations of the time responses of systems in various combinations of values of the amplitude and frequency.

(3) To study the friction induced vibration of a five-degree-of-freedom mass-on-oscillating-belt model considering multiple types of nonlinearities. The significant effects of each type of nonlinearity on the linear stability and nonlinear steady-state responses of the system are investigated. This study is also extended to a continuous slider-on-disc model.

(4) To propose a new pin-on-disc system with an L-mechanism to create a state-dependent normal force and couple with the friction induced stick-slip tangential vibration of the system. Especially the friction induced dynamics with a non-uniform friction interface on the disc is investigated.

1.3 Original contributions

The original contributions in this thesis can be summarised in five aspects as follows:

(1) A numerical algorithm for the transient dynamic analysis of friction induced vibration involving three different states of motion (slip and stick in contact, and separation; and considering the impact when re-contact happens) is proposed.

(2) The friction induced dynamics of a slider-on-disc system at time-varying spinning disc speeds, is investigated. The distinct dynamic behaviours of the system under time-varying disc speeds from those under constant disc speeds indicate the necessity to consider the time-variant sliding velocity when studying the friction induced vibration in mechanical systems.

(3) The ranges of amplitude and frequency of the intentionally introduced tangential high-frequency harmonic excitation to suppress the friction induced vibration in

two theoretical mechanical models are determined both analytically and numerically. This research can provide theoretical guidance for the suppression of friction induced vibration in real mechanical systems by application of a tangential harmonic excitation.

(4) A comprehensive analysis of the effects of multiple types of nonlinearities on the friction induced vibration is conducted. It is discovered that each type of nonlinearity has significant effects on the linear stability and nonlinear steady-state responses of the mechanical models proposed, therefore it is essential to take multiple types of nonlinearities into account in the research of friction induced vibration.

(5) A new pin-on-disc model with an L-mechanism to adjust the normal force is proposed and the friction induced dynamics of the system with non-uniform friction interface, where a sector of disc surface is assigned with a different set of friction property from that on the rest of the disc surface, is studied. It is found that with appropriate friction coefficients on the sector and an appropriate span angle of the sector, the range of disc speeds and normal preloads at which the stick-slip limit cycle exists will be greatly diminished. Therefore a promising approach to suppress the friction induced stick-slip vibration is provided.

1.4 Outline of the thesis

This thesis consists of eight chapters and the content of each chapter is briefly stated as follows:

Chapter 1 introduces the background and motivations, the aim and objectives, the original contributions and the outline of this thesis.

Chapter 2 provides a comprehensive literature review concerning friction induced vibration in five aspects: the main physical mechanisms for initiating friction induced vibration, the friction force models, the dynamic behaviours of friction induced vibration in a variety of mechanical models, the dynamics of the spinning disc in contact with stationary parts and the experimental investigations on the friction induced vibration in mechanical systems.

Chapter 3 presents the fundamental knowledge and analysis tools that are utilized in the present thesis. Firstly three principal mechanisms for generating friction induced vibration, that are the negative friction-velocity slope, the stick-slip oscillation and the mode-coupling instability, are presented in low-degree-of freedom lumped models. Secondly, two main kinds of theoretical methods of friction induced vibration, i.e. the complex eigenvalue analysis (CEA) and the transient dynamic analysis (TDA), are introduced. Finally the basic theory about the vibration of elastic thin plates is stated.

Chapter 4 studies friction induced vibration of a mass-slider with in-plane and transverse springs and dampers in sliding contact with a spinning elastic disc in three different situations of spinning speeds, i.e. constant deceleration, constant acceleration and constant speed. The non-smooth dynamic responses of the system including three different states of motion, i.e., slip, stick and separation, are calculated. And the dynamic responses in the three different situations of disc speed are compared to reveal the effects of time-variant disc speed on the friction induced dynamics of the system.

Chapter 5 investigates the effects of tangential high-frequency harmonic excitation on the friction induced vibration in multi-degree-of-freedom (MDoF) systems that are coupled in the tangential and normal directions. It is observed the friction induced vibration of the systems can be suppressed by the tangential harmonic excitation when the amplitude and frequency of the excitation are in certain ranges. The ranges of amplitude and frequency of the tangential harmonic excitation to suppress the friction induced vibration in the systems are then determined both analytically and numerically.

Chapter 6 studies the friction induced vibration of a five-degree-of-freedom mass-on-oscillating-belt model considering multiple types of nonlinearities. The first type of nonlinearity is the nonlinear contact stiffness, the second is the non-smooth behaviour including stick, slip and separation, and the third is the geometrical nonlinearity caused by the moving-load feature of the mass on the rigid belt. Both the linear stability of the system and the nonlinear steady-state responses are studied. The effects of each type of nonlinearity on the system dynamics are revealed. The similar study is also conducted on a continuous slider-on-disc model.

Chapter 7 studies the friction induced stick-slip vibration of a new pin-on-disc system with an L-mechanism to adjust the normal force. And the friction induced dynamics with a non-uniform friction interface on the disc is investigated.

Chapter 8 presents important findings and conclusions in this PhD project and points out some future directions of research.

Chapter 2

Literature review

There have been a large number of published studies on the friction induced vibration, which greatly enhances understanding of the problem. In this chapter, the literature of this subject is reviewed in five aspects. Firstly several main physical mechanisms for initiating friction induced vibration are reviewed; then a review of various friction force models is conducted; thirdly the works on investigation of the dynamic behaviours of friction induced vibration in a diverse variety of mechanical models are presented; The fourth part focuses on the literature concerning the dynamics of the spinning disc in contact with stationary parts. Finally in the fifth part the experimental investigations on the friction induced vibration in mechanical systems are reviewed.

2.1 Mechanisms for generation of friction induced vibration

From previous studies, the mechanisms for the occurrence of friction induced vibration generally fall into four categories [5]: (1) stick–slip oscillation, which usually happens when the value of static friction coefficient is greater than the kinetic friction coefficient; (2) sprag-slip instability for which the origin of instability is geometrical rather than tribological; (3) negative gradient in friction coefficient–velocity relationship; and (4) mode-coupling instability or mode-locking, which is generally acknowledged as the main mechanism for self-excited vibration in automobile brakes.

2.1.1 Stick-slip oscillation

Stick-slip oscillation features two distinct states of motion, sticking (when the two objects in contact are at rest relatively and the static friction force between them does

not exceed the maximum static friction capacity) and slipping (when the two objects are in relative motion). The stick-slip vibration serves to be the cause of vibration instability in a number of mechanical systems [6-14] or in geodynamics [15-17]. In [18], Feeny et al. gave a substantial historical review on the friction influenced dynamics and stick-slip phenomena in mechanical, civil and transportation systems.

Since the dynamic states of a system experience non-smooth transitions, such a system belongs to the class of non-smooth systems, which can exhibit chaotic behaviour [19]. Popp et al. [2, 19, 20] investigated stick-slip dynamics of discrete and continuous models and observed the rich bifurcation and chaotic behaviour could appear for the models with the governing equations which could be expressed as three- or higher-dimension first-order ordinary differential equations. The observations of the bifurcation and chaotic behaviour associated with stick-slip were also made by other researchers [21-23]. The works investigated the characteristics of stick-slip motion which are influenced by the system parameter values and friction property [24-27]. Kinkaid et al. [28] studied the dynamics of a 4-DoF (degree-of-freedom) system with a two-dimension friction force and found the change of direction of the friction force could excite unstable vibration even with the Coulomb's friction law, thereby introducing a new mechanism for brake squeal. Behrendt et al. [29] conducted a finite element analysis on the stick-slip motion of an elastic brake pad sliding over a rigid surface under constant load and constant velocity.

In [30], a systematic procedure to find both stable and unstable periodic stick-slip vibrations of autonomous dynamic systems with dry friction was derived, in which the discontinuous friction forces were approximated by a smooth function. Hetzler [31] studied the effect of damping due to non-smooth Coulomb friction on a simple oscillator on the belt exhibiting self-excitation due to negative damping in the case of negative friction force-relative velocity slope. Tonazzi et al. [32] performed an experimental and numerical analysis of frictional contact scenarios from macro stick-slip to continuous sliding. Papangelo [33] investigated the subcritical bifurcation of a slider-on-belt system which experienced friction induced vibration in the case of a weakening-strengthening friction law, and the results showed that there was a range of parameters where two stable solutions coexist, i.e., a stable sliding equilibrium and a stable stick-slip limit cycle. The approximate analytical expressions for the amplitude and frequency of friction induced stick-slip oscillations were derived in [34]. The

stick-slip vibration in the situation of decelerating sliding was investigated in [35, 36], the results showed that decelerating sliding can induce stick-slip whereas no stick-slip appears during steady sliding.

The literature showed that the stick-slip oscillation is widespread in engineering and other fields, and it can produce complex dynamic behaviours.

2.1.2 Sprag-slip instability

The sprag-slip is not tribological but geometrical instability. The concept of sprag-slip was firstly proposed by Spurr [37], in which the variations of normal and tangential forces due to the deformations of contacting structures were considered to cause the vibration instability. Jarvis and Mills [38] employed a cantilevered beam on disc to examine sprag-slip instability in braking systems. Earles et al. [39] showed the necessary condition for instability in terms of the contact orientation in a simple pin-on-disc model. Sinou et al. [40] studied the instability in a nonlinear sprag-slip model with a constant coefficient of friction by a central manifold theory and the effects of parameters on the sprag-slip instability were examined.

Another notable line of research focused on the existence and uniqueness of the solutions of the frictional systems. Painlevé [41] investigated the existence and uniqueness properties of the solutions of rigid bodies subjected to the Coulomb-type sliding friction by using a rigid beam model. It was noticed that there was a possibility of multiple solutions and non-existence of (static) solutions due to the nonlinearity arising from the friction model. The phenomenon is called the Painlevé paradox. Leine et al. [42] studied the periodic motion and bifurcations of a frictional impact oscillator which consisted of an object with normal and tangential degrees of freedom in contact with a rigid surface. It was shown that this type of systems could exhibit the Painlevé paradox, i.e. non-uniqueness and non-existence of solutions, for physically realistic values of the friction coefficient. Hoffmann et al. [43, 44] examined the dynamics of sprag-slip instability and found that there were parameter combinations for which the system did not possess a static solution corresponding to a steady sliding state, which could be a sufficient condition for occurrence of sprag-slip oscillation. Kang and Krousgrill [45] developed simple friction-coupled models with spragging forces by using a mass on a traveling belt in both one- and two-dimension spaces and determined

the condition for non-existence of steady-sliding response through analytical and numerical procedures.

Although the interest on the sprag-slip mechanism has lessened since the mode-coupling mechanism gained acceptance as a dominant factor in the initiation of brake squeal, it is still studied today as a mechanism for the dynamic instability in many applications.

2.1.3 Negative gradient in friction coefficient–relative velocity relationship

The idea that the negative slope in friction coefficient–relative velocity relationship accounted for the instability of a brake system was previously proposed by Mills [46], Fosberry and Holubecki [47], Sinclair and Manville [48]. The decreasing feature of friction force with the increase of relative velocity was considered to bring in a negative damping to the system and lead to dynamic instability. The negative damping effect due to the negative friction-velocity slope was investigated by many researchers [49-51]. Ouyang et al. [52] demonstrated the effect of the negative friction-velocity slope on the parametric resonances of a flexible annular disc excited by a rotating mass-spring-damper system together with a frictional follower force. In [33], the negative slope of friction force at the static equilibrium determined the linear stability boundary for the system.

There was not much literature on this kind of mechanism as it can only explain a limited number of fiction-induced-vibration problems [3, 53].

2.1.4 Mode-coupling instability

The mode-coupling instability originates from the modal behaviour of the structures in contact. The complex eigenvalue analysis shows that some modes become unstable when coupling with other modes of the friction system. This phenomenon was considered to be mainly responsible for brake squeal and has been widely studied [54-62].

North firstly observed the mode-coupling phenomenon when studying brake squeal that could also happen for a constant friction coefficient [54]. Hoffmann et al. [55] used a minimal two degree-of-freedom model to clarify the physical mechanisms underlying the mode-coupling instability of friction induced oscillations from an

intuitive perspective. It was shown that the friction force acts like a cross-coupling force linking motion normal to the contact surface to motion parallel to it and that a necessary condition for the onset of instability is that the friction induced cross-coupling force balances the corresponding structural cross-coupling force of the system. In a later work [56], Hoffmann and Gaul clarified the influence of structural damping on this type of instability mechanism. It was shown that linear viscous structural damping changes the eigenvalue characteristics of mode-coupling friction induced instability. Kang et al. [57] presented the mathematical formulation for determining the dynamic in terms of the self-excited transverse vibration of a thin annular plate, in which the mode-coupling instability of the disc doublet modes was investigated.

Huang et al. [63] showed that the compatibility of mode shapes needed for mode coupling is one of the factors dictating the onset of squeal in drum brake system. Elmaian et al. [4] presented a wide diversity of responses on a same dynamic system by changing the parameter values and showed the squeal was mainly due to the mode-coupling phenomenon. Hultén [64] proposed a new kind of mode-coupling mechanism that the coupling of the system was not due to the inclined spring but the friction forces in two orthogonal directions. Chen et al. [61] investigated the eigenvalues of several car brakes through experimental and numerical analysis and predicted that the coupling of the in-plane and out-of-plane modes of the brake was the main reason for squeals above 3 kHz.

2.1.5 Additional Mechanisms

Apart from the four principal mechanisms above, there are other mechanisms proposed to explain the occurrence of friction induced vibration in specific systems. Chan et al. [65] analysed the destabilizing effect of the friction force as a follower force. Hochlenert et al. [66] established an accurate formulation of the kinematics of the frictional contact in two and three dimensions and worked out the essential properties of the contact kinematics leading to self-excited vibration. Ouyang and Mottershead [67] investigated the instability of the transverse vibration of a disc excited by two co-rotating sliders on either side of the disc and found that the moving normal forces and friction couple produced by the sliders bring about dynamic instability. Chen et al. [68] analysed the instability of a friction system caused by the time delay between the

normal force and the friction force. Graf and Ostermeyer [69] utilized a dynamic friction law with an internal variable in the classical mass-on-belt model and found the stability of the system was dependent on the relation between the eigenfrequency of the oscillator and the time constants in the dynamic friction law, where the unstable vibration could even happen in the case of a positive friction-velocity relationship.

2.2 Friction force models for dynamic analysis

Friction forces of complicated nature can be found in all practical mechanical systems which have contacting surfaces with relative motion. To obtain accurate dynamic responses of the systems with friction force, rigorous evaluation of friction forces is required. There has been a great amount of literature devoted to developing friction force models that can be used to capture the frictional behaviour, such as stick-slip effect, Stribeck effect and pre-sliding displacement, etc. Generally, the friction force models can be classified into two groups, namely the 'static' and 'dynamic' friction models. The former group usually describes the steady-state behaviour of friction force, while the latter can capture more friction characteristics due to the inclusion of extra state variables.

2.2.1 'Static' friction models

One of the first models of friction was put forward by Amontons [70] and Coulomb [71], who stated that the friction force is proportional to the normal force and independent of the magnitude of relative velocity. Besides, the static coefficient of friction is assumed to be equivalent to the kinetic coefficient of friction, therefore the Coulomb friction law involves a single parameter, that is, the kinetic coefficient of friction. The mathematical expression of Coulomb friction law can be written as,

$$\begin{cases} \mathbf{F}_{\mathrm{T}} = \mu_{\mathrm{k}} \|\mathbf{F}_{\mathrm{N}}\| \mathrm{sgn}(\mathbf{v}_{\mathrm{rel}}) & \|\mathbf{v}_{\mathrm{rel}}\| \neq 0 \\ \|\mathbf{F}_{\mathrm{T}}\| \leq \mu_{\mathrm{k}} \|\mathbf{F}_{\mathrm{N}}\| & \|\mathbf{v}_{\mathrm{rel}}\| = 0 \end{cases} \tag{2.1}$$

where $\mathrm{sgn}(\mathbf{v}_{\mathrm{rel}}) = \mathbf{v}_{\mathrm{rel}}/\|\mathbf{v}_{\mathrm{rel}}\|$, $\mathbf{F}_{\mathrm{T}}$, $\mathbf{F}_{\mathrm{N}}$ and $\mathbf{v}_{\mathrm{rel}}$ represent the friction force, the normal force and the relative velocity between the contacting surfaces, respectively. The friction force during sticking when $\|\mathbf{v}_{\mathrm{rel}}\| = 0$ serves to sustain the relative static state and thus can be obtained from the equations of motion of systems, while the magnitude of static friction force cannot exceed the maximum static friction capacity $\mu_{\mathrm{k}}\|\mathbf{F}_{\mathrm{N}}\|$. Further studies on frictional behaviour suggested the maximum static friction force

should be larger than the kinetic friction force, which led to consideration of two different friction coefficients, namely the coefficient of static friction μ_s and the coefficient of kinetic friction μ_k ($\mu_s > \mu_k$). As a modification of the Coulomb's friction law, a viscous friction component was introduced to describe the linear relationship between the friction force related to the lubricant viscosity and the relative velocity. The friction force during relative sliding can be written as,

$$\mathbf{F}_T = \mu_k \|\mathbf{F}_N\| \mathrm{sgn}(\mathbf{v}_{rel}) + F_v \mathbf{v}_{rel} \tag{2.2}$$

where F_v is the viscous friction coefficient related to the viscosity of the lubricant. Stribeck [72] found experimentally that the friction force decreases with the increase in the relative velocity at low velocities, which led to the expression of friction force during relative sliding as a continuous and decreasing function of the relative velocity. A popular expression of the friction force during the relative sliding which considered the Stribeck effect was written as [73],

$$\mathbf{F}_T = \left(\mu_k + (\mu_s - \mu_k) \mathrm{e}^{-\left(\frac{\|\mathbf{v}_{rel}\|}{v_s}\right)^{\delta}} \right) \|\mathbf{F}_N\| \mathrm{sgn}(\mathbf{v}_{rel}) \tag{2.3}$$

where v_s denotes the Stribeck velocity, δ is a factor relying on the geometry of the contacting surfaces. The examples of variations of the friction force with the relative velocity in the above four different friction models for the one-dimensional (1D) case are illustrated in Figure 2.1.

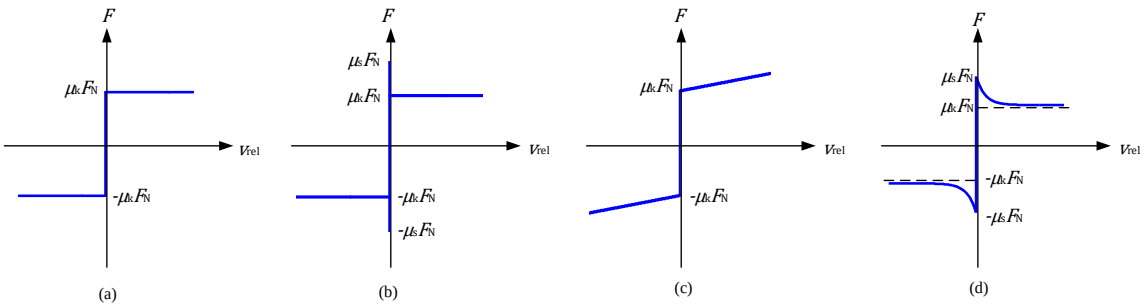

Figure 2.1 Friction force versus relative velocity for 1D case: (a) Coulomb friction model, (b) Coulomb model with larger static friction force, (c) Coulomb friction with viscous friction, (d) Model with Stribeck effect.

In the aforementioned static friction models, the friction force at zero relative velocity is multivalued and needs to be determined from the equations of motion of systems. Thus it is essential to accurately capture the transition between the stick mode and the

slip mode, which brings about numerical difficulty for the dynamic analysis of the frictional systems. To improve the computational efficiency, several researches proposed friction models which replaced the discontinuity at zero velocity by finite slopes. Two approaches were widely used, which employ a linear function [74] or a hyperbolic tangent function [30, 75] to describe the friction force-relative velocity relationship around zero velocity. The mathematical expressions of the two smoothing approaches for the Coulomb's friction model can be written as,

$$\mathbf{F}_{\mathrm{T}} = \begin{cases} \mu_{\mathrm{k}} \|\mathbf{F}_{\mathrm{N}}\| \mathrm{sgn}(\mathbf{v}_{\mathrm{rel}}) & \|\mathbf{v}_{\mathrm{rel}}\| > v_{\mathrm{tol}} \\ \mu_{\mathrm{k}} \|\mathbf{F}_{\mathrm{N}}\| \mathbf{v}_{\mathrm{rel}} / v_{\mathrm{tol}} & \|\mathbf{v}_{\mathrm{rel}}\| \leq v_{\mathrm{tol}} \end{cases} \tag{2.4}$$

for linear function, where v_{tol} is the tolerance velocity, and

$$\mathbf{F}_{\mathrm{T}} = \mu_{\mathrm{k}} \|\mathbf{F}_{\mathrm{N}}\| \tanh(\sigma \|\mathbf{v}_{\mathrm{rel}}\|) \mathrm{sgn}(\mathbf{v}_{\mathrm{rel}}) \tag{2.5}$$

for hyperbolic tangent function, where σ is the smoothness factor. The examples of these two friction models for 1D case are shown in Figure 2.2.

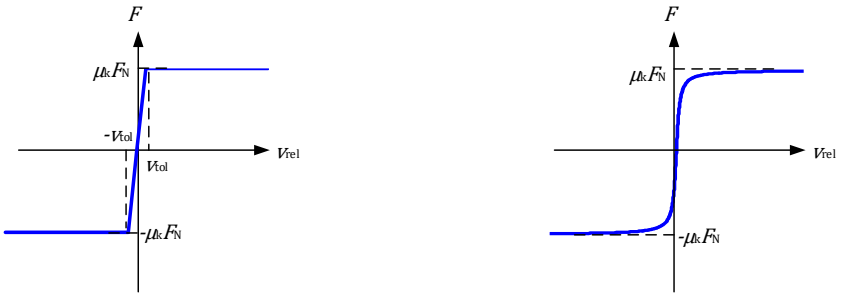

Figure 2.2 Smooth functions to approximate the Coulomb friction model for 1D case.

In addition, several acceleration-based friction models have been proposed, in which friction force is dependent on another variable besides the relative velocity, i.e. the relative acceleration between the contacting surfaces. Stefański et al. [76] put forward a friction model which showed non-reversible friction characteristic. The function of this model is described as,

$$\mathbf{F}_{\mathrm{T}} = \mu_{\mathrm{k}} \|\mathbf{F}_{\mathrm{N}}\| \left(1 + \frac{\mu_{\mathrm{s}} - \mu_{\mathrm{k}}}{\mu_{\mathrm{k}}} \exp(-\|\mathbf{v}_{\mathrm{rel}}\|) \mathrm{sign}(\mathbf{v}_{\mathrm{rel}} \cdot \dot{\mathbf{v}}_{\mathrm{rel}})\right) \mathrm{sgn}(\mathbf{v}_{\mathrm{rel}}) \tag{2.6}$$

where $\mathrm{sign}(*)$ is the sign function. Wojewoda et al. [77] proposed a static friction model of hysteretic type with a stochastic component. This model is divided into three

different states, sticking and sliding in acceleration and deceleration. Its mathematical expression is written as,

$$\mathbf{F}_{\mathrm{T}} = \begin{cases} F_{\mathrm{st}}\mathrm{sgn}(\mathbf{v}_{\mathrm{rel}}) & \text{if } F_{\mathrm{st}} \leq F_{\mathrm{d+}} \cap \ \mathrm{sign}(\mathbf{v}_{\mathrm{rel}} \cdot \dot{\mathbf{v}}_{\mathrm{rel}}) \geq 0 \\ F_{\mathrm{d+}}\mathrm{sgn}(\mathbf{v}_{\mathrm{rel}}) & \text{if } F_{\mathrm{st}} > F_{\mathrm{d+}} \cap \ \mathrm{sign}(\mathbf{v}_{\mathrm{rel}} \cdot \dot{\mathbf{v}}_{\mathrm{rel}}) \geq 0 \\ F_{\mathrm{d-}}\mathrm{sgn}(\mathbf{v}_{\mathrm{rel}}) & \text{if } \mathrm{sign}(\mathbf{v}_{\mathrm{rel}} \cdot \dot{\mathbf{v}}_{\mathrm{rel}}) < 0 \end{cases} \tag{2.7}$$

with

$$F_{\mathrm{st}} = \frac{1}{2} k_{\mathrm{S}} \frac{\|\mathbf{v}_{\mathrm{rel}}\|^2}{\|\dot{\mathbf{v}}_{\mathrm{rel}}\|} - F_0 \tag{2.8}$$

$$F_{\mathrm{d+}} = F_{\mathrm{C}} + \left(F_{\mathrm{S}} + \Delta F_{\mathrm{S}} \frac{1}{1+\frac{\|\mathbf{v}_{\mathrm{rel}}\|}{v_{\mathrm{S}}}} - F_{\mathrm{C}} \right) \left(g(\mathbf{v}_{\mathrm{rel}}, \dot{\mathbf{v}}_{\mathrm{rel}}) + f_{\mathrm{R}}(\mathbf{x}, \mathbf{v}_{\mathrm{rel}}) \right) \tag{2.9}$$

$$F_{\mathrm{d-}} = F_{\mathrm{C}} - (F_{\mathrm{S}} - F_{\mathrm{C}}) \left(g(\mathbf{v}_{\mathrm{rel}}, \dot{\mathbf{v}}_{\mathrm{rel}}) + f_{\mathrm{R}}(\mathbf{x}, \mathbf{v}_{\mathrm{rel}}) \right) \tag{2.10}$$

where $F_{\mathrm{C}} = \mu_{\mathrm{k}} \|\mathbf{F}_{\mathrm{N}}\|$, $F_{\mathrm{S}} = \mu_{\mathrm{s}} \|\mathbf{F}_{\mathrm{N}}\|$, k_{S} is the contact stiffness, F_0 is the initial value for sticking force, $f_{\mathrm{R}}(\mathbf{x}, \mathbf{v}_{\mathrm{rel}})$ is a stochastic function and $g(\mathbf{v}_{\mathrm{rel}}, \dot{\mathbf{v}}_{\mathrm{rel}})$ represents a function to model the Stribeck curve. An example of the friction characteristics of this model is displayed in Figure 2.3.

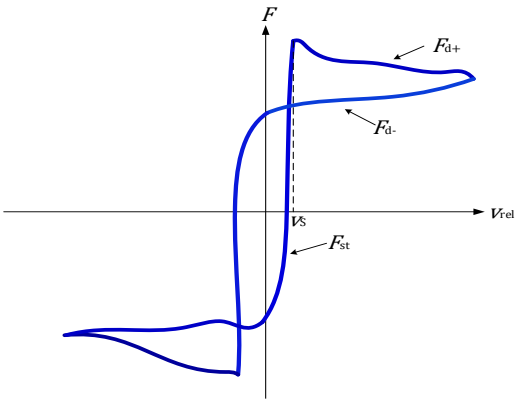

Figure 2.3 Hysteretic behaviour of friction force.

Besides, Karnopp [78] developed a model where the velocity is considered zero for a prescribed small range. Leine et al. [79] proposed the switch model as a modification of Karnopp model. Ambrósio [80] proposed a modified Coulomb's friction law. Awrejcewicz et al. [81] presented a model which is dependent on both the tangential force and the relative velocity.

2.2.2 'Dynamic' friction models

The 'dynamic' friction models are capable of capturing some friction phenomena such as pre-sliding displacement or friction lag which are not reflected in the 'static' friction models by introducing extra state variables.

The Dahl friction model [82, 83] introduced the pre-sliding displacement through a new state variable $\mathbf{z}$ and its formulation is expressed as a first-order differential equation,

$$\frac{\mathrm{d}\mathbf{z}}{\mathrm{d}t} = \left(1 - \frac{\sigma_0 \mathbf{z} \cdot \mathrm{sgn}(\mathbf{v}_{\mathrm{rel}})}{\mu_{\mathrm{k}} \|\mathbf{F}_{\mathrm{N}}\|}\right) \mathbf{v}_{\mathrm{rel}} \tag{2.11}$$

The friction force $\mathbf{F}_{\mathrm{T}} = \sigma_0 \mathbf{z}$, where σ_0 represents the stiffness coefficient of the bonds between the two contacting surfaces. In the steady state, the Dahl friction model is actually the Coulomb's friction model.

Haessig and Friedland [84] proposed a model which considers that the friction force results from the deformation of the asperities. Each contact is modelled as a bond of a rigid bristle and a flexible bristle which behaves as a linear spring. The total friction force is the resultant of all the spring forces due to relative motion, i.e.,

$$\mathbf{F}_{\mathrm{T}} = \sum_{i=1}^{n} \sigma_i (\mathbf{x}_i - \mathbf{b}_i) \tag{2.12}$$

where n is the number of bristles bonded, σ_i denotes the stiffness of the ith flexible bristle, $\mathbf{x}_i$ is the position of the flexible bristle, $\mathbf{b}_i$ represents the position of the rigid bristle. This model is inefficient for numerical simulation, therefore it is not usually used.

Canudas de Wit et al. [85, 86] developed the LuGre model in which the friction force is also considered as the result of deformation of bristles while the average bristle deflection is utilized. An internal state variable $\mathbf{z}$ is introduced to quantify the average bristle deflection, and the friction force is expressed as,

$$\begin{cases} \dfrac{\mathrm{d}\mathbf{z}}{\mathrm{d}t} = \left(1 - \dfrac{\sigma_0 \mathbf{z} \cdot \mathrm{sgn}(\mathbf{v}_{\mathrm{rel}})}{g(\mathbf{v}_{\mathrm{rel}})}\right) \mathbf{v}_{\mathrm{rel}} \\ \mathbf{F}_{\mathrm{T}} = \sigma_0 \mathbf{z} + \sigma_1 \dfrac{\mathrm{d}\mathbf{z}}{\mathrm{d}t} + \sigma_2 \mathbf{v}_{\mathrm{rel}} \end{cases} \tag{2.13}$$

where σ_0, σ_1 are the stiffness and damping of the bristles, respectively, $f(\mathbf{v}_{\mathrm{rel}})$ is a function that describes the viscous effect, $g(\mathbf{v}_{\mathrm{rel}})$ is a function that considers the

Stribeck effect. The LuGre model can be regarded as a derivation from the Dahl model. In [87], Piatkowski presented a method of determination of parameters for LuGre and Dahl friction models.

The reset integrator model [88] is also an evolution of the Dahl model. In this model, the friction force originates from the elastic and plastic deformation of the surface asperities. Similarly, an extra state variable **z** is used to determine the deformation of bristles in contact as,

$$\frac{\mathrm{d}\mathbf{z}}{\mathrm{d}t} = \begin{cases} \mathbf{0} & \text{if } \|\mathbf{z}\| \geq z_0 \cap \mathbf{z} \cdot \mathbf{v}_{\mathrm{rel}} > 0 \\ \mathbf{v}_{\mathrm{rel}} & \text{otherwise} \end{cases} \tag{2.14}$$

The friction force is defined as,

$$\mathbf{F}_{\mathrm{T}} = \begin{cases} \sigma_0 z_0 \mathrm{sgn}(\boldsymbol{z}) & \text{if } \|\mathbf{z}\| \geq z_0 \\ \sigma_0(1+a)\mathbf{z} + \sigma_1 \frac{\mathrm{d}\mathbf{z}}{\mathrm{d}t} & \text{if } \|\mathbf{z}\| < z_0 \end{cases} \tag{2.15}$$

As shown above, the reset integrator model consists of two state equations, one for slipping and another for sticking. The transition between the two states occurs when the deformation reaches its maximum value z_0, which makes this model discontinuous.

Besides, Dupont et al. [89] developed the elasto-plastic model, which divided the body's displacement into the elastic displacement that represents the bristle deflection and the plastic displacement that represents the macroscopic sliding displacement. Swevers et al. [90] proposed the Leuven model which was an improvement over the LuGre model. Gonthier et al. [91] introduced a two-dimensional friction model based on the LuGre model. Liang et al. [92] extended the model proposed by Haessig and Friedland [83] to the three-dimensional space.

2.3 Investigation of friction induced vibration in mechanical models

Friction induced vibration in mechanical systems can exhibit rich dynamic behaviours, which have been revealed in a number of publications. To study this problem, various mechanical models have been established, which can usually be classified into three categories, namely the lumped models, the continuous models and the finite element models.

2.3.1 Lumped models

Popp and Stelter [20] analysed the stick-slip oscillation of a 1-DoF slider-on-belt system with external harmonic excitation and a 2-DoF slider-on-belt system. The results showed the bifurcation behaviours of the dynamic responses in the two systems, depending on the ratio between the excitation frequency and the natural frequency of the oscillator and the ratio between two damping coefficients, respectively. Elmaian et al. [4] investigated the friction induced vibration of a three degree-of-freedom model and found that three distinct dynamic states, i.e, stick, slip and separation can appear in the vibration of this model and the time ratios of the three states in the whole process vary with the system parameters, which can be linked to the appearance of different categories of noises, i.e., no noise, creak, squeal and squeak. Li and Feng [93] examined the dynamics of a single-degree-of-freedom oscillator sliding over a rigid surface with the LuGre friction model and found the chaotic motions can appear which is not expected in a single-degree-of-freedom system because the LuGre friction model contains one internal variable. Pikunov and Stefanski [94] analysed the friction induced dynamics of a 1-DoF mass-on-belt model with cubic nonlinearity and a modified LuGre friction model. By means of a method of estimation for non-smooth systems, Lyapunov exponent spectrum of the friction oscillator was calculated to be used for observations of the nature of the oscillator's response.

In Ref. [95], a three-degree-of-freedom model of a pin-on-disc system was presented and the effects of parameters including the normal force, the rotational speed and the pin stiffness on the system responses were revealed. In Ref. [96], the combined problem of friction and impact of a single-degree-freedom oscillator colliding with an obstacle and excited by a moving belt was studied. Li et al. [97] analysed the mode-coupling phenomenon of a 2-DoF model with nonlinear contact stiffness and the effects of separation and reattachment on the vibration amplitudes of dynamic responses were studied. Zhang et al. [98] compared the results of system instability obtained from three different methods, i.e., the complex eigenvalue analysis (CEA), the net work analysis and the nonlinear instability analysis, in a 4-DoF friction oscillator and found both the net work analysis and CEA under-predict the instability due to their inability to detect the subcritical Hopf bifurcation. Some work on friction induced dynamics using low-degree-of freedom lumped models was also done in Refs. [2, 19, 28, 33, 55, 56, 62, 99-102].

Kruse et al. [103] explored the effect of joints on the stability and bifurcation behaviour of a system subject to friction induced flutter. It was shown that subcritical bifurcations, bifurcations from infinity and detached limit cycles can arise when the joint with nonlinear dynamic behaviour is integrated in the system, which indicate the severe limitations of linear stability analysis based on the eigenvalue calculation of the linearized model. Pilipchuck et al. [104] examined the non-stationary effects in friction induced vibration of a two-degree-of-freedom brake model. It was observed that the system responses experienced qualitative transitions due to the linearly deceasing velocity of the belt. In particular, there was a significant widening of frequency spectrum of the dynamics in the final phase of the process. Brunetti et al. [105] studied the dynamics of a periodic modular lumped model in which each module consists of a mass in contact with the moving belt and a mass linked with the adjacent modules. It was shown that although the eigenvalues allow to indicate the stability of the system, they fail to indicate the frequency of the steady-state responses including the contact nonlinearities, i.e., stick-slip transition in the tangential direction and contact-no contact in the normal direction. A new energy index quantifying the capability of each mode to exchange energy with the external environment was then introduced as a more reliable indicator of the unstable frequency in the friction induced dynamic responses. In Ref. [106], the stick-slip induced brake creep-groan phenomenon was investigated by using a lumped torsional model and experiment.

Li et al. [107] investigated the dynamics of an archetypal self-excited smooth and discontinuous oscillator driven by dry friction from the moving belt. The complicated dynamic behaviours of double tangency bifurcation, the bifurcation of sliding homoclinic orbit to a saddle, subcritical Hopf bifurcation and grazing bifurcation for this system can be demonstrated with the variations of parameters such as the friction coefficients and the belt velocity. In Ref. [58], a novel two-degree-of-freedom model involving a wobbling disc which can be easily associated with a disc brake was proposed and its stability behaviour was analysed. Wei et al. [108] established a 3-DoF dynamic model of a brake system consisting of two-layer pads and a rigid disc and the bifurcation and chaotic behaviour of system responses dependent on the variation of brake pressure and the parameters of double-layer pads were observed. In Ref. [109], the vibration of a slider on the rough surface was examined by using a 2-DoF theoretical model and experiment. The Poisson's impact law and Coulomb's

friction law were employed on the contact surfaces to incorporate the roughness effects in the numerical simulation and the numerical solutions were found to agree with the experiments. In Ref. [110], the impact of contact stiffness heterogeneities on friction induced vibration was studied.

Thomsen et al. [34] considered the classical "mass-on-moving-belt" model with a discontinuous friction law and derived the approximate analytical expressions for the conditions, the amplitudes and the base frequencies of friction induced stick-slip and pure-slip oscillations. Hetzler et al. [111] presented an analytical investigation on stability and local bifurcation behaviour due to exponentially decreasing friction characteristic in a "mass-on-belt" oscillator. The analytical work on the stability analysis and limit cycles of the 1-DoF friction oscillator can also be seen from Refs. [112-114]. In Ref. [115], the Lyapunov exponents of the non-smooth 1-DoF mass-on-belt model with external excitation were derived, which was highly useful in identifying the chaotic behaviour in the system. Besides, the smooth functions were used to approximate the discontinuous friction law in some work. Van de Vrande et al. [30] investigated the friction induced vibration of 1 and 2-DoF mass-on-belt models and a 1-DoF drill string model by using smooth functions to approximate the discontinuous friction forces and the results showed the smoothing procedure accurately describes the behaviour of discontinuous systems. Divenyi et al. [116] adopted a smoothing procedure to model the non-smooth dry friction between the formation and drill bit to study the drill string vibration in a two-degree-of-freedom model.

Some literature focuses on the uncertainty analysis of friction induced vibration in lumped models. Nobari et al. [117] studied the uncertainty quantification of the complex eigenvalue of a 4-DoF lumped model in presence of uncertain input parameters and the expressions for calculating the mean value, variance and pseudo-variance of the complex eigenvalues were derived via perturbation method. Nechak and Sinou [118] presented a hybrid surrogate model for the prediction of friction induced instability in a 4-DoF friction system with random and interval uncertain parameters. In Ref. [119], two methods based on the generalized polynomial chaos coupled with the Lyapunov indirect method were proposed to deal with the stability of a 2-DoF nonlinear friction system with uncertain friction coefficients.

2.3.2 Continuous models

In the research of friction induced vibration, continuous structures which possess an infinite number of degrees-of-freedom have also been widely used for investigation.

Hoffmann et al. [43] used the dynamic model of an inclined flexible beam on the moving belt to examine the sprag-slip instability and found that there were parameter combinations for which a static solution corresponding to a steady sliding state did not exist, which thus provided a sufficient condition for self-excited vibration in the system. In Ref. [120], the dynamics of brake system was studied by modelling the brake disc as a flexible beam and the brake pads as elastic foundations. The results showed the mode coupling resulting from the deformation of the pad was the major factor in the generation of dynamic instability and brake squeal. Meziane et al. [121] proposed an experimental and numerical study of friction induced vibration of a system composed of two beams in contact. Transient dynamic and complex eigenvalue analysis with a Lagrange multiplier for imposing contact constraints were performed, the results of which correlated with experimental results with good precision with frequency content and vibrations in time. Won and Chung [122] presented a numerical analysis for the vibration of a transversely moving beam in contact with a frictional wall. The stick and slip states which occurred in the vibration were investigated and the effects of the axial load and the moving speed on the dynamic response were also examined.

Hochlenert et al. [66] examined the friction induced vibration of the moving continua including a travelling Euler-Bernoulli beam and a rotating annular Kirchhoff plate in frictional point contact with idealized brake pads and the influence of the design parameters on the occurrence of self-excited vibration in the system was shown. Ibrahim and Somnay [123] analysed the nonlinear dynamic behaviour of an elastic beam sliding on two frictional supports under sinusoidal and random excitations. Tonazzi et al. [124] conducted a numerical analysis of the dynamics of two finite elastic media in sliding contact with Coulomb friction law. The results showed that either the stick-slip phenomenon or mode coupling instability can happen to the system, and it was revealed how the system parameters affect the frictional behaviour switching from stick-slip oscillation to harmonic vibration due to mode coupling instability. Jung and Feeny [125] investigated the dynamic of a one-dimensional elastic

medium subjected to the distributed friction force and periodic boundary conditions. It was found the dynamic instability occurred in the form of unstable travelling waves, which were dependent on the friction coefficient and the Poisson ratio. Loyer et al. [126] studied the dynamic behaviour of an elastic layer with frictional contact in which the mode coupling phenomenon was responsible for the dynamic instability. Both the linear stability analysis and the time simulation of the nonlinear response were carried out and the model reduction was performed to save the computation time of temporal solution.

Disc is an integral component in many mechanical systems, such as the car brake system, the clutches, the computer drives, etc. In some literature, the disc was modelled by an elastic circular plate for the research of friction induced vibration in the relevant mechanical systems. Chan et al. [65] examined the parametric resonance of a stationary elastic disc excited by a rotating mass-spring-damper system with a frictional follower force. Ouyang et al. [127] investigated the in-plane vibration of a slider which is driven around the surface of a flexible disc and the transverse vibration of the disc. Shen [128] demonstrated that axisymmetric plate damping was capable of suppressing unbounded response of a stationary, elastic, circular plate excited by a rotating slider. In Ref. [129], the authors studied the coupling of in-plane and out-of-plane vibrations of a rotating annular Kirchhoff plate in the presence of a distributed frictional loading on its surface. As friction induced vibration of discs is a key focus in the research of the present thesis, more existing literature on the dynamics of disc under frictional contacts will be reviewed in Section 2.4.

2.3.3 Finite element models

Mechanical systems in practice, e.g., an automobile brake system, are usually composed of components with irregular geometry and complicated boundary condition, which makes it difficult to precisely model them by using lumped models or continuous models. With the advancement of computation capacity and introduction of model reduction techniques, finite element models have been used by many researchers for the study of friction induced vibration in complex mechanical systems.

Cao et al. [130] presented a numerical method to calculate the unstable frequencies of a car disc brake in which the stationary components of the brake were modelled using finite elements and the disc as a thin plate. The predicted unstable frequencies obtained

from the complex eigenvalues showed good agreement with the experimentally established brake squeal frequencies. Dai and Lim [131] developed an enhanced dynamic finite element model with friction coupling in which a pair of spectral-based assurance criteria for modelling and validating the structural coupling and boundary condition of the rotor-pad assembly was successfully applied. Kang et al. [132-134] used the finite element models of the pad-disc system for investigation of the dynamic instability in disc brakes in a series of works. In Ref. [132], the finite element model of a rotating hat-disc in contact with two stationary pads was constructed to conduct the squeal analysis and two types of mechanisms for the occurrence of squeal, i.e., mode coupling and negative friction slope, were found. In Ref. [133], a new modelling methodology for the moving load model with the rotating finite element of an asymmetric automotive brake disc in friction contact with stationary pads was proposed. The numerical results showed the system eigenvalues were variable for the disc rotation angle and therefore the appearance of dynamic instability and squeal events was time-dependent when the disc is asymmetric, which was in stark contrast with the results of axisymmetric disc. In Ref. [134], the squeal propensity of the in-plane modes and the constrained-layer type damping shims for disc brake system was investigated by using the finite element method. It was highlighted that the in-plane torsion modes of the disc were essential in squeal generation in presence of effective damping shim and negative friction slope.

Blaschke [135] examined the squeal propensity by a finite element model in which the contact force between the brake pad and the brake disc was directly calculated from the state of the system rather than being obtained from the imaginary springs. Wei at al. [136] used Abaqus to investigate the effects of key parameters including the rotational speed, the braking pressure and the friction coefficient on the dynamic instability of a brake model. The comparison between the experimental results and the results of complex eigenvalue analysis (CEA) demonstrated that the CEA may overestimate or underestimate the unstable frequencies. Some work on the friction induced vibration using finite element models were also done in Refs. [137-141].

Besides the linear stability analysis on the finite element models, some literature focused on the nonlinear time-domain analysis. Sinou [142] developed a nonlinear finite element model of a disc brake system and studied the transient and stationary nonlinear self-excited vibration. The results showed that nonlinear transient and

stationary self-excited vibration can be very complex and include more unstable modes than those predicted by a linearized stability analysis around a nonlinear equilibrium point. Soobbarayen et al. [143] presented a numerical analysis of the influence of the loading conditions on the vibration and acoustic responses of a finite element model. The numerical results showed that a sufficiently fast ramp loading can destabilize a stable configuration predicted by the stability analysis. Moreover, the ramp loading can result in higher amplitudes of time response than that for the static load and activate new harmonic components due to nonlinearity.

In order to solve the problem of expensive computational cost in the large finite element models of frictional systems, the model reduction techniques were proposed or employed in some studies [144-149]. In Ref. [144], a novel nonlinear method which works for nonlinear systems subject to flutter instability called the Constrained Harmonic Balance Method (CHBM) was proposed and applied effectively to the analysis of disc brake squeal. In Ref. [145], the performances of two popular model reduction methods were investigated in the case of a disc/pads system. Besset and Sinou [146] put forward a new efficient reduction method based on complex interface modes for predicting the stability analysis of a damped nonlinear brake system subject to friction induced vibration. Li et al. [149] proposed a model reduction strategy based on mode synthesis for complicated frictional system, which was then applied to the analysis of friction induced vibration of a real pad-on-disc structure and validated by the experimental results.

2.4 Dynamics of spinning disc in contact with stationary parts

Discs rotating relative to stationary parts can be found in a wide variety of industrial applications, such as car disc brakes, disc drives, circular saws, clutches, etc. During the normal operations of these mechanical devices, the contact of the disc with the stationary parts may excite unstable vibrations in the system, which seriously affect the performance of the devices. In the last several decades, there has been lots of research on this problem.

The early works on the instability of rotating elastic disc under stationary loading system were done by Iwan [150, 151]. In Ref. [150], the dynamic instabilities of a stationary elastic disc under a mass-spring-damper loading system rotating at constant

speed were studied. In Ref. [151], the dynamic instabilities of a rotating elastic disc under a stationary mass-spring-damper loading system were investigated. The centrifugal stresses due to rotation of disc was considered. Hutton et al. [152] analysed the response of a rotating disc clamped at the inside and free at the perimeter subject to the excitation produced by stationary point loads and restrained by stationary point springs for the analysis and design of guided circular saws. Ono et al. [153] built the theoretical formulation and conducted the eigenvalue analysis for a system of a spinning flexible disc and a pair of head and suspension systems that contact the disc on its two sides for the stability analysis of disc drive system. Chen and Bogy [154] examined the modal interactions in a spinning disc-stationary load system by use if a numerical finite element method and by an eigenfunction expansion method. Young and Lin [155] studied the stability of a spinning annular plate transversely in contact with a stationary oscillating unit which consists of two parallel combinations of springs and dampers attached above and under a mass. The numerical results demonstrated that taking account of the stiffness between the disc and the mass may cause extra flutter-type instability between the predominantly disc modes and the predominantly mass mode. Ouyang [156] presented the numerical analysis of the vibration in a refined dynamic model of atomising discs where the disc was modelled as a thin Kirchhoff plate with centrifugal and gyroscopic effects. And Ouyang [157] presented a tutorial for moving load problems among which the vibration of a circular plate excited by a moving oscillator was described.

The role of friction force between the rotating disc and the stationary parts on the dynamics of system has also been studied. In Ref. [158], the critical rotational speeds of an annular laminated disc and instability due to the existence of a stationary frictional follower load were examined. Pei et al. [159] studied the stability and steady-state response of a rotating flexible disc under stationary sliders in consideration of the initial transverse runout of the disc. It was found that amplitude of the steady-state response can be suppressed by the increase of disc damping, slider damping and friction force at the disc-slider interface. Ouyang et al. [52, 67, 127] investigated the vibration of a stationary elastic disc under the circumferentially moving mass loading system, in which the friction fore between the disc and the slider was taken into account. In Ref. [67], the friction force acted as a rotating bending moment and a follower force. In Refs. [52, 127], the friction force influenced the circumferential

motion of the slider which then affected the dynamics of the disc, and the effect of a negative friction-velocity relationship was examined in Ref. [52]. Kang [57] studied the dynamic instability of a thin annular plate due to circumferential friction between the plate and two fixed sector contact interfaces under steady-sliding conditions. It was observed that the angle of the sectors was a key parameter for the modal stability of the plate. Zhang et al. [160] used a flexible pin-on-disc system to simulate how the squeal noise can be generated in frictional contact and the features of time-varying squeal because of periodic friction coefficient were studied.

In Ref. [161], the dynamic response of a rotating disc subject to distributed nonlinear contact stresses from two fixed and rigid pads was examined. It was shown that high-frequency vibrations in the form of standing or travelling waves were produced, which resulted from the mode-coupling mechanism. And the stick zone of the contact area when the self-excited vibration was produced, i.e., the points in the state of sticking on the disc surface, was determined by a smooth friction-velocity curve. In Ref. [162], the dynamics of an asymmetric disc subjected to sector-shaped frictional contact on both sides of the disc was investigated. The results showed that breaking the axisymmetry changed the stability boundary of the system. Li et al. [163] investigated the transverse vibration of an elastic disc excited by a preloaded mass-damper-spring slider which experienced in-plane stick-slip oscillation and incorporated the separation and reattachment phenomena considering the possibility of loss of contact due to growing transverse disc vibration. The results highlighted the important role of separation on friction induced vibration. Sui and Ding [164] investigated the instability of a pad-on-disc in moving interactions and a stochastic analysis was carried out. In Ref. [165], a nonlinear stability analysis of a realistic disc brake model was described and it was exemplified that the effect of parameters on the linear and on the nonlinear stability boundary can be oppositional.

2.5 Experimental investigations on the friction induced vibration

Among the literature on the study of friction induced vibration, part of them focused on the investigations by physical experiments. Butlin and Woodhouse [166] presented a comparison between theoretical predictions and experimental results from a pin-on-disc test rig exploring friction induced vibration. A large number of measured squeal initiations were used to reveal the complex-valued frequency-dependent parameters

for a theoretical model of linearized dynamic friction. The results highlighted the importance of an accurate description of dynamic friction at the sliding interface in predicting the squeal events. In Ref. [167], the experimental estimates of parametric uncertainties with a first-order perturbation analysis provided a foundation for exploring the effect of uncertainty on predictions of squeal. In Ref. [168], an experimental investigation on a pin-on-disc rig was performed to validate the results on the prediction of instability of the system by a theoretical model composed of two linear sub-systems coupled by a frictional point contact.

Neis et al. [169] investigated the friction property of brake materials by means of a rotating stick-slip tester. Experimental results were compared with the computational model implemented in Simulink. In Ref. [170], the acoustic emission technique was used to record and study the elastic waves which appear during transition from static to kinetic friction in a stick-slip experiment carried out using a sheet of soft steel and a clamp of quenched steel. Giannini et al. [171] built an experimental setup where two pads carried by clamped beams were brought to be in contact with a disc and measured the dynamic behaviour and squeal behaviour of the system. The experimental results provided guidelines to build a representative model of the setup and a better understanding of the physics of the squeal mechanism. In Ref. [172], an experimental analysis was performed on a simplified brake apparatus where the squeal events were correlated with the modal behaviour of the system as a function of main parameters. A clear distinction between the squeal events involving the dynamics of the pad and the squeal events involving the dynamic of the calliper was performed. In Ref. [173], the experimental methods were presented to characterize the nonlinearities in brake system and a novel simulation approach that allows the calculation of limit cycles considering nonlinearities was then introduced.

Chen and Zhou [174] studied an initiation process of friction induced vibration based on three-dimensional vibration accelerations and tangential force in a friction system under reciprocating sliding conditions. Two modes of vibration were found where Mode one is present as soon as the reciprocating sliding starts and Mode two does not occur until the coefficient of friction reaches a large value. In Ref. [175], an experimental setup of a drill-string system was built and the limit cycle of friction-induced torsional vibration was observed. Nishiwaki et al. [176] examined the out-of-plane deformation of a rotating disc using the double-pulsed technique in order to

visualise the vibration pattern of the disc and pad when squeal vibration occurs. Their results showed that squeal vibration was generated when both the rotating disc and pads vibrated in bending mode. Oberst and Lai [177] carried out an experimental work using a noise dynamometer to determine the influence of geometry of brake pads on vibration of the system. The experimental results were evaluated with a noise index and it was indicated that pads with a single slot perform better than pads with no slots or double vertical slots.

Abu Baker and Ouyang [178] presented the wear prediction of the friction material in brake pads subject to brake applications. The wear progress predicted in the finite element simulation was verified using measured static contact pressure distribution from contact tests and measured surface topography of the friction material. In Ref. [179], the experimental study on the reduction of noise from the disc brake system using constrained layer damping was carried out. It was recommended to use modal analysis and frequency response function measurements in the selection of the damping material for the reduction of brake noise so as to avoid excessive time consumption with extensive dynamometer tests in the "trial and error" procedure. In Ref. [180], an experimental study was conducted to investigate the effect of surface sandblasting on squeal generation. The experimental results indicated that the surface roughness has important influence on the friction wear process and the evolution of the friction induced noise and the suppression of friction induced noise can be achieved by increasing the surface roughness appropriately.

Some researchers conducted studies on the friction induced vibration and noise of the train brake. Quan et al. [181] carried out experiments to evaluate the effects of friction block shape and installation angles on the brake noise of high-speed trains on a customized small-scale brake dynamometer. Wang et al. [182] studied the effect of grooved disc surface on the tribological and noise behaviours of train brakes by experimental observations on a specifically designed dynamometer. Kanki et al. [183] proposed to attach an oil damper to the train brake system to suppress the brake squeal and the capability of the proposed damper in squeal suppression was demonstrated by test results. Sinou et al. [184] presented an experimental and numerical analysis of the squeal vibration on industrial railway brakes.

2.6 Conclusion

Abundant studies involving the friction induced vibration in mechanical systems from various aspects are presented in the literature review, which enhances understanding of this problem enormously and on the other hand, reflects the complexity of this problem that is related to multiple factors. The literature of this subject constitutes the important foundation and inspirations for the research in the present thesis.

Chapter 3

Basic theories and analytical methods of friction induced vibration

In this chapter, the fundamental knowledge and analysis tools that are utilized in the present thesis are presented. In Section 3.1 the principal mechanisms for generation of friction induced vibration including the negative friction-velocity slope, the stick-slip oscillation and the mode-coupling instability are clarified in low-degree-of freedom lumped models. In Section 3.2, two main kinds of theoretical methods for the analysis of friction-induced-vibration problems, i.e. the complex eigenvalue analysis (CEA) and the transient dynamic analysis (TDA), are introduced. Finally in Section 3.3 the basic theory about the vibration of elastic thin plates are stated.

3.1 Principal mechanisms of friction induced vibration

3.1.1 Negative friction-velocity slope

Because friction force decreases with the increase in the relative velocity at low velocities in a number of experimental observations, the expression of friction force during relative sliding as a continuous and decreasing function of the relative velocity was proposed. The negative slope of the function of friction force introduced a negative damping into the system, which can thus lead to the dynamic instability of the system. In the following this mechanism is elaborated in a single-degree-of-freedom dynamic model.

A mass-damper-spring oscillator on a moving belt is displayed in Fig. 3.1, where the vibration of the oscillator is influenced by the friction force between the mass and the belt. As shown in the figure, the equation of motion of the mass can be written as,

$$m\ddot{x} + c\dot{x} + kx = F_{\mathrm{f}} \tag{3.1}$$

where $v_{\mathrm{r}} = v - \dot{x}$. Suppose that friction force in relative sliding is a linearly decreasing function of the relative velocity, i.e.,

$$F_{\mathrm{f}} = \mathrm{sgn}(v_{\mathrm{r}})(F_0 + \alpha_0 v_{\mathrm{r}}) \tag{3.2}$$

where α represents the negative slope, the equations of motion of the mass around the equilibrium point ($\ddot{x} = \dot{x} = 0$) can be rewritten as,

$$m\ddot{x} + (c + \alpha_0)\dot{x} + kx = F_0 + \alpha v \tag{3.3}$$

It is observed from Eq. (3.3) that the dynamic instability occurs when $c + \alpha_0 < 0$, i.e. $\alpha_0 < -c$. This example explains how the negative friction-velocity slope results in the generation of self-excited vibration.

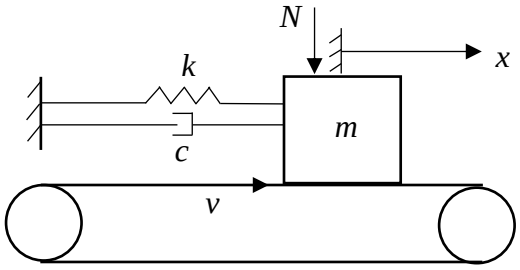

Figure 3.1 A single-degree-of-freedom friction oscillator.

3.1.2 Stick-slip oscillation

Stick-slip oscillation is formed when two distinct states of motion, sticking (if the two objects in contact are at rest relatively and the static friction force between them does not exceed the maximum static friction capacity) and slipping (if the two objects are in relative motion) take place successively. In the following this mechanism is elaborated also by using the classical mass-on-moving-belt model.

3.1.2.1 Periodic stick-slip oscillation

The stick-slip motion of a single-degree-of-freedom mass-on-belt model as shown in Fig. 3.2 is examined. It is easy to obtain the equation of motion of the system, i.e.,

$$m\ddot{x} + kx = F_{\mathrm{f}} \tag{3.4}$$

where F_{f} represents the friction force between the mass slider and the belt, and the Coulomb's law of friction is assumed on the interface. The friction force adopts different formulations in the two distinct states of motion, i.e. sticking and slipping. In the state of slipping, the friction force can be written as,

$$F_{\mathrm{f}} = \mathrm{sgn}(v_{\mathrm{r}})\mu_{\mathrm{k}}N \tag{3.5}$$

where μ_{k} is the coefficient of kinetic friction, and the condition for the mass to stay in the state of slipping is,

$$v_{\mathrm{r}} = v - \dot{x} \neq 0 \tag{3.6}$$

In the state of sticking, the friction force is used to sustain the relative static state and thus it follows,

$$F_{\mathrm{f}} = kx \tag{3.7}$$

and the motion of the mass in the state of sticking follows,

$$\ddot{x} = 0, \dot{x} = v, x = v(t - t_{\mathrm{s}}) \tag{3.8}$$

where t_{s} is the time when the sticking starts. The condition for the mass to stay in the state of sticking is,

$$|F_{\mathrm{f}}| \leq \mu_{\mathrm{s}}N \tag{3.9}$$

where μ_{s} is the coefficient of static friction.

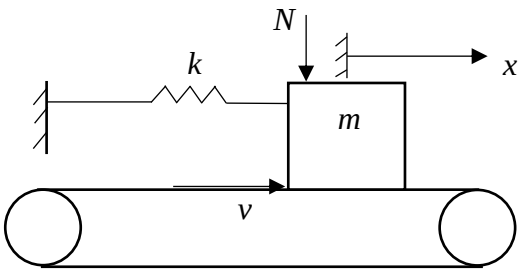

Figure 3.2 A single-degree-of-freedom mass-on-moving-belt model.

The dynamic behaviour of the system based on the above equations is then obtained. Suppose that the values of parameters are: $m = 1$, $k = 1$, $N = 10$, $\mu_k = 0.23$, $\mu_s = 0.4$, $v = 1$, the phase-plane plots of the mass with various initial conditions are shown in Fig. 3.3. It is clearly seen that there exists a stable limit cycle (highlighted by the thick curve in the figure) for the motion of the mass, which indicates that the steady-state motion of the mass is a periodic stick-slip oscillation as long as the initial condition is far enough from the equilibrium point.

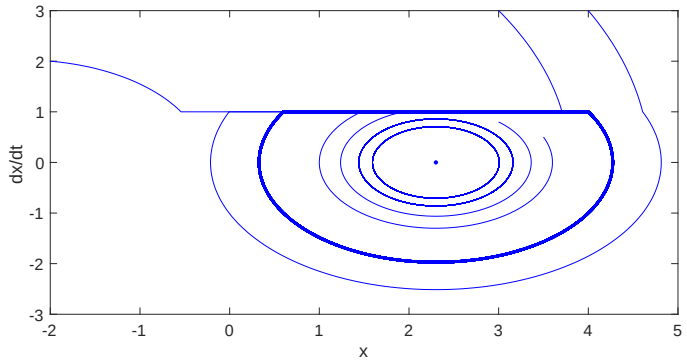

Figure 3.3 The phase-plane plots of the single-degree-of-freedom friction oscillator with various initial conditions.

3.1.2.2 Bifurcations of stick-slip oscillation

The bifurcation behaviour of stick-slip oscillation is exhibited in this section. Firstly the motion of a single-degree-of-freedom mass-on-belt model under a harmonic external excitation, which was studied in Ref. [20], is considered, as shown in Fig. 3.4.

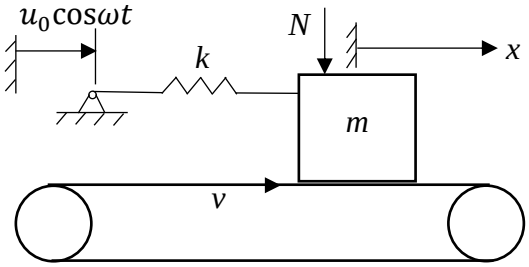

Figure 3.4 A single-degree-of-freedom mass-on-moving-belt model with harmonic external excitation.

The equation of motion of the system reads,

$$m\ddot{x} + k(x - u_0 \cos\omega t) = F_f \tag{3.10}$$

With the Coulomb's law of friction used, the formulation of the friction force in the state of slipping is the same as that in the above section while the friction force in the state of sticking is influenced by the external excitation, which can be written as,

$$F_{\mathrm{f}} = k(x - u_0 \cos\omega t) \tag{3.11}$$

Suppose $u_0 = 0.5$ and other parameters are identical to those in the above section, the phase-plane plots and frequency spectrums with different excitation frequencies are shown in Fig. 3.5. It is observed that the dynamic responses with distinct features result from different excitation frequencies. For $\omega = 0.85$ and $\omega = 1.2$, the dynamic responses are periodic, although with different periods, while for $\omega = 0.5$, non-periodic oscillation is present. Next the bifurcation behaviour of the system response with the excitation frequency as the controlling parameter is shown in Fig. 3.6. It is observed that the system response experiences transitions from periodic to non-periodic oscillations with variation of the excitation frequency.

Besides, the system response is examined under the friction law with Stribeck effect, whose expression in the state of slipping can be written as,

$$F_{\mathrm{f}} = \mathrm{sgn}(v_{\mathrm{r}})\left(\mu_{\mathrm{k}} + (\mu_{\mathrm{s}} - \mu_{\mathrm{k}})e^{-|v_{\mathrm{r}}|}\right)N \tag{3.12}$$

while the friction force is still capped by $\mu_s N$. Suppose $\mu_{\mathrm{k}} = 0.23$, $\mu_{\mathrm{s}} = 0.4$, the bifurcation behaviour of the system response is shown in Fig. 3.7.

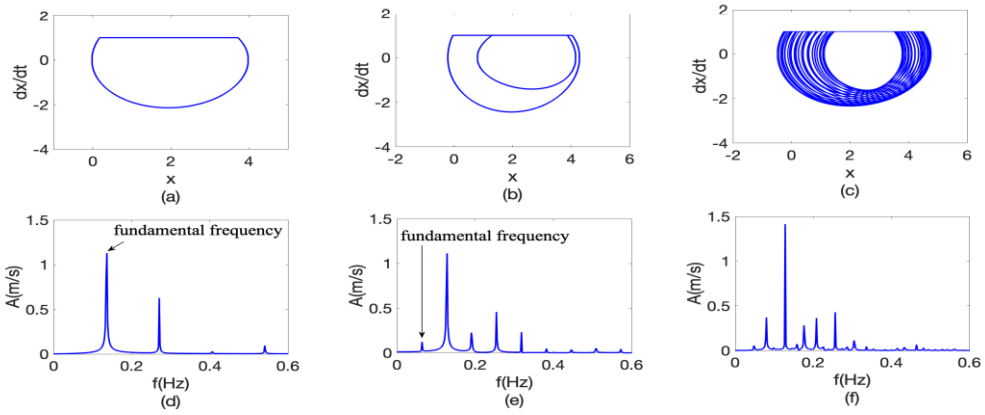

Figure 3.5 The phase-plane plots and frequency spectrums with different excitation frequencies: (a) and (d) $\omega = 0.85$; (b) and (e) $\omega = 1.2$; (c) and (f) $\omega = 0.5$.

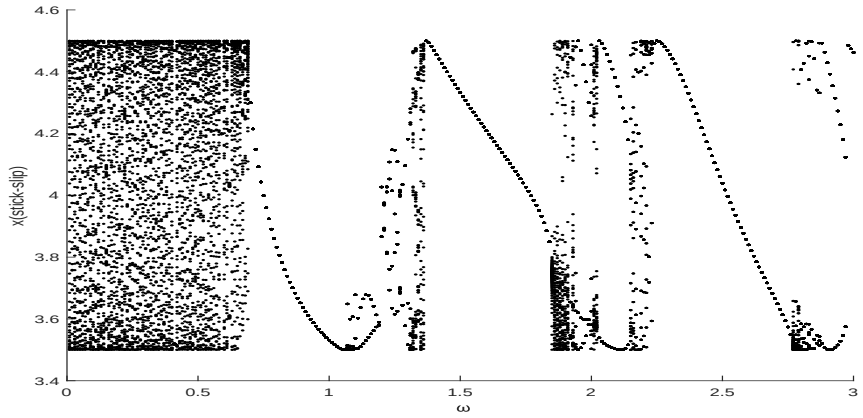

Figure 3.6 The bifurcation behaviour of the system response dependent on the excitation frequency under the Coulomb's law.

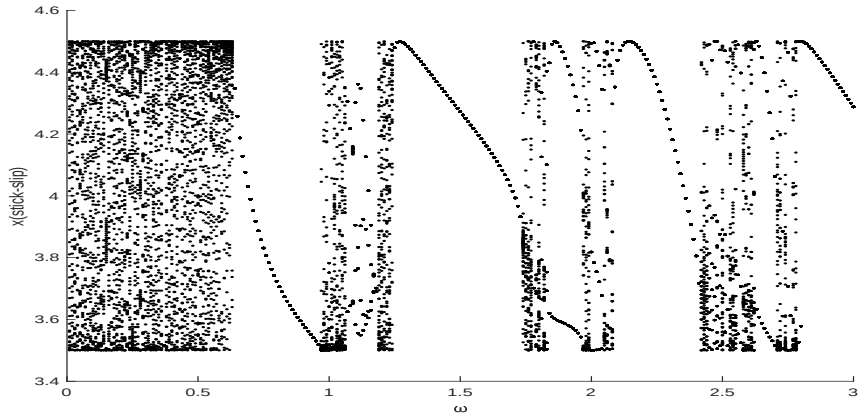

Figure 3.7 The bifurcation behaviour of the system response dependent on the excitation frequency under the friction law with Stribeck effect.

Secondly the motion of a two-degree-of-freedom mass-on-belt model [20] is considered, as shown in Fig. 3.8. The equations of motion of the system are,

$$m_1\ddot{x}_1 + (c_1 + c_2)\dot{x}_1 - c_2\dot{x}_2 + (k_1 + k_2)x_1 - k_2x_2 = F_{\mathrm{f1}} \tag{3.13}$$

$$m_2\ddot{x}_2 + c_2(\dot{x}_2 - \dot{x}_1) + k_2(x_2 - x_1) = F_{\mathrm{f2}} \tag{3.14}$$

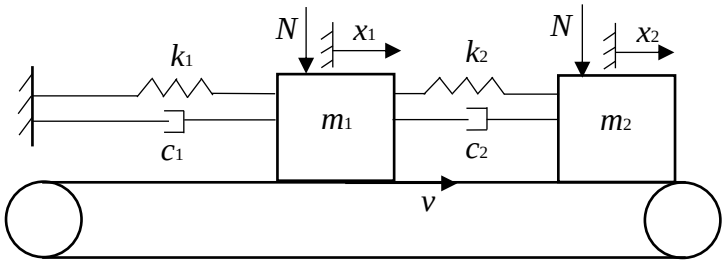

Figure 3.8 A two-degree-of-freedom mass-on-moving-belt model.

Similarly the friction forces in the state of slipping for both masses can be written as,

$$F_{\mathrm{f}i} = \mathrm{sgn}(v_{\mathrm{r}i})\mu(v_{\mathrm{r}i})N,\ i=1,\ 2 \tag{3.15}$$

where $v_{\mathrm{r}i} = v - \dot{x}_i$, i=1, 2. The friction force in the state of sticking of m_1 or m_2 is derived from Eq. (3.13) setting $\ddot{x}_1 = 0$ and $\dot{x}_1 = v$ or from Eq. (3.14) setting $\ddot{x}_2 = 0$ and $\dot{x}_2 = v$, respectively. Therefore while m_1 is in the state of sticking,

$$F_{\mathrm{f}1} = (c_1 + c_2)v - c_2\dot{x}_2 + (k_1 + k_2)x_1 - k_2x_2 \tag{3.16}$$

while m_2 is in the state of sticking,

$$F_{\mathrm{f}2} = c_2(v - \dot{x}_1) + k_2(x_2 - x_1) \tag{3.17}$$

And the motion of m_1 while m_1 is in the state of sticking follows,

$$\ddot{x}_1 = 0,\ \dot{x}_1 = v,\ x_1 = v(t - t_1) \tag{3.18}$$

where t_1 is the time when m_1 starts to stick. The condition for m_1 to stay in the state of sticking is,

$$|F_{\mathrm{f}1}| \le \mu_{\mathrm{s}}N \tag{3.19}$$

Similarly, the motion of m_2 while m_2 is in the state of sticking follows,

$$\ddot{x}_2 = 0,\ \dot{x}_2 = v,\ x_2 = v(t - t_2) \tag{3.20}$$

where t_2 is the time when m_2 starts to stick. The condition for m_2 to stay in the state of sticking is,

$$|F_{\mathrm{f}2}| \le \mu_{\mathrm{s}}N \tag{3.21}$$

Suppose the values of basic system parameters are: $m_1 = 2.5,\ m_2 = 1,\ k_1 = 2,\ k_2 = 1,\ N = 20,\ c_1/c_2 = 1,\ v = 1$ and the friction law with Stribeck effect expressed as Eq. (3.12) is adopted with $\mu_{\mathrm{k}} = 0.1$, $\mu_{\mathrm{s}} = 0.4$, the phase-plane plots and frequency spectrums with different damping ratios D ($D = c_2/2\sqrt{m_2k_2}$) are shown in Fig. 3.9. It is observed that the dynamic responses of the system are periodic for $D = 0.3$ and $D = 0.2$, and aperiodic for $D = 0.1$. Fig. 3.10 shows the bifurcation behaviour of the system responses, which is quite different from that of the single-degree-of-freedom model under harmonic external excitation. It is indicated from Fig. 3.10 that the non-periodic oscillation happens only when the damping ratio D is quite small in the two-degree-of-freedom mass-on-moving-belt model.

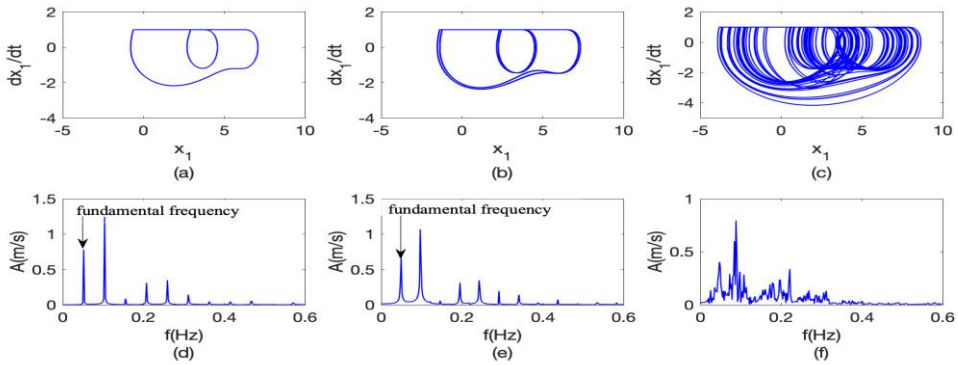

Figure 3.9 The phase-plane plots and frequency spectrums with damping ratios D: (a) and (d) $D = 0.3$; (b) and (e) $D = 0.2$; (c) and (f) $D = 0.1$.

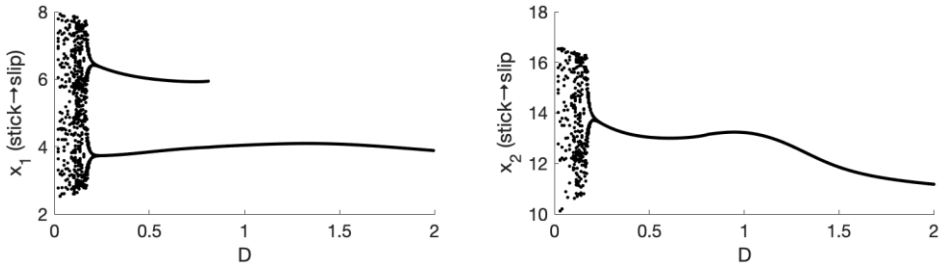

Figure 3.10 The bifurcation behaviour of the system responses of the two-degree-of-freedom model dependent on the damping ratio.

3.1.3 Mode-coupling instability

The mode-coupling instability has been considered to be mainly responsible for brake squeal. The complex eigenvalue analysis shows that some modes become unstable when coupling with other mode(s) of the system. Next this mechanism is clarified in a simple two-degree-of-freedom model.

As shown in Fig. 3.11, a two-degree-of-freedom model [55, 56] is considered. In this model, a point mass m is connected to the base by a damper c_1 in the horizontal direction and a damper c_2 in the vertical direction, and two linear springs k_1 and k_2 at the angles of inclination to the horizontal direction α_1 and α_2 respectively. The mass is pressed by a preload F to bring it into frictional contact with a belt moving at constant velocity v. A spring k_3 is used to model the contact stiffness between the mass and the belt. The equations of motion of the 2-DoF system can be obtained as,

$$\begin{bmatrix} m & 0 \\ 0 & m \end{bmatrix} \begin{bmatrix} \ddot{x} \\ \ddot{y} \end{bmatrix} + \begin{bmatrix} c_1 & 0 \\ 0 & c_2 \end{bmatrix} \begin{bmatrix} \dot{x} \\ \dot{y} \end{bmatrix} + \begin{bmatrix} k_{11} & k_{12} \\ k_{21} & k_{22} \end{bmatrix} \begin{bmatrix} x \\ y \end{bmatrix} = \begin{bmatrix} F_{\mathrm{f}} \\ -F \end{bmatrix} \tag{3.22}$$

where,

$$\left.\begin{array}{c} k_{11} = k_1\cos^2\alpha_1 + k_2\cos^2\alpha_2, \\ k_{12} = k_{21} = -k_1\sin\alpha_1\cos\alpha_1 + k_2\sin\alpha_2\cos\alpha_2 \\ k_{22} = k_1\sin^2\alpha_1 + k_2\sin^2\alpha_2 + k_3 \end{array}\right\} \tag{3.23}$$

The normal force between the mass and the belt is expressed as,

$$N = -k_3 y \tag{3.24}$$

Since the friction force is assumed to be proportional to the normal force $F_\mathrm{f} = \mu N$, the equations of motion of the system can be rewritten as,

$$\begin{bmatrix} m & 0 \\ 0 & m \end{bmatrix}\begin{bmatrix} \ddot{x} \\ \ddot{y} \end{bmatrix} + \begin{bmatrix} c_1 & 0 \\ 0 & c_2 \end{bmatrix}\begin{bmatrix} \dot{x} \\ \dot{y} \end{bmatrix} + \begin{bmatrix} k_{11} & k_{12} + \mu k_3 \\ k_{21} & k_{22} \end{bmatrix}\begin{bmatrix} x \\ y \end{bmatrix} = \begin{bmatrix} 0 \\ -F \end{bmatrix} \tag{3.25}$$

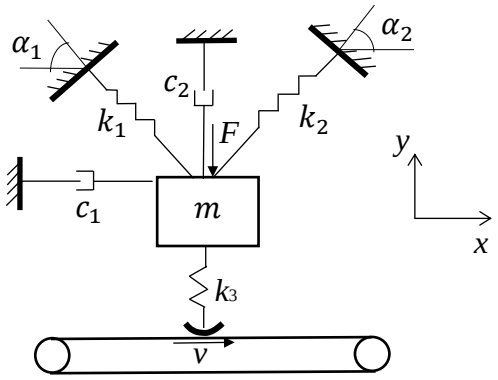

Figure 3.11 A two-degree-of-freedom friction model.

The stiffness matrix of the system is now non-symmetric, which can bring about dynamic instability. Denoting $\bar{x} = x - x_\mathrm{e}$, $\bar{y} = y - y_\mathrm{e}$, where ($x_\mathrm{e}$, y_e) is the equilibrium point of the system, the dynamic equations with respect to $\bar{x}$ and $\bar{y}$ are,

$$\begin{bmatrix} m & 0 \\ 0 & m \end{bmatrix}\begin{bmatrix} \ddot{\bar{x}} \\ \ddot{\bar{y}} \end{bmatrix} + \begin{bmatrix} c_1 & 0 \\ 0 & c_2 \end{bmatrix}\begin{bmatrix} \dot{\bar{x}} \\ \dot{\bar{y}} \end{bmatrix} + \begin{bmatrix} k_{11} & k_{12} + \mu k_3 \\ k_{21} & k_{22} \end{bmatrix}\begin{bmatrix} \bar{x} \\ \bar{y} \end{bmatrix} = \begin{bmatrix} 0 \\ 0 \end{bmatrix} \tag{3.26}$$

Assuming the solution of the homogeneous differential equations as Eq. (3.26) is,

$$\begin{bmatrix} \bar{x} \\ \bar{y} \end{bmatrix} = \begin{bmatrix} x_0 \\ y_0 \end{bmatrix} \mathrm{e}^{st} \tag{3.27}$$

and substituting Eq. (3.27) into Eq. (3.26), a generalized eigenvalue problem is resulted,

$$\left(s^2\begin{bmatrix} m & 0 \\ 0 & m \end{bmatrix} + s\begin{bmatrix} c_1 & 0 \\ 0 & c_2 \end{bmatrix} + \begin{bmatrix} k_{11} & k_{12} + \mu k_3 \\ k_{21} & k_{22} \end{bmatrix}\right)\begin{bmatrix} x_0 \\ y_0 \end{bmatrix} = \begin{bmatrix} 0 \\ 0 \end{bmatrix} \tag{3.28}$$

By setting

$$\left| s^2 \begin{bmatrix} m & 0 \\ 0 & m \end{bmatrix} + s \begin{bmatrix} c_1 & 0 \\ 0 & c_2 \end{bmatrix} + \begin{bmatrix} k_{11} & k_{12} + \mu k_3 \\ k_{21} & k_{22} \end{bmatrix} \right| = 0 \qquad (3.29)$$

the eigenvalue s can be solved. If one of the solution of s has positive real part, the equilibrium point of the system becomes unstable and self-excited vibration will happen.

Suppose the values of parameter are: $m = 1$, $k_1 = 1$, $k_2 = 1$, $k_3 = 2$, $\alpha_1 = \frac{\pi}{4}$, $\alpha_2 = \frac{\pi}{6}$, the eigenvalues of the undamped system ($c_1 = c_2 = 0$) as a function of μ are shown in Fig. 3.12, where the left figure shows the imaginary parts and the right figure shows the real parts. It is seen that when $\mu > 4.2$, the two imaginary parts coalesce and one real part becomes positive. The time histories of $\bar{x}$ and $\bar{y}$ at two different values of μ (one is a little smaller than 4.2, the other is a little larger than 4.2) are shown in Fig. 3.13. From Fig. 3.12 and 3.13 the significant role of friction on the stability of the system is observed. When μ is smaller than the critical value 4.2, the real parts of eigenvalues are zero and the vibration does not grow meaning the equilibrium point of the system is stable; when μ is larger than the critical value, the real part of one of the eigenvalues becomes positive and the vibration grows unbounded meaning the equilibrium point is unstable and self-excited vibration will arise in the system.

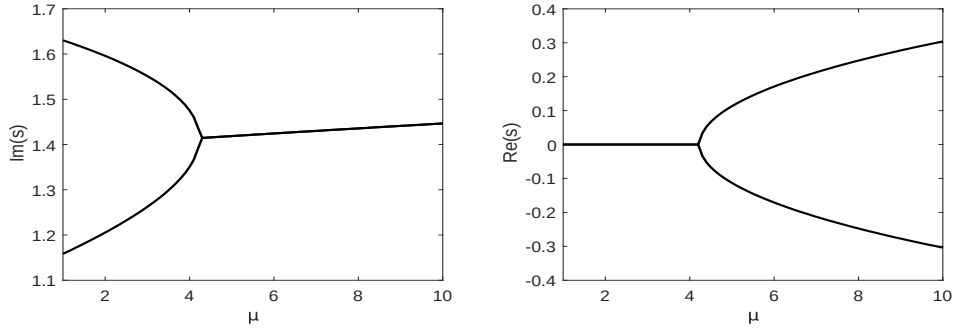

Figure 3.12 The eigenvalues of the system as a function of μ.

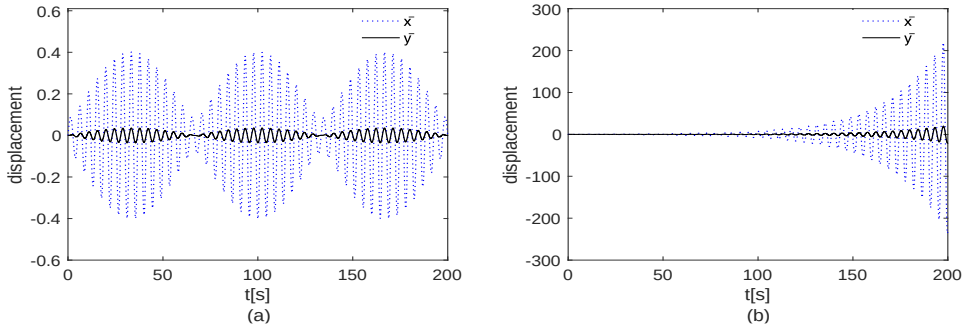

Figure 3.13 The time histories of the dynamic responses: (a) $\mu = 4.1$; (b) $\mu = 4.3$.

Next the system with structural damping in terms of the mode-coupling instability is investigated. Two cases of damping, which are proportional damping ($c_1 = c_2$) and non-proportional damping ($c_1 \neq c_2$), are considered. In Fig. 3.14, the eigenvalues of the system with proportional damping for $c_1 = 0, 0.2, 0.5$ are plotted. It is observed that the imaginary parts of eigenvalues for different damping coefficients merge at nearly identical value of μ, i.e., at about $\mu = 4.2$, while the positive real part occurs at greater value of μ for larger damping coefficient. Defining the value of the friction coefficient at which one of the real parts become positive as the critical friction coefficient μ_c, Fig. 3.15 displays μ_c as a function of c_1. It is seen that the critical friction coefficient increases with the increase of damping, indicating that the structural damping stabilizes the system, which is consistent with the normal function of structural damping. In Fig. 3.16, the eigenvalues of the system with non-proportional damping $c_2 = 2c_1$ for $c_1 = 0, 0.2, 0.5$ are plotted. It is seen that for the system with non-proportional damping, the imaginary parts of eigenvalues approach with the increase of μ, but no merging of imaginary parts occurs any more. The critical friction coefficient μ_c as a function of c_1 in this case is displayed in Fig, 3.17. It is observed that the critical friction coefficient firstly decreases and then increases with the increase of damping. Therefore the small structural damping may lead to destabilization, and the structural damping plays the role of stabilizing the system only after the damping exceed a certain value. This behaviour is called "viscous instability" or "damping instability".

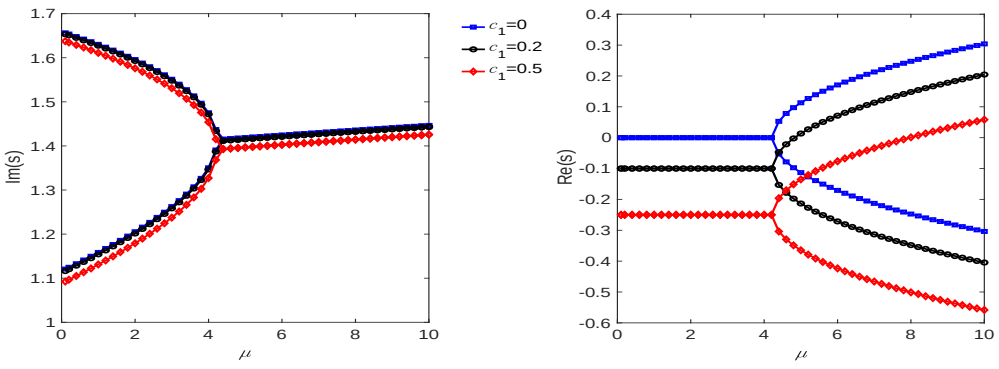

Figure 3.14 The eigenvalues of the system with proportional damping as a function of μ.

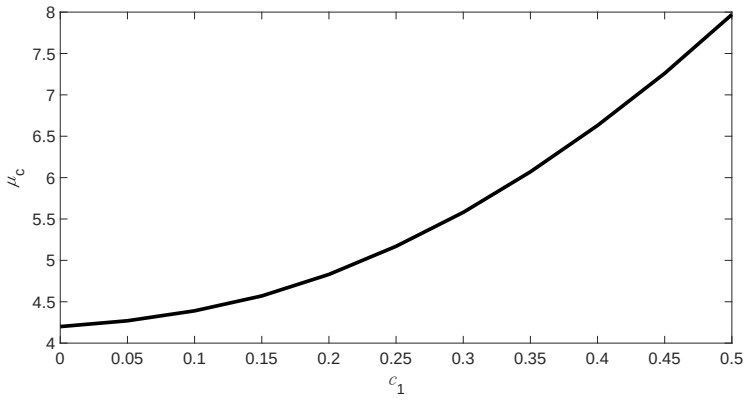

Figure 3.15 The critical friction coefficient μ_c as a function of damping coefficient c_1 for the system with proportional damping.

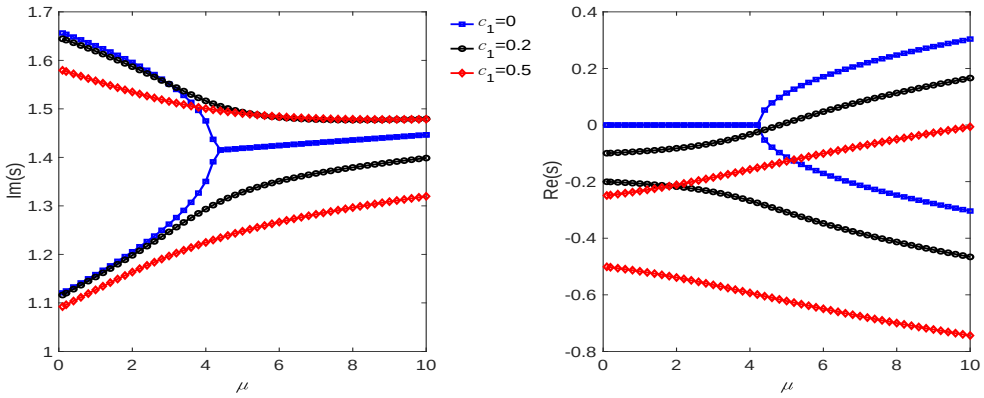

Figure 3.16 The eigenvalues of the system with non-proportional damping as a function of μ.

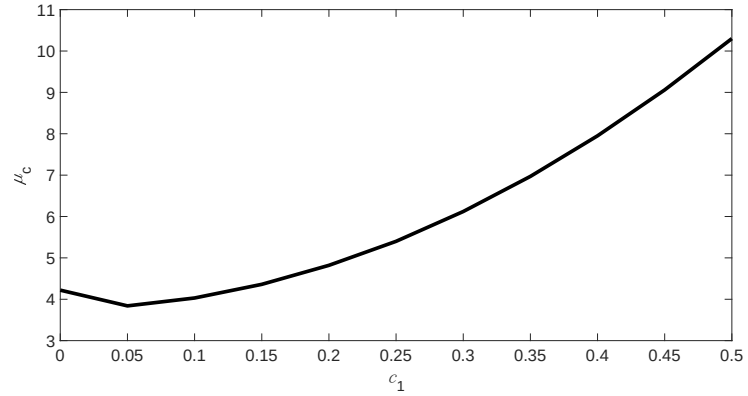

Figure 3.17 The critical friction coefficient μ_c as a function of damping coefficient c_1 for the system with non-proportional damping.

3.2 Analytical methods of friction induced vibration

There are two main categories of methods for the analysis of friction-induced-vibration problems, i.e., the complex eigenvalue analysis (CEA) and the transient dynamic analysis (TDA). The linear complex eigenvalue approach is often employed for the stability analysis of the steady sliding state. It can be used for the initial estimations of unstable modes which possibly lead to limit cycle vibration. The transient dynamic analysis is used to observe the dynamic behaviour of the system during the whole dynamic process, which enables acquiring the system behaviours in the steady state, incorporating nonstationary features such as time-dependent loading, and detecting the instability that may be omitted by CEA in some situations, e.g., when subcritical Hopf bifurcation exists.

3.2.1 Complex eigenvalue analysis

The equations of motion of an *n*-degree-of-freedom system with friction induced vibration can be generally expressed as,

$$\mathbf{M}\ddot{\mathbf{x}} + \mathbf{C}\dot{\mathbf{x}} + \mathbf{K}\mathbf{x} = \mathbf{F}_{\text{con}}(\mathbf{x}) + \mathbf{F}_{\text{ext}} \tag{3.30}$$

where $\mathbf{x} = [x_1 \quad x_2 \quad \cdots \quad x_n]^{\mathrm{T}}$. $\mathbf{M}$, $\mathbf{C}$, $\mathbf{K}$ are the mass matrix, damping matrix and stiffness matrix of the system, respectively. $\mathbf{F}_{\text{con}}$ contains the contact forces at the friction interface, i.e., the normal contact force and the tangential friction force. The contact forces can be linear or nonlinear functions with respect to the displacements. $\mathbf{F}_{\text{ext}}$ is the external force applied on the system, e.g. the brake pressure. Next the procedure of the stability analysis of the system is presented.

Firstly the equilibrium point $\mathbf{x}_0$ corresponding to a steady sliding state is obtained,

$$\mathbf{K}\mathbf{x}_0 = \mathbf{F}_{\text{con}}(\mathbf{x}_0) + \mathbf{F}_{\text{ext}} \tag{3.31}$$

Substituting $\mathbf{x} = \bar{\mathbf{x}} + \mathbf{x}_0$ into Eq. (3.30) results in,

$$\mathbf{M}\ddot{\bar{\mathbf{x}}} + \mathbf{C}\dot{\bar{\mathbf{x}}} + \mathbf{K}(\bar{\mathbf{x}} + \mathbf{x}_0) = \mathbf{F}_{\text{con}}(\bar{\mathbf{x}} + \mathbf{x}_0) + \mathbf{F}_{\text{ext}} \tag{3.32}$$

By expanding the $\mathbf{F}_{\text{con}}$ into the Taylor series and keeping only the first-order term, as well as the use of Eq. (3.31), the linearized system can be expressed as,

$$\mathbf{M}\ddot{\bar{\mathbf{x}}} + \mathbf{C}\dot{\bar{\mathbf{x}}} + (\mathbf{K} - \mathbf{K}_{\text{L}})\bar{\mathbf{x}} = \mathbf{0} \tag{3.33}$$

where $\mathbf{K}_{\mathrm{L}}$ is the Jacobian matrix of $\mathbf{F}_{\mathrm{con}}$, and the entry of $\mathbf{K}_{\mathrm{L}}$ is,

$$\mathbf{K}_{\mathrm{L}}(i,j) = \frac{\partial F_i(\mathbf{x})}{\partial x_j}\Big|_{\mathbf{x}_0} \tag{3.34}$$

where $F_i(\mathbf{x})$ is the *i*th element of $\mathbf{F}_{\mathrm{con}}$. And matrix $\mathbf{K}_{\mathrm{L}}$ is generally asymmetric, which may result in the dynamic instability.

According to the theory of second-order linear homogeneous ordinary differential equations, the solution of Eq. (3.33) can be written as,

$$\bar{\mathbf{x}} = \boldsymbol{\varphi}\mathrm{e}^{\lambda t} \tag{3.35}$$

By substituting Eq. (3.35) into Eq. (3.33), a quadratic eigenvalue equation is obtained,

$$(\lambda^2\mathbf{M} + \lambda\mathbf{C} + \mathbf{K} - \mathbf{K}_{\mathrm{L}})\boldsymbol{\varphi} = \mathbf{0} \tag{3.36}$$

Generally there are *n* pairs of conjugate complex numbers as the eigenvalues that are solved from Eq. (3.36), i.e.,

$$\lambda_i = \sigma_i \pm \omega_i \mathrm{i},\ i = 1,2,\dots,n \tag{3.37}$$

where $\mathrm{i} = \sqrt{-1}$ is the imaginary unit, σ_i and ω_i are the real part and imaginary part of the *i*th pair of eigenvalues, respectively. σ_i and ω_i indicate the growth rate and frequency of the *i*th mode in the response of the linearized system, therefore the stability of the equilibrium point of the frictional system which corresponds to steady sliding state can be evaluated by the signs of σ_i,

(1) if all σ_i are negative, the equilibrium point which corresponds to a steady sliding state is asymptotically stable, therefore unstable vibration will not happen in the system.

(2) if one $\sigma_i = 0$ and other real parts are negative, the stability of the equilibrium point cannot be determined by the complex eigenvalue analysis, and a further transient analysis is required.

(3) if at least one of σ_i is positive, the equilibrium point is unstable, therefore the vibration will grow from the equilibrium point and the system will show self-excited vibration. However, the vibration amplitudes are dependent on the nonlinearities in the system.

3.2.2 Transient dynamic analysis

3.2.2.1 Runge-Kutta method for ordinary differential equations

The equations of motion governing the dynamics of systems are usually ordinary differential equations (ODE) whose analytical solutions are difficult to obtain. Numerical methods can be employed to calculate the dynamic responses with good accuracy and efficiency. The numerical methods often used in dynamic simulations include Runge-Kutta method, Newmark-β method, central difference method, etc [185].

The fourth-order Runge-Kutta method is a popular numerical method in non-stiff dynamic problems because it is convenient to use and has high accuracy and stability. The standard procedure of the fourth-order Runge-Kutta method is for the first-order ODE and the integration for the second-order ODE requires the conversion of the second-order ODE to the first-order ODE. In Ref. [186], however, the formula for the direct integration of the second-order ODE was given that is exhibited below.

The second-order differential equations can be generally written as,

$$\ddot{\mathbf{y}} = \mathbf{f}(t, \mathbf{y}, \dot{\mathbf{y}}) \tag{3.38}$$

with the initial condition $\mathbf{y}(t_0) = \mathbf{y}_0$ and $\dot{\mathbf{y}}(t_0) = \dot{\mathbf{y}}_0$. If a time step h is assumed, the state variables $\mathbf{y}(t)$ and $\dot{\mathbf{y}}(t)$ at $t = t_0 + h$ are obtained by the following formulations,

$$\mathbf{y}(t_0 + h) = \mathbf{y}(t_0) + \frac{1}{6}(\mathbf{v}_1 + 2\mathbf{v}_2 + 2\mathbf{v}_3 + \mathbf{v}_4) \tag{3.39}$$

$$\dot{\mathbf{y}}(t_0 + h) = \dot{\mathbf{y}}(t_0) + \frac{1}{6}(\mathbf{w}_1 + 2\mathbf{w}_2 + 2\mathbf{w}_3 + \mathbf{w}_4) \tag{3.40}$$

where,

$$\mathbf{v}_1 = h\dot{\mathbf{y}}_0,\ \mathbf{w}_1 = h\mathbf{f}(t_0, \mathbf{y}_0, \dot{\mathbf{y}}_0),$$

$$\mathbf{v}_2 = h\left(\dot{\mathbf{y}}_0 + \frac{1}{2}\mathbf{w}_1\right),\ \mathbf{w}_2 = h\mathbf{f}\left(t_0 + \frac{1}{2}h, \mathbf{y}_0 + \frac{1}{2}\mathbf{v}_1, \dot{\mathbf{y}}_0 + \frac{1}{2}\mathbf{w}_1\right),$$

$$\mathbf{v}_3 = h\left(\dot{\mathbf{y}}_0 + \frac{1}{2}\mathbf{w}_2\right),\ \mathbf{w}_3 = h\mathbf{f}\left(t_0 + \frac{1}{2}h, \mathbf{y}_0 + \frac{1}{2}\mathbf{v}_2, \dot{\mathbf{y}}_0 + \frac{1}{2}\mathbf{w}_2\right),$$

$$\mathbf{v}_3 = h\left(\dot{\mathbf{y}}_0 + \frac{1}{2}\mathbf{w}_3\right),\ \mathbf{w}_4 = h\mathbf{f}(t_0 + h, \mathbf{y}_0 + \mathbf{v}_3, \dot{\mathbf{y}}_0 + \mathbf{w}_3)$$

After obtaining $\mathbf{y}(t_0 + h)$ and $\dot{\mathbf{y}}(t_0 + h)$, the values of $\mathbf{y}(t)$ and $\dot{\mathbf{y}}(t)$ at $t = t_0 + 2h$ can be derived from Eqs. (3.39) and (3.40), and so on.

3.2.2.2 Numerical techniques for non-smooth dynamic system

As is introduced in the literature review, the dry friction characteristic normally consists of two qualitatively different parts resulting in a non-smooth behaviour, i.e., stick-slip oscillation. Besides, the unilateral contact between two objects with relative motion in a frictional system allows the loss of contact. Therefore friction induced dynamics in many cases belongs to the class of non-smooth mechanics. Different states of motion (slip, stick and separation) take place successively during the vibration, which are governed by different sets of ordinary differential equations.

To obtain the whole time histories of the dynamic responses of the system, the fourth-order Runge–Kutta method suitable for the second-order ordinary differential equations is employed to obtain the responses in every single state while conditions for state transitions are monitored at each time step. Within the time step in which a state transition happens, the bisection method is used to capture the exact transition time instant. After the transition point, the state changes and the original set of equations of motion is replaced by another one. The general procedure for the numerical simulation of the non-smooth friction induced vibration is shown by the flowchart as follows.

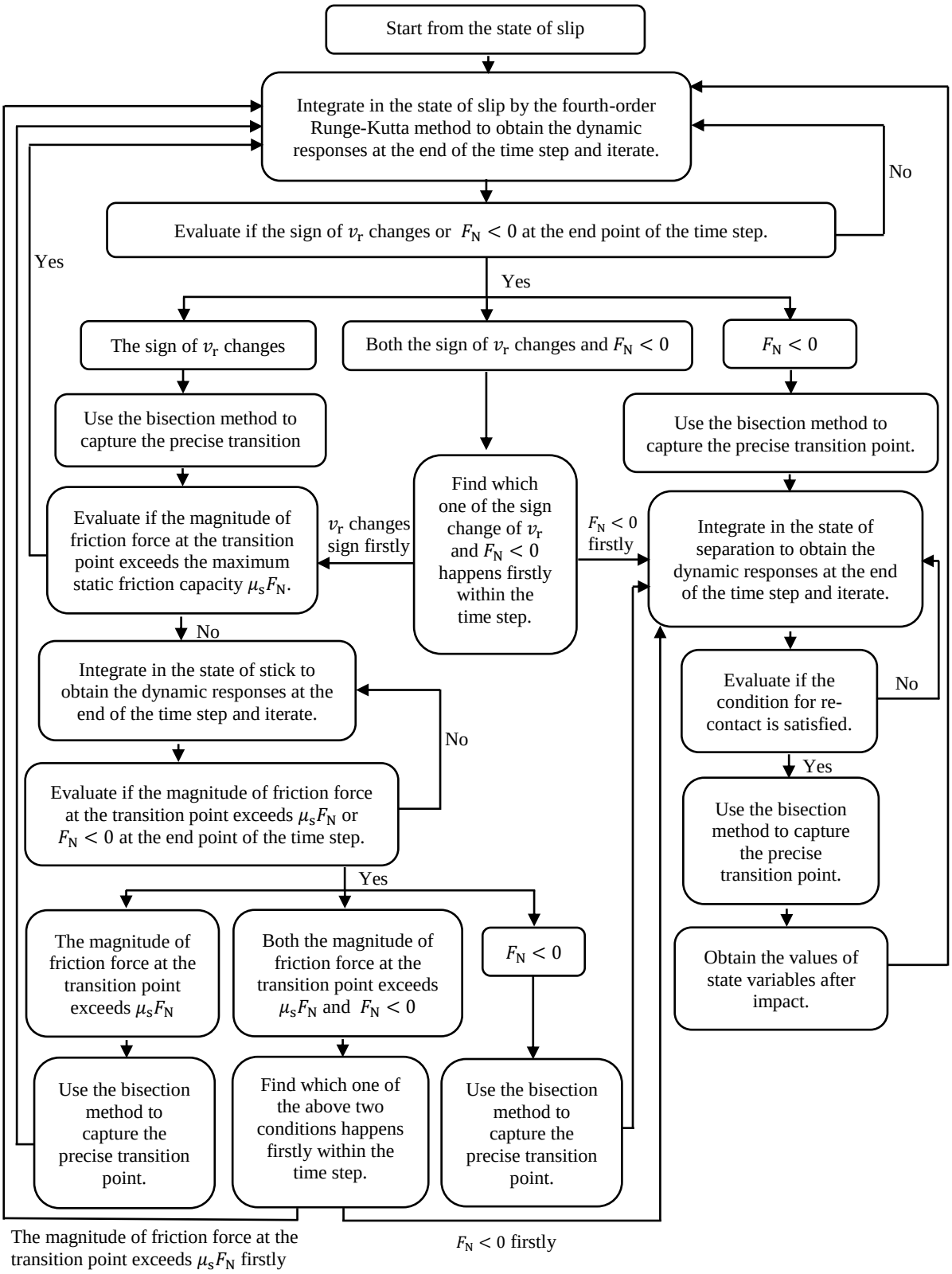

Figure 3.18 The flowchart of the computation procedure for the time histories of the non-smooth friction induced vibration.

3.3 Basic theories of the vibration of elastic thin plates

3.3.1 Free vibration of elastic thin plates

According to the classical plate theory [187], the equation of motion for the free transverse vibration of an elastic thin annular plate can be written as,

$$\rho h \frac{\partial^2 w}{\partial t^2} + D^* \nabla^4 w = 0 \tag{3.41}$$

where $w = w(r, \theta, t)$ is the transverse displacement of the plate, ρ is the density of material, h is the thickness of the plate, $D^* = \frac{Eh^3}{12(1-\nu^2)}$ is the bending rigidity, E and ν are the Young's modulus and Poisson's ratio of the material, respectively. And the partial differential $\nabla^4 w$ is,

$$\nabla^4 w = \nabla^2(\nabla^2 w),\ \nabla^2 = \frac{\partial^2}{\partial r^2} + \frac{1}{r}\frac{\partial}{\partial r} + \frac{1}{r^2}\frac{\partial^2}{\partial \theta^2} \tag{3.42}$$

The transverse displacement can be expressed as a linear superposition of mode shape functions, i.e.,

$$w(r, \theta, t) = \sum_{m=0}^{\infty} \sum_{n=0}^{\infty} W_{mn}(r, \theta) T_{mn}(t) \tag{3.43}$$

where $W_{mn}(r, \theta)$ represents the mode shape function, $T_{mn}(t)$ represents the modal coordinates. With substitution of Eq. (3.43) into Eq. (3.41), the following differential equations with respect to $W_{mn}(r, \theta)$ and $T_{mn}(t)$ are resulted,

$$\nabla^4 W_{mn}(r, \theta) - \beta_{mn}^4 W_{mn}(r, \theta) = 0 \tag{3.44}$$

$$\frac{\mathrm{d}^2 T_{mn}(t)}{\mathrm{d}t^2} + \omega_{mn}^2 T_{mn}(t) = 0 \tag{3.45}$$

where $\beta_{mn}^4 = \frac{\rho h \omega_{mn}^2}{D}$. The general solutions of Eq. (3.44) and Eq. (3.45) are,

$$W_{mn}(r, \theta) = [C_{mn}^1 J_n(\beta_{mn} r) + C_{mn}^2 Y_n(\beta_{mn} r) + C_{mn}^3 I_n(\beta_{mn} r) + C_{mn}^4 K_n(\beta_{mn} r)] \cdot [A_{mn} \sin(n\theta) + B_{mn} \cos(n\theta)] \tag{3.46}$$

$$T_{mn}(t) = X_{mn} \sin(\omega_{mn} t + \phi_{mn}) \tag{3.47}$$

where J_n, Y_n, I_n, K_n are Bessel functions. By substituting Eqs. (3.46) and (3.47) into Eq. (3.43), the transverse displacement of the annular plate in the case of free vibration can be obtained as,

$$w(r,\theta,t)=\sum_{m=0}^{\infty}\sum_{n=0}^{\infty}[C_{mn}^{1}J_n(\beta_{mn}r)+C_{mn}^{2}Y_n(\beta_{mn}r)+C_{mn}^{3}I_n(\beta_{mn}r)+ C_{mn}^{4}K_n(\beta_{mn}r)]\cdot[A_{mn}\sin(n\theta)+B_{mn}\cos(n\theta)]X_{mn}\sin(\omega_{mn}t+\phi_{mn}) \quad (3.48)$$

3.3.2 Natural frequencies and mode shapes of an annular plate with clamped inner boundary and free outer boundary

For a clamped boundary, both the deflection and slope are zero. For a free boundary, both the bending moment and resultant shear force are zero. Therefore the boundary conditions for the annular plate with clamped inner boundary (r=a) and free outer boundary (r=b) can be written as,

$$W_{mn}(a,\theta)=0,\ \frac{\partial W_{mn}(r,\theta)}{\partial r}|_{r=a}=0,\ M_r|_{r=b}=0,\ \left(Q_r+\frac{1}{r}\frac{\partial M_{r\theta}}{\partial\theta}\right)|_{r=b}=0 \quad (3.49)$$

where,

$$M_r=-D^*\left(\frac{\partial^2 W_{mn}}{\partial r^2}+\frac{\nu}{r}\frac{\partial W_{mn}}{\partial r}+\frac{\nu}{r^2}\frac{\partial^2 W_{mn}}{\partial\theta^2}\right) \quad (3.50)$$

$$M_{r\theta}=-(1-\nu)D^*\frac{\partial}{\partial r}\left(\frac{1}{r^2}\frac{\partial W_{mn}}{\partial\theta}\right) \quad (3.51)$$

$$Q_r=-D^*\frac{\partial}{\partial r}\left(\frac{\partial^2 W_{mn}}{\partial r^2}+\frac{\nu}{r}\frac{\partial W_{mn}}{\partial r}+\frac{\nu}{r^2}\frac{\partial^2 W_{mn}}{\partial\theta^2}\right) \quad (3.52)$$

By substituting Eq. (3.46) into Eqs. (3.49)-(3.52), it is derived that,

$$\begin{bmatrix}H_{11}&H_{12}&H_{13}&H_{14}\\H_{21}&H_{22}&H_{23}&H_{24}\\H_{31}&H_{32}&H_{33}&H_{34}\\H_{41}&H_{42}&H_{43}&H_{44}\end{bmatrix}\begin{bmatrix}C_{mn}^{1}\\C_{mn}^{2}\\C_{mn}^{3}\\C_{mn}^{4}\end{bmatrix}=\mathbf{0} \quad (3.53)$$

where,

$$H_{11}=J_n(\beta_{mn}a),\ H_{12}=Y_n(\beta_{mn}a),\ H_{13}=I_n(\beta_{mn}a),\ H_{14}=K_n(\beta_{mn}a)$$

$$H_{21}=\frac{n}{a}J_n(\beta_{mn}a)-\lambda J_{n+1}(\beta_{mn}a),\ H_{22}=\frac{n}{a}Y_n(\beta_{mn}a)-\beta_{mn}Y_{n+1}(\beta_{mn}a)$$

$$H_{23}=\frac{n}{a}I_n(\beta_{mn}a)+\beta_{mn}I_{n+1}(\beta_{mn}a),\ H_{24}=\frac{n}{a}K_n(\beta_{mn}a)-\beta_{mn}K_{n+1}(\beta_{mn}a)$$

$$H_{31}=\left[\frac{n(n-1)(1-\nu)}{b^2}-\beta_{mn}^2\right]J_n(\beta_{mn}b)+\beta_{mn}J_{n+1}(\beta_{mn}b)$$

$$H_{32}=\left[\frac{n(n-1)(1-\nu)}{b^2}-\beta_{mn}^2\right]Y_n(\beta_{mn}b)+\beta_{mn}Y_{n+1}(\beta_{mn}b)$$

$$H_{33}=\left[\frac{n(n-1)(1-\nu)}{b^2}+\beta_{mn}^2\right]I_n(\beta_{mn}b)+\beta_{mn}I_{n+1}(\beta_{mn}b)$$

$$H_{34} = \left[\frac{n(n-1)(1-\nu)}{b^2} + \beta_{mn}^2\right] K_n(\beta_{mn}b) + \beta_{mn} K_{n+1}(\beta_{mn}b)$$

$$H_{41} = \left[\frac{-n\beta_{mn}^2 b^2 + (1-n)(1-\nu)n^2}{b^3}\right] J_n(\beta_{mn}b) + \left[\frac{\beta_{mn}^3 b^3 + \beta_{mn} b(1-\nu)n^2}{b^3}\right] J_{n+1}(\beta_{mn}b)$$

$$H_{42} = \left[\frac{-n\beta_{mn}^2 b^2 + (1-n)(1-\nu)n^2}{b^3}\right] Y_n(\beta_{mn}b) + \left[\frac{\beta_{mn}^3 b^3 + \beta_{mn} b(1-\nu)n^2}{b^3}\right] Y_{n+1}(\beta_{mn}b)$$

$$H_{43} = \left[\frac{n\beta_{mn}^2 b^2 + (1-n)(1-\nu)n^2}{b^3}\right] I_n(\beta_{mn}b) + \left[\frac{\beta_{mn}^3 b^3 - \beta_{mn} b(1-\nu)n^2}{b^3}\right] I_{n+1}(\beta_{mn}b)$$

$$H_{44} = \left[\frac{n\beta_{mn}^2 b^2 + (1-n)(1-\nu)n^2}{b^3}\right] K_n(\beta_{mn}b) + \left[\frac{-\beta_{mn}^3 b^3 + \beta_{mn} b(1-\nu)n^2}{b^3}\right] K_{n+1}(\beta_{mn}b)$$

β_{mn} and the vector $[C_{mn}^1 \quad C_{mn}^2 \quad C_{mn}^3 \quad C_{mn}^4]^{\mathrm{T}}$ can be determined from Eq. (3.53), therefore the mode shape function $W_{mn}(r,\theta)$ is derived. And the natural frequency can be obtained as,

$$\omega_{mn} = \beta_{mn}^2 \left(\frac{D^*}{\rho h}\right)^{\frac{1}{2}} \tag{3.54}$$

Similarly, the natural frequencies and mode shapes of the annular plate in other boundary conditions can be obtained, which are not presented here as only the boundary condition of clamped inner boundary and free outer boundary is used in this thesis.

3.3.3 Forced vibration of elastic thin plates

Suppose the transverse external force $f(r,\theta,t)$ is applied on the plate, the equations of motion for the transverse vibration of the plate can be written as,

$$\rho h \frac{\partial^2 w}{\partial t^2} + D^* \nabla^4 w = f(r,\theta,t) \tag{3.55}$$

The solution of Eq. (3.55) can also be expressed as a linear superposition of mode shape functions in the form below,

$$w(r,\theta,t) = \sum_{m=0}^{\infty} \sum_{n=0}^{\infty} R_{mn}(r)[\cos(n\theta) Q_{mn}(t) + \sin(n\theta) S_{mn}(t)] \tag{3.56}$$

where,

$$R_{mn}(r) = [C_{mn}^1 J_n(\beta_{mn}r) + C_{mn}^2 Y_n(\beta_{mn}r) + C_{mn}^3 I_n(\beta_{mn}r) + C_{mn}^4 K_n(\beta_{mn}r)] \tag{3.57}$$

that can be solved by the method described in the above section. $Q_{mn}(t)$, $S_{mn}(t)$ are the modal coordinates. The orthogonal conditions of modal functions are,

$$\int_a^b \int_0^{2\pi} \rho h R_{mn}(r) R_{kl}(r) \cos(n\theta)\cos(l\theta) r \mathrm{d}r\mathrm{d}\theta = \int_a^b \int_0^{2\pi} \rho h R_{mn}(r) R_{kl}(r) \sin(n\theta)\sin(l\theta) r \mathrm{d}r = M_{kl}\delta_{mk}\delta_{nl}$$

$$\int_a^b \int_0^{2\pi} D R_{kl}(r) \cos(l\theta) \nabla^4 [R_{mn}(r)\cos(n\theta)] r \mathrm{d}r\mathrm{d}\theta = \int_a^b \int_0^{2\pi} D R_{kl}(r) \sin(l\theta) \nabla^4 [R_{mn}(r)\sin(n\theta)] r \mathrm{d}r\mathrm{d}\theta = \omega_{kl}^2 M_{kl}\delta_{mk}\delta_{nl}$$

$$\int_a^b \int_0^{2\pi} \rho h R_{mn}(r) R_{kl}(r) \sin(n\theta)\cos(l\theta) r \mathrm{d}r\mathrm{d}\theta = \int_a^b \int_0^{2\pi} \rho h R_{mn}(r) R_{kl}(r) \cos(n\theta)\sin(l\theta) r \mathrm{d}r\mathrm{d}\theta = 0$$

$$\int_a^b \int_0^{2\pi} D R_{kl}(r) \cos(l\theta) \nabla^4 [R_{mn}(r)\sin(n\theta)] r \mathrm{d}r\mathrm{d}\theta = \int_a^b \int_0^{2\pi} D R_{kl}(r) \sin(l\theta) \nabla^4 [R_{mn}(r)\cos(n\theta)] r \mathrm{d}r\mathrm{d}\theta = 0 \quad (3.58)$$

where,

$$M_{kl} = \begin{cases} \rho h \pi \int_a^b R_{kl}^2(r) r \mathrm{d}r & l = 1,2,\dots,\infty \\ 2\rho h \pi \int_a^b R_{kl}^2(r) r \mathrm{d}r & l = 0 \end{cases} \quad (3.59)$$

By substituting Eq. (3.56) into Eq. (3.55), then multiplying both sides of the equation by $R_{kl}(r)\cos(l\theta)$ or $R_{kl}(r)\sin(l\theta)$ and integrating them over the whole plate surface, and by using the orthogonal conditions of modal functions, the ordinary differential equations with respect to the modal coordinates can be obtained,

$$M_{kl}\ddot{Q}_{kl} + \omega_{kl}^2 M_{kl} Q_{kl} = \int_a^b \int_0^{2\pi} R_{kl}(r)\cos(l\theta) f(r,\theta,t)\, r \mathrm{d}r\mathrm{d}\theta \quad (3.60)$$

$$M_{kl}\ddot{S}_{kl} + \omega_{kl}^2 M_{kl} S_{kl} = \int_a^b \int_0^{2\pi} R_{kl}(r)\sin(l\theta) f(r,\theta,t)\, r \mathrm{d}r\mathrm{d}\theta \quad (3.61)$$

From Eqs. (3.60) and (3.61), the modal coordinates are determined, which are then substituted into Eq. (3.56) and the transverse displacement of the annular plate in the case of forced vibration can be thus derived.

Chapter 4

Friction induced vibration of a slider on an elastic disc spinning at time-varying speeds

In this chapter, the friction induced vibration of a mass slider with in-plane and transverse springs and dampers in sliding contact with a spinning elastic disc in three different situations of spinning speed, i.e. constant deceleration, constant acceleration and constant speed, is investigated. The stick–slip motion in the circumferential direction and separation–re-contact behaviour in the transverse direction are considered, which make the system responses non-smooth. It is observed that the decelerating rotation of the disc can make the in- plane stick–slip motion of the slider more complicated in comparison with constant disc rotation and thereby exerting significant influence on the transverse vibration of the disc, while the accelerating rotation of the disc contributes to the occurrence of separation during the vibration and thus influencing the vibration behaviour of the system. Numerical simulation results show that distinct dynamic behaviours can be observed in the three situations of spinning speed of disc and two kinds of particular characteristics of differences are revealed.

4.1 Introduction

As introduced in the literature review, dry friction induced vibration has been studied extensively and several significant mechanisms were proposed to explain the occurrence of friction induced self-excited vibration: the negative friction slope, the stick-slip motion, the sprag-slip motion and the mode-coupling instability. Yuan [50] revealed the negative damping effect due to the negative friction-velocity slope. Popp

and Stelter [20] investigated the discrete and continuous models exhibiting stick-slip motion and rich bifurcation and chaotic behaviours were revealed. Two kinds of friction laws: the Coulomb friction with stiction and the friction model with Stribeck effect were applied. Sinou et al. [40] studied the instability in a nonlinear sprag-slip model with constant coefficient of friction by a central manifold theory. The mode-coupling instability occurred as some modes of the system became unstable when coupling with other modes as a result of friction induced cross-coupling force. Hoffmann et al. [55] used a 2-DoF model to clarify the physical mechanisms underlying the mode-coupling instability of self-excited friction induced vibration. The effect of viscous damping on the mode-coupling instability in friction induced vibration was investigated in [56]. Besides, other mechanisms were proposed to explain the occurrence of friction induced vibration in specific systems. Chen et al. [68] analysed the instability of a friction system caused by the time delay between the normal force and the friction force. Kinkaid et al. [28] studied the dynamics of a 4-DoF system with a two-dimension friction force and found the change of direction of the friction force could excite unstable vibration.

Some researchers treated the friction induced vibration in mechanical system as a moving load problem. Chan et al. [65] examined the parametric resonance of a stationary elastic disc excited by a rotating mass-spring-damper system with a frictional follower force. Hochlenert et al. [66] analysed the stability behaviour of a minimal disc brake model consisting of the rotating Kirchhoff plate and idealized brake pads. Ouyang et al. [52, 67, 127] investigated the vibration of a stationary elastic disc under the circumferentially moving mass loading system. Li et al. [163] investigated the transverse vibration of an elastic disc excited by a preloaded mass-damper-spring slider which experienced in-plane stick-slip oscillation and incorporated the separation and reattachment phenomena considering the possibility of loss of contact due to growing transverse disc vibration. Kang [57] studied the dynamic instability of a thin annular plate due to circumferential friction between the plate and two fixed sector contact interfaces under steady-sliding conditions.

The models used to study the friction-induced-vibration (FIV) problems in the existing literature usually employ a constant sliding velocity, e.g., constant belt velocity in the slider-on-belt model or constant spinning speed of the disc. There has been little research that has considered the decelerating or accelerating sliding, which should not

be neglected as an important influential factor in friction induced vibration. In [35], a mathematical model was presented to prove that stick-slip oscillation could be induced by deceleration. Pilipchuk et al. [104] examined the friction induced dynamics of a two-DoF 'belt–spring–block' model and showed that due to the decelerating belt, the system response experiences transitions which could be regarded as simple indicators of onset of squeal. However, the work on the friction induced dynamics under decelerating/accelerating sliding motion is still quite limited. To investigate the influences of decelerating/accelerating sliding on the dynamic behaviour of frictional systems and study the problems such as brake noise in a more realistic model because the braking process is practically a decelerating process for the brake disc, the friction induced vibration of a mass slider on a spinning elastic disc at time-varying speeds is examined in this chapter.

The rest of the chapter is arranged as follows. In Section 4.2 the system configuration of the slider-on-disc model is introduced and the equations of motion for the system in three different states: stick, slip and separation are derived. The conditions for the transitions among these states are determined. Subsequently the numerical simulation and analysis are conducted to investigate the distinct dynamic behaviours of the system in the three different situations of spinning speed of disc in Section 4.3 and to help reveal the effects of deceleration and acceleration on the friction induced dynamics of the system, the system responses under the decelerating and accelerating sliding motion are compared with the results under constant sliding speed. The significant differences that the deceleration and acceleration make to the vibration behaviour of the frictional system from that in the constant disc speed underlie the necessity to consider the time-variant spinning speed in the research of friction induced vibration and noise. Finally in Section 4.4 the conclusions on the effects of the decelerating and accelerating sliding motion on the dynamics of the frictional system are drawn.

4.2 Model description and theoretical analysis

The dynamics of a slider-on-disc system subject to friction force is studied in this paper. The disc is modelled as a Kirchhoff plate clamped at inner boundary and free at outer boundary. A slider, which is assumed to be a point mass, is connected to the rigid base with transverse and in-plane (circumferential) springs and dashpots and in point contact with the spinning disc. Without loss of generality, the circumferential

coordinate of the fixed base is set as $\theta = 0$. The slider is assumed to be fixed radially at r_0 from the disc centre and pre-compressed on the disc by N_0 in the normal direction. The system configuration is illustrated in Fig. 4.1. Three different situations of spinning speed of disc, i.e. constant deceleration, constant acceleration and constant speed, are considered, which can be expressed as,

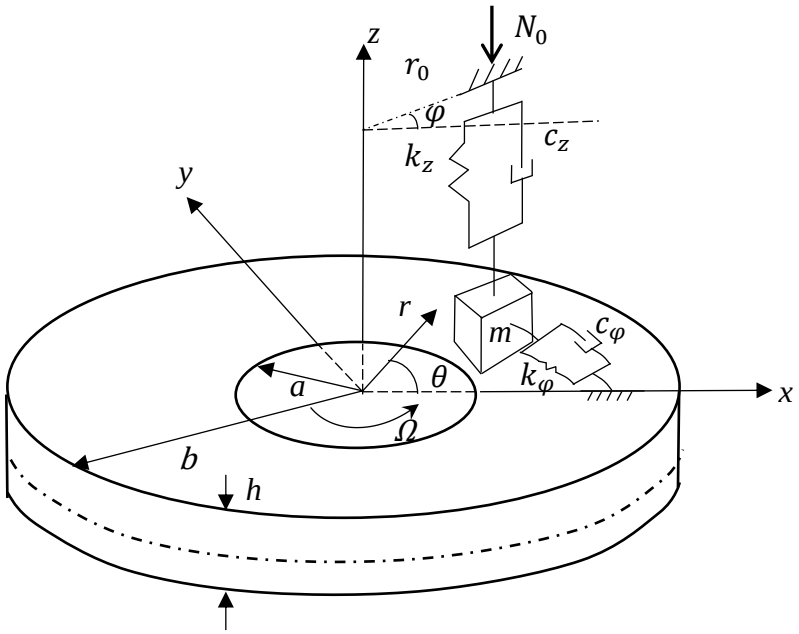

Figure 4.1 The system configuration of a slider on an elastic disc.

$$\Omega(t) = \Omega_0 \left(1 - \frac{t}{t_{\max}}\right), \text{ decelerating} \tag{4.1}$$

$$\Omega(t) = \Omega_1 + a_{\mathrm{d}} t, \text{ accelerating} \tag{4.2}$$

$$\Omega(t) = \Omega_{\mathrm{c}}, \text{ constant speed} \tag{4.3}$$

for the three situations, respectively, as shown in Fig. 4.2. In Eq. (4.1), Ω_0 is the initial spinning speed of the disc, $t_{\max}$ is the time duration of the deceleration process. In Eq. (4.2), Ω_1 is the initial spinning speed of the disc, a_{d} is the acceleration of the disc speed and always positive. In Eq. (4.3), Ω_{c} is a constant value which is independent of time.

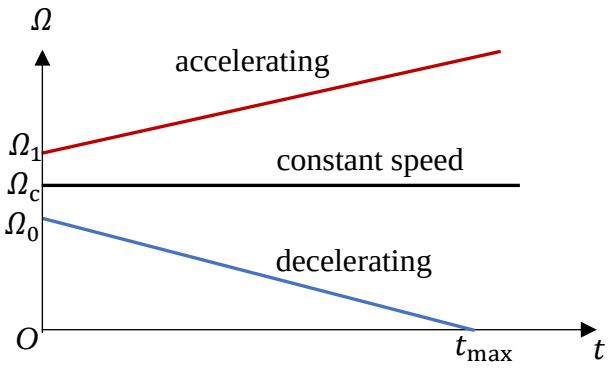

Figure 4.2 The three situations of spinning speed of the disc.

4.2.1 Circumferential stick-slip vibration of the slider

When the circumferential relative velocity between the slider and the disc is not equal to zero, the slider slips on the disc. In the slip phase, the slider is subject to the kinetic friction force, thus the equation of circumferential motion of the slider can be written as,

$$I\ddot{\varphi} + r_0^2 c_\varphi \dot{\varphi} + r_0^2 k_\varphi \varphi = r_0 \mathrm{sgn}(\Omega - \dot{\varphi})\mu N \tag{4.4}$$

where φ is the circumferential angular displacement of the slider, $I = mr_0^2$, c_φ and k_φ are its moment of inertia, in-plane damping coefficient and in-plane spring stiffness, respectively. m is the slider's mass, N represents the normal force between the disc and the slider. μ is the kinetic friction coefficient, and here it is taken as a function of the relative velocity as follows,

$$\mu = \mu_1 + (\mu_0 - \mu_1)\mathrm{e}^{-\alpha|r_0(\Omega - \dot{\varphi})|} \tag{4.5}$$

where μ_0, μ_1, α are the parameters determining the maximum value, the asymptotic value and the initial slope of the friction coefficient with respect to the relative velocity.

When the circumferential velocity of slider reaches the instantaneous disc speed and the magnitude of the friction force acting on the slider does not exceed the static friction force, the slider sticks to the disc. In the sticking phase, the circumferential angular velocity and acceleration of the slider remain identical to the disc's rotary speed and acceleration, i.e.,

$$\dot{\varphi} = \Omega, \ddot{\varphi} = \dot{\Omega} \tag{4.6}$$

Substituting Eqs. (4.1)-(4.3) into Eq. (4.6), it is easy to derive that,

$$\dot{\varphi} = \Omega_0 \left(1 - \frac{t}{t_{\max}}\right), \ddot{\varphi} = -\frac{\Omega_0}{t_{\max}} \tag{4.7}$$

$$\dot{\varphi} = \Omega_1 + a_\mathrm{d} t, \ddot{\varphi} = a_\mathrm{d} \tag{4.8}$$

$$\dot{\varphi} = \Omega_\mathrm{c}, \ddot{\varphi} = 0 \tag{4.9}$$

in the sticking phase for the situations of decelerating disc, accelerating disc and constant disc speed, respectively. The instantaneous circumferential position of the slider in the sticking phase is thus given by,

$$\varphi(t) = \varphi(t_\mathrm{s}) + \int_{t_\mathrm{s}}^{t} \Omega_0 \left(1 - \frac{t}{t_\mathrm{max}}\right) \mathrm{d}t = \varphi(t_\mathrm{s}) + \Omega_0 (t - t_\mathrm{s}) - \frac{\Omega_0}{2t_\mathrm{max}} (t^2 - t_\mathrm{s}^2) \tag{4.10}$$

$$\varphi(t) = \varphi(t_\mathrm{s}) + \int_{t_\mathrm{s}}^{t} (\Omega_1 + a_\mathrm{d} t)\, \mathrm{d}t = \varphi(t_\mathrm{s}) + \Omega_1 (t - t_\mathrm{s}) + \frac{1}{2} a_\mathrm{d} (t^2 - t_\mathrm{s}^2) \tag{4.11}$$

$$\varphi(t) = \varphi(t_\mathrm{s}) + \int_{t_\mathrm{s}}^{t} \Omega_\mathrm{c}\, \mathrm{d}t = \varphi(t_\mathrm{s}) + \Omega_\mathrm{c} (t - t_\mathrm{s}) \tag{4.12}$$

for the situations of decelerating disc, accelerating disc and constant disc speed, respectively, where t_s is the time instant when a sticking phase starts. And the friction force in the sticking phase is a reaction force, which can be obtained as,

$$f_\mathrm{stick} = \frac{1}{r_0} \left(I\ddot{\varphi} + r_0^2 c_\varphi \dot{\varphi} + r_0^2 k_\varphi \varphi\right) \tag{4.13}$$

Thus the condition for the slider to remain sticking to the disc is,

$$\left|\frac{1}{r_0} \left(I\ddot{\varphi} + r_0^2 c_\varphi \dot{\varphi} + r_0^2 k_\varphi \varphi\right)\right| \leq \mu_\mathrm{s} N \tag{4.14}$$

where μ_s is the static friction coefficient between the slider and the disc. When the magnitude of the friction force reaches the maximum static friction capacity, the slider starts to slip on the disc again.

4.2.2 Transverse vibration of the disc

The slider is located at the polar coordinate $\left(r_0, \varphi(t)\right)$ at an arbitrary time t. When the slider is in contact with the disc, the normal displacement $z(t)$ of the slider equals to the local transverse displacement of the disc at $\left(r_0, \varphi(t)\right)$ in the space-fixed coordinate system, i.e.,

$$z(t) = w(r_0, \varphi(t), t) \tag{4.15}$$

and thus,

$$\dot{z} = \frac{\partial w}{\partial t} + \dot{\varphi} \frac{\partial w}{\partial \theta} \tag{4.16}$$

$$\ddot{z} = \frac{\partial^2 w}{\partial t^2} + 2\dot{\varphi}\frac{\partial^2 w}{\partial \theta \partial t} + \dot{\varphi}^2\frac{\partial^2 w}{\partial \theta^2} + \ddot{\varphi}\frac{\partial w}{\partial \theta} \tag{4.17}$$

By the force balance in the normal direction of the slider, the normal force between the slider and the disc is obtained as,

$$N = N_0 + m\ddot{z} + c_z\dot{z} + k_z z \tag{4.18}$$

Meanwhile, the friction force between the slider and disc presents a bending moment in the circumferential direction of the disc [57, 67], which is,

$$M_\theta = hf/2 \tag{4.19}$$

where h is the thickness of the disc. During the slip phase, the friction force reads,

$$f = \mathrm{sgn}(\Omega - \dot{\varphi})\mu N = \mathrm{sgn}(\Omega - \dot{\varphi})\mu(N_0 + m\ddot{z} + c_z\dot{z} + k_z z) \tag{4.20}$$

While in the stick phase, the friction force, given in Eq. (4.13), can be written as,

$$f = \frac{1}{r_0}\left[-I\frac{\Omega_0}{t_{\max}} + r_0^2 c_\varphi \Omega_0\left(1 - \frac{t}{t_{\max}}\right) + r_0^2 k_\varphi \varphi\right] \tag{4.21}$$

$$f = \frac{1}{r_0}\left[Ia_{\mathrm{d}} + r_0^2 c_\varphi(\Omega_1 + a_{\mathrm{d}}t) + r_0^2 k_\varphi \varphi\right] \tag{4.22}$$

$$f = \frac{1}{r_0}\left(r_0^2 c_\varphi \Omega_{\mathrm{c}} + r_0^2 k_\varphi \varphi\right) \tag{4.23}$$

for the situations of decelerating, accelerating and constant speed, respectively, where φ can be obtained from Eqs. (4.10)-(4.12) respectively. The transverse displacement of the disc in the space-fixed coordinate system can be approximated by a linear superposition of a set of orthogonal basis functions as [188],

$$w(r,\theta,t) = \sum_{k=0}^{\infty}\sum_{l=0}^{\infty} R_{kl}(r)[\cos(l\theta)\cdot C_{kl}(t) + \sin(l\theta)\cdot D_{kl}(t)] \tag{4.24}$$

where k and l denote the number of nodal circles and nodal diameters respectively, $C_{kl}(t)$, $D_{kl}(t)$ are modal coordinates, $R_{kl}(r)$ is a combination of Bessel functions satisfying the inner and outer boundary conditions of the nonrotating disc and orthogonality conditions. And the equations of motion with respect to the modal coordinates can be obtained from Lagrange's equations,

$$\frac{\mathrm{d}}{\mathrm{d}t}\left[\frac{\partial L}{\partial \dot{C}_{kl}}\right] - \frac{\partial L}{\partial C_{kl}} = P_{kl}, k = 0,1,2,\ldots,\infty, l = 0,1,2,\ldots,\infty \tag{4.25}$$

$$\frac{\mathrm{d}}{\mathrm{d}t}\left[\frac{\partial L}{\partial \dot{D}_{kl}}\right] - \frac{\partial L}{\partial D_{kl}} = Q_{kl}, k = 0,1,2,\ldots,\infty, l = 1,2,\ldots,\infty \tag{4.26}$$

in which,

$$L = T - U \tag{4.27}$$

$$T = \frac{1}{2}\rho h \iint_S \left(\frac{\partial w(r,\theta,t)}{\partial t} + \Omega \frac{\partial w(r,\theta,t)}{\partial \theta}\right)^2 r\mathrm{d}r\mathrm{d}\theta \tag{4.28}$$

$$U = \frac{1}{2}D^* \iint_S (\nabla^2 w)^2 - 2(1-\nu)\left[\frac{\partial^2 w}{\partial r^2}\left(\frac{1}{r}\frac{\partial w}{\partial r} + \frac{1}{r^2}\frac{\partial^2 w}{\partial \theta^2}\right) - \left(\frac{1}{r}\frac{\partial^2 w}{\partial r \partial \theta} - \frac{1}{r^2}\frac{\partial w}{\partial \theta}\right)^2\right] r\mathrm{d}r\mathrm{d}\theta \tag{4.29}$$

$$P_{kl} = -N \cdot \frac{\partial w(r_0,\varphi,t)}{\partial C_{kl}} + M_\theta \frac{\partial \gamma}{\partial C_{kl}} \tag{4.30}$$

$$Q_{kl} = -N \cdot \frac{\partial w(r_0,\varphi,t)}{\partial D_{kl}} + M_\theta \frac{\partial \gamma}{\partial D_{kl}} \tag{4.31}$$

$$\gamma = \frac{\partial w(r_0,\varphi,t)}{r_0 \partial \theta} \tag{4.32}$$

In the above equations, T and U represent the kinetic energy and strain energy of the disc respectively, P_{kl} and Q_{kl} represent the generalized forces obtained from the virtual work of the normal force and bending moment acting on the disc. S is the area of the disc surface, ρ is the density of material, $D^* = \frac{Eh^3}{12(1-\nu^2)}$ is the bending rigidity, E and ν are the Young's modulus and the Poisson's ratio of the disc material, respectively.

4.2.3 Coupled in-plane and out-of-plane vibration

Substituting Eqs. (4.15)-(4.20) and (4.24) into Eqs. (4.25)-(4.32), the equations of the transverse motion of the disc with respect to the modal coordinates during the slip phase are given,

$$M_{kl}\ddot{C}_{kl} + 2lM_{kl}\Omega\dot{D}_{kl} + (\omega_{kl}^2 M_{kl} - l^2 M_{kl}\Omega^2)C_{kl} = \left[-R_{kl}(r_0)\cos(l\varphi) - \frac{h}{2r_0}sgn(\Omega-\dot{\varphi})\mu l R_{kl}(r_0)\sin(l\varphi)\right]\cdot$$
$$\left(N_0 + \sum_{r=0}^{\infty}\sum_{s=0}^{\infty} R_{rs}(r_0)\{m\cos(s\varphi)\ddot{C}_{rs} + m\sin(s\varphi)\ddot{D}_{rs} + [-2m\dot{\varphi}s\sin(s\varphi) + c_z\cos(s\varphi)]\dot{C}_{rs} + [2m\dot{\varphi}s\cos(s\varphi) + c_z\sin(s\varphi)]\dot{D}_{rs}\right.$$
$$\left.+[-m\ddot{\varphi}s\sin(s\varphi) - m\dot{\varphi}^2 s^2\cos(s\varphi) - c_z\dot{\varphi}s\sin(s\varphi) + k_z\cos(s\varphi)]C_{rs} + [m\ddot{\varphi}s\cos(s\varphi) - m\dot{\varphi}^2 s^2\sin(s\varphi) + c_z\dot{\varphi}s\cos(s\varphi) + k_z\sin(s\varphi)]D_{rs}\}\right) \tag{4.33}$$

$$M_{kl}\ddot{D}_{kl} - 2lM_{kl}\Omega\dot{C}_{kl} + (\omega_{kl}^2 M_{kl} - l^2 M_{kl}\Omega^2)D_{kl} = \left[-R_{kl}(r_0)\sin(l\varphi) + \frac{h}{2r_0}sgn(\Omega-\dot{\varphi})\mu l R_{kl}(r_0)\cos(l\varphi)\right]\cdot$$
$$\left(N_0 + \sum_{r=0}^{\infty}\sum_{s=0}^{\infty} R_{rs}(r_0)\{m\cos(s\varphi)\ddot{C}_{rs} + m\sin(s\varphi)\ddot{D}_{rs} + [-2m\dot{\varphi}s\sin(s\varphi) + c_z\cos(s\varphi)]\dot{C}_{rs} + [2m\dot{\varphi}s\cos(s\varphi) + c_z\sin(s\varphi)]\dot{D}_{rs}\right.$$
$$\left.+[-m\ddot{\varphi}s\sin(s\varphi) - m\dot{\varphi}^2 s^2\cos(s\varphi) - c_z\dot{\varphi}s\sin(s\varphi) + k_z\cos(s\varphi)]C_{rs} + [m\ddot{\varphi}s\cos(s\varphi) - m\dot{\varphi}^2 s^2\sin(s\varphi) + c_z\dot{\varphi}s\cos(s\varphi) + k_z\sin(s\varphi)]D_{rs}\}\right) \tag{4.34}$$

where Ω is given by Eqs (4.1)-(4.3) for the situations of decelerating disc, accelerating disc and constant disc speed respectively, ω_{kl} is the natural frequency of the mode with *k* nodal circles and *l* nodal diameters of the corresponding nonrotating plate, and

$$M_{kl} = \begin{cases} \rho h \pi \int_a^b R_{kl}^2(r) r \mathrm{d}r, & l = 1,2,\ldots \\ 2\rho h \pi \int_a^b R_{kl}^2(r) r \mathrm{d}r, & l = 0 \end{cases} \tag{4.35}$$

During the slip phase, the equation of motion of φ reads,

$$I\ddot{\varphi} + r_0^2 c_\varphi \dot{\varphi} + r_0^2 k_\varphi \varphi = r_0 sgn(\Omega - \dot{\varphi})\mu \left(N_0 + \sum_{r=0}^{\infty}\sum_{s=0}^{\infty} R_{rs}(r_0)\{m\cos(s\varphi)\ddot{C}_{rs} + m\sin(s\varphi)\ddot{D}_{rs} + [-2m\dot{\varphi}s\sin(s\varphi) + c_z\cos(s\varphi)]\dot{C}_{rs} \right.$$
$$+[2m\dot{\varphi}s\cos(s\varphi) + c_z\sin(s\varphi)]\dot{D}_{rs} + [-m\ddot{\varphi}s\sin(s\varphi) - m\dot{\varphi}^2 s^2\cos(s\varphi) - c_z\dot{\varphi}s\sin(s\varphi) + k_z\cos(s\varphi)]C_{rs}$$
$$\left. +[m\ddot{\varphi}s\cos(s\varphi) - m\dot{\varphi}^2 s^2\sin(s\varphi) + c_z\dot{\varphi}s\cos(s\varphi) + k_z\sin(s\varphi)]D_{rs}\} \right) \tag{4.36}$$

In the stick phase, the equations of the transverse motion of the disc can be derived by substituting Eqs. (4.15)-(4.19) and (4.24) into Eqs. (4.25)-(4.32) as,

$$M_{kl}\ddot{C}_{kl} + 2lM_{kl}\Omega\dot{D}_{kl} + (\omega_{kl}^2 M_{kl} - l^2 M_{kl}\Omega^2)C_{kl} = -\frac{h}{2r_0} lR_{kl}(r_0)\sin(l\varphi)f - R_{kl}(r_0)\cos(l\varphi) \cdot$$
$$\left(N_0 + \sum_{r=0}^{\infty}\sum_{s=0}^{\infty} R_{rs}(r_0)\{m\cos(s\varphi)\ddot{C}_{rs} + m\sin(s\varphi)\ddot{D}_{rs} + [-2m\dot{\varphi}s\sin(s\varphi) + c_z\cos(s\varphi)]\dot{C}_{rs} + [2m\dot{\varphi}s\cos(s\varphi) + c_z\sin(s\varphi)]\dot{D}_{rs} \right.$$
$$\left. +[-m\ddot{\varphi}s\sin(s\varphi) - m\dot{\varphi}^2 s^2\cos(s\varphi) - c_z\dot{\varphi}s\sin(s\varphi) + k_z\cos(s\varphi)]C_{rs} + [m\ddot{\varphi}s\cos(s\varphi) - m\dot{\varphi}^2 s^2\sin(s\varphi) + c_z\dot{\varphi}s\cos(s\varphi) + k_z\sin(s\varphi)]D_{rs}\} \right) \tag{4.37}$$

$$M_{kl}\ddot{D}_{kl} - 2lM_{kl}\Omega\dot{C}_{kl} + (\omega_{kl}^2 M_{kl} - l^2 M_{kl}\Omega^2)D_{kl} = \frac{h}{2r_0} lR_{kl}(r_0)\cos(l\varphi)f - R_{kl}(r_0)\sin(l\varphi) \cdot$$
$$\left(N_0 + \sum_{r=0}^{\infty}\sum_{s=0}^{\infty} R_{rs}(r_0)\{m\cos(s\varphi)\ddot{C}_{rs} + m\sin(s\varphi)\ddot{D}_{rs} + [-2m\dot{\varphi}s\sin(s\varphi) + c_z\cos(s\varphi)]\dot{C}_{rs} + [2m\dot{\varphi}s\cos(s\varphi) + c_z\sin(s\varphi)]\dot{D}_{rs} \right.$$
$$\left. +[-m\ddot{\varphi}s\sin(s\varphi) - m\dot{\varphi}^2 s^2\cos(s\varphi) - c_z\dot{\varphi}s\sin(s\varphi) + k_z\cos(s\varphi)]C_{rs} + [m\ddot{\varphi}s\cos(s\varphi) - m\dot{\varphi}^2 s^2\sin(s\varphi) + c_z\dot{\varphi}s\cos(s\varphi) + k_z\sin(s\varphi)]D_{rs}\} \right) \tag{4.38}$$

where f is given by Eqs. (4.21)-(4.23) for the situations of decelerating disc, accelerating disc and constant disc speed respectively, $\varphi, \dot{\varphi}, \ddot{\varphi}$ during the stick phase for the three different situations are given in Eqs. (4.7)-(4.12). The condition for remaining in the stick state, which is given in Eq. (4.14), is thus obtained as,

$$\left|\frac{1}{r_0}\left(I\ddot{\varphi} + r_0^2 c_\varphi \dot{\varphi} + r_0^2 k_\varphi \varphi\right)\right| \le \mu_s \left(N_0 + \sum_{r=0}^{\infty}\sum_{s=0}^{\infty} R_{rs}(r_0)\{m\cos(s\varphi)\ddot{C}_{rs} + m\sin(s\varphi)\ddot{D}_{rs} + [-2m\dot{\varphi}s\sin(s\varphi) + c_z\cos(s\varphi)]\dot{C}_{rs} \right.$$
$$+[2m\dot{\varphi}s\cos(s\varphi) + c_z\sin(s\varphi)]\dot{D}_{rs} + [-m\ddot{\varphi}s\sin(s\varphi) - m\dot{\varphi}^2 s^2\cos(s\varphi) - c_z\dot{\varphi}s\sin(s\varphi) + k_z\cos(s\varphi)]C_{rs}$$
$$\left. +[m\ddot{\varphi}s\cos(s\varphi) - m\dot{\varphi}^2 s^2\sin(s\varphi) + c_z\dot{\varphi}s\cos(s\varphi) + k_z\sin(s\varphi)]D_{rs}\} \right) \tag{4.39}$$

4.2.4 Separation and re-contact

With the increase of the amplitude of the transverse motion, the slider may separate from the disc. Separation happens when the normal force between the disc and the slider drops to $N = 0$. And in the separation phase, both the slider and the disc experience free vibration, therefore the equations of motion of the disc and the slider read,

$$M_{kl}\ddot{C}_{kl} + 2lM_{kl}\Omega\dot{D}_{kl} + (\omega_{kl}^2 M_{kl} - l^2 M_{kl}\Omega^2)C_{kl} = 0 \tag{4.40}$$

$$M_{kl}\ddot{D}_{kl} - 2lM_{kl}\Omega\dot{C}_{kl} + (\omega_{kl}^2 M_{kl} - l^2 M_{kl}\Omega^2)D_{kl} = 0 \tag{4.41}$$

for the transverse displacement of the disc, and

$$I\ddot{\varphi} + r_0^2 c_\varphi \dot{\varphi} + r_0^2 k_\varphi \varphi = 0 \tag{4.42}$$

$$m\ddot{z} + c\dot{z} + kz + N_0 = 0 \tag{4.43}$$

for the circumferential and normal motions of the slider. The state of separation is maintained when the following condition is satisfied,

$$z(t) > w(r_0, \varphi(t), t) \tag{4.44}$$

After separation, the above condition is monitored for re-contact. Re-contact occurs when the slider's normal motion become equal to the transverse displacement of the disc at the polar coordinate of the slider. And when this happens, a very short-lived impact force is considered to act between the slider and the disc within time duration of (t_r^-, t_r^+). The method for determining the values of the dynamic state variables immediately after re-contact, which was given in Ref. [189], is adopted in this paper.

For simplification, an assumption for the re-contact is that the impact is perfectly plastic and the slider sticks onto the disc after the impact. Suppose the impulse at t_r is p, thus the distributed load on the disc due to the impact is $-p\delta(r - r_0)\delta\big(\theta - \varphi(t)\big)\delta(t - t_r)$, which causes the equations of motion of the disc to become,

$$M_{kl}\ddot{C}_{kl} + 2lM_{kl}\Omega\dot{D}_{kl} + (\omega_{kl}^2 M_{kl} - l^2 M_{kl}\Omega^2)C_{kl} = -pR_{kl}(r_0)\cos\big(l\varphi(t)\big)\delta(t - t_r) \tag{4.45}$$

$$M_{kl}\ddot{D}_{kl} - 2lM_{kl}\Omega\dot{C}_{kl} + (\omega_{kl}^2 M_{kl} - l^2 M_{kl}\Omega^2)D_{kl} = -pR_{kl}(r_0)\sin\big(l\varphi(t)\big)\delta(t - t_r) \tag{4.46}$$

The velocity jump for the disc due to the impact can be thus obtained as,

$$\dot{C}_{kl}(t_r^+) - \dot{C}_{kl}(t_r^-) = -\frac{pR_{kl}(r_0)\cos(l\varphi(t_r))}{M_{kl}} \tag{4.47}$$

$$\dot{D}_{kl}(t_r^+) - \dot{D}_{kl}(t_r^-) = -\frac{pR_{kl}(r_0)\sin(l\varphi(t_r))}{M_{kl}} \tag{4.48}$$

Similarly, the velocity jump of the slider is,

$$\dot{z}(t_r^+) - \dot{z}(t_r^-) = \frac{p}{m} \tag{4.49}$$

Combining Eq. (4.49) and Eqs. (4.47) and (4.48) gives,

$$\dot{C}_{kl}(t_r^+) - \dot{C}_{kl}(t_r^-) = -\frac{mR_{kl}(r_0)\cos(l\varphi(t_r))\left[\dot{z}(t_r^+) - \dot{z}(t_r^-)\right]}{M_{kl}} \tag{4.50}$$

$$\dot{D}_{kl}(t_r^+) - \dot{D}_{kl}(t_r^-) = -\frac{mR_{kl}(r_0)\sin(l\varphi(t_r))\left[\dot{z}(t_r^+) - \dot{z}(t_r^-)\right]}{M_{kl}} \tag{4.51}$$

For perfectly plastic impact, the slider has the same velocity as that of the disc at time t_r^+, therefore,

$$\begin{aligned}\dot{z}(t_r^+) = \left(\frac{\partial w}{\partial t} + \dot{\varphi}\frac{\partial w}{\partial \varphi}\right)_{t=t_r^+} = \sum_{r=0}^{\infty}\sum_{s=0}^{\infty} R_{rs}(r_0)\left[\cos\left(s\varphi(t_r^+)\right)\dot{C}_{rs}(t_r^+) + \sin\left(s\varphi(t_r^+)\right)\dot{D}_{rs}(t_r^+)\right.\\ \left.-\dot{\varphi}(t_r^+)s\sin\left(s\varphi(t_r^+)\right)C_{rs}(t_r^+) + \dot{\varphi}(t_r^+)s\cos\left(s\varphi(t_r^+)\right)D_{rs}(t_r^+)\right]\end{aligned} \tag{4.52}$$

Because the transverse displacement and the in-plane motion of the slider are unchanged by the normal impact, the following equations hold,

$$\begin{gathered}C_{kl}(t_r^+) = C_{kl}(t_r^-) = C_{kl}(t_r), D_{kl}(t_r^+) = D_{kl}(t_r^-) = D_{kl}(t_r),\\ \varphi(t_r^+) = \varphi(t_r^-) = \varphi(t_r), \dot{\varphi}(t_r^+) = \dot{\varphi}(t_r^-) = \dot{\varphi}(t_r)\end{gathered} \tag{4.53}$$

By substituting Eq. (4.52) into Eqs. (4.50) and (4.51) and utilizing Eq. (4.53), the normal velocity of the slider and the modal velocities of the disc after the impact can be derived as,

$$\dot{z}(t_r^+) = \frac{\sum_{r=0}^{\infty}\sum_{s=0}^{\infty} R_{rs}(r_0)\left[\cos\left(s\varphi(t_r)\right)\dot{C}_{rs}(t_r^-) + \sin\left(s\varphi(t_r)\right)\dot{D}_{rs}(t_r^-) + \frac{mR_{rs}(r_0)}{M_{rs}}\dot{z}(t_r^-) - \dot{\varphi}(t_r)s\sin\left(s\varphi(t_r)\right)C_{rs}(t_r) + \dot{\varphi}(t_r)s\cos\left(s\varphi(t_r)\right)D_{rs}(t_r)\right]}{1 + \sum_{r=0}^{\infty}\sum_{s=0}^{\infty}\frac{mR_{rs}^2(r_0)}{M_{rs}}} \tag{4.54}$$

$$\dot{C}_{kl}(t_r^+) = \dot{C}_{kl}(t_r^-) - \frac{mR_{kl}(r_0)\cos(l\varphi(t_r))}{M_{kl}}\left\{\frac{\sum_{r=0}^{\infty}\sum_{s=0}^{\infty} R_{rs}(r_0)\left[\cos\left(s\varphi(t_r)\right)\dot{C}_{rs}(t_r^-) + \sin\left(s\varphi(t_r)\right)\dot{D}_{rs}(t_r^-) + \frac{mR_{rs}(r_0)}{M_{rs}}\dot{z}(t_r^-) - \dot{\varphi}(t_r)s\sin\left(s\varphi(t_r)\right)C_{rs}(t_r) + \dot{\varphi}(t_r)s\cos\left(s\varphi(t_r)\right)D_{rs}(t_r)\right]}{1 + \sum_{r=0}^{\infty}\sum_{s=0}^{\infty}\frac{mR_{rs}^2(r_0)}{M_{rs}}} - \dot{z}(t_r^-)\right\} \tag{4.55}$$

$$\dot{D}_{kl}(t_r^+) = \dot{D}_{kl}(t_r^-) - \frac{mR_{kl}(r_0)\sin(l\varphi(t_r))}{M_{kl}} \left\{ \frac{\sum_{r=0}^{\infty}\sum_{s=0}^{\infty} R_{rs}(r_0)\left[\cos(s\varphi(t_r))\dot{C}_{rs}(t_r^-)+\sin(s\varphi(t_r))\dot{D}_{rs}(t_r^-)+\frac{mR_{rs}(r_0)}{M_{rs}}\dot{z}(t_r^-)-\dot{\varphi}(t_r)s\sin(s\varphi(t_r))C_{rs}(t_r)+\dot{\varphi}(t_r)s\cos(s\varphi(t_r))D_{rs}(t_r)\right]}{1+\sum_{r=0}^{\infty}\sum_{s=0}^{\infty}\frac{mR_{rs}^2(r_0)}{M_{rs}}} - \dot{z}(t_r^-) \right\}$$

(4.56)

4.3 Numerical simulation and analysis

Because there are three distinct dynamic phases with different governing equations of motion throughout the process of vibration, the dynamic system in question is non-smooth, which brings about a difficulty in numerical calculation. To obtain the whole time histories of the dynamic responses of the system, the numerical algorithm introduced in Section 3.2.2.2 is employed. In the following, the dynamic behaviours of the frictional system in the three situations of spinning speed of disc are investigated and relevant interesting phenomena are analysed.

The basic system parameters whose values are constant in the numerical examples are listed in Table 4.1. It should be noted that numbers *k* and *l* in the expression of the transverse displacement of the disc can be chosen to include as many modes as needed to represent the dynamics of the system with acceptable accuracy. To avoid excessive computations, the modal series in Eq. (4.24) are truncated at suitable values of indices k and l. The first seven natural frequencies of the disc are 1492, 1517, 1517, 1824, 1824, 2774 and 2774 rad/s, which are 237, 241, 241, 290, 290, 442 and 442 in Hz. It is found that the first seven disc modes (one single mode with zero nodal circle and zero nodal diameter and three pairs of doublet modes with zero nodal circle and one, two or three nodal diameters) are good enough in terms of the convergence of the results.

Table 4.1 The values of constant system parameters

a	b	r_0	ρ	E	h	ν
0.044m	0.12m	0.1m	7200kg/m^3	150GPa	0.002m	0.211
m	k_z	$r_0^2 k_\varphi$	N_0	μ_0	μ_1	μ_s
0.1kg	$3\cdot10^4$N/m	2000N·m/rad	500N	0.6	0.35	0.8

4.3.1 Stable sliding equilibrium under the constant speed and the effects of time-variant speed

In this sub-section, the dynamic responses in the three different situations of disc speed are obtained and compared to reveal the effects of time-variant disc speed on the friction induced dynamics of the system.

In the situation of constant disc speed, it is viable to find an equilibrium point in the slip state for the system by solving the algebraic nonlinear equations obtained by setting all the terms involving velocity and acceleration in Eqs. (4.33), (4.34) and (4.36) to be zero. The algebraic nonlinear equations to determine the equilibrium point are solved numerically using *fsolve* in MATLAB. Then the Lyapunov stability at this equilibrium point is investigated. That is, if the solutions of Eqs. (4.33), (4.34) and (4.36) with a small initial perturbation from the equilibrium point converge to the equilibrium point with time approaching infinity, the sliding equilibrium under study is considered to be asymptotically stable; while if the solutions move away from the equilibrium point with time increasing, the sliding equilibrium under study is unstable. Based on the system parameters listed in Table 4.1, the regions of stability with respect to four parameters c_z, c_φ, α and Ω_c which are found to have significant effects on the stability are obtained. Fig. 4.3 illustrates some combinations of c_z and $r_0^2 c_\varphi$ which correspond to stable sliding equilibriums with different values of α under two different constant spinning speed $\Omega_c = 1$ and $10\mathrm{rad/s}$.

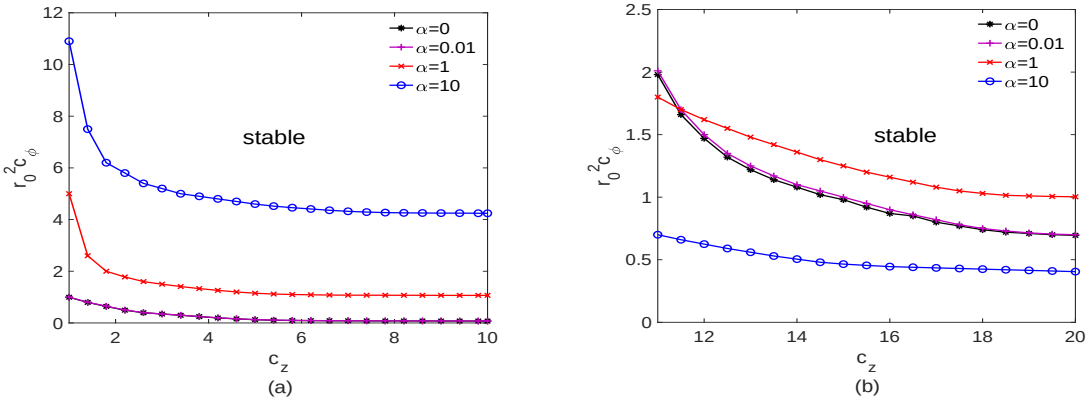

Figure 4.3 Combinations of c_z and $r_0^2 c_\varphi$ corresponding to stable sliding equilibrium with different values of α under two spinning speed: (a) $\Omega_c = 1\mathrm{rad/s}$, (b) $\Omega_c = 10\mathrm{rad/s}$. ('stable' refers to the region above the respective curve).

Considering a parameter combination in the 'stable' area ($c_z = 11\ \mathrm{N \cdot s/m}$, $r_0^2 c_\varphi = 1\ \mathrm{N \cdot m \cdot s/rad}$, α=10, $\Omega_c = 10\ \mathrm{rad/s}$), it can be seen from Fig. 4.4 that the amplitudes of dynamic responses of the system decay fast with time until the sliding equilibrium is reached. For comparison, the vibration in the situation of decelerating disc ($\Omega_0 = 10\ \mathrm{rad/s}$, $t_{\max} = 20\ \mathrm{s}$) with the same parameter values and initial condition as those in the situation of constant disc speed is investigated and the results are depicted in Fig. 4.5. An interesting phenomenon arises that the vibration decays in the early stage, similarly to that in the situation of constant speed, but then grows in the final stage and the stick-slip motion is induced. The reason for this phenomenon is the negative slope of the friction force-relative velocity relationship, which is usually considered a contributor to system instability. With the decrease of disc speed, the magnitude of the relative velocity $|\Omega - \dot{\varphi}|$ can become sufficiently low (please note that $\dot{\varphi}$ becomes approximately zero before the vibration grows in the end of the process), leading to a large negative slope of the friction force-relative velocity dependence, which, acting like a negative damping, can cancel out the positive viscous damping and then cause the vibration of the system to grow towards the end of the decelerative process.

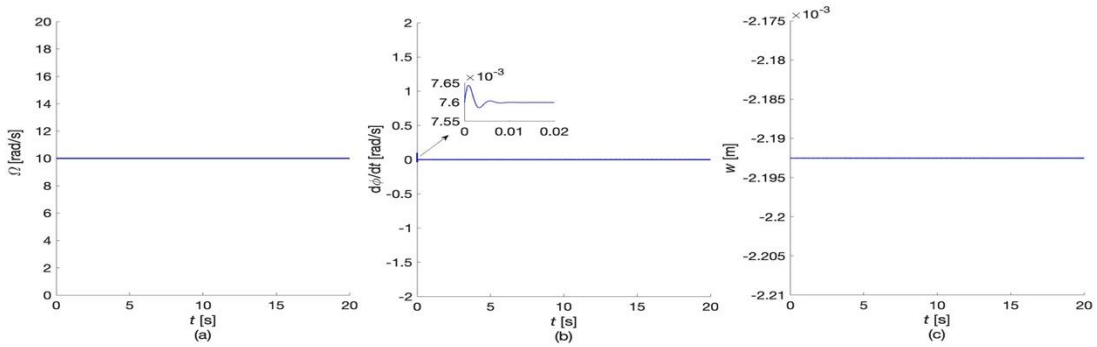

Figure 4.4 The system dynamic responses under the constant disc speed: (a) the spinning speed of disc, (b) the circumferential velocity of the slider, (c) the transverse displacement of a specific point on the disc at $r = r_0$ and $\theta = 0$. ($c_z = 11\ \mathrm{N \cdot s/m}$, $r_0^2 c_\varphi = 1\ \mathrm{N \cdot m \cdot s/rad}$, α=10, $\Omega_c = 10\mathrm{rad/s}$).

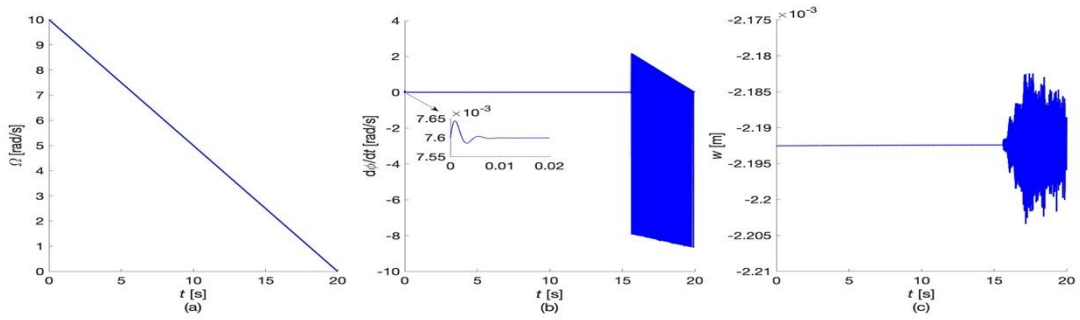

Figure 4.5 The system dynamic responses under the decelerating disc: (a) the spinning speed of disc, (b) the circumferential velocity of the slider, (c) the transverse displacement of a specific point on the disc at $r = r_0$ and $\theta = 0$. ($c_z = 11\ \mathrm{N \cdot s/m}$, $r_0^2 c_\varphi = 1\ \mathrm{N \cdot m \cdot s/rad}$, α=10, $\Omega_0 = 10\mathrm{rad/s}$, $t_{\max} = 20\mathrm{s}$).

A similar phenomenon occurs in the situation of accelerating disc but the mechanism is different. Another parameter combination leading to a stable sliding equilibrium under constant disc speed ($c_z = 1\ \mathrm{N \cdot s/m}$, $r_0^2 c_\varphi = 2\ \mathrm{N \cdot m \cdot s/rad}$, $\alpha = 0$, $\Omega_c = 1\ \mathrm{rad/s}$) is used. The time histories of responses starting from a small perturbation from the sliding equilibrium under constant disc speed are shown in Fig. 4.6. Similarly, the vibration decays fast until the sliding equilibrium is reached. Meanwhile, the system responses under accelerating disc ($\Omega_1 = 1\ \mathrm{rad/s}$, $a_d = 3\ \mathrm{rad/s^2}$) with the same parameter values and initial condition as those under constant disc speed are obtained and plotted in Fig. 4.7. As shown in this figure, the vibration decays firstly but grows at a time point later due to the increase of disc speed. This phenomenon can be explained by the effect of moving load which causes speed-dependent instability [67, 163]. The two examples above reflect the time-varying features of the friction-induced vibration of the system due to the time-variant disc speed.

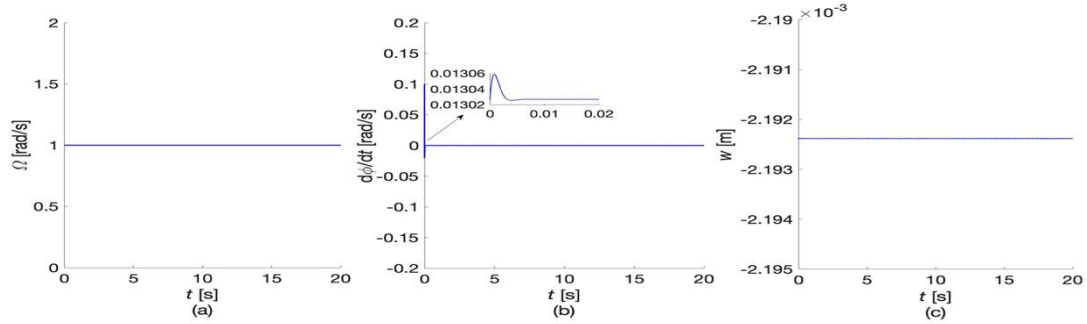

Figure 4.6 The system dynamic responses under the constant disc speed: (a) the spinning speed of disc, (b) the circumferential velocity of the slider, (c) the transverse displacement of disc at $(r_0, 0)$. ($c_z = 1\mathrm{N \cdot s/m}$, $r_0^2 c_\varphi = 2\ \mathrm{N \cdot m \cdot s/rad}$, α=0, $\Omega_c = 1\mathrm{rad/s}$).

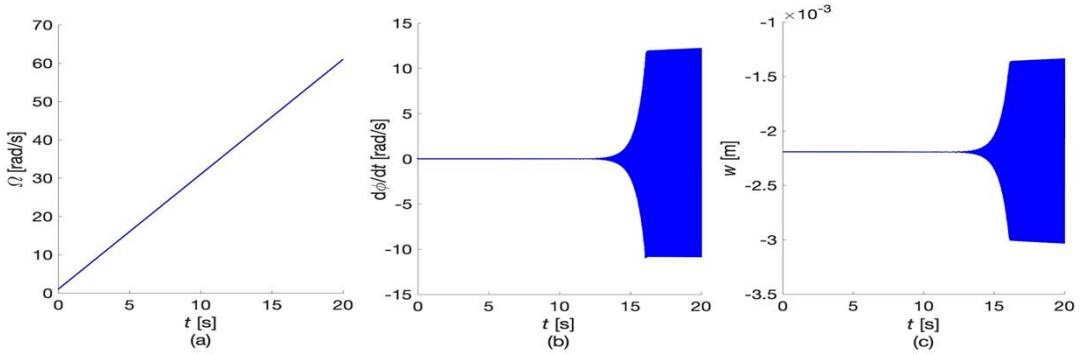

Figure 4.7 The system dynamic responses under the accelerating disc: (a) the spinning speed of disc, (b) the circumferential velocity of the slider, (c) the transverse displacement of disc at $(r_0, 0)$. ($c_z = 1\text{N} \cdot \text{s/m}$, $r_0^2 c_\varphi = 2\ \text{N} \cdot \text{m} \cdot \text{s/rad}$, α=0, $\Omega_1 = 1\text{rad/s}$, $a_\text{d} = 3\text{rad/s}^2$).

4.3.2 Non-stationary dynamic behaviour under the time-variant disc speed

Next, the parameter combinations corresponding to unstable sliding equilibrium in the situation of constant disc speed are considered and the dynamic responses in the three situations of disc speed are compared. The initial conditions are set to be a small perturbation from the equilibrium point of the system in all the numerical examples below. The parameter values used in the first example are: $c_z = 0.1\text{N} \cdot \text{s/m}$, $r_0^2 c_\varphi = 0.1\ \text{N} \cdot \text{m} \cdot \text{s/rad}$, α=1 and $\Omega_\text{c} = 2\pi\text{rad/s}$ in the situation of constant speed. The results about the in-plane angular motion of the slider and the transverse vibration of the disc under the constant disc speed are illustrated in Figs. 4.8 and 4.9, respectively.

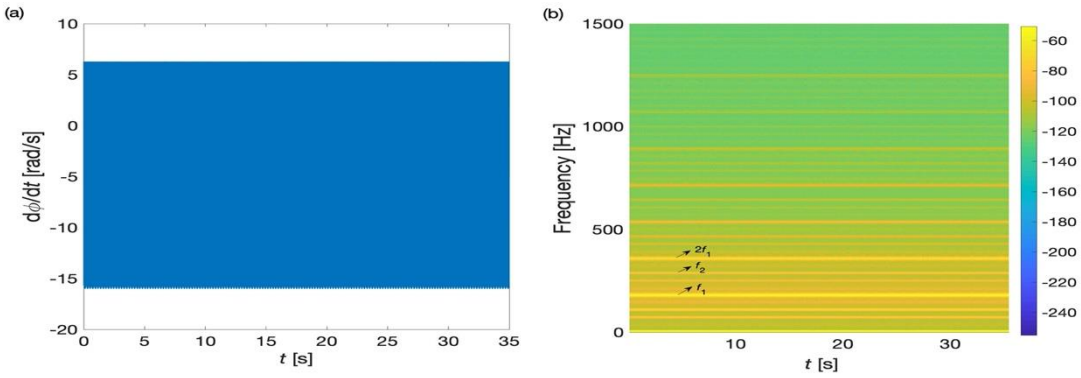

Figure 4.8 The time history of the circumferential angular velocity of the slider and time-frequency plot of the circumferential angular displacement of the slider under the constant disc speed: (a) the time history of the circumferential angular velocity, (b) the time-frequency plot of the circumferential angular displacement.($c_z = 0.1\text{N} \cdot \text{s/m}$, $r_0^2 c_\varphi = 0.1\ \text{N} \cdot \text{m} \cdot \text{s/rad}$, α=1, $\Omega_\text{c} = 2\pi\text{rad/s}$).

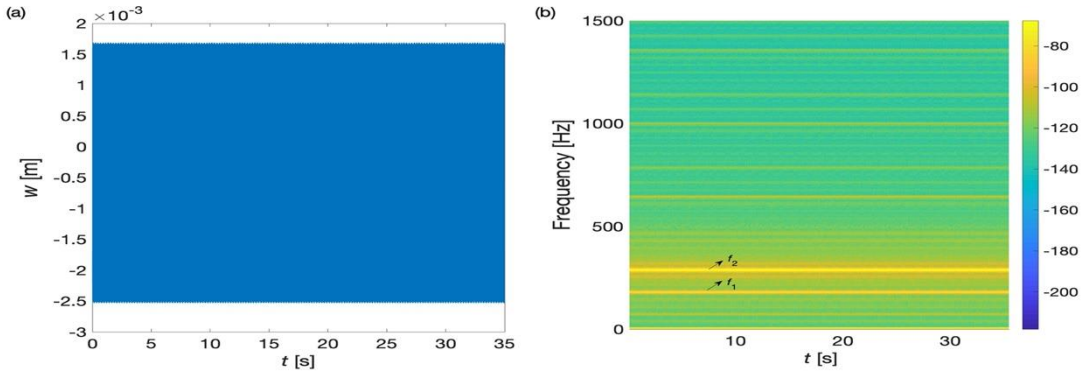

Figure 4.9 The time history and time-frequency plot of the transverse displacement of the disc at $r = r_0$ and $\theta = 1\text{rad}$ under the constant disc speed: (a) the time history, (b) the frequency spectrum plot.

In these figures, the time-frequency plots are obtained from the short-time Fourier transform, from which it can be observed that the frequency compositions of the responses remain unchanged throughout the whole process, indicating that the dynamic responses are stationary. Besides, both the frequency spectra of the in-plane angular motion of the slider and the transverse vibration of the disc consist of several incommensurate frequencies and two common incommensurate frequencies $f_1 = 181$ Hz and $f_2 = 290.5$ Hz can be identified, which suggests that both dynamic responses are quasi-periodic. The vibration of the system in the situation of decelerating disc is then investigated and the results concerning the in-plane angular motion of the slider and the transverse vibration of the disc are illustrated in Figs. 4.10 and 4.11.

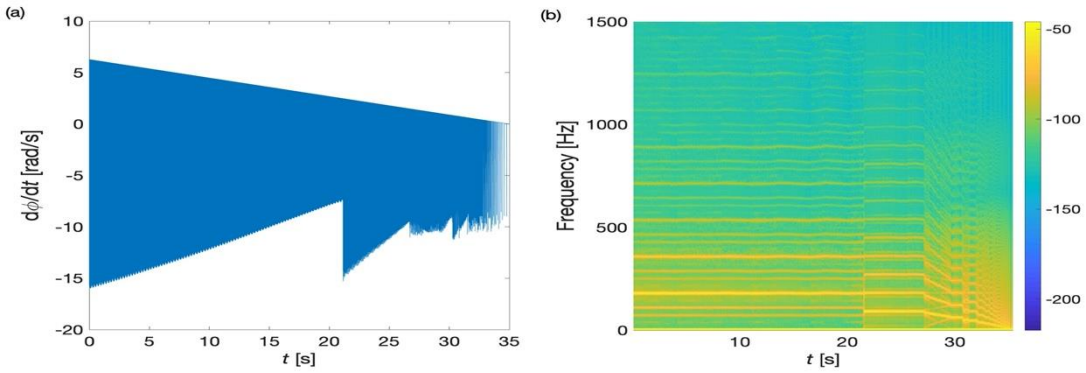

Figure 4.10 The time history of the circumferential angular velocity of the slider and time-frequency plot of the circumferential angular displacement of the slider under the decelerating disc: (a) the time history of the circumferential angular velocity, (b) the time-frequency plot of the circumferential angular displacement.($c_z = 0.1\text{N} \cdot \text{s/m}$, $r_0^2 c_\varphi = 0.1\ \text{N} \cdot \text{m} \cdot \text{s/rad}$, α=1, $\Omega_0 = 2\pi\text{rad/s}$, $t_{\max} = 35\text{s}$).

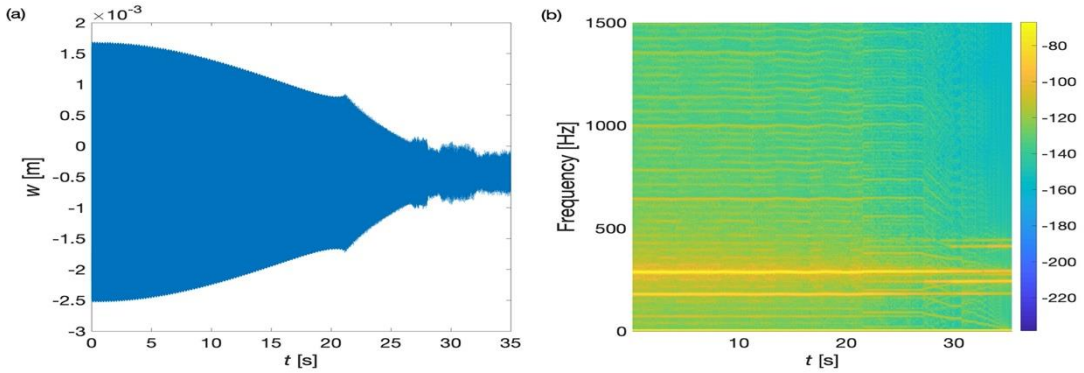

Figure 4.11 The time history and time-frequency plot of the transverse displacement of the disc at $r = r_0$ and $\theta = 1\text{rad}$ under the decelerating disc: (a) the time history, (b) the frequency spectrum plot.

The time-frequency plots show the time-variant characteristic of frequency spectra of the responses, especially the in-plane motion of the slider, in the situation of decelerating disc. In the early stage of vibration, the frequency spectra of responses are similar to those in the situation of constant speed, but lower-frequency components arise in the dynamic responses towards the end of the process, and the frequency spectrum of the in-plane motion of the slider gets very fuzzy and dense in the final stage of the process. The variation of the frequencies of the response during the process can also be observed from the time histories during two different time spans in the early and late stages, as depicted in Fig. 4.12.

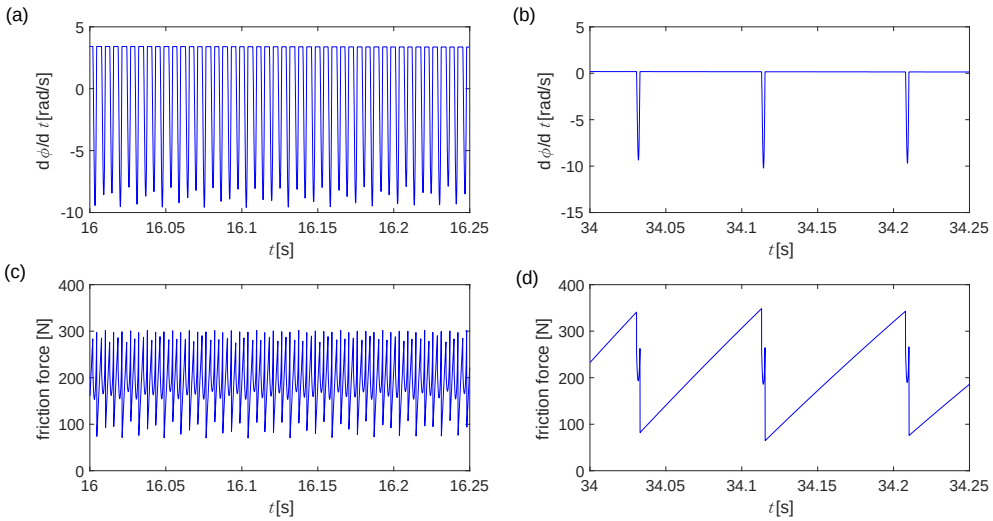

Figure 4.12 The short-term time histories during two different time spans under the decelerating disc: (a and b) the circumferential angular velocity of the slider, (c and d) the friction force.

The second example uses the parameter values: $c_z = 2\text{N} \cdot \text{s/m}$, $r_0^2 c_\varphi = 0.5\ \text{N} \cdot \text{m} \cdot \text{s/rad}$, α=1 and $\Omega_c = 2\pi\text{rad/s}$ in the situation of constant speed. Figs. 4.13 and 4.14 illustrate the time histories and time-frequency plots of the in-plane motion of the slider and transverse vibration of the disc. The frequency compositions of the responses remain unchanged and both the frequency spectra of the in-plane angular displacement of the slider and the transverse displacement of the disc consist of the fundamental frequency f_0 (206 Hz) and its superharmonics ($nf_0, n = 2,3,\ldots$), indicating that the in-plane motion of the slider and the transverse motion of the disc are periodic at the same frequency. Correspondingly, the results of the dynamic responses in the situation of decelerating disc are illustrated in Figs. 4.15 and 4.16. As shown in Fig. 4.15b, at least six segments with distinct frequency compositions, which are in time intervals $0 < t < 15\text{s}$, $15 < t < 20\text{s}$, $20 < t < 28\text{s}$, $28 < t < 30\text{s}$, $30 < t < 31\text{s}$, $31 < t < 35\text{s}$, can be identified based on visual inspection. The phase portraits of the circumferential motion of the slider and trajectories of the friction force during certain time spans in the six segments are shown in Fig. 4.17. As is seen, stick-slip vibration with different periods in the six time intervals can be identified for the in-plane motion of the slider.

The third example considers a higher disc speed, where the parameter values in the situation of constant speed are: $c_z = 2\text{N} \cdot \text{s/m}$, $r_0^2 c_\varphi = 0.5\ \text{N} \cdot \text{m} \cdot \text{s/rad}$, α=1 and $\Omega_c = 6\pi\text{rad/s}$. The in-plane motions of the slider and the transverse motions of the disc under the constant disc speed and under the decelerating disc are shown in Figs. 4.18-21. Similarly, the frequency spectra of responses in the situation of decelerating disc are more time-variant than those in the situation of constant disc speed, especially lower-frequency components arise in the dynamic responses and the frequency spectra get fuzzy and dense towards the end of the process.

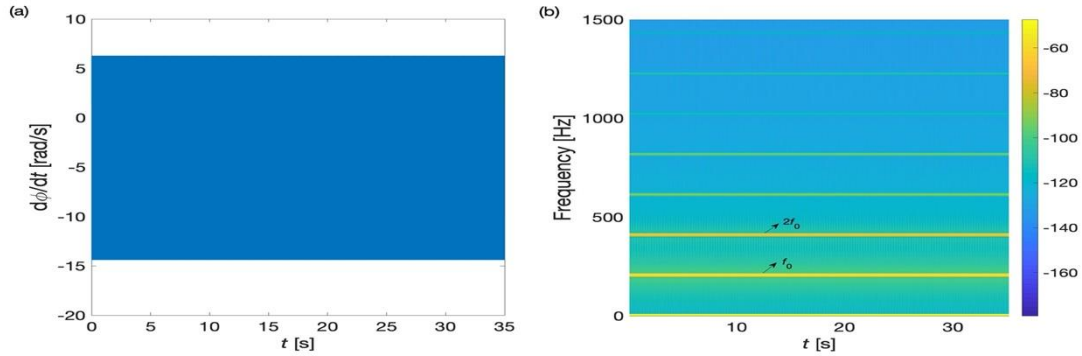

Figure 4.13 The time history of the circumferential angular velocity of the slider and time-frequency plot of the circumferential angular displacement of the slider under the constant disc speed: (a) the time history of the circumferential angular velocity, (b) the time-frequency plot of the circumferential angular displacement.($c_z = 2\text{N} \cdot \text{s/m}$, $r_0^2 c_\varphi = 0.5\ \text{N} \cdot \text{m} \cdot \text{s/rad}$, α=1, $\Omega_{\text{c}} = 2\pi\text{rad/s}$).

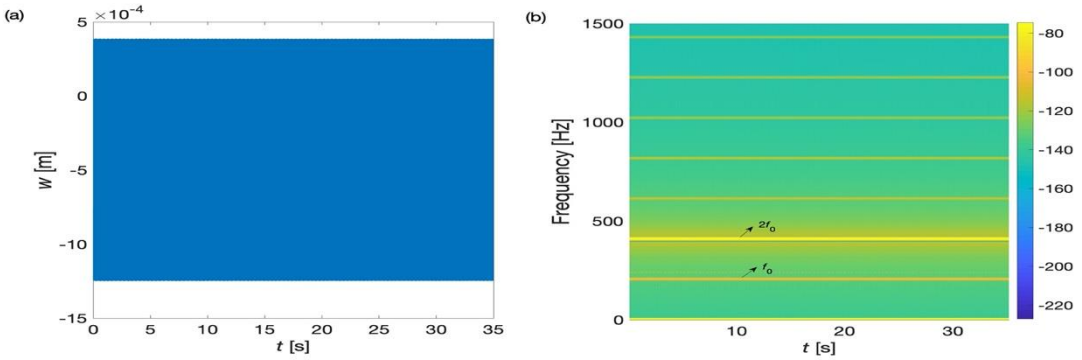

Figure 4.14 The time history and time-frequency plot of the transverse displacement of the disc at $r = r_0$ and $\theta = 1\text{rad}$ under the constant disc speed: (a) the time history, (b) the frequency spectrum plot.

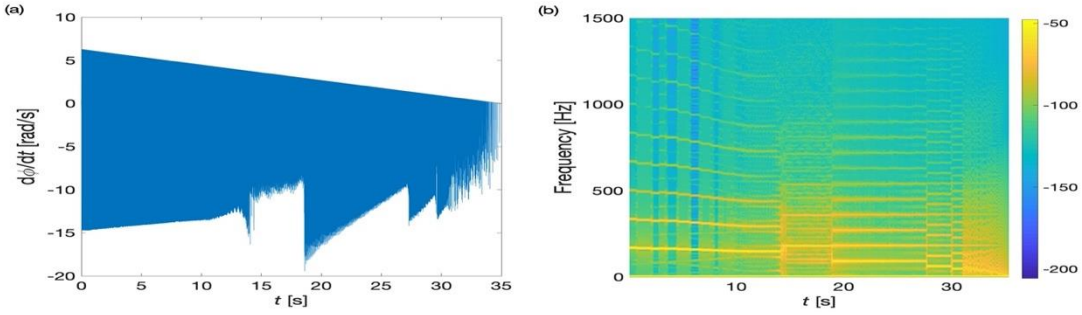

Figure 4.15 The time history of the circumferential angular velocity of the slider and time-frequency plot of the circumferential angular displacement of the slider under the decelerating disc: (a) the time history of the circumferential angular velocity, (b) the time-frequency plot of the circumferential angular displacement.($c_z = 2\text{N} \cdot \text{s/m}$, $r_0^2 c_\varphi = 0.5\ \text{N} \cdot \text{m} \cdot \text{s/rad}$, α=1, $\Omega_0 = 2\pi\text{rad/s}$, $t_{\max} = 35\text{s}$).

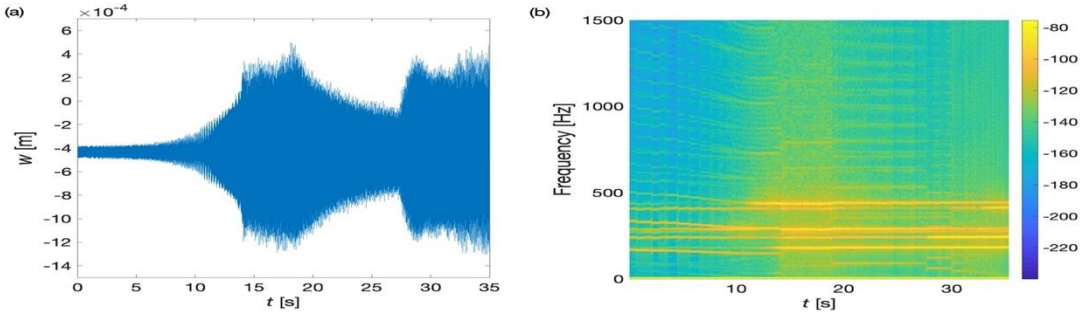

Figure 4.16 The time history and time-frequency plot of the transverse displacement of the disc at $r = r_0$ and $\theta = 1\text{rad}$ under the decelerating disc: (a) the time history, (b) the frequency spectrum plot.

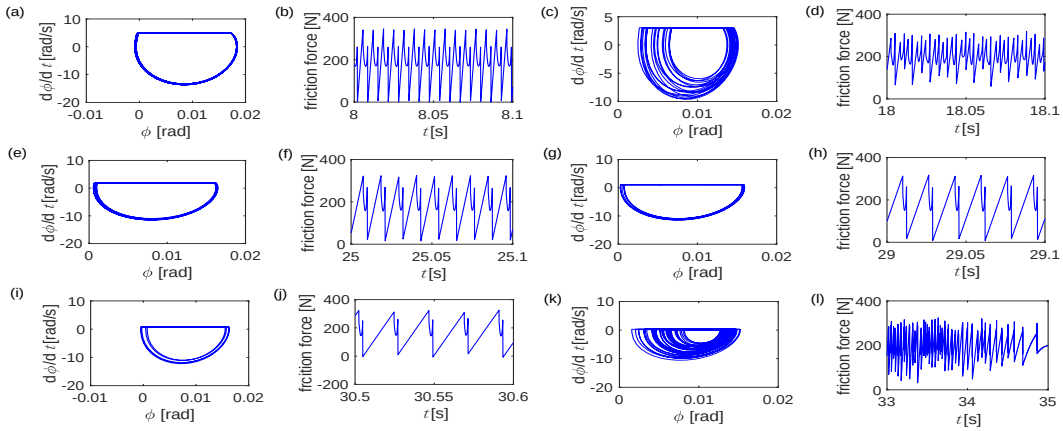

Figure 4.17 The phase portraits of the circumferential motion of the slider and trajectories of friction force time spans within six different time segments under the decelerating disc: (a,b) $8 < t < 8.1$s, (c,d) $18 < t < 18.1$s, (e,f) $25 < t < 20.1$s, (g,h) $29 < t < 29.1$s, (i,j) $30.5 < t < 30.6$s, (k,l) $33 < t < 35$s.

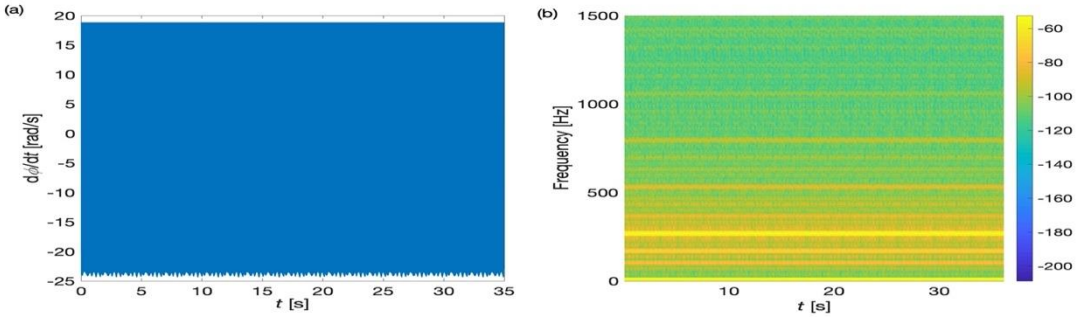

Figure 4.18 The time history of the circumferential angular velocity of the slider and time-frequency plot of the circumferential angular displacement of the slider under the constant disc speed: (a) the time history of the circumferential angular velocity, (b) the time-frequency plot of the circumferential angular displacement.($c_z = 2\text{N} \cdot \text{s/m}$, $r_0^2 c_\varphi = 0.5\ \text{N} \cdot \text{m} \cdot \text{s/rad}$, α=1, $\Omega_c = 6\pi\text{rad/s}$).

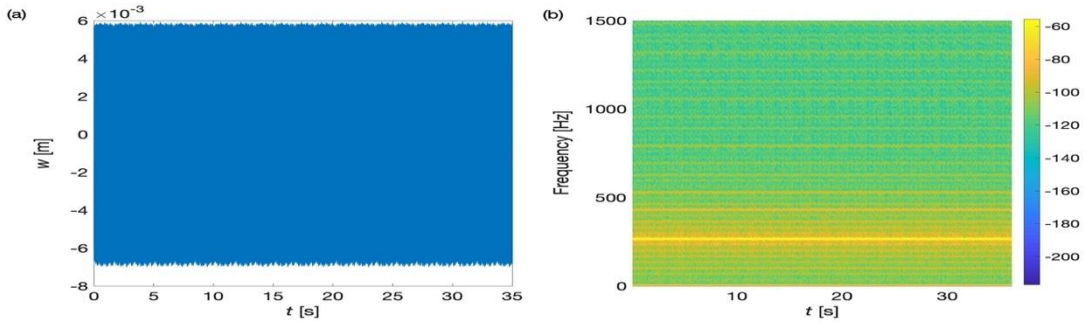

Figure 4.19 The time history and time-frequency plot of the transverse displacement of the disc at $r = r_0$ and $\theta = 1\text{rad}$ under the constant disc speed: (a) the time history, (b) the frequency spectrum plot.

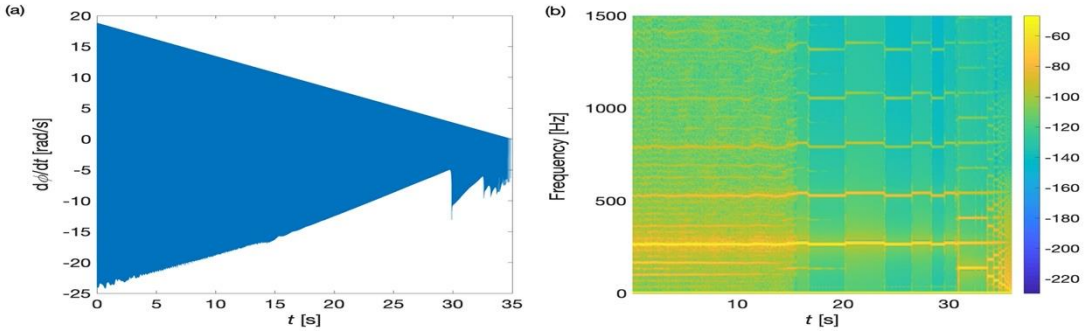

Figure 4.20 The time history of the circumferential angular velocity of the slider and time-frequency plot of the circumferential angular displacement of the slider under the decelerating disc: (a) the time history of the circumferential angular velocity, (b) the time-frequency plot of the circumferential angular displacement.($c_z = 2\text{N} \cdot \text{s/m}$, $r_0^2 c_\varphi = 0.5\ \text{N} \cdot \text{m} \cdot \text{s/rad}$, α=1, $\Omega_0 = 6\pi\text{rad/s}$, $t_{\max} = 35\text{s}$).

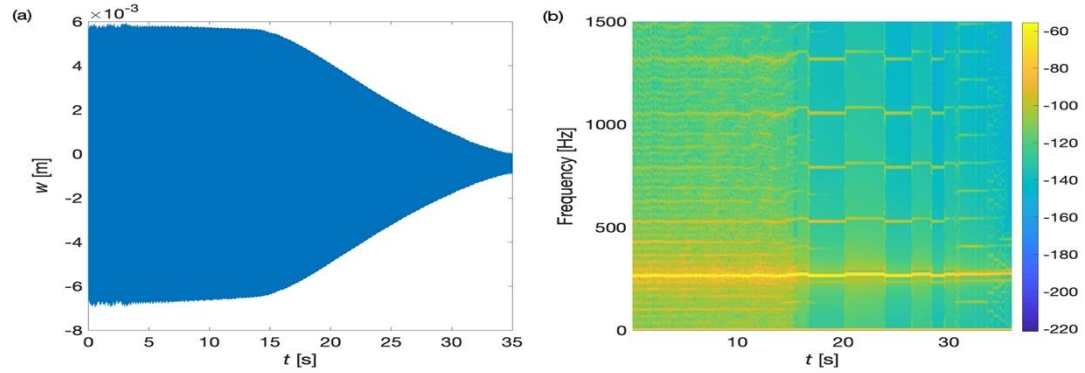

Figure 4.21 The time history and time-frequency plot of the transverse displacement of the disc at $r = r_0$ and $\theta = 1\text{rad}$ under the decelerating disc: (a) the time history, (b) the frequency spectrum plot.

The effect of accelerating disc on the system dynamics is also investigated. The variations of normal force are plotted in Fig. 4.22, from which it is seen that separation happens with the increase of disc speed in the process, while there is no separation occurring for the corresponding system in the situation of constant disc speed. The dynamic responses under the accelerating disc are illustrated in Figs. 4.23 and 4.24. It is noticed that separation happening in the process leads to shift of frequency spectra of the system responses.

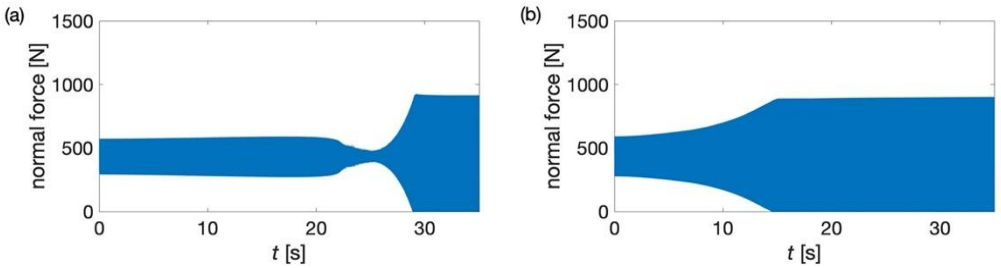

Figure 4.22 The variation of normal force with time in the situation of accelerating disc in the two cases: (a) $c_z = 0.1\text{N} \cdot \text{s/m}$, $r_0^2 c_\varphi = 0.1\ \text{N} \cdot \text{m} \cdot \text{s/rad}$, α=1, $\Omega_1 = 2\pi\text{rad/s}$, $a_\text{d} = 0.2\text{rad/s}^2$, (b) $c_z = 2\text{N} \cdot \text{s/m}$, $r_0^2 c_\varphi = 0.5\ \text{N} \cdot \text{m} \cdot \text{s/rad}$, α=1, $\Omega_1 = 2\pi\text{rad/s}$, $a_\text{d} = 0.2\text{rad/s}^2$.

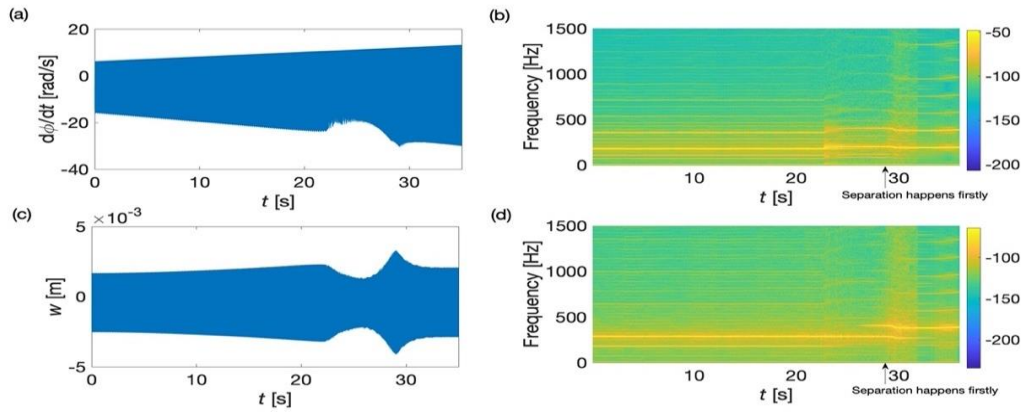

Figure 4.23 The time histories and time-frequency plots of the dynamic responses under the accelerating disc: (a) (b) the in-plane motion of the slider, (c) (d) the transverse motion of the disc. ($c_z = 0.1\text{N} \cdot \text{s/m}$, $r_0^2 c_\varphi = 0.1\ \text{N} \cdot \text{m} \cdot \text{s/rad}$, α=1, $\Omega_1 = 2\pi\text{rad/s}$, $a_\text{d} = 0.2\text{rad/s}^2$).

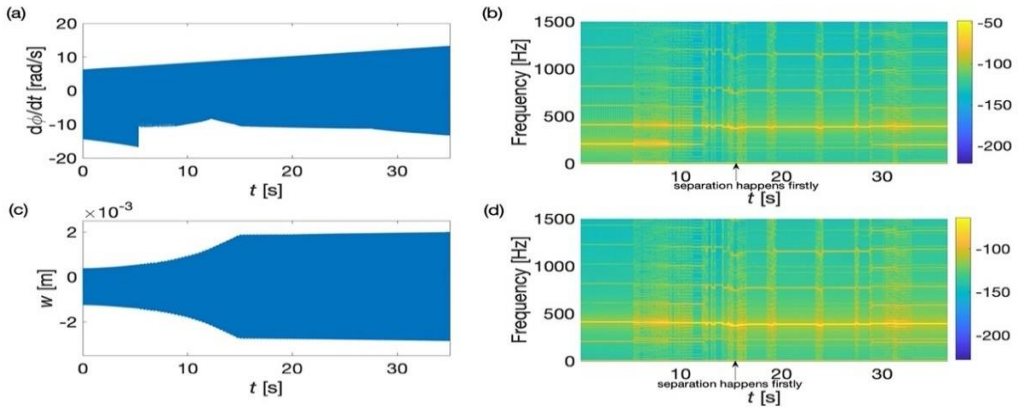

Figure 4.24 The time histories and time-frequency plots of the dynamic responses under the accelerating disc: (a) (b) the in-plane motion of the slider, (c) (d) the transverse motion of the disc. ($c_z = 2\text{N} \cdot \text{s/m}$, $r_0^2 c_\varphi = 0.5\ \text{N} \cdot \text{m} \cdot \text{s/rad}$, α=1, $\Omega_1 = 2\pi\text{rad/s}$, $a_\text{d} = 0.2\text{rad/s}^2$).

4.3.3 Impact during vibration

As the amplitude of transverse vibration of the disc increases, the slider may separate from the disc and then recontact with disc. The role of the impact happening at the instants of recontact on the system dynamics is examined. The dynamic responses of the system under the constant disc speed in two conditions: with impact and without impact are obtained to exemplify the effect of the impact on the vibration. When the impact is ignored, the transverse velocity of the disc is not changed during the recontact. Fig. 4.25 shows the time histories of the transverse displacement at $(r_0, 0)$ of the disc with a certain parameter combinations. It is seen that the transverse vibration with impact considered is much weaker compared with that without impact, which can be explained by the fact that the impact is assumed to be fully plastic in this paper and thus dissipates energy in the vibration.

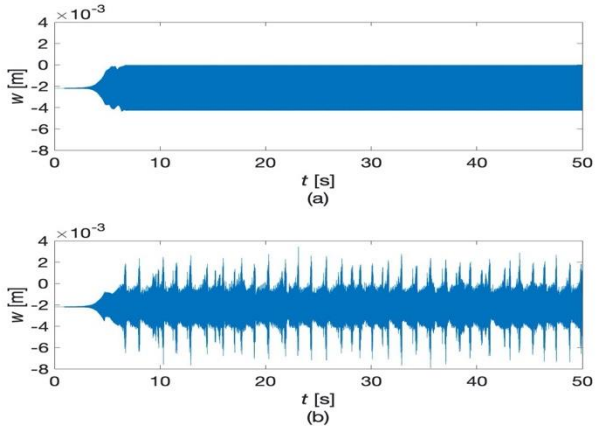

Figure 4.25 The time histories of the transverse displacement in the situation of constant disc speed under two conditions: (a) with impact, (b) without impact. ($c_z = 0$, $r_0^2 c_\varphi = 0$, α=1, $\Omega_c = 50\text{rad/s}$).

4.4 Conclusions

In this chapter, the dynamics of a slider-on-disc system subject to friction force in three different situations of spinning speed, i.e. constant deceleration, constant acceleration and constant speed, is investigated. Due to the non-smooth nature of the friction force between the slider and the disc, the slider experiences stick-slip vibration in the circumferential direction of the disc. Meanwhile, the in-plane motion of the slider causes time-varying normal force and bending moment on the disc, which can be seen as moving loads to excite the transverse vibration of the elastic disc. The transverse vibration of the disc will, in turn, influence the in-plane motion of the slider by affecting the magnitude of friction force through the varying normal force. Therefore the transverse vibration and the in-plane vibration of the slider are coupled. It is observed the decelerating and accelerating disc rotation results in distinct dynamic behaviours of the frictional system from that under the constant disc speed. The following conclusions can be reached,

1. In the situation of constant speed, a sliding equilibrium of the system can be found. The parameter combinations corresponding to the stable or unstable equilibrium points in the sense of Lyapunov stability are identified.

2. For the system with the parameter combinations corresponding to the stable sliding equilibrium in the situation of constant speed, the vibration starting from an initial condition near the equilibrium point decays with time and ceases eventually. While

in the situation of time-varying disc speed, stability may change with time due to the variation of disc speed with time, resulting in an interesting phenomenon that the system vibration decays with time in the early stage but grows in the later stage. This kind of time-varying characteristic of friction induced vibration results from the negative-slope friction force-relative velocity relationship in the situation of decelerating disc and the speed-dependent instability caused by the moving load in the situation of accelerating disc.

3. The time-variant disc speed increases the non-stationary characteristics of the system dynamics as opposed to the constant disc speed, especially the in-plane motion of the slider, which means there are more shifts of frequency spectra of the dynamic responses throughout the process in the situation of time-variant disc speed than that in the situation of constant speed.

4. When impact is considered, the transverse vibration of the disc becomes lower than without.

Chapter 5

Suppression of friction induced vibration in MDoF systems using tangential harmonic excitation

This chapter investigates the effects of tangential harmonic excitation on the friction induced vibration in multi-degree-of-freedom (MDoF) systems that are coupled in the tangential and normal directions. A minimal two-degree-of-freedom system and a more complicated slider-on-disc system are considered. It is observed the friction induced vibration of the systems can be suppressed with the tangential harmonic excitation when the amplitude and frequency of the excitation are in certain ranges. The analytical method to determine the ranges where the systems are stabilized by the tangential excitation is established. To verify the analytical results, a great amount of computational effort is also made to simulate the time responses of systems in various combinations of values of the amplitude and frequency, by which the parameter ranges where the friction induced vibration is suppressed can also be obtained.

5.1 Introduction

Friction induced self-excited vibration are usually undesirable and should be avoided. The published studies revealed numerous factors leading to friction induced dynamic instability, e.g. stick-slip oscillation [19,20], sprag-slip instability [43-45], mode-coupling instability [55-57], moving-load follower force and friction couple [65-67], etc.

Understanding the factors leading to friction induced dynamic instability may help to select appropriate parameter values corresponding to stable systems in a design.

Additionally, some structural modification approaches were developed to suppress friction induced vibration and noise, such as installing damping shims on the brake pads [179], modifying brake disc surface topography [190, 191], applying yawing angular misalignment [192], etc. All these methods mentioned above change the dynamic properties of the systems permanently. On the other hand, Cunefare and Graf [193] proposed using an actuator to produce a fluctuating friction force with high frequency between the pad and the disc to eliminate brake squeal. Feeny and Moon [194] applied a high-frequency excitation to quench stick-slip chaos. Zhao et al. [195] integrated the piezoceramic actuators into a disc brake system to provide harmonic high-frequency vibrations to eliminate the stick-slip limit cycle vibration of the system. This approach of applying an external periodic excitation offers a more flexible way to suppress the unwanted friction induce vibration in mechanical systems. However, there has been little theoretical study on this topic. It was observed in [196] that sufficiently strong high-frequency excitation in the tangential direction can smoothen the discontinuity in dry friction and produce behaviour like viscous damping. Thomsen [197] conduced a theoretical analysis of the effects of high-frequency external excitation on the stick-slip vibration of a single-DoF mass-on-belt system. Nevertheless, real mechanical systems such as a disc brake system usually involve multiple degrees of freedom, in which mechanisms responsible for friction induced vibration such as mode-coupling instability may appear. In order to provide more practical theoretical guidance for suppression of friction induced vibration in real mechanical systems, this chapter investigates the effects of the tangential high-frequency harmonic excitation on the friction induced dynamics of a two-degree-of-freedom mass-on-belt system and a slider-on-disc system.

The rest of the chapter is arranged as follows. In Section 5.2, the equations of motion are formulated and the analytical formulas for the parameter ranges where the systems are stabilized by the tangential excitation are derived for the two-DoF mass-on-belt system. In Section 5.3, the corresponding formulation and derivation for the slider-on-disc system are presented. Subsequently a detailed numerical study is conducted in Section 5.4 and the results obtained from the analytical formulas are examined in relation to the time responses calculated by the Runge-Kutta algorithm. Finally in Section 5.5 the conclusions are drawn.

5.2 A minimal 2-DoF frictional system

The model of the 2-DoF frictional system is shown in Fig. 5.1, which was previously investigated in [55] in terms of mode-coupling instability. In this model, a point mass m is connected to the base by two sets of spring-damper systems (k_1, c_1 and k_2, c_2) at the angles of inclination to the horizontal direction α_1 and α_2, respectively. The mass is pressed by a preload F to bring it into frictional contact with a belt moving at constant velocity v. A spring k_3 is used to model the contact stiffness between the mass and the belt. A tangential harmonic force $F_\mathrm{b}(t) = A_\mathrm{b}\sin\omega t$ is now applied to the mass and its effects on the dynamic instability of the system is examined.

The equations of motion of the 2-DoF system can be derived as,

$$\begin{bmatrix} m & 0 \\ 0 & m \end{bmatrix}\begin{bmatrix} \ddot{x} \\ \ddot{y} \end{bmatrix} + \begin{bmatrix} c_{11} & c_{12} \\ c_{21} & c_{22} \end{bmatrix}\begin{bmatrix} \dot{x} \\ \dot{y} \end{bmatrix} + \begin{bmatrix} k_{11} & k_{12} \\ k_{21} & k_{22} \end{bmatrix}\begin{bmatrix} x \\ y \end{bmatrix} = \begin{bmatrix} F_\mathrm{f} + A_\mathrm{b}\sin\omega t \\ -F \end{bmatrix} \tag{5.1}$$

where,

$$\left.\begin{array}{c} c_{11} = c_1\cos^2\alpha_1 + c_2\cos^2\alpha_2,\ k_{11} = k_1\cos^2\alpha_1 + k_2\cos^2\alpha_2, \\ c_{12} = c_{21} = -c_1\sin\alpha_1\cos\alpha_1 + c_2\sin\alpha_2\cos\alpha_2, k_{12} = k_{21} = -k_1\sin\alpha_1\cos\alpha_1 + k_2\sin\alpha_2\cos\alpha_2 \\ c_{22} = c_1\sin^2\alpha_1 + c_2\sin^2\alpha_2,\ k_{22} = k_1\sin^2\alpha_1 + k_2\sin^2\alpha_2 + k_3 \end{array}\right\} \tag{5.2}$$

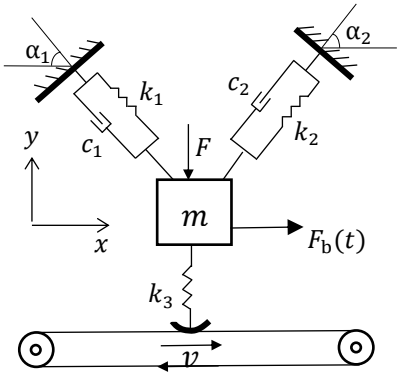

Figure 5.1 Two-degree-of-freedom frictional system.

And F_f represents the friction force between the mass and the belt, $F_\mathrm{f} = \mu(v_\mathrm{r})N$, in which $\mu(v_\mathrm{r})$ and N denote the coefficient of friction and the normal force, respectively. Here a Coulomb's law of friction is utilized, i.e.,

$$\mu(v_\mathrm{r}) = \mathrm{sign}(v_\mathrm{r})\mu_\mathrm{k} \tag{5.3}$$

where $v_\mathrm{r} = v - \dot{x}$. Eq. (5.3) is valid during relative sliding when $v_\mathrm{r} \neq 0$. In the stick phase when $v_\mathrm{r} = 0$, friction force F_f is obtained from the equations of motion, Eq. (5.1). Additionally, the normal force is expressed as,

$$N = -k_3 y \tag{5.4}$$

By defining the following quantities and operator,

$$\omega_1 = \sqrt{\frac{k_1}{m}},\ \tau = \omega_1 t,\ \eta_2 = \frac{k_2}{k_1},\ \eta_3 = \frac{k_3}{k_1},\ \zeta = \frac{c_1}{2m\omega_1},\ \delta = \frac{c_2}{c_1},\ B_\mathrm{b} = \frac{A_\mathrm{b}}{k_1},\ R = \frac{\omega}{\omega_1},\ (*)' = \frac{\mathrm{d}(*)}{\mathrm{d}\tau} \tag{5.5}$$

Eq. (5.1) can be rewritten as,

$$x'' + 2\zeta(\cos^2\alpha_1 + \delta\cos^2\alpha_2)x' + 2\zeta(-\sin\alpha_1\cos\alpha_1 + \delta\sin\alpha_2\cos\alpha_2)y' + (\cos^2\alpha_1 + \eta_2\cos^2\alpha_2)x + (-\sin\alpha_1\cos\alpha_1 + \eta_2\sin\alpha_2\cos\alpha_2)y = -\mu(v_r)\eta_3 y + B_\mathrm{b}\sin(R\tau) \tag{5.6a}$$

$$y'' + 2\zeta(-\sin\alpha_1\cos\alpha_1 + \delta\sin\alpha_2\cos\alpha_2)x' + 2\zeta(\sin^2\alpha_1 + \delta\sin^2\alpha_2)y' + (-\sin\alpha_1\cos\alpha_1 + \eta_2\sin\alpha_2\cos\alpha_2)x + (\sin^2\alpha_1 + \eta_2\sin^2\alpha_2 + \eta_3)y = -\frac{F}{k_1} \tag{5.6b}$$

Suppose the solutions consist of a slowly varying component and a small-amplitude fast varying component, i.e.,

$$x(\tau) = \overline{x}(\tau) + \frac{1}{R}\underline{x}(R\tau) \tag{5.7a}$$

$$y(\tau) = \overline{y}(\tau) + \frac{1}{R}\underline{y}(R\tau) \tag{5.7b}$$

Substituting Eq. (5.7) into Eq. (5.6) results in,

$$\overline{x}'' + R\frac{\mathrm{d}^2\underline{x}}{\mathrm{d}(R\tau)^2} + 2\zeta a_1\left(\overline{x}' + \frac{\mathrm{d}\underline{x}}{\mathrm{d}(R\tau)}\right) + 2\zeta a_2\left(\overline{y}' + \frac{\mathrm{d}\underline{y}}{\mathrm{d}(R\tau)}\right) + a_4\left(\overline{x} + \frac{1}{R}\underline{x}\right) + (a_5 + \mu(v_r)\eta_3)\left(\overline{y} + \frac{1}{R}\underline{y}\right) - B_\mathrm{b}\sin(R\tau) = 0 \tag{5.8a}$$

$$\left(\overline{y}'' + R\frac{\mathrm{d}^2\underline{y}}{\mathrm{d}(R\tau)^2}\right) + 2\zeta a_2\left(\overline{x}' + \frac{\mathrm{d}\underline{x}}{\mathrm{d}(R\tau)}\right) + 2\zeta a_3\left(\overline{y}' + \frac{\mathrm{d}\underline{y}}{\mathrm{d}(R\tau)}\right) + a_5\left(\overline{x} + \frac{1}{R}\underline{x}\right) + a_6\left(\overline{y} + \frac{1}{R}\underline{y}\right) + \frac{F}{k_1} = 0 \tag{5.8b}$$

where,

$$a_1 = \cos^2\alpha_1 + \delta\cos^2\alpha_2,\ a_2 = -\sin\alpha_1\cos\alpha_1 + \delta\sin\alpha_2\cos\alpha_2,\ a_3 = \sin^2\alpha_1 + \delta\sin^2\alpha_2,$$
$$a_4 = \cos^2\alpha_1 + \eta_2\cos^2\alpha_2,\ a_5 = -\sin\alpha_1\cos\alpha_1 + \eta_2\sin\alpha_2\cos\alpha_2,\ a_6 = \sin^2\alpha_1 + \eta_2\sin^2\alpha_2 + \eta_3 \tag{5.9}$$

Assuming $B_\mathrm{b} = C_\mathrm{b}R$ and grouping the terms on the left-hand sides of Eq. (5.8) into the coefficients of R, 1, $\frac{1}{R}$ lead to,

$$\left[\frac{\mathrm{d}^2\underline{x}}{\mathrm{d}(R\tau)^2} - C_\mathrm{h}\sin(R\tau)\right]R + \left[\overline{x}'' + 2\zeta a_1\left(\overline{x}' + \frac{\mathrm{d}\underline{x}}{\mathrm{d}(R\tau)}\right) + 2\zeta a_2\left(\overline{y}' + \frac{\mathrm{d}\underline{y}}{\mathrm{d}(R\tau)}\right) + a_4\overline{x} + a_5\overline{y} + \mu(v_r)\eta_3\overline{y}\right] + \left[a_4\underline{x} + a_5\underline{y} + \mu(v_r)\eta_3\underline{y}\right]\frac{1}{R} = 0 \quad (5.10a)$$

$$\frac{\mathrm{d}^2\underline{y}}{\mathrm{d}(R\tau)^2}R + \left[\overline{y}'' + 2\zeta a_2\left(\overline{x}' + \frac{\mathrm{d}\underline{x}}{\mathrm{d}(R\tau)}\right) + 2\zeta a_3\left(\overline{y}' + \frac{\mathrm{d}\underline{y}}{\mathrm{d}(R\tau)}\right) + a_5\overline{x} + a_6\overline{y} + \frac{F}{k_1}\right] + \left[a_5\underline{x} + a_6\underline{y}\right]\frac{1}{R} = 0 \quad (5.10b)$$

When $R \gg 1$, the following equations are resulted,

$$\frac{\mathrm{d}^2\underline{x}}{\mathrm{d}(R\tau)^2} = C_\mathrm{b}\sin(R\tau) + O(\frac{1}{R}) \quad (5.11a)$$

$$\overline{x}'' + 2\zeta a_1\left(\overline{x}' + \frac{\mathrm{d}\underline{x}}{\mathrm{d}(R\tau)}\right) + 2\zeta a_2\left(\overline{y}' + \frac{\mathrm{d}\underline{y}}{\mathrm{d}(R\tau)}\right) + a_4\overline{x} + a_5\overline{y} + \mu(v_r)\eta_3\overline{y} = O(\frac{1}{R}) \quad (5.11b)$$

$$\frac{\mathrm{d}^2\underline{y}}{\mathrm{d}(R\tau)^2} = O(\frac{1}{R}) \quad (5.11c)$$

$$\overline{y}'' + 2\zeta a_2\left(\overline{x}' + \frac{\mathrm{d}\underline{x}}{\mathrm{d}(R\tau)}\right) + 2\zeta a_3\left(\overline{y}' + \frac{\mathrm{d}\underline{y}}{\mathrm{d}(R\tau)}\right) + a_5\overline{x} + a_6\overline{y} + \frac{F}{k_1} = O(\frac{1}{R}) \quad (5.11d)$$

It can be derived from Eqs. (5.11a) and (5.11c) that

$$\underline{x}(R\tau) = -C_\mathrm{b}\sin(R\tau) + C_1R\tau + O(\frac{1}{R}) \quad (5.12a)$$

$$\underline{y}(R\tau) = C_2R\tau + O(\frac{1}{R}) \quad (5.12b)$$

where C_1 and C_2 are constants, and C_1 and C_2 should be zero as it is unlikely for $\underline{x}$ and $\underline{y}$ to grow infinitely with time. By substituting Eqs. (5.12a) and (5.12b) into Eqs. (5.11b) and (5.11d) and applying a fast-time-average operator $\frac{1}{2\pi}\int_0^{2\pi}(*)\mathrm{d}(R\tau)$ to Eqs. (5.11b) and (5.11d) as well as omitting the small quantity $O(\frac{1}{R})$, the new differential equations with respect to the slowly varying components $\overline{x}(\tau)$ and $\overline{y}(\tau)$ are,

$$\overline{x}'' + 2\zeta a_1\overline{x}' + 2\zeta a_2\overline{y}' + a_4\overline{x} + a_5\overline{y} + \left[\frac{1}{2\pi}\int_0^{2\pi}\mu\left(v - \omega_1\overline{x}' + \omega_1C_\mathrm{b}\cos R\tau\right)\mathrm{d}(R\tau)\right]\eta_3\overline{y} = 0 \quad (5.13a)$$

$$\overline{y}'' + 2\zeta a_2\overline{x}' + 2\zeta a_3\overline{y}' + a_5\overline{x} + a_6\overline{y} + \frac{F}{k_1} = 0 \quad (5.13b)$$

Because the amplitudes of the fast varying components are in the order of $\frac{1}{R}$, the behaviour of the overall system responses can be observed via the behaviour of the slowly varying components $\overline{x}(\tau)$ and $\overline{y}(\tau)$. By utilizing the friction law of Eq. (5.3), it is obtained that,

$$\frac{1}{2\pi}\int_0^{2\pi}\mu\left(v-\omega_1\overline{x}'+\omega_1 C_\mathrm{b}\cos(R\tau)\right)\mathrm{d}(R\tau)=$$

$$\begin{cases}\operatorname{sign}\left(v-\omega_1\overline{x}'\right)\mu_k & \left|v-\omega_1\overline{x}'\right|\geq\omega_1 C_\mathrm{b}\\ \left[-1+\frac{2}{\pi}\arccos\left(-\frac{v-\omega_1\overline{x}'}{\omega_1 C_\mathrm{b}}\right)\right]\mu_k & \left|v-\omega_1\overline{x}'\right|<\omega_1 C_\mathrm{b}\end{cases} \tag{5.14}$$

Converting Eq. (5.13) into the first-order differential equations and linearizing the differential equations at the equilibrium point, a Jacobian matrix with respect to $\overline{x}(\tau)$ and $\overline{y}(\tau)$ can be obtained as,

$$J=\begin{bmatrix}0 & 1 & 0 & 0\\ -a_4 & -2\zeta a_1 & -a_5-\mu_\mathrm{k}\eta_3 & 0\\ 0 & 0 & 0 & 1\\ -a_5 & -2\zeta a_2 & -a_6 & -2\zeta a_3\end{bmatrix},\quad \text{when } v\geq\omega_1 C_\mathrm{b} \tag{5.15a}$$

or,

$$J=\begin{bmatrix}0 & 1 & 0 & 0\\ -a_4 & -2\zeta a_1+\frac{2\mu_\mathrm{k}\omega_1}{\pi\sqrt{\omega_1^2 C_\mathrm{b}^2-v^2}}\eta_3\overline{y}_e & -a_5-\left[-1+\frac{2}{\pi}\arccos\left(-\frac{v}{\omega_1 C_\mathrm{b}}\right)\right]\mu_\mathrm{k}\eta_3 & 0\\ 0 & 0 & 0 & 1\\ -a_5 & -2\zeta a_2 & -a_6 & -2\zeta a_3\end{bmatrix},$$

$$\text{when } v<\omega_1 C_\mathrm{b} \tag{5.15b}$$

in which $\overline{y}_e$ is the normal displacement of the equilibrium point obtained from the differential equation Eq. (5.13). The stability of the system at the equilibrium point can be then revealed by the real parts of the eigenvalues of the Jacobian matrix. The range of the amplitude and frequency of the excitation where the system is stabilized is thus derived.

5.3 Slider-on-disc system

The configuration of the slider-on-disc system is illustrated in Fig. 5.2. It is a simplified model of a car brake system. The disc is modelled as a Kirchhoff plate clamped at inner boundary and free at outer boundary. The lumped-mass slider is constrained by fixtures consisting of a tangential spring k_1, an inclined spring k_3 at 45 degree to the tangential direction and dashpots c_1 and c_2 in the tangential and normal directions. Without loss of generality, the circumferential coordinate of the fixtures is set as $\theta=0$. The contact stiffness is represented by a linear spring k_2. The slider is assumed to be fixed radially at r_0 from the disc centre and pressed by a preload F that forces the

mass into frictional contact with the disc, which is rotating at the speed Ω. Likewise, a harmonic force $F_{\mathrm{d}}(t) = A\sin\omega t$ in the tangential direction is applied to the slider to suppress the friction-induced vibration of the system.

In this system, the vibration of the slider in the normal and tangential directions and the transverse vibration of the disc are considered. The equations of motion of the slider can be written as,

$$mr_0\ddot{\varphi} + c_1 r_0\dot{\varphi} + k_1 r_0\varphi + \frac{1}{2}k_3 r_0\varphi - \frac{1}{2}k_3 u = F_{\mathrm{f}} + A\sin\omega t \tag{5.16}$$

$$m\ddot{u} + c_2\dot{u} + k_2\big(u - w(r_0,\varphi,t)\big) - \frac{1}{2}k_3 r_0\varphi + \frac{1}{2}k_3 u = -F \tag{5.17}$$

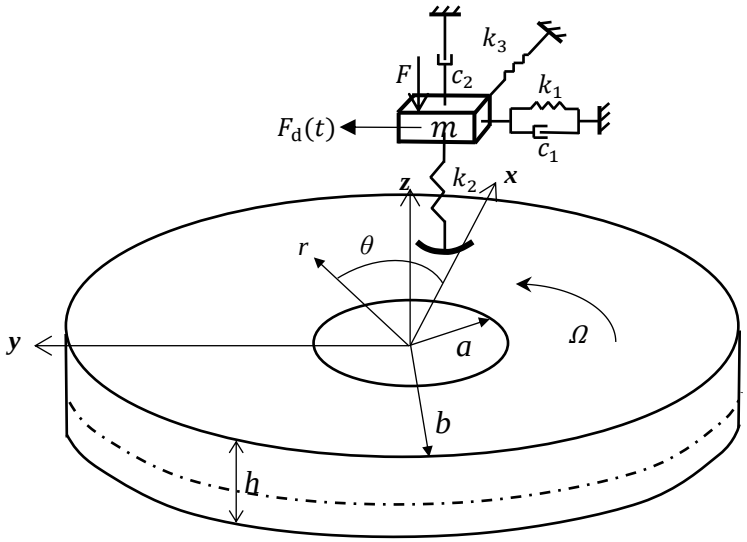

Figure 5.2 The slider-on-disc system.

where φ and u represent the angular displacement in the tangential direction and the translational displacement in the normal direction of the slider, respectively. $w(r_0,\varphi,t)$ denotes the transverse displacement of the disc at the polar coordinate (r_0,φ) in the space-fixed coordinate system, which is the location of the contact point at an arbitrary time t. F_{f} represents the friction force between the slider and the disc, $F_{\mathrm{f}} = \mu(v_{\mathrm{r}})N$, where $\mu(v_{\mathrm{r}})$ and N denote the coefficient of friction and the normal force, respectively. In many cases the friction force decreases with the increase in the relative velocity at low velocities, therefore the friction law with a negative friction-velocity slope [198] is considered here, i.e.,

$$\mu(v_{\mathrm{r}}) = \mathrm{sign}(v_{\mathrm{r}})\left[\mu_{\mathrm{k}} + (\mu_{\mathrm{s}} - \mu_{\mathrm{k}})\mathrm{e}^{-\alpha|v_{\mathrm{r}}|}\right] \tag{5.18}$$

where $v_{\mathrm{r}} = r_0(\Omega - \dot{\varphi})$, μ_{s} and μ_{k} are the coefficients of static and kinetic friction respectively. α determines the initial negative slope, and the friction law actually turns into the Coulomb law when $\alpha = 0$. And the normal force is expressed as,

$$N = k_2(w(r_0, \varphi, t) - u) \tag{5.19}$$

The transverse displacement of the disc can be approximated by a linear superposition of a set of orthogonal basis functions as,

$$w(r, \theta, t) = \sum_{k=0}^{\infty} \sum_{l=0}^{\infty} R_{kl}(r)[\cos(l\theta) \cdot C_{kl}(t) + \sin(l\theta) \cdot D_{kl}(t)] \tag{5.20}$$

where k and l denote the numbers of nodal circles and nodal diameters respectively, $C_{kl}(t)$, $D_{kl}(t)$ are modal coordinates, $R_{kl}(r)$ is a combination of Bessel functions satisfying the inner and outer boundary conditions of the nonrotating disc and orthogonality conditions. The equations of motion with respect to the modal coordinates can be obtained from Lagrange's equations,

$$\frac{\mathrm{d}}{\mathrm{d}t}\left[\frac{\partial L}{\partial \dot{C}_{kl}}\right] - \frac{\partial L}{\partial C_{kl}} = P_{kl}, k = 0,1,2,\ldots,\infty, l = 0,1,2,\ldots,\infty \tag{5.21}$$

$$\frac{\mathrm{d}}{\mathrm{d}t}\left[\frac{\partial L}{\partial \dot{D}_{kl}}\right] - \frac{\partial L}{\partial D_{kl}} = Q_{kl}, k = 0,1,2,\ldots,\infty, l = 1,2,\ldots,\infty \tag{5.22}$$

in which,

$$L = T - U \tag{5.23}$$

$$T = \frac{1}{2}\rho h \iint_S \left(\frac{\partial w(r,\theta,t)}{\partial t} + \Omega \frac{\partial w(r,\theta,t)}{\partial \theta}\right)^2 r\mathrm{d}r\mathrm{d}\theta \tag{5.24}$$

$$U = \frac{1}{2}D^* \iint_S (\nabla^2 w)^2 - 2(1-\nu)\left[\frac{\partial^2 w}{\partial r^2}\left(\frac{1}{r}\frac{\partial w}{\partial r} + \frac{1}{r^2}\frac{\partial^2 w}{\partial \theta^2}\right) - \left(\frac{1}{r}\frac{\partial^2 w}{\partial r \partial \theta} - \frac{1}{r^2}\frac{\partial w}{\partial \theta}\right)^2\right] r\mathrm{d}r\mathrm{d}\theta \tag{5.25}$$

$$P_{kl} = -N \cdot \frac{\partial w(r_0,\varphi,t)}{\partial C_{kl}} + M_\theta \frac{\partial \gamma}{\partial C_{kl}} \tag{5.26}$$

$$Q_{kl} = -N \cdot \frac{\partial w(r_0,\varphi,t)}{\partial D_{kl}} + M_\theta \frac{\partial \gamma}{\partial D_{kl}} \tag{5.27}$$

$$\gamma = \frac{\partial w(r_0,\varphi,t)}{r_0 \partial \theta} \tag{5.28}$$

In the above equations, T and U denote the kinetic energy and strain energy of the disc respectively, P_{kl} and Q_{kl} represent the generalized forces obtained from the virtual work of the normal contact force and bending moment acting on the disc. S is the area of the disc surface, ρ is the density of material, $D^* = \frac{Eh^3}{12(1-\nu^2)}$ is the bending rigidity,

E and ν are the Young's modulus and the Poisson's ratio of the disc material, respectively. The bending moment M_θ can be expressed as,

$$M_\theta = hF_f/2 \tag{5.29}$$

By substituting Eqs. (5.19), (5.20) and (5.29) into Eqs. (5.21)- (5.28), the equations of transverse vibration of the disc with respect to the modal coordinates can be derived,

$$M_{kl}\ddot{C}_{kl} + 2lM_{kl}\Omega\dot{D}_{kl} + (\omega_{kl}^2 M_{kl} - l^2 M_{kl}\Omega^2)C_{kl} = \left[-R_{kl}(r_0)\cos(l\varphi) - \frac{h}{2r_0}\mu(v_r)lR_{kl}(r_0)\sin(l\varphi)\right]\cdot \left[k_2\left(\sum_{k=0}^{\infty}\sum_{l=0}^{\infty}R_{kl}(r_0)\left(\cos(l\varphi)\cdot C_{kl}(t) + \sin(l\varphi)\cdot D_{kl}(t)\right) - u\right)\right] \tag{5.30a}$$

$$M_{kl}\ddot{D}_{kl} - 2lM_{kl}\Omega\dot{C}_{kl} + (\omega_{kl}^2 M_{kl} - l^2 M_{kl}\Omega^2)D_{kl} = \left[-R_{kl}(r_0)\sin(l\varphi) + \frac{h}{2r_0}\mu(v_r)lR_{kl}(r_0)\cos(l\varphi)\right]\cdot \left[k_2\left(\sum_{k=0}^{\infty}\sum_{l=0}^{\infty}R_{kl}(r_0)\left(\cos(l\varphi)\cdot C_{kl}(t) + \sin(l\varphi)\cdot D_{kl}(t)\right) - u\right)\right] \tag{5.30b}$$

in which ω_{kl} is the natural frequency of the mode with k nodal circles and l nodal diameters of the corresponding nonrotating plate, and

$$M_{kl} = \begin{cases} \rho h\pi \int_a^b R_{kl}^2(r) r\mathrm{d}r, & l = 1,2,\ldots \\ 2\rho h\pi \int_a^b R_{kl}^2(r) r\mathrm{d}r, & l = 0 \end{cases} \tag{5.31}$$

The equations of motion for the whole system are therefore the coupled equations consisting of Eqs. (5.16), (5.17) and (5.30). Similar to the 2-DoF frictional system, the analytical formulas to determine the range of the amplitude and frequency of the excitation where the system can be stabilized are derived.

By defining the following quantities and operator,

$$\tau = \omega_{cr}t,\ \omega_1 = \sqrt{k_1/m},\ \omega_2 = \sqrt{k_2/m},\ \omega_3 = \sqrt{k_3/m},\ \beta_i = \frac{\omega_i}{\omega_{cr}}(i = 1,2,3),\ \beta_{kl} = \frac{\omega_{kl}}{\omega_{cr}},\ \bar{\Omega} = \frac{\Omega}{\omega_{cr}},\ \gamma_{kl} = \frac{m}{M_{kl}},\ \zeta_i = \frac{c_i}{2\sqrt{mk_i}},\ B_d = \frac{A}{m\omega_{cr}^2},\ R = \frac{\omega}{\omega_{cr}},\ (*)' = \frac{\mathrm{d}(*)}{\mathrm{d}\tau} \tag{5.32}$$

The coupled differential equations Eqs. (5.16), (5.17) and (5.30) governing the motion of the slider-on-disc system can be rewritten as,

$$r_0\left(\varphi'' + 2\zeta_1\beta_1\varphi' + \beta_1^2\varphi + \frac{1}{2}\beta_3^2\varphi\right) - \frac{1}{2}\beta_3^2 u = \mu(v_r)\beta_2^2(w-u) + B_d\sin(R\tau) \tag{5.33}$$

$$u'' + 2\zeta_2\beta_2 u' + \beta_2^2(u-w) - \frac{1}{2}\beta_3^2 r_0\varphi + \frac{1}{2}\beta_3^2 u = \frac{-F}{m\omega_{cr}^2} \tag{5.34}$$

$$C_{kl}'' + 2l\bar{\Omega}D_{kl}' + (\beta_{kl}^2 - l^2\bar{\Omega}^2)C_{kl} = \gamma_{kl}\beta_2^2\left[-R_{kl}(r_0)\cos(l\varphi) - \frac{h}{2r_0}\mu(v_r)lR_{kl}(r_0)\sin(l\varphi)\right]\cdot \left(\sum_{k=0}^{\infty}\sum_{l=0}^{\infty}R_{kl}(r_0)[\cos(l\varphi)\cdot C_{kl} + \sin(l\varphi)\cdot D_{kl}] - u\right) \tag{5.35}$$

$$D_{kl}'' - 2l\bar{\Omega}C_{kl}' + (\beta_{kl}^2 - l^2\bar{\Omega}^2)D_{kl} = \gamma_{kl}\beta_2^2\left[-R_{kl}(r_0)\sin(l\varphi) + \frac{h}{2r_0}\mu(v_r)lR_{kl}(r_0)\cos(l\varphi)\right]\cdot \left(\sum_{k=0}^{\infty}\sum_{l=0}^{\infty}R_{kl}(r_0)[\cos(l\varphi)\cdot C_{kl} + \sin(l\varphi)\cdot D_{kl}] - u\right) \quad (5.36)$$

Suppose the solutions consist of a slowly varying component and a small-amplitude fast varying component, i.e.,

$$\varphi(\tau) = \overline{\varphi}(\tau) + \frac{1}{R}\underline{\varphi}(R\tau) \quad (5.37)$$

$$u(\tau) = \overline{u}(\tau) + \frac{1}{R}\underline{u}(R\tau) \quad (5.38)$$

$$C_{kl}(\tau) = \overline{C_{kl}}(\tau) + \frac{1}{R}\underline{C_{kl}}(R\tau) \quad (5.39)$$

$$D_{kl}(\tau) = \overline{D_{kl}}(\tau) + \frac{1}{R}\underline{D_{kl}}(R\tau) \quad (5.40)$$

Substituting Eqs. (5.37)-(5.40) into Eqs. (5.33)-(5.36) results in,

$$r_0\left[\left(\overline{\varphi}'' + R\frac{\mathrm{d}^2\underline{\varphi}}{\mathrm{d}(R\tau)^2}\right) + 2\zeta_1\beta_1\left(\overline{\varphi}' + \frac{\mathrm{d}\underline{\varphi}}{\mathrm{d}(R\tau)}\right) + \left(\beta_1^2 + \frac{1}{2}\beta_3^2\right)\left(\overline{\varphi} + \frac{1}{R}\underline{\varphi}\right)\right] - \frac{1}{2}\beta_3^2\left(\overline{u} + \frac{1}{R}\underline{u}\right) = \mu\beta_2^2\left[w - \left(\overline{u} + \frac{1}{R}\underline{u}\right)\right] + B_{\mathrm{d}}\sin R\tau \quad (5.41)$$

$$\left(\overline{u}'' + R\frac{\mathrm{d}^2\underline{u}}{\mathrm{d}(R\tau)^2}\right) + 2\zeta_2\beta_2\left(\overline{u}' + \frac{\mathrm{d}\underline{u}}{\mathrm{d}(R\tau)}\right) + \beta_2^2\left(\overline{u} + \frac{1}{R}\underline{u} - w\right) - \frac{1}{2}\beta_3^2 r_0\left(\overline{\varphi} + \frac{1}{R}\underline{\varphi}\right) + \frac{1}{2}\beta_3^2\left(\overline{u} + \frac{1}{R}\underline{u}\right) = \frac{-F}{m\omega_{\mathrm{cr}}^2} \quad (5.42)$$

$$\left(\overline{C_{kl}}'' + R\frac{\mathrm{d}^2\underline{C_{kl}}}{\mathrm{d}(R\tau)^2}\right) + 2l\bar{\Omega}\left(\overline{D_{kl}}' + \frac{\mathrm{d}\underline{D_{kl}}}{\mathrm{d}(R\tau)}\right) + (\beta_{kl}^2 - l^2\bar{\Omega}^2)\left(\overline{C_{kl}} + \frac{1}{R}\underline{C_{kl}}\right) = \gamma_{kl}\beta_2^2\left[-R_{kl}(r_0)\mathrm{cos}l\left(\overline{\varphi} + \frac{1}{R}\underline{\varphi}\right) - \frac{h}{2r_0}\mu lR_{kl}(r_0)\mathrm{sin}l\left(\overline{\varphi} + \frac{1}{R}\underline{\varphi}\right)\right]\cdot\left(\sum_{k=0}^{\infty}\sum_{l=0}^{\infty}R_{kl}(r_0)\left[\mathrm{cos}l\left(\overline{\varphi} + \frac{1}{R}\underline{\varphi}\right)\cdot\left(\overline{C_{kl}} + \frac{1}{R}\underline{C_{kl}}\right) + \mathrm{sin}l\left(\overline{\varphi} + \frac{1}{R}\underline{\varphi}\right)\cdot\left(\overline{D_{kl}} + \frac{1}{R}\underline{D_{kl}}\right)\right] - \left(\overline{u} + \frac{1}{R}\underline{u}\right)\right) \quad (5.43)$$

$$\left(\overline{D_{kl}}'' + R\frac{\mathrm{d}^2\underline{D_{kl}}}{\mathrm{d}(R\tau)^2}\right) - 2l\bar{\Omega}\left(\overline{C_{kl}}' + \frac{\mathrm{d}\underline{C_{kl}}}{\mathrm{d}(R\tau)}\right) + (\beta_{kl}^2 - l^2\bar{\Omega}^2)\left(\overline{D_{kl}} + \frac{1}{R}\underline{D_{kl}}\right) = \gamma_{kl}\beta_2^2\left[-R_{kl}(r_0)\mathrm{sin}l\left(\overline{\varphi} + \frac{1}{R}\underline{\varphi}\right) + \frac{h}{2r_0}\mu lR_{kl}(r_0)\mathrm{cos}l\left(\overline{\varphi} + \frac{1}{R}\underline{\varphi}\right)\right]\cdot\left(\sum_{k=0}^{\infty}\sum_{l=0}^{\infty}R_{kl}(r_0)\left[\mathrm{cos}l\left(\overline{\varphi} + \frac{1}{R}\underline{\varphi}\right)\cdot\left(\overline{C_{kl}} + \frac{1}{R}\underline{C_{kl}}\right) + \mathrm{sin}l\left(\overline{\varphi} + \frac{1}{R}\underline{\varphi}\right)\cdot\left(\overline{D_{kl}} + \frac{1}{R}\underline{D_{kl}}\right)\right] - \left(\overline{u} + \frac{1}{R}\underline{u}\right)\right) \quad (5.44)$$

By assuming $B_{\mathrm{d}} = C_{\mathrm{d}}R$ and grouping the terms of Eqs. (5.41)-(5.44) into the coefficients of R, 1, $\frac{1}{R}$, the following equations can be obtained when $R \gg 1$,

$$r_0\frac{\mathrm{d}^2\underline{\varphi}}{\mathrm{d}(R\tau)^2} - C_{\mathrm{d}}\sin(R\tau) = O\left(\frac{1}{R}\right),\ \frac{\mathrm{d}^2\underline{u}}{\mathrm{d}(R\tau)^2} = O\left(\frac{1}{R}\right),\ \frac{\mathrm{d}^2\underline{C_{kl}}}{\mathrm{d}(R\tau)^2} = O\left(\frac{1}{R}\right),\ \frac{\mathrm{d}^2\underline{D_{kl}}}{\mathrm{d}(R\tau)^2} = O\left(\frac{1}{R}\right) \quad (5.45)$$

$$r_0\left[\overline{\varphi}'' + 2\zeta_1\beta_1\left(\overline{\varphi}' + \frac{\mathrm{d}\varphi}{\mathrm{d}(R\tau)}\right) + \left(\beta_1^2 + \frac{\beta_3^2}{2}\right)\overline{\varphi}\right] - \frac{\beta_3^2}{2}\overline{u} - \mu(v_r)\beta_2^2\left[\sum_{k=0}^{\infty}\sum_{l=0}^{\infty}R_{kl}(r_0)\left(\mathrm{cos}l\left(\overline{\varphi} + \frac{1}{R}\underline{\varphi}\right)\cdot\overline{C_{kl}} + \mathrm{sin}l\left(\overline{\varphi} + \frac{1}{R}\underline{\varphi}\right)\cdot\overline{D_{kl}}\right) - \overline{u}\right] = O\left(\frac{1}{R}\right) \quad (5.46)$$

$$\overline{u}'' + 2\zeta_2\beta_2\left(\overline{u}' + \frac{\mathrm{d}u}{\mathrm{d}(R\tau)}\right) + \beta_2^2\left[\overline{u} - \sum_{k=0}^{\infty}\sum_{l=0}^{\infty}R_{kl}(r_0)\left(\mathrm{cos}l\left(\overline{\varphi} + \frac{1}{R}\underline{\varphi}\right)\cdot\overline{C_{kl}} + \mathrm{sin}l\left(\overline{\varphi} + \frac{1}{R}\underline{\varphi}\right)\cdot\overline{D_{kl}}\right)\right] - \frac{1}{2}\beta_3^2 r_0\overline{\varphi} + \frac{1}{2}\beta_3^2\overline{u} + \frac{F}{m\omega_{\mathrm{cr}}^2} = O\left(\frac{1}{R}\right) \quad (5.47)$$

$$\overline{C_{kl}}'' + 2l\bar{\Omega}\left(\overline{D_{kl}}' + \frac{\mathrm{d}D_{kl}}{\mathrm{d}(R\tau)}\right) + (\beta_{kl}^2 - l^2\bar{\Omega}^2)\,\overline{C_{kl}} - \gamma_{kl}\beta_2^2\left[-R_{kl}(r_0)\mathrm{cos}l\left(\overline{\varphi} + \frac{1}{R}\underline{\varphi}\right) - \frac{h}{2r_0}\mu(v_\mathrm{r})lR_{kl}(r_0)\mathrm{sin}l\left(\overline{\varphi} + \frac{1}{R}\underline{\varphi}\right)\right]\cdot$$
$$\left[\sum_{k=0}^{\infty}\sum_{l=0}^{\infty}R_{kl}(r_0)\left(\mathrm{cos}l\left(\overline{\varphi} + \frac{1}{R}\underline{\varphi}\right)\cdot\overline{C_{kl}} + \mathrm{sin}l\left(\overline{\varphi} + \frac{1}{R}\underline{\varphi}\right)\cdot\overline{D_{kl}}\right) - \overline{u}\right] = O\left(\frac{1}{R}\right) \quad (5.48)$$

$$\overline{D_{kl}}'' - 2l\bar{\Omega}\left(\overline{C_{kl}}' + \frac{\mathrm{d}C_{kl}}{\mathrm{d}(R\tau)}\right) + (\beta_{kl}^2 - l^2\bar{\Omega}^2)\,\overline{D_{kl}} - \gamma_{kl}\beta_2^2\left[-R_{kl}(r_0)\mathrm{sin}l\left(\overline{\varphi} + \frac{1}{R}\underline{\varphi}\right) + \frac{h}{2r_0}\mu(v_\mathrm{r})lR_{kl}(r_0)\mathrm{cos}l\left(\overline{\varphi} + \frac{1}{R}\underline{\varphi}\right)\right]\cdot$$
$$\left[\sum_{k=0}^{\infty}\sum_{l=0}^{\infty}R_{kl}(r_0)\left(\mathrm{cos}l\left(\overline{\varphi} + \frac{1}{R}\underline{\varphi}\right)\cdot\overline{C_{kl}} + \mathrm{sin}l\left(\overline{\varphi} + \frac{1}{R}\underline{\varphi}\right)\cdot\overline{D_{kl}}\right) - \overline{u}\right] = O\left(\frac{1}{R}\right) \quad (5.49)$$

It can be derived from (5.45) that,

$$\underline{\varphi}(R\tau) = -\frac{C_\mathrm{d}}{r_0}\sin(R\tau) + C_1R\tau + O(\frac{1}{R}) \quad (5.50a)$$

$$\underline{u}(R\tau) = C_2R\tau + O(\frac{1}{R}) \quad (5.50b)$$

$$\underline{C_{kl}}(R\tau) = C_3R\tau + O(\frac{1}{R}) \quad (5.50c)$$

$$\underline{D_{kl}}(R\tau) = C_4R\tau + O(\frac{1}{R}) \quad (5.50d)$$

where C_1, C_2, C_3 and C_4 are constants, and they should be zero as it is unlikely for the fast varying components to grow infinitely with time. By substituting Eqs. (5.50a)-(5.50d) into Eqs. (5.46)-(5.49) and applying a fast-time-average operator $\frac{1}{2\pi}\int_0^{2\pi}(*)\mathrm{d}(R\tau)$ to Eqs. (5.46)-(5.49) as well as omitting the small quantity $O(\frac{1}{R})$, the new differential equations with respect to the slowly varying components are,

$$r_0\left[\overline{\varphi}'' + 2\zeta_1\beta_1\overline{\varphi}' + \left(\beta_1^2 + \frac{1}{2}\beta_3^2\right)\overline{\varphi}\right] - \frac{1}{2}\beta_3^2\overline{u} - \beta_2^2f(\overline{\varphi}')\cdot\left[\sum_{k=0}^{\infty}\sum_{l=0}^{\infty}\left(\mathrm{cos}l\overline{\varphi}\cdot\overline{C_{kl}} + \mathrm{sin}l\overline{\varphi}\cdot\overline{D_{kl}}\right) - \overline{u}\right] = 0 \quad (5.51)$$

$$\overline{u}'' + 2\zeta_2\beta_2\overline{u}' + \beta_2^2\left[\overline{u} - \sum_{k=0}^{\infty}\sum_{l=0}^{\infty}R_{kl}(r_0)\left(\mathrm{cos}l\overline{\varphi}\cdot\overline{C_{kl}} + \mathrm{sin}l\overline{\varphi}\cdot\overline{D_{kl}}\right)\right] - \frac{1}{2}\beta_3^2r_0\overline{\varphi} + \frac{1}{2}\beta_3^2\overline{u} + \frac{F}{m\omega_\mathrm{cr}^2} = 0 \quad (5.52)$$

$$\overline{C_{kl}}'' + 2l\bar{\Omega}\overline{D_{kl}}' + (\beta_{kl}^2 - l^2\bar{\Omega}^2)\,\overline{C_{kl}} - \gamma_{kl}\beta_2^2\left[-R_{kl}(r_0)\mathrm{cos}l\overline{\varphi} - \frac{h}{2r_0}lR_{kl}(r_0)f(\overline{\varphi}')\mathrm{sin}l\overline{\varphi}\right]\cdot$$
$$\left[\sum_{k=0}^{\infty}\sum_{l=0}^{\infty}R_{kl}(r_0)\left(\mathrm{cos}l\overline{\varphi}\cdot\overline{C_{kl}} + \mathrm{sin}l\overline{\varphi}\cdot\overline{D_{kl}}\right) - \overline{u}\right] = 0 \quad (5.53)$$

$$\overline{D_{kl}}'' - 2l\bar{\Omega}\overline{C_{kl}}' + (\beta_{kl}^2 - l^2\bar{\Omega}^2)\,\overline{D_{kl}} - \gamma_{kl}\beta_2^2\left[-R_{kl}(r_0)\mathrm{sin}l\overline{\varphi} + \frac{h}{2r_0}lR_{kl}(r_0)f(\overline{\varphi}')\mathrm{cos}l\overline{\varphi}\right]\cdot$$
$$\left[\sum_{k=0}^{\infty}\sum_{l=0}^{\infty}R_{kl}(r_0)\left(\mathrm{cos}l\overline{\varphi}\cdot\overline{C_{kl}} + \mathrm{sin}l\overline{\varphi}\cdot\overline{D_{kl}}\right) - \overline{u}\right] = 0 \quad (5.54)$$

where $f(\overline{\varphi}') = \frac{1}{2\pi}\int_0^{2\pi}\mu(\Omega - \omega_\mathrm{cr}\overline{\varphi}' + \frac{\omega_\mathrm{cr}C_\mathrm{d}}{r_0}\cos(R\tau))\mathrm{d}(R\tau)$. It is difficult to derive the analytical solution of the integral here, therefore the Gaussian quadrature [199] is utilized to obtain the function values of $f(\overline{\varphi}')$. Furthermore, the derivative of $f(\overline{\varphi}')$ at $\overline{\varphi}' = 0$ can be obtained by the finite difference method [185]. Subsequently Eqs. (5.51)-(5.54) can be linearized at the equilibrium point and the Jacobian matrix is extracted from the linearized system, whose eigenvalues indicate the stability of the

system at the equilibrium point, i.e., if the self-excited vibration will happen, when the harmonic excitation is applied.

5.4 Numerical study

In this section, a detailed numerical study is conducted to demonstrate the effect of tangential harmonic excitation in suppressing the friction induced vibration of the 2-DoF system and the slider-on-disc system. For the determination of the parameter range that will suppress the friction induced vibration of the systems, the results obtained both from the analytical method and from the time domain integration by the Runge-Kutta algorithm are presented. To avoid the numerical difficulty brought about by the discontinuity at the zero relative velocity of the discontinuous type of friction laws, the smooth functions [30, 75] that can accurately describe the behaviour of the discontinuous systems are used to approximate the discontinuous friction forces in the calculation of the time responses. In this paper, the smooth functions used are $\mu(v_{\mathrm{r}}) = \mu_{\mathrm{k}} \tanh(\sigma v_{\mathrm{r}})$ in the 2-DoF frictional system and $\mu(v_{\mathrm{r}}) = \left[\mu_{\mathrm{k}} + (\mu_{\mathrm{s}} - \mu_{\mathrm{k}})\mathrm{e}^{-\alpha|v_{\mathrm{r}}|}\right] \tanh(\sigma v_{\mathrm{r}})$ in the slider-on-disc system, respectively. σ is the smoothness factor and its value is set as 50 in all the time responses simulations of both systems.

5.4.1 Numerical study of the 2-DoF frictional system

In the numerical examples for the 2-DoF friction system, the basic system parameters assigned with constant values are: $m = 1$, $\alpha_1 = 30^{\circ}$, $\alpha_2 = 45^{\circ}$, $k_1 = 1$, $k_2 = 0.5$, $k_3 = 0.5$, $c_1 = 0.001$, $c_2 = 0.001$, $F = 2$. Firstly the dynamics of the original system, i.e. when the tangential harmonic excitation is not applied, is examined. The eigenvalues of the Jacobian matrix of the original system as a function of μ_k are shown in Fig. 5.3, which reflects the local stability of the system at the equilibrium point. If there exists an eigenvalue with a positive real part, the equilibrium point is unstable and the system exhibits growing self-excited vibration. It is clearly shown that the mode-coupling instability appears at the onset of a positive real part and the merging of imaginary parts in the original frictional system. And the equilibrium point of the system becomes destabilized when μ_{k} is larger than its critical value 0.37. Fig. 5.4 displays the time histories of the tangential and normal displacements of the original system at $\mu_{\mathrm{k}} = 0.4$ and $\mu_{\mathrm{k}} = 0.7$, where it can be seen that the amplitudes of the dynamic responses, especially the normal displacement of the mass, grow with time

until the mass separates with the disc (when $y > 0$). Then the mass will re-contact with and separate from the belt repetitively, as has been observed in [97]. The time histories after separation are not shown here as the present work is devoted to suppressing the friction induced vibration of the system by means of tangential harmonic excitation.

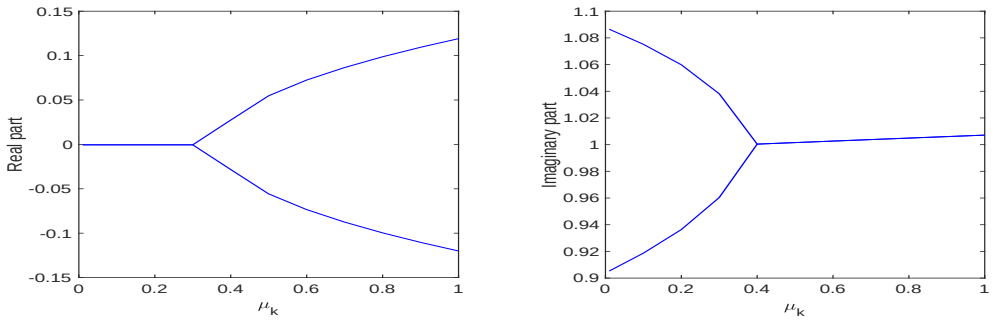

Figure 5.3 Eigenvalues of Jacobian matrix of the original system as a function of μ_k.

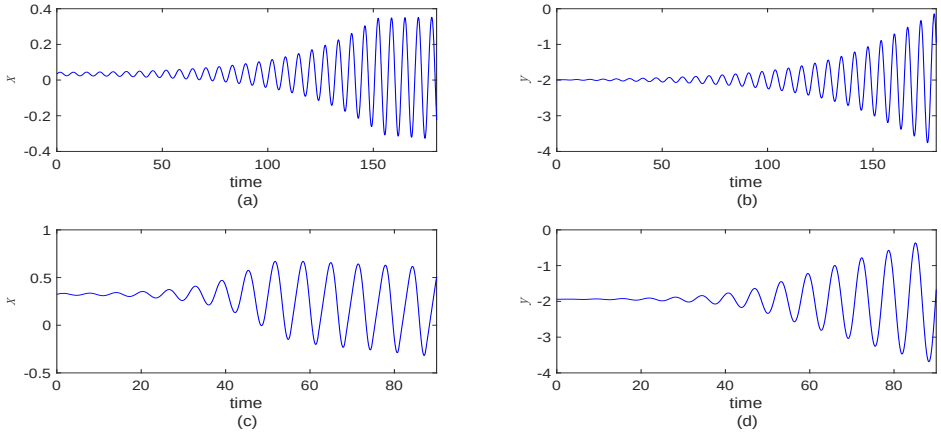

Figure 5.4 The time histories of tangential and normal displacements of the original system when μ_k is larger than its critical value: (a) (b) $\mu_k = 0.4$; (c) (d) $\mu_k = 0.7$.

Then the dynamic responses of the system under the above two values of μ_k in the presence of the harmonic excitation with appropriate amplitude and frequency are shown in Fig. 5.5, from which it is observed that although the amplitudes of the dynamic responses are increased in the initial stage under the influence of the external excitation, they are greatly attenuated in the steady-state phase, especially for the normal displacements of the mass. These two cases demonstrate the effectiveness of the tangential harmonic excitation in suppressing the friction induced self-excited vibration of the system.

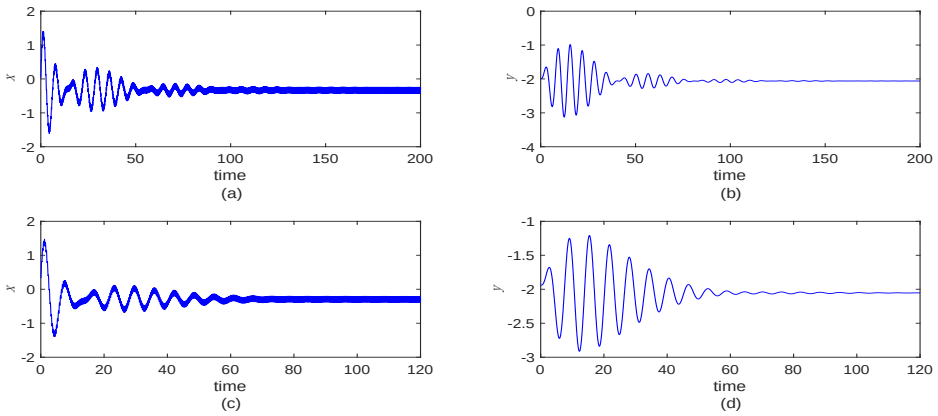

Figure 5.5 The dynamic responses of the system after application of the harmonic excitation with amplitude $A_{\mathrm{b}} = 35$ and frequency ratio $R = \frac{\omega}{\omega_1} = 20$: (a) (b) $\mu_{\mathrm{k}} = 0.4$; (c) (d) $\mu_{\mathrm{k}} = 0.7$. (The belt velocity is 0.3).

Next the range of the amplitude and frequency of the harmonic excitation to stabilize the frictional system is derived. The results obtained from the analytical method and from the extensive time response simulations are compared, as shown in Fig. 5.6. In this figure, the region above each curve incorporates the parameter combinations to stabilize the system under the specific coefficient of friction (greater than the critical value). It is seen that there is fairly good agreement between the stability boundaries obtained from the analytical method and from the time response simulations when the frequency ratio ($R = \omega/\omega_1$) is sufficiently large. Besides, it should be noted here the mode-coupling instability of the original system is not dependent on belt velocity v, which, however, has an effect on the stability boundary for the harmonic excitation. Fig. 5.7 shows the range of the amplitude and frequency of the harmonic excitation to stabilize the system under three different values of belt velocity, from which it is observed that a larger-amplitude excitation is needed to suppress the unstable vibration of the frictional system in the situation of higher belt velocity.

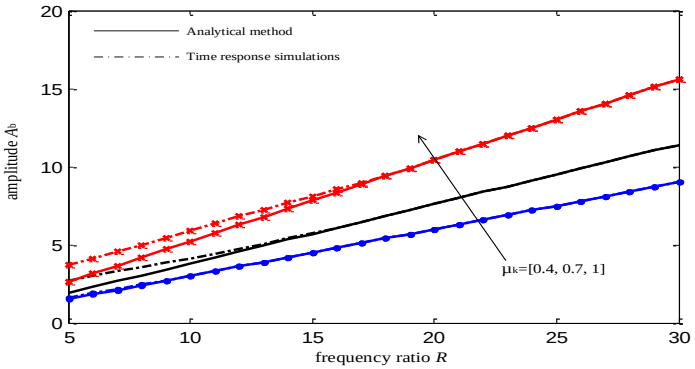

Figure 5.6 The range of the amplitude and frequency of the harmonic excitation to stabilize the system obtained from both the analytical method and the extensive time response simulations. ($v = 0.3$, the parameter range to stabilize the system is above the corresponding curve).

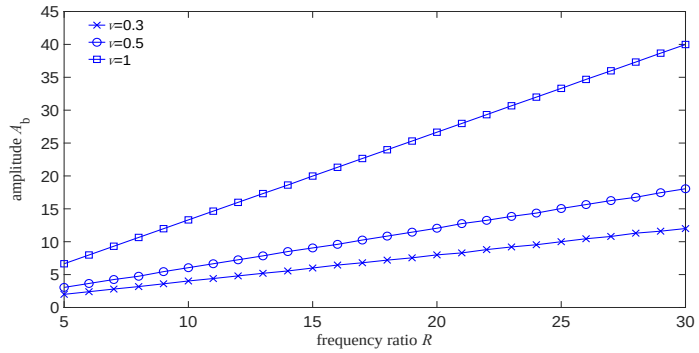

Figure 5.7 The range of the amplitude and frequency of the harmonic excitation to stabilize the system under three different values of belt velocity ($\mu_{\mathrm{k}} = 0.7$, the parameter range to stabilize the system is above the corresponding curve).

5.4.2 Numerical study of the slider-on-disc system

The basic system parameters whose values are constant in the numerical examples are listed in Table 5.1. It should be noted that numbers *k* and *l* in the expression of the transverse displacement of the disc can be chosen to include as many modes as needed to represent the dynamics of the system with acceptable accuracy. To avoid excessive computations, the modal series in Eq. (5.20) are truncated at suitable values of *k* and *l*. The first seven natural frequencies of the disc are 1492, 1517, 1517, 1824, 1824, 2774 and 2774 rad/s and the critical speed of the disc is $\omega_{\mathrm{cr}} = \frac{1824}{2} = 912$ rad/s. It is found that the first seven disc modes (one single mode with zero nodal circle and zero nodal

diameter and three pairs of doublet modes with zero nodal circle and one, two or three nodal diameters) are adequate in terms of the convergence of the results.

Table 5.1 The values of constant parameters of the slider-on-disc system

a	b	r_0	ρ	E	h	ν
0.044 m	0.12 m	0.1 m	7200 kg/m^3	150 GPa	0.002 m	0.211
m	k_1	k_2	k_3	c_1	c_2	
1 kg	10^5N/m	$5 \cdot 10^4$N	$6 \cdot 10^4$N/m	5 N · s/m	5 N · s/m	

Firstly, the dynamic characteristics of the original system (when the tangential harmonic excitation is not applied) is analysed. The dynamic instability in the original system can be contributed by three factors, i.e. the negative slope in the friction force-relative velocity relationship, the mode coupling instability of the normal and tangential motion of the slider and the effect of moving load which causes speed-dependent instability, all of which the frictional systems may encounter in practice [3, 200]. The local stability of the system at the sliding equilibrium can be used to evaluate if the self-excited vibration will be generated, which is studied in the following procedures.

First of all, the sliding equilibrium of this system is found by solving the algebraic nonlinear equations derived from setting all the terms involving velocity and acceleration in the coupled equations Eqs. (5.16), (5.17) and (5.30) to be zero. In the second step, the nonlinear coupled equations governing the motion of the system are linearized at the sliding equilibrium and the Jacobian matrix is extracted from the linearized system. In the last step, the eigenvalues of the Jacobian matrix are calculated to reveal the local stability of the system at the sliding equilibrium for various values of parameters. Fig. 5.8 plots the regions of instability (RI) dependent on the normal preload versus the disc speed under three different values of the coefficients of friction. In Fig. 5.8(a) when $\alpha = 0$, the coefficients of friction are set as constant at $\mu(v_r) = \mu_s = 1$, the dynamic instability stems from only the moving load which causes instability as disc speed $\Omega > 10.5$ rad/s. In Fig. 5.8(b), the coefficients of friction are not large enough to bring about the mode-coupling instability, but the large negative slope of the friction-velocity relationship in the vicinity of zero relative velocity and the moving load lead to the dynamic instability in low and high disc speeds,

respectively. In Fig. 5.8(c), the mode-coupling instability exists, therefore the dynamic instability occurs in the system independent of the normal preload and disc speed.

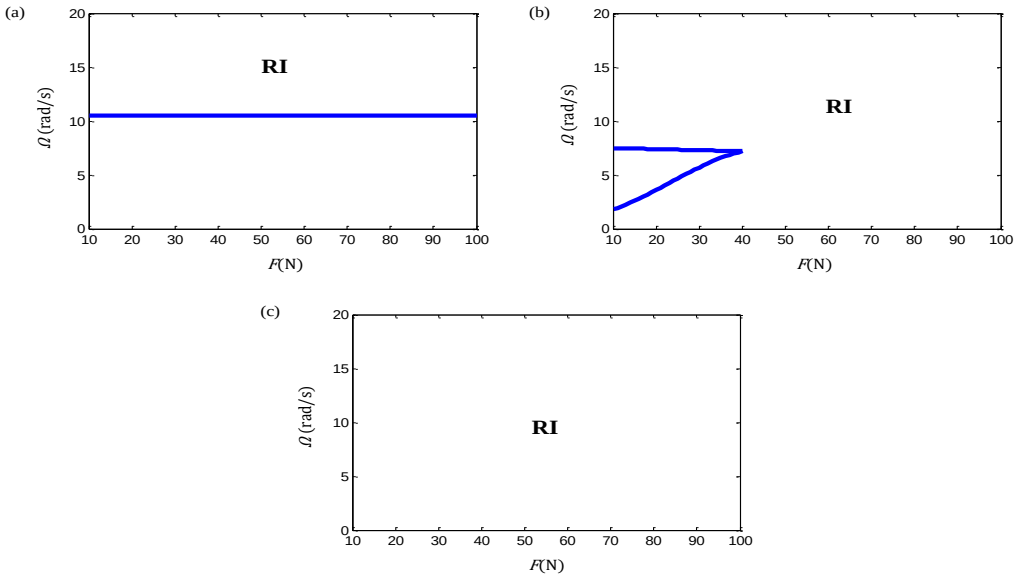

Figure 5.8 Region of instability of normal preload vs disc speed in three cases of friction coefficients: (a) $\mu_s = 1$, $\alpha = 0$, (b) $\mu_s = 1.5$, $\mu_k = 1.2$, $\alpha = 1$, (c) $\mu_s = 2.25$, $\mu_k = 2$, $\alpha = 1$.

The time histories of the dynamic responses of the system with two sets of parameters whose values are in the region of instability are displayed in Fig. 5.9, where the friction induced self-excited vibration is clearly exhibited in the two cases. It should be noted that since the interest here is only to identify the occurrence of friction induced vibration in the original system, the behaviour of separation and re-contact between the slider and the disc is not considered, which thus allows the dynamic responses to grow boundlessly. Then the dynamic responses of the system for the two cases after application of the tangential harmonic excitation with appropriate amplitude and frequency are shown in Fig. 5.10, which obviously indicates that the friction induced vibration in the original system is suppressed by the high-frequency tangential harmonic excitation.

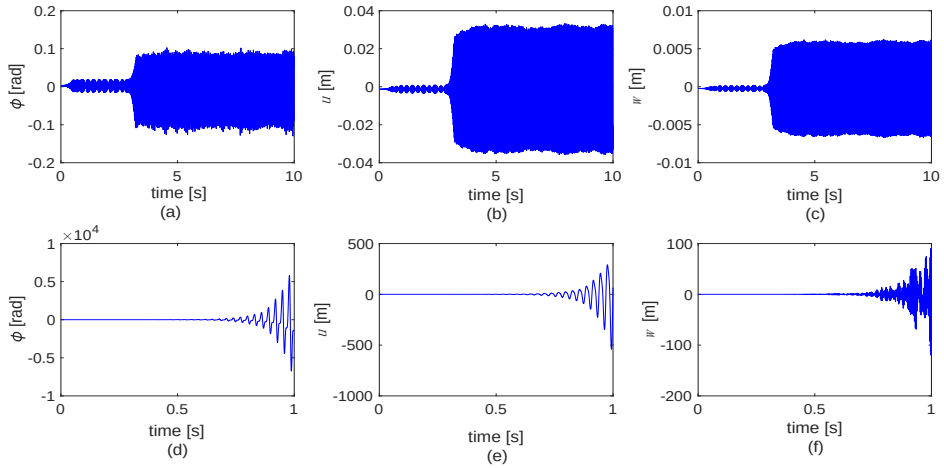

Figure 5.9 The dynamic responses when $F = 100\text{N}$ and $\Omega = 5\text{rad}/s$ including the angular displacement of the slider in the tangential direction, the normal displacement of the slider and the transverse displacement of the disc at the point $(r_0, 0)$: (a)-(c) $\mu_s = 1.5$, $\mu_k = 1.2$, $\alpha = 1$; (d)-(f) $\mu_s = 2.25$, $\mu_k = 2$, $\alpha = 1$.

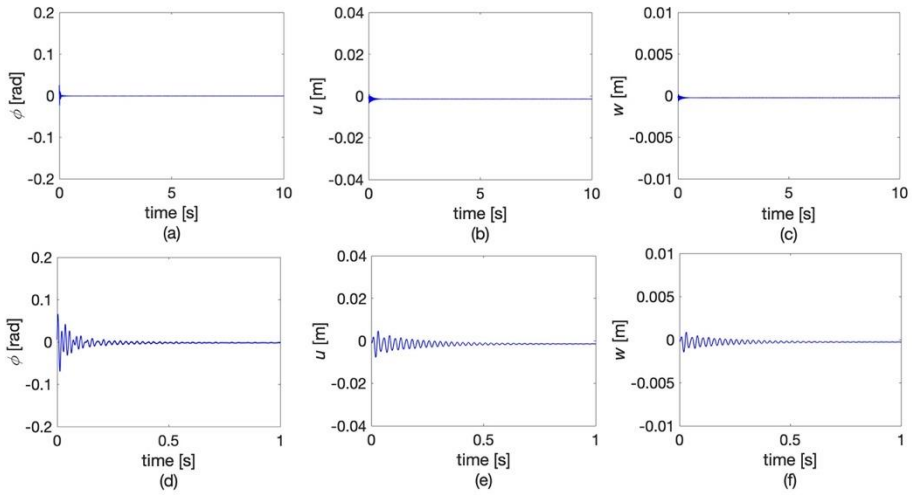

Figure 5.10 The dynamic responses of system after application of the harmonic excitation for the two cases in Fig. 5.9: (a)-(c) for the first case with the excitation amplitude $A = 2{\cdot}10^4$ N and frequency ratio $R = \frac{\omega}{\omega_{cr}} = 22$; (d)-(f) for the second case with the excitation amplitude $A = 5{\cdot}10^4$ N and frequency ratio $R = \frac{\omega}{\omega_{cr}} = 22$.

Next the ranges of the amplitude and frequency of the harmonic excitation to suppress the friction induced vibration of the system are derived, when the values of system parameters are identical to those in Fig. 5.9. Both the results obtained from the analytical method and from time responses simulations are shown for the first case in Fig. 5.11(a) and second case in Fig. 5.11(b), where good agreements between the

results from the two approaches are observed for both cases when the frequency ratio is sufficiently large. It can thus be concluded that the analytical method is a reliable approach, while the time responses simulations can also be performed for verification in the practical applications. Besides, the regions of instability of the original system shown in Fig. 5.8 can be greatly diminished by application of the tangential harmonic excitation with appropriate amplitude and frequency, as depicted in Fig. 5.12.

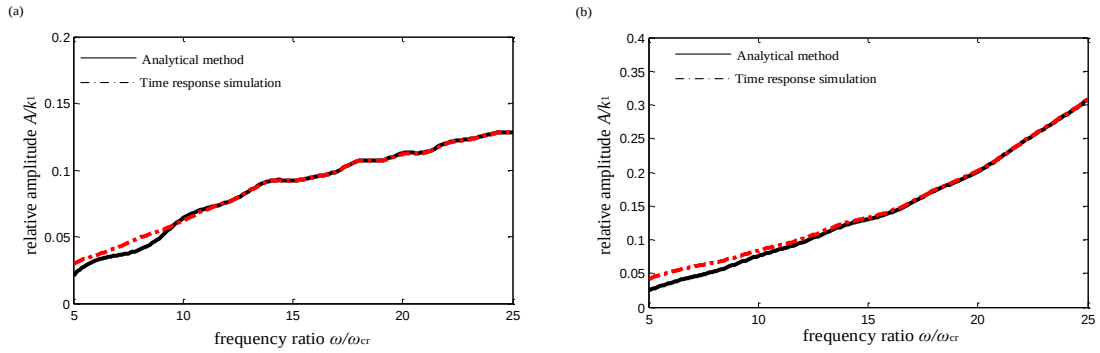

Figure 5.11 Range of amplitude and frequency of the harmonic excitation to suppress the friction induced vibration of the system: (a) the first case (b) the second case. (The range to suppress the friction induced vibration is above the corresponding curve).

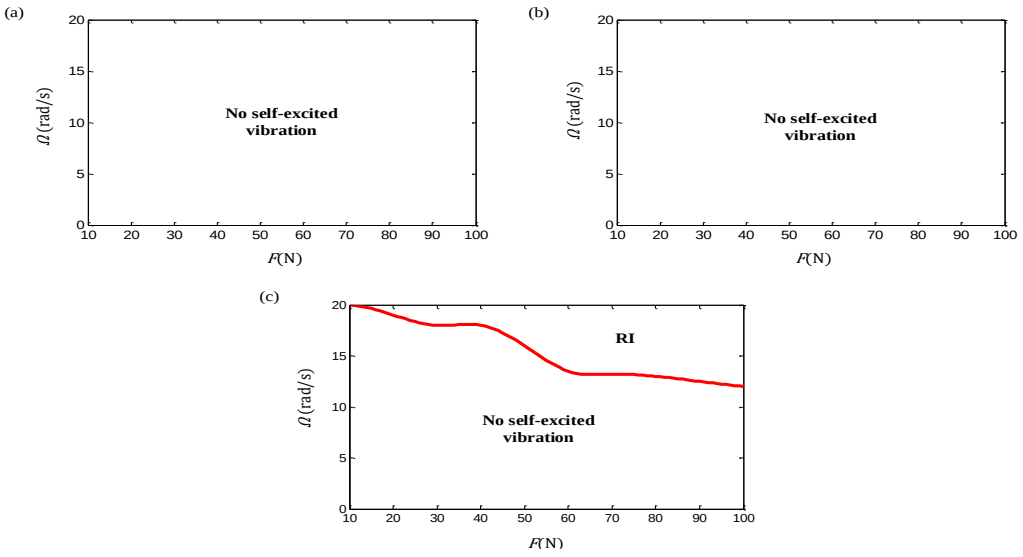

Figure 5.12 Region of instability in three cases of friction coefficients in application of the harmonic excitation with the amplitude $A = 5{\cdot}10^4$ N and frequency ratio $R = 20$: (a) $\mu_s = 1$, $\alpha = 0$, (b) $\mu_s = 1.5$, $\mu_k = 1.2$, $\alpha = 1$, (c) $\mu_s = 2.25$, $\mu_k = 2$, $\alpha = 1$.

It should be noted here the application of high-frequency tangential excitation with considerable amplitude will cause the reversal of relative velocity and thus the reversal

of friction force, i.e., the friction force will be in both directions rather than in a single direction during the process. The reversal of friction force may affect the braking capacity when applying the high-frequency tangential excitation to suppress the noise in brake systems, which is worth careful attention. As for brake squeal, since it tends to occur at very low disc speeds when a car nearly comes to a stop, the friction force reversal should not be an issue.

5.5 Conclusions

In this chapter, the friction induced vibration of a two-degree-of-freedom mass-on-belt system and a complicated slider-on-disc system, as well as the application of the harmonic excitation in the direction tangential to the friction interface for suppressing the friction induced vibration in the systems, are studied. In the multi-degree-of-freedom frictional systems, there is one or several friction-related factors, e.g., the mode-coupling instability, the negative slope in the friction force-relative velocity relationship, the moving load, contributing to the occurrence of self-excited vibration. The results show the tangential harmonic excitation with appropriate amplitude and frequency is very effective in suppressing the friction induced self-excited vibration of the systems. The ranges of the amplitude and frequency of the harmonic excitation that stabilize the friction systems are obtained by both an analytical method and extensive time response simulations. The results by the two approaches are in good agreement when the ratio between the excitation frequency and the reference frequency (associated with a natural frequency of the system and in the same order as it) is sufficiently large. This research provides theoretical guidance for applying the tangential harmonic excitation to suppress the friction induced vibration in real mechanical systems such as the disc brake system. In practice, piezoactuators are usually used to drive the brake pad into high-frequency tangential vibration to suppress squeal, which use voltage as input. Therefore, some experimental tests must be carried out to establish the correlation between the amplitudes of the external excitation in the numerical simulations and the amplitudes of the input voltage for the piezoactuators in the practical application.

Chapter 6

Friction induced vibration considering multiple types of nonlinearities

The friction induced vibration of a novel 5-DoF (degree-of-freedom) mass-on-oscillating-belt model considering multiple types of nonlinearities is studied in this chapter. The first type of nonlinearity in the system is the nonlinear contact stiffness, the second is the non-smooth states of motion including stick, slip and separation, and the third is the geometrical nonlinearity brought about by the moving-load feature of the mass slider on the rigid belt. Both the linear stability of the system and the nonlinear steady-state responses are investigated. The numerical results indicate the necessity of the transient dynamic analysis in the study of friction-induced-vibration problems as the linear stability analysis fails to detect the occurrence of self-excited vibration when two stable solutions coexist in the system. The bifurcation behaviour of the steady-state responses of the system versus some parameters is determined. The significant effects of each type of nonlinearity on the linear stability and nonlinear steady-state responses of the system are discovered. Moreover, a similar study is conducted on a continuous slider-on-disc model.

6.1 Introduction

There are two main categories of methods for the analysis of friction-induced-vibration problems, i.e., the complex eigenvalue analysis (CEA) and the transient dynamic analysis (TDA). The linear complex eigenvalue approach is often employed for the stability analysis of the steady sliding state. If at least one of the eigenvalues of the linearized system has positive real part, the steady sliding state becomes unstable and

the system will show self-excited vibration. Hoffmann et al. [55] used a 2-DoF model to clarify the mechanism of mode-coupling instability of friction induced vibration. It was observed that as the friction coefficient increases, the imaginary parts of eigenvalues coalesce and one real part becomes positive, which indicates the occurrence of self-excited vibration in the system. Ouyang and Mottershead [201] introduced the velocity-dependent friction with the Stribeck effect into the moving load model for the vibration of a car disc brake. The dynamic instability of the system was identified by solving a nonlinear complex eigenvalue problem. Kang [202] analytically investigated the mode-coupling instability of a stationary disc and two stationary brake pads with circumferential friction under steady-sliding condition. Liu et al. [203] investigated the effects of key parameters on the dynamic instability of a finite element brake model by employing the CEA method. Because the CEA allows all unstable eigenvalues to be found in one run and is thus computationally efficient, it becomes a standard analysis tool to predict brake squeal propensity in industry [204-206].

The transient dynamic analysis of friction induced vibration has been performed by numerous researchers. Li et al. [97] examined the dynamics of a 2-DoF model with nonlinear contact stiffness and the effects of separation and reattachment on the vibration amplitudes of dynamic responses were studied. Sinou [142] studied the transient and stationary self-excited vibration in a nonlinear finite element model of a disc brake. Soobbarayen et al. [143] presented a numerical analysis of the influence of the loading conditions on the vibration and acoustic responses of a finite element model. The numerical results showed that a sufficiently fast ramp loading can destabilize a stable configuration predicted by the stability analysis. Papangelo et al. [33] investigated the subcritical bifurcation of a slider-on-belt system in the case of a weakening-strengthening friction law, and the results showed that there was a range of the belt velocity where two stable solutions coexisted, i.e., a stable sliding equilibrium and a stable stick-slip limit cycle. Zhang et al. [98] examined the dynamics of a 4-DoF friction oscillator and found the CEA under-predicts the instability of the system due to its inability to detect the subcritical Hopf bifurcation. From the studies above, the drawbacks of the CEA method for the analysis of nonlinear friction induced vibration can be observed. Firstly, the CEA may miss the dynamic instabilities in some situations, e.g., when subcritical Hopf bifurcation exists. Secondly, the real part and

imaginary part of an unstable eigenvalue does not necessarily describe the amplitude and frequency of the steady-state response of the system.

The nonlinearities in friction-induced-vibration problems can originate from multiple sources, e.g., nonlinear contact stiffness [97,98,142,173,207], non-smooth behaviours including stick/slip and contact/separation [4,163,208-210]. Although quite a few published papers on friction induced vibration took the nonlinearities into account, a comprehensive study of the effects of multiple types of nonlinearities on the friction induced self-excited vibration is still lacking. In this chapter, the dynamics of a 5-DoF friction-excited slider-on-moving-belt model is firstly studied, in which three representative types of nonlinearities in the friction-induced-vibration problems are present. The first type of nonlinearity is the nonlinear contact stiffness, the second is the non-smooth states of motion including stick, slip and separation, and the third is the geometrical nonlinearity brought about by the moving-load feature of the slider on the belt. Both the linear stability of the system and the steady-state responses are investigated by means of the CEA and the TDA, respectively. Subsequently a similar study on a continuous slider-on-disc model is also done.

The rest of the chapter is arranged as follows. In Section 6.2 the system configuration of the slider-on-belt model is introduced and the equations of motion for the system in three different states: slip, stick and separation are derived. The conditions for the transitions among these states are determined. In Section 6.3 the procedures of the linear stability analysis of the discrete system and the numerical simulation scheme of the transient dynamic analysis are stated. In Section 6.4 the numerical study of the linear stability and nonlinear steady-state responses of the discrete system is conducted, where the effects of each type of nonlinearity are examined. In Section 6.5 the effects of multiple nonlinearities on the dynamics of slider-on-disc model are investigated. Finally in Section 6.6 the important conclusions are reached.

6.2 The mechanical model and dynamic equations

The model of the 5-DoF frictional system is shown in Fig. 6.1, which consists of two parts, i.e., the mass slider and the belt. The point mass slider, with mass *M*, is constrained by a spring k_1 and a damper c_1 in the horizontal direction and a damper c_2 in the vertical direction. Besides, a spring k_3 at 45 degree relative to the horizontal

direction, which couples the vibration in the two directions, is connected to the slider. The belt, with mass m and rotational inertia about the mass centre J, is moving at a constant speed v around two wheels what are constrained by a set of spring-damper system (k_4, c_4) in the horizontal direction and two sets of spring-damper systems (k_5, c_5 and k_6, c_6) in the vertical direction. The vertical spring-damper systems, which are located at the centres of the two wheels at distances l_1 and l_2 from the mass centre of the belt, respectively, also constrain the rotational motion of the belt. A preload F is applied to press the slider to be in frictional contact with the moving belt, and Coulomb's law of friction is utilized to model the friction force on the interface. The contact between the slider and the belt is assumed to be unilateral, and a combination of a linear spring k_2 and a nonlinear spring k_{nl} with cubic stiffness is used to model the contact stiffness. In this model, the horizontal and vertical motion of the slider, as well as the horizontal, vertical and rotational motion of the belt, are investigated. Without loss of generality, the slider is assumed to be right above the mass centre of the belt at zero displacements.

The equations of motion of the 5-DoF system can be written as,

$$\begin{cases} M\ddot{x}_1 + c_1\dot{x}_1 + k_1x_1 + \frac{1}{2}k_3x_1 - \frac{1}{2}k_3y_1 = F_{\mathrm{T}} \\ M\ddot{y}_1 + c_2\dot{y}_1 - \frac{1}{2}k_3x_1 + \frac{1}{2}k_3y_1 + F = F_{\mathrm{N}} \\ m\ddot{x}_2 + c_4\dot{x}_2 + k_4x_2 = -F_{\mathrm{T}} \\ m\ddot{y}_2 + c_5(\dot{y}_2 + l_1\dot{\varphi}) + k_5(y_2 + l_1\varphi) + c_6(\dot{y}_2 - l_2\dot{\varphi}) + k_6(y_2 - l_2\varphi) = -F_{\mathrm{N}} \\ J\ddot{\varphi} + c_5(\dot{y}_2 + l_1\dot{\varphi})l_1 + k_5(y_2 + l_1\varphi)l_1 - c_6(\dot{y}_2 - l_2\dot{\varphi})l_2 - k_6(y_2 - l_2\varphi)l_2 = F_{\mathrm{N}}(x_1 - x_2) \end{cases} \tag{6.1}$$

where F_{T} and F_{N} represent the tangential friction force and the normal force between the slider and the belt, respectively. As the system may experience non-smooth states of motion including slip, stick and separation, F_{T} and F_{N} will take different forms in distinct states of motion.

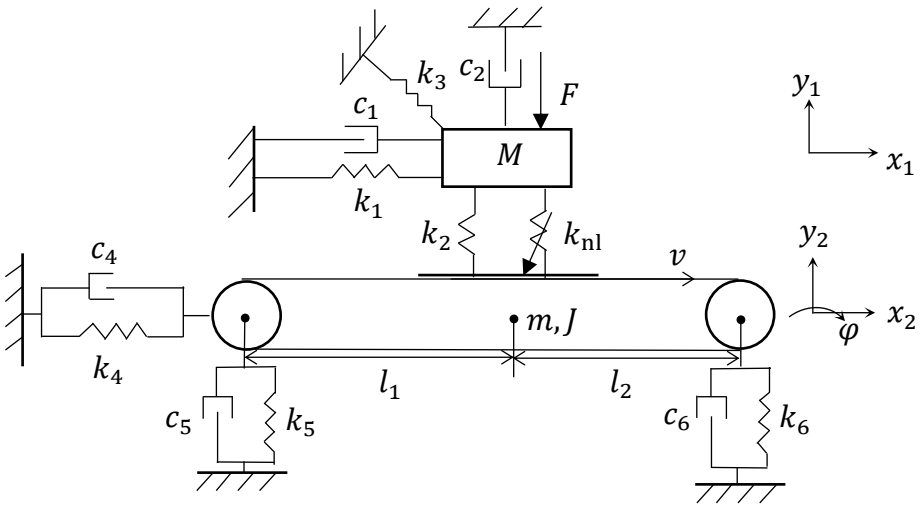

Figure 6.1 The model of the 5-DoF frictional system.

When the slider is in contact with the belt, in the states of slip and stick, the normal force is the resultant force of the linear spring k_2 and the nonlinear spring k_{nl}, i.e.,

$$F_{\mathrm{N}} = k_2(y_2 - (x_1 - x_2)\varphi - y_1) + k_{\mathrm{nl}}(y_2 - (x_1 - x_2)\varphi - y_1)^3 \tag{6.2}$$

The friction force takes different forms in the states of slip and stick. In the state of slip, the friction force is expressed as,

$$F_{\mathrm{T}} = \mathrm{sgn}(v_{\mathrm{r}})\mu_{\mathrm{k}}F_{\mathrm{N}} \tag{6.3}$$

where $v_{\mathrm{r}} = v + \dot{x}_2 - \dot{x}_1$ and μ_{k} is the coefficient of kinetic friction. The condition for the system to stay in the state of slip is,

$$\begin{cases} v_{\mathrm{r}} \neq 0 \\ F_{\mathrm{N}} > 0 \end{cases} \tag{6.4}$$

In the state of stick, the friction force serves to sustain the relative static state, i.e., $v_{\mathrm{r}} = 0$, and thus can be obtained from the equations of motion of the system, Eq. (6.1). As the absolute belt velocity here is $v + \dot{x}_2$, which is not known a priori, the tangential velocity of the slider $\dot{x}_1$ during sticking is not known a priori either. In the following, a method to derive the state variables and the friction force during sticking is presented.

Firstly, it is obtained from $v_{\mathrm{r}} = 0$ that,

$$\begin{cases} \dot{x}_2 = \dot{x}_1 - v \\ \ddot{x}_2 = \ddot{x}_1 \\ x_2(t) = x_1(t) - x_1(t_{\mathrm{s}}) - v \times (t - t_{\mathrm{s}}) + x_2(t_{\mathrm{s}}) \end{cases} \tag{6.5}$$

where t_s is the time at the onset of stick. Then, by adding the third equation in Eq. (6.1) into the first equation in Eq. (6.1), it is obtained that,

$$M\ddot{x}_1 + m\ddot{x}_2 + c_1\dot{x}_1 + c_4\dot{x}_2 + \left(k_1 + \frac{1}{2}k_3\right)x_1 - \frac{1}{2}k_3y_1 + k_4x_2 = 0 \tag{6.6}$$

By substituting Eq. (6.5) into Eq. (6.6), the terms involving x_2, $\dot{x}_2$, $\ddot{x}_2$ in Eq. (6.6) can be eliminated, i.e.,

$$(M+m)\ddot{x}_1 + (c_1+c_4)\dot{x}_1 + \left(k_1 + \frac{1}{2}k_3 + k_4\right)x_1 - \frac{1}{2}k_3y_1 = c_4v + k_4[x_1(t_s) + v \times (t-t_s) - x_2(t_s)] \tag{6.7}$$

Similarly, the expression of x_2 in Eq. (6.5) are substituted into other equations in Eq. (6.1) to eliminate the terms involving x_2. Therefore, the original 5-DoF equations of motion involving x_1, y_1, x_2, y_2, φ and their velocities and accelerations are converted into a 4-DoF equations of motion involving x_1, y_1, y_2, φ and their velocities and accelerations, in the state of stick. By integrating the 4-DoF equations of motion, the values of x_1, y_1, y_2, φ (also including velocities and accelerations) during sticking are obtained, and the values of x_2 (also including velocity and acceleration) during sticking can also be acquired from Eq. (6.5). Besides, the value of friction force during sticking can be derived from the first or the third equation in Eq. (6.1). The condition for the system to stay in the state of stick is,

$$\begin{cases} |F_\mathrm{T}| \le \mu_\mathrm{s} F_\mathrm{N} \\ F_\mathrm{N} > 0 \end{cases} \tag{6.8}$$

where μ_s is the coefficient of static friction.

While in the state of separation, the slider and the belt are not in contact, therefore $F_\mathrm{N} = 0$, $F_\mathrm{T} = 0$. The condition for the system to stay in the state of separation is,

$$y_2 - (x_1 - x_2)\varphi - y_1 < 0 \tag{6.9}$$

With the formulations of F_T and F_N in each of the three states obtained, the equations of motion for each of the states are determined. After separation, the condition Eq. (6.9) is monitored for re-contact. Re-contact happens when the slider's vertical motion become equal to the vertical motion of the belt at the contact point. And a very short-lived impact force is considered to act between the slider and the belt within a tiny time duration of (t_r^-, t_r^+). The method for determining the values of the dynamic state variables immediately after re-contact, which was given in Ref. [189], is employed in

this paper. For simplification, an assumption for the re-contact is that the impact is perfectly plastic. Suppose the impulse at t_r is p and based on the theorem of momentum, the velocity jump for the slider and the belt due to the impact can be thus obtained as,

$$\dot{y}_1(t_r^+) - \dot{y}_1(t_r^-) = \frac{p}{M} \tag{6.10}$$

$$\dot{y}_2(t_r^+) - \dot{y}_2(t_r^-) = -\frac{p}{m} \tag{6.11}$$

$$\dot{\varphi}(t_r^+) - \dot{\varphi}(t_r^-) = \frac{p\cdot(x_1(t_r)-x_2(t_r))}{J} \tag{6.12}$$

For perfectly plastic impact, the slider has the same vertical velocity as that of the belt at the contact point at time t_r^+, therefore

$$\dot{y}_1(t_r^+) = \dot{y}_2(t_r^+) - \big(x_1(t_r) - x_2(t_r)\big)\dot{\varphi}(t_r^+) \tag{6.13}$$

By substituting Eqs. (6.10)-(6.12) into Eq. (6.13), the values of the impulse p and the state variables immediately after re-contact can be obtained, which are,

$$p = \frac{\dot{y}_2(t_r^-)-\dot{y}_1(t_r^-)-\big(x_1(t_r)-x_2(t_r)\big)\dot{\varphi}(t_r^-)}{\frac{1}{M}+\frac{1}{m}+\frac{(x_1(t_r)-x_2(t_r))^2}{J}} \tag{6.14}$$

$$\dot{y}_1(t_r^+) = \dot{y}_1(t_r^-) + \frac{\dot{y}_2(t_r^-)-\dot{y}_1(t_r^-)-\big(x_1(t_r)-x_2(t_r)\big)\dot{\varphi}(t_r^-)}{M\left[\frac{1}{M}+\frac{1}{m}+\frac{(x_1(t_r)-x_2(t_r))^2}{J}\right]} \tag{6.15}$$

$$\dot{y}_2(t_r^+) = \dot{y}_2(t_r^-) - \frac{\dot{y}_2(t_r^-)-\dot{y}_1(t_r^-)-\big(x_1(t_r)-x_2(t_r)\big)\dot{\varphi}(t_r^-)}{m\left[\frac{1}{M}+\frac{1}{m}+\frac{(x_1(t_r)-x_2(t_r))^2}{J}\right]} \tag{6.16}$$

$$\dot{\varphi}(t_r^+) = \dot{\varphi}(t_r^-) + \frac{(x_1(t_r)-x_2(t_r))\big[\dot{y}_2(t_r^-)-\dot{y}_1(t_r^-)-\big(x_1(t_r)-x_2(t_r)\big)\dot{\varphi}(t_r^-)\big]}{J\left[\frac{1}{M}+\frac{1}{m}+\frac{(x_1(t_r)-x_2(t_r))^2}{J}\right]} \tag{6.17}$$

6.3 Linear stability analysis and transient dynamic analysis

6.3.1 Linear stability analysis of the 5-DoF model

In this section, the procedure to carry out the linear stability analysis is introduced. Firstly the equilibrium points of the system are determined by solving the nonlinear static equations. Then, the equations of motion of the system are linearized around the equilibrium points and a linearized system is derived. Finally, the eigenvalues of

linearized system are calculated to determine the stability of the steady sliding state for various values of key parameters.

6.3.1.1 Equilibrium points

By setting all the terms involving velocity and acceleration in the equations of motion for the state of slip to zero, the nonlinear algebraic equations whose solutions are the equilibrium points are obtained as

$$\begin{bmatrix} k_1+\frac{1}{2}k_3 & -\frac{1}{2}k_3 & 0 & 0 & 0 \\ -\frac{1}{2}k_3 & \frac{1}{2}k_3 & 0 & 0 & 0 \\ 0 & 0 & k_4 & 0 & 0 \\ 0 & 0 & 0 & k_5+k_6 & k_5l_1-k_6l_2 \\ 0 & 0 & 0 & k_5l_1-k_6l_2 & k_5l_1^2+k_6l_2^2 \end{bmatrix} \begin{bmatrix} x_1 \\ y_1 \\ x_2 \\ y_2 \\ \varphi \end{bmatrix} + \begin{bmatrix} a_1 \\ a_2 \\ a_3 \\ a_4 \\ a_5 \end{bmatrix} = \begin{bmatrix} 0 \\ -F \\ 0 \\ 0 \\ 0 \end{bmatrix} \quad (6.18)$$

where

$$a_1 = -\mu_{\mathrm{k}}[k_2(y_2-(x_1-x_2)\varphi-y_1)+k_{\mathrm{nl}}(y_2-(x_1-x_2)\varphi-y_1)^3]$$
$$a_2 = -k_2(y_2-(x_1-x_2)\varphi-y_1)-k_{\mathrm{nl}}(y_2-(x_1-x_2)\varphi-y_1)^3$$
$$a_3 = \mu_{\mathrm{k}}[k_2(y_2-(x_1-x_2)\varphi-y_1)+k_{\mathrm{nl}}(y_2-(x_1-x_2)\varphi-y_1)^3]$$
$$a_4 = k_2(y_2-(x_1-x_2)\varphi-y_1)+k_{\mathrm{nl}}(y_2-(x_1-x_2)\varphi-y_1)^3$$
$$a_5 = -(x_1-x_2)[k_2(y_2-(x_1-x_2)\varphi-y_1)+k_{\mathrm{nl}}(y_2-(x_1-x_2)\varphi-y_1)^3]$$

By solving Eq. (6.18), the equilibrium points can be determined.

6.3.1.2 Complex eigenvalue analysis

By linearizing the nonlinear equations of motion around the equilibrium points, a linearized system results:

$$\mathbf{M}\ddot{\bar{\mathbf{x}}} + \mathbf{C}\dot{\bar{\mathbf{x}}} + \mathbf{K}\bar{\mathbf{x}} = \mathbf{0} \quad (6.19)$$

where $\bar{\mathbf{x}} = \mathbf{x} - \mathbf{x}_{\mathrm{e}}$, $\mathbf{x} = [x_1, y_1, x_2, y_2, \varphi\,]^{\mathrm{T}}$, $\mathbf{x}_{\mathrm{e}} = [x_{1\mathrm{e}}, y_{1\mathrm{e}}, x_{2\mathrm{e}}, y_{2\mathrm{e}}, \varphi_{\mathrm{e}}\,]^{\mathrm{T}}$ is an equilibrium point. The mass matrix, damping matrix and stiffness matrix of the linearized system are,

$$\mathbf{M} = \mathrm{diag}(M, M, m, m, J)$$

$$\mathbf{C} = \begin{bmatrix} c_1 & 0 & 0 & 0 & 0 \\ 0 & c_2 & 0 & 0 & 0 \\ 0 & 0 & c_4 & 0 & 0 \\ 0 & 0 & 0 & c_5 + c_6 & c_5 l_1 - c_6 l_2 \\ 0 & 0 & 0 & c_5 l_1 - c_6 l_2 & c_5 l_1^2 + c_6 l_2^2 \end{bmatrix}$$

$\mathbf{K} =$

$$\begin{bmatrix} k_1 + \frac{1}{2}k_3 + \Lambda\mu_{\mathrm{k}}\varphi_{\mathrm{e}} & -\frac{1}{2}k_3 + \Lambda\mu_{\mathrm{k}} & -\Lambda\mu_{\mathrm{k}}\varphi_{\mathrm{e}} & -\Lambda\mu_{\mathrm{k}} & \Lambda\mu_{\mathrm{k}}(x_1 - x_2) \\ -\frac{1}{2}k_3 + \Lambda\varphi_{\mathrm{e}} & \frac{1}{2}k_3 + \Lambda & -\Lambda\varphi_{\mathrm{e}} & -\Lambda & \Lambda(x_1 - x_2) \\ -\Lambda\mu_{\mathrm{k}}\varphi_{\mathrm{e}} & -\Lambda\mu_{\mathrm{k}} & k_4 + \Lambda\mu_{\mathrm{k}}\varphi_{\mathrm{e}} & \Lambda\mu_{\mathrm{k}} & -\Lambda\mu_{\mathrm{k}}(x_1 - x_2) \\ -\Lambda\varphi_{\mathrm{e}} & -\Lambda & \Lambda\varphi_{\mathrm{e}} & \Lambda + k_5 + k_6 & -\Lambda(x_1 - x_2) + k_5 l_1 - k_6 l_2 \\ -\Pi & \Lambda(x_1 - x_2) & \Pi & -\Lambda(x_1 - x_2) + k_5 l_1 - k_6 l_2 & \Lambda(x_1 - x_2)^2 + k_5 l_1^2 + k_6 l_2^2 \end{bmatrix}$$

and,

$$\Lambda = k_2 + 3k_{\mathrm{nl}}[y_{2\mathrm{e}} - (x_{1\mathrm{e}} - x_{2\mathrm{e}})\varphi_{\mathrm{e}} - y_{1\mathrm{e}}]^2$$

$$\Pi = k_2[y_{2\mathrm{e}} - y_{1\mathrm{e}} - 2\varphi_{\mathrm{e}}\,(x_{1\mathrm{e}} - x_{2\mathrm{e}})] + k_{\mathrm{nl}}\{-3\varphi_{\mathrm{e}}(x_{1\mathrm{e}} - x_{2\mathrm{e}}) \cdot [y_{2\mathrm{e}} - (x_{1\mathrm{e}} - x_{2\mathrm{e}})\varphi_{\mathrm{e}} - y_{1\mathrm{e}}]^2 + [y_{2\mathrm{e}} - (x_{1\mathrm{e}} - x_{2\mathrm{e}})\varphi_{\mathrm{e}} - y_{1\mathrm{e}}]^3\}$$

Then, the eigenvalues of the linearized system above are calculated. If the real parts of all the eigenvalues are negative, the equilibrium point corresponding to the steady sliding state is stable. If at least one of the eigenvalues has a positive real part, the equilibrium point is unstable, which leads to self-excited vibration in the nonlinear system.

6.3.2 Transient dynamic analysis

Because F_{T} and F_{N} take different mathematical forms in distinct states of motion, the dynamic system in question is non-smooth. To obtain the whole time histories of the dynamic responses of the system, the numerical algorithm for the transient dynamic analysis introduced in Section 3.2.2.2 is utilized.

6.4 Numerical study of the 5-DoF model

6.4.1 Stability analysis

According to the procedure given in Section 6.3.1, the stability of the system at the equilibrium point is analysed in this section, where the effects of different types of

nonlinearities are examined. Some basic parameters are assigned constant values if not specified otherwise, which are listed in Table 6.1.

Table 6.1 The values of constant system parameters of the 5-DoF frictional model

M	m	J	c_1	c_2	c_4	c_5	c_6	v
1kg	1kg	0.1kg·m^2	0.1N·m·s	0.1N·m·s	0.1N·m·s	0.1N·m·s	0.1N·m·s	1m/s
k_1	k_2	k_3	k_4	k_5	k_6	l_1	l_2	
10^4N	$5{\cdot}10^3$N	$6{\cdot}10^3$N	10^4N/m	10^4N/m	10^4N/m	0.2m	0.2m	

The results show that the mode-coupling instability arises in the system with the variations of parameter values, namely, the imaginary parts of two eigenvalues coalesce and one of the real parts becomes positive. In Fig. 6.2 and Fig. 6.3, the complex eigenvalues of a pair of modes as a function of the friction coefficient μ_{k} with different nonlinear contact stiffness k_{nl} is exhibited. For each value of k_{nl}, the mode-coupling instability occurs in the system with the increase of μ_{k}. The value of the friction coefficient at which the instability occurs can be called the critical friction coefficient. The comparison between the results of different k_{nl} indicates that a larger nonlinear contact stiffness leads to a smaller critical friction coefficient for the instability. Besides, the comparison between Fig. 6.2 and Fig. 6.3 suggests that the preload also influence the critical friction coefficient. The relationship between the critical friction coefficient and the preload is depicted in Fig.6.4, from which it is seen that the critical friction coefficient for the instability decreases with the increase of the preload.

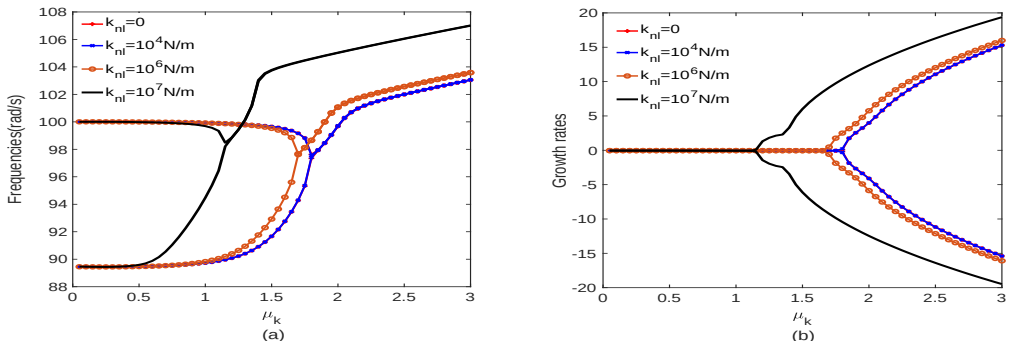

Figure 6.2 Stability analysis of the 5-DoF frictional model with different nonlinear contact stiffness k_{nl} when the preload $F = 100$N: (a) frequencies and (b) growth rates.

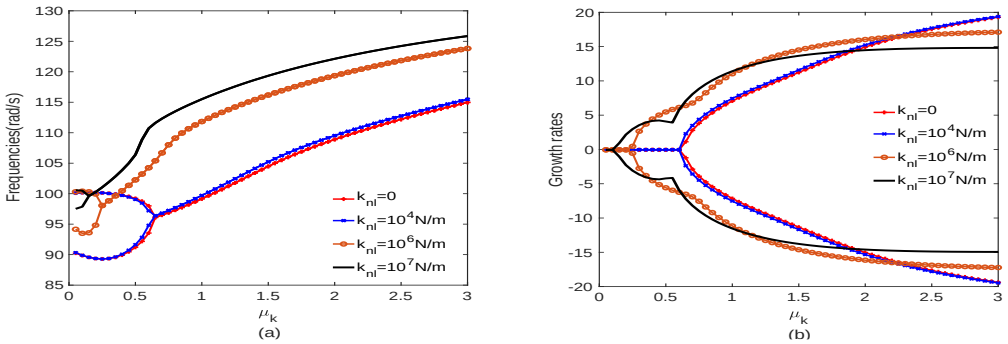

Figure 6.3 Stability analysis of the 5-DoF frictional model with different nonlinear contact stiffness k_{nl} when the preload $F = 1000\mathrm{N}$: (a) frequencies and (b) growth rates.

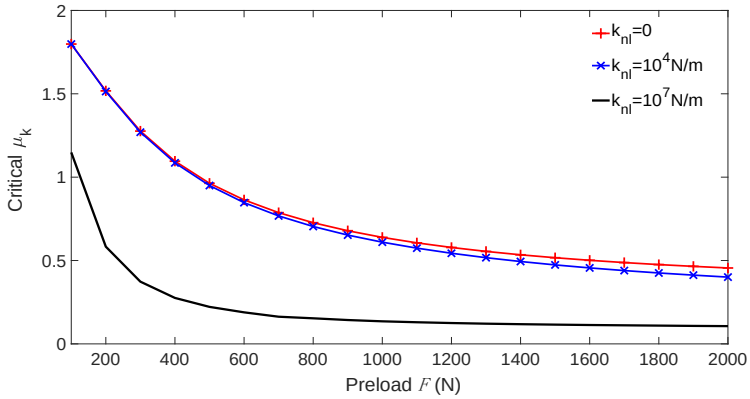

Figure 6.4 The critical friction coefficient μ_{k} for the instability of the 5-DoF frictional model as a function of the preload F.

Next the effects of the geometrical nonlinearity (GN) in the system on the stability are investigated. The geometrical nonlinearity in the system is produced by the combination of the relative motion between the slider and the belt with the rotational motion of the belt. In Fig. 6.5, the critical friction coefficient for the instability as a function of the preload when the rotational motion of the belt is not considered, i.e., without the geometrical nonlinearity, is compared with that of the original 5-DoF system, i.e., with the geometrical nonlinearity. It is clearly observed that the critical friction coefficient for the instability with the geometrical nonlinearity is quite smaller than without. In another word, the geometrical nonlinearity promotes the occurrence of the instability. Besides, another effect of the geometrical nonlinearity on the stability is found. Fig. 6.6 shows the complex eigenvalues analysis results of the system in the two situations, i.e., with and without geometrical nonlinearity, when $F = 1000\mathrm{N}$, $l_1 = 0.1\mathrm{m}$, $l_2 = 0.3\mathrm{m}$. It is seen that the system with the geometrical nonlinearity exhibits

more complex behaviour of instability than without. For the system without the geometrical nonlinearity, there is only one instability when μ_k is larger than its critical value. For the system with the geometrical nonlinearity, however, two instabilities arise (the real parts of two pairs of conjugate eigenvalues become positive) when μ_k is within a certain range and one of the instabilities disappears for large value of μ_k. This example indicates that the geometrical nonlinearity increases the complexity of the instability in the system.

Lastly, the nonlinearity with respect to the non-smooth states of motion has no effect on the stability of the system at the equilibrium point because the system is in the state of slip near the equilibrium point.

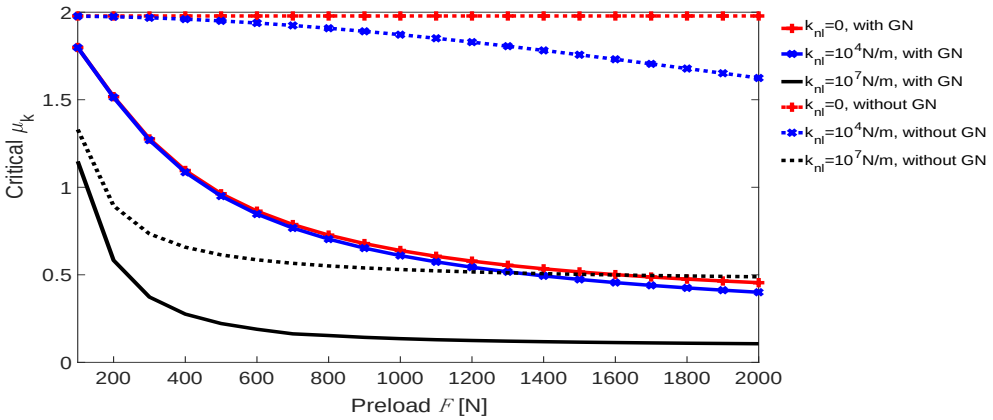

Figure 6.5 The effect of the geometrical nonlinearity (GN) on the critical friction coefficient μ_k for the instability of the 5-DoF frictional model.

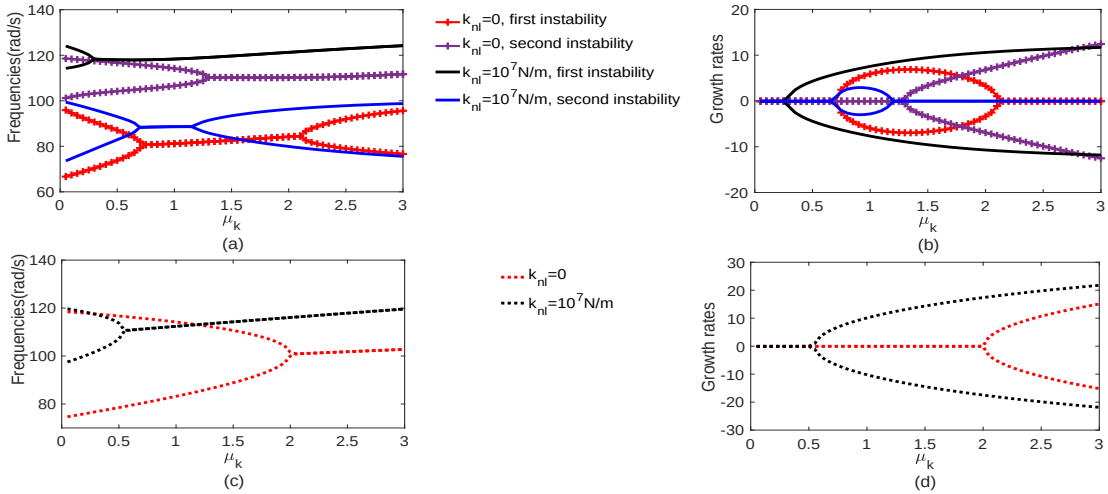

Figure 6.6 The effect of the geometrical nonlinearity on the instability of the 5-DoF frictional model: (a)(b) with the geometrical nonlinearity and (c)(d) without the geometrical nonlinearity. ($F = 1000$N, $l_1 = 0.1$m, $l_2 = 0.3$m).

6.4.2 Nonlinear steady-state responses

In this section, the nonlinear steady-state responses of the system are investigated by means of the transient dynamic analysis. The values of the basic system parameters are the same as those in Table 6.1. The effects of different types of nonlinearities on the steady-state responses of the system are examined.

6.4.2.1 The characteristics of the steady-state responses of the system

Firstly, the time responses of the system under three different values of μ_{k} $(0.3, 1.4, 2.5)$ with $\mu_{\mathrm{s}} = 3$, $k_{\mathrm{nl}} = 10^4 \mathrm{N/m}$ and $F = 200\mathrm{N}$ are obtained in Fig. 6.7. For each μ_{k}, the solutions of the nonlinear algebraic equations in Eq. (6.18) consists of a solution of real numbers and a pair of solutions of conjugate complex numbers. The solution of real numbers is the equilibrium point of the system, which is,

$$\mathbf{x}_{\mathrm{e}} = [-0.0042\mathrm{m}, -0.0304\mathrm{m}, -0.0036\mathrm{m}, -0.0061\mathrm{m}, -0.0001\mathrm{rad}]^{\mathrm{T}}, \text{ for } \mu_{\mathrm{k}} = 0.3,$$

$$\mathbf{x}_{\mathrm{e}} = [-0.0053\mathrm{m}, -0.0263\mathrm{m}, -0.0147\mathrm{m}, -0.0053\mathrm{m}, 0.0026\mathrm{rad}]^{\mathrm{T}}, \text{ for } \mu_{\mathrm{k}} = 1.4,$$

$$\mathbf{x}_{\mathrm{e}} = [0.0124\mathrm{m}, -0.0233\mathrm{m}, -0.0232\mathrm{m}, -0.0046\mathrm{m}, 0.0041\mathrm{rad}]^{\mathrm{T}}, \text{ for } \mu_{\mathrm{k}} = 2.5.$$

It is worth noting that a mode-coupling instability happens in the system with the increase of μ_{k}. The eigenvalues of the coupled modes for the three values of μ_{k} are $[-0.05 \pm 100\mathrm{i},\ -0.04 \pm 89.4\mathrm{i}]$, $[-0.05 \pm 98.7\mathrm{i},\ -0.048 \pm 93.7\mathrm{i}]$ and $[11.98 \pm 102.6\mathrm{i},\ -12.08 \pm 102.6\mathrm{i}]$ respectively, therefore $\mu_{\mathrm{k}} = 0.3$ and 1.4 lead to a stable equilibrium point and $\mu_{\mathrm{k}} = 2.5$ leads to an unstable equilibrium point. In Fig. 6.7, the exhibited time responses for each value of μ_{k} are acquired from two different initial conditions, i.e., one near the equilibrium point and the other far from the equilibrium point. When $\mu_{\mathrm{k}} = 0.3$, the dynamic responses from both initial conditions approach the equilibrium point, indicating there is only one stable solution for the system responses, i.e., the equilibrium point. When $\mu_{\mathrm{k}} = 2.5$, the dynamic responses from both initial conditions approach the same limit cycle, indicating there is only one stable solution for the system responses, i.e., the limit cycle vibration. When $\mu_{\mathrm{k}} = 1.4$, however, the two initial conditions lead to different steady-state responses. The dynamic responses from the initial condition near the equilibrium point approach the equilibrium point while the dynamic responses from the initial condition far from the equilibrium approach the limit cycle vibration, which indicates the coexistence of two stable solutions in the system. This example shows that the linear stability analysis at

the equilibrium point in the friction-excited system fails to detect the occurrence of self-excited vibration when the system is bi-stable, which can only be found out by a transient dynamic analysis.

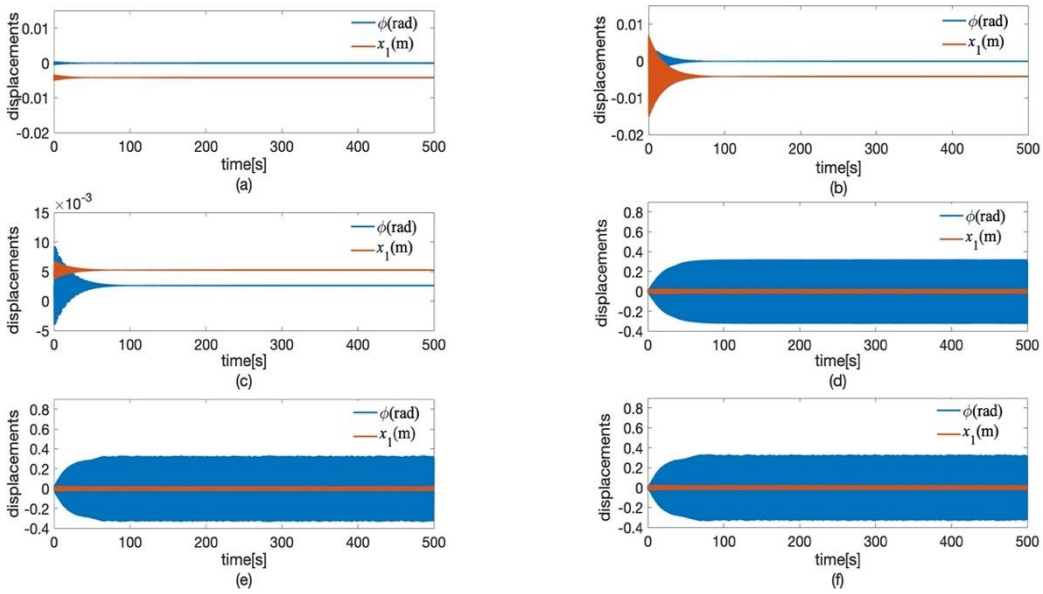

Figure 6.7 The time responses of the 5-DoF frictional model under three different values of μ_{k} $(0.3, 1.4, 2.5)$ with $\mu_{\mathrm{s}} = 3$, $k_{\mathrm{nl}} = 10^4 \mathrm{N/m}$ and $F = 200\mathrm{N}$ from two initial conditions: (a)(c)(e) near the equilibrium point and (b)(d)(f) far from the equilibrium point.

In Fig. 6.8, the steady-state limit cycle vibration when $\mu_{\mathrm{k}} = 1.4$ and $\mu_{\mathrm{k}} = 2.5$ is further compared in terms of the contact forces, the phase plots and the frequency spectra. It is deduced from Fig. 6.8(a)(c)(e) that the steady-state dynamic responses of the system when $\mu_{\mathrm{k}} = 1.4$ are periodic with the frequency of around 1.58Hz, while Fig. 6.8(b)(d)(f) demonstrate that the steady-state dynamic responses when $\mu_{\mathrm{k}} = 2.5$ are non-periodic. Therefore the system responses bifurcate with the variation of μ_{k} and the bifurcation behaviour of the system with the given parameter values is displayed in Fig. 6.9, which shows the values of x_1 at the transition points from slip to stick. It shows that the system has periodic steady-state responses when $0.9 \leq \mu_{\mathrm{k}} < 1.8$ and non-periodic responses when $0.4 \leq \mu_{\mathrm{k}} < 0.9$ or $1.8 \leq \mu_{\mathrm{k}} < 3$. Besides, an index is defined to measure the intensity of steady-state vibration of the system, which is,

$$L_{\mathrm{s}} = \sum_{i=1}^{5} \frac{\int_T [(X_i - X_{ie})^2] \mathrm{d}t}{T} \tag{6.20}$$

where X_i $(i = 1,2,3,4,5)$ represents the dynamic response x_1 , y_1 , x_2 , y_2 , φ respectively, X_{ie} is the value of the equilibrium point and T represents a time period in the steady state. Index L_s as a function of μ_k is shown in Fig. 6.10, from which it is observed that the system has a single stable equilibrium point when $\mu_k < 0.4$ and a single stable limit cycle when $\mu_k > 1.5$, while two stable steady-state solutions coexist when $\mu_k \in [0.4, 1.5]$.

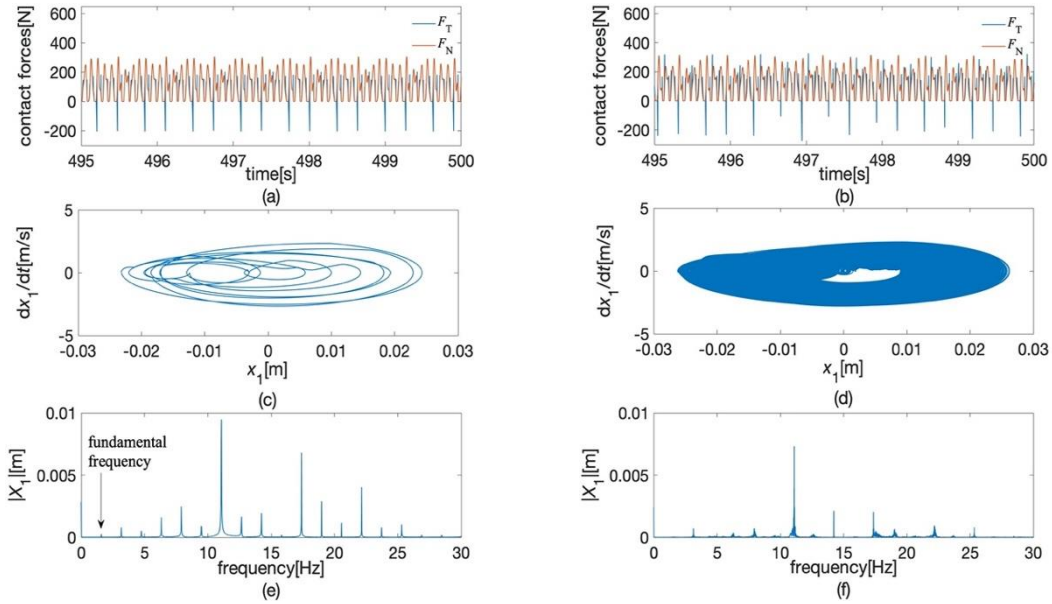

Figure 6.8 The steady-state limit cycle vibration of the 5-DoF frictional model in terms of the contact forces, the phase plots and the frequency spectra: (a)(c)(e) $\mu_k = 1.4$ and (b)(d)(f) $\mu_k = 2.5$.

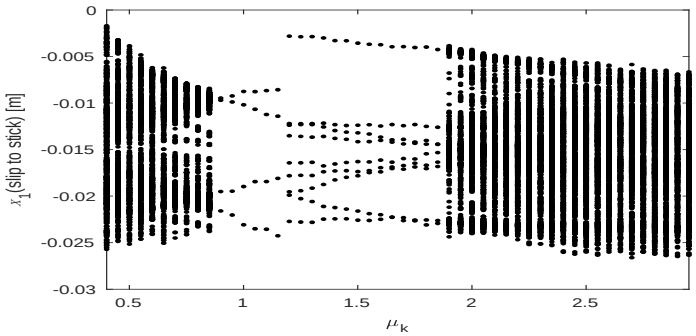

Figure 6.9 The bifurcation behaviour of the steady-state limit cycle vibration of the 5-DoF friction model dependent on μ_k.

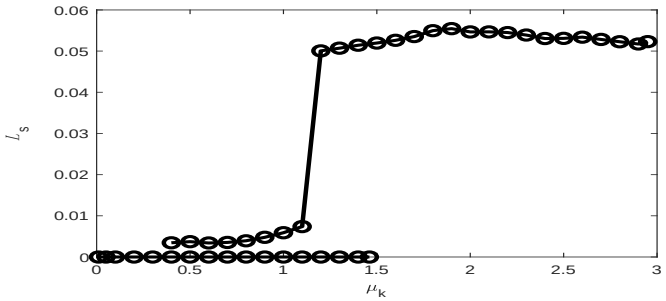

Figure 6.10 Index L_s as a function of μ_k of the 5-DoF frictional model.

6.4.2.2 The effects of nonlinearities on the steady-state responses of the system

First of all, the effects of the nonlinear contact stiffness on the steady-state responses are investigated. With different values of k_{nl} and the same values of other parameters as those in Section 6.4.2.1, the bifurcation behaviours of the steady-state limit cycle vibration of the system, which reveal the periodicity of the steady-state responses with the variation of μ_k, are shown in Fig. 6.11. By comparing the results in Fig. 6.11 with those in Fig. 6.9, it is observed that the bifurcation behaviours of the steady-state responses when $k_{nl} = 0$ and $k_{nl} = 10^4 \mathrm{N/m}$ are alike, while the bifurcation behaviour of the steady-state responses when $k_{nl} = 10^7 \mathrm{N/m}$ is quite different. Fig. 6.11(a) shows that the system in the case of $k_{nl} = 0$ also has periodic steady-state responses when $0.9 \leq \mu_k < 1.8$, except $\mu_k = 1.3$. Besides, the system when $k_{nl} = 0$ has stable periodic limit cycle vibration at $\mu_k = 0.05$, which is different from the result of the system with $k_{nl} = 10^4 \mathrm{N/m}$. Fig. 6.11(b) demonstrates that the system has periodic steady-state responses when $0.75 \leq \mu_k \leq 2.9$ or $\mu_k = 0.1$, and the values of x_1 at the transition points from slip to stick are approximately identical when μ_k lies in the above range, as shown in the figure, indicating that the system responses in the above range of μ_k are close. In Fig. 6.12, index L_s as the function of μ_k with three values of k_{nl}, i.e., $k_{nl} = 0$, $10^4 \mathrm{N/m}$ and $10^7 \mathrm{N/m}$, is depicted. The range of μ_k in which two stable steady-state solutions (the equilibrium point and the limit cycle) coexist in the system is identified, which is $[0.4, 1.5]$ for both $k_{nl} = 0$ and $k_{nl} = 10^4 \mathrm{N/m}$, and $(0, 0.6]$ for $k_{nl} = 10^7 \mathrm{N/m}$. Besides, the values of L_s as the function of μ_k roughly reflect the intensity of steady-state vibration of the system at different values of μ_k. For $k_{nl} = 0$ and $k_{nl} = 10^4 \mathrm{N/m}$, the steady-state vibration generally gets stronger for larger values of μ_k. For $k_{nl} = 10^7 \mathrm{N/m}$, however, the steady-state vibration is weaker when $0.75 \leq \mu_k \leq 2.9$, namely, when the system has periodic oscillations, than that

when the system has non-periodic oscillations. Based on the above observations, it is concluded that the nonlinearity from the contact stiffness has a significant effect on the steady-state responses of the system.

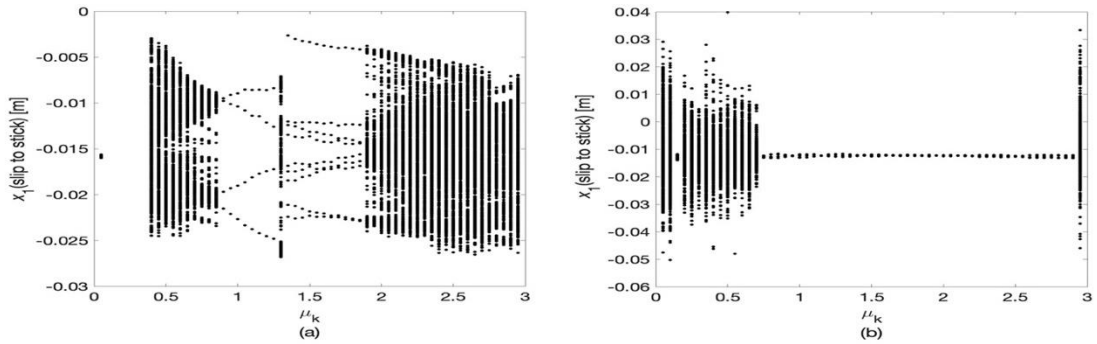

Fig. 6.11 The bifurcation behaviours of the steady-state limit cycle vibration of the 5-DoF frictional model with different values of k_{nl}: (a) $k_{\mathrm{nl}} = 0$ and (b) $k_{\mathrm{nl}} = 10^7\mathrm{N/m}$.

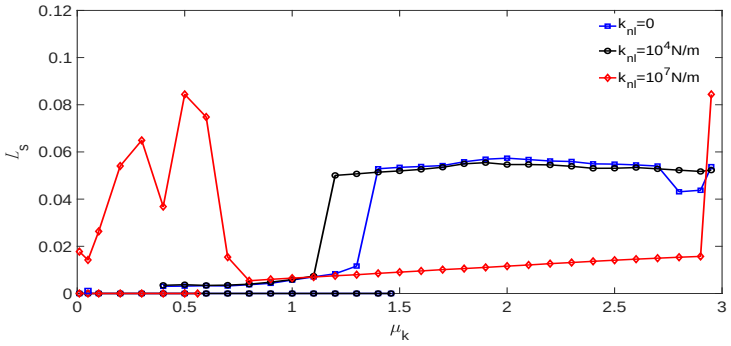

Figure 6.12 Index L_{s} as the function of μ_{k} for the 5-DoF frictional model with different values of k_{nl}.

Secondly, the effects of the geometrical nonlinearity in the system on the steady-state responses are investigated. To reveal the effects of the geometrical nonlinearity, the steady-state responses of the system without the geometrical nonlinearity are calculated and compared with the results of the original system with the geometrical nonlinearity. In Fig. 6.13, the bifurcation behaviours of the steady-state limit cycle vibration of the system without the geometrical nonlinearity are plotted. It is seen that the system experiences nearly unchanged periodic oscillations when μ_{k} varies within $[0.38, 2.95]$ in the case of $k_{\mathrm{nl}} = 0$ and $k_{\mathrm{nl}} = 10^4\mathrm{N/m}$, and the representative phase-plane plots of the periodic oscillations are depicted in Fig. 6.13(d) and (e). In the case of $k_{\mathrm{nl}} = 10^7\mathrm{N/m}$, the system has non-periodic steady-state responses when μ_{k} is very small and similar periodic responses as μ_{k} varies within $[0.05, 2.95]$. The

representative phase-plane plot of the periodic responses is depicted in Fig. 6.13(f), which is different from those in the case of $k_{\mathrm{nl}} = 0$ and $k_{\mathrm{nl}} = 10^4\mathrm{N/m}$. Index L_{s} as a function of μ_{k} for the system without the geometrical nonlinearity is presented in Fig. 6.14, which shows a much more steady pattern of the values of L_{s} with the variation of μ_{k} than the counterpart of the system with the geometrical nonlinearity. Besides, the steady-state responses with different values of preload F when $\mu_{\mathrm{k}} = 2.5$ and $k_{\mathrm{nl}} = 10^7\mathrm{N/m}$ in the two situations, i.e., with and without the geometrical nonlinearity, are calculated, and the bifurcation behaviours and index L_{s} are shown in Fig. 6.15. By the comparison between the results in the two situations, it is clearly seen that the system responses with the geometrical nonlinearity experience more fluctuations than those without the geometrical nonlinearity as preload F varies, in terms of the periodicity and intensity of the steady-state vibration. Based on the above observations, it is concluded that the geometrical nonlinearity has a significant effect on the steady-state responses of the system, and the system responses in the presence of geometrical nonlinearity are more changeable with the variations of parameters (e.g., μ_{k} and F) than those without geometrical nonlinearity.

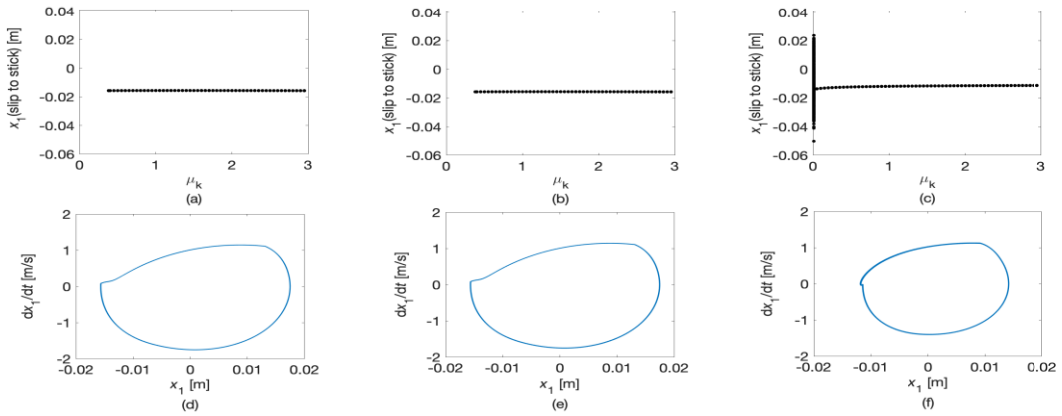

Figure 6.13 The bifurcation behaviours of the steady-state limit cycle vibration (a-c) and phase-plane plots when $\mu_{\mathrm{k}} = 2$ (d-f) for the 5-DoF frictional model without the geometrical nonlinearity: (a)(d) $k_{\mathrm{nl}} = 0$, (b)(e) $k_{\mathrm{nl}} = 10^4\mathrm{N/m}$ and (c)(f) $k_{\mathrm{nl}} = 10^7\mathrm{N/m}$.

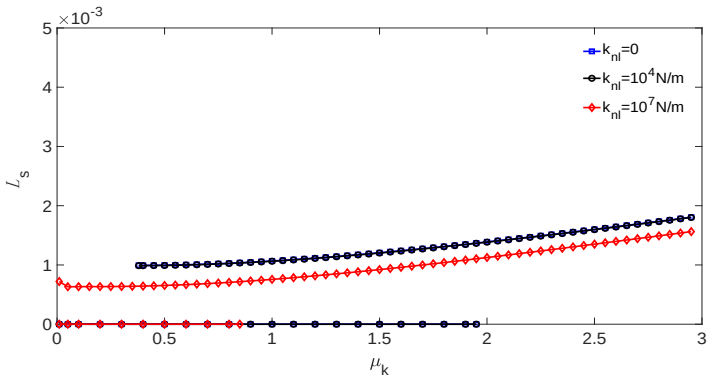

Figure 6.14 Index L_s as a function of μ_k for the 5-DoF frictional model without the geometrical nonlinearity.

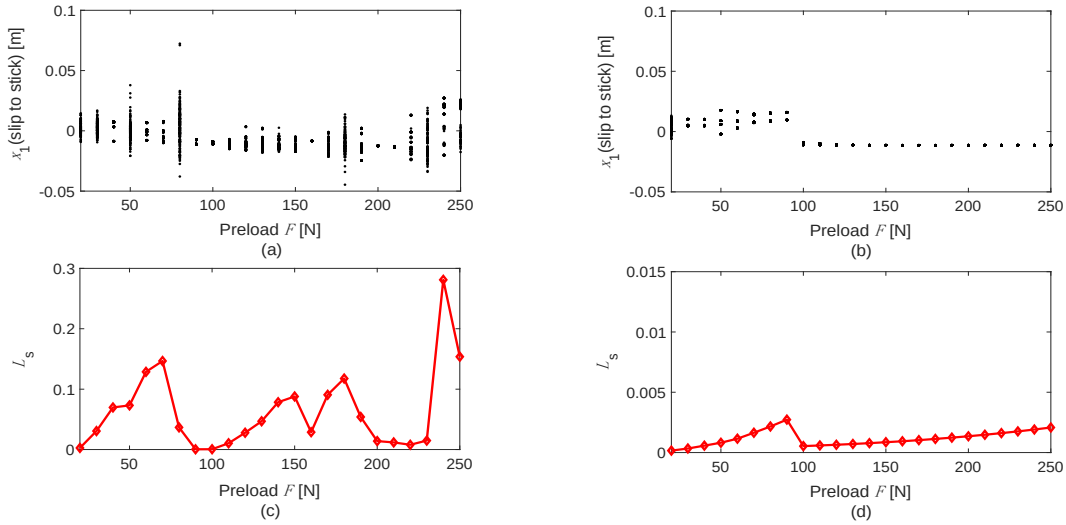

Figure 6.15 The bifurcation behaviour and index L_s of the steady-state responses of the 5-DoF frictional model as the function of the preload F when $\mu_k = 2.5$ and $k_{nl} = 10^7 N/m$ in the two situations: (a)(c) with the geometrical nonlinearity and (b)(d) without the geometrical nonlinearity.

Thirdly, the effects of the non-smooth states of motion on the steady-state responses of the system are investigated. Many previous studies [98,103,160,211] only took the state of relative sliding into account when investigating the dynamics of frictional systems, while the states of stick and separation will actually happen in the vibration of frictional systems because of the discontinuous friction force and the unilateral contact. To reveal the effects of the non-smooth states of motion including stick/slip and contact/separation on the steady-state responses of the system, the dynamic responses when the non-smooth states of motion are not considered, i.e., there exists the single state of relative sliding in the vibration, are calculated and compared with the results of the original system. In Fig. 6.16, the dynamic responses of the system in

the two situations, i.e., including and excluding the non-smooth behaviours, are depicted for comparison, where $\mu_{\mathrm{k}} = 2.5$, $\mu_{\mathrm{s}} = 3$, $k_{\mathrm{nl}} = 10^7\mathrm{N/m}$, $F = 800\mathrm{N}$ and the values of other basic parameters are the same as those in Table 6.1 except $k_4 = k_5 = k_6 = 5{\cdot}10^6\mathrm{N/m}$ in this example. From this figure it is observed that the amplitudes of dynamic responses when excluding the non-smooth behaviours are much larger than those when including the non-smooth behaviours in the vibration. It should be noted here the contact between the slider and the belt is assumed to be bilateral (i.e., maintained) when the non-smooth behaviours are excluded, therefore normal force F_{N} is allowed to become negative.

With the values of other parameters unchanged and μ_{k} as the control parameter, the bifurcation behaviour and index L_{s} of the steady-state responses in the two situations are plotted in Fig. 6.17. In the bifurcation diagram for the situation when the non-smooth behaviours are excluded, the values of x_1 when $\dot{x}_1 = 0$ at each μ_{k} are displayed, which indicate that the steady-state dynamic responses are periodic for all $\mu_{\mathrm{k}} \geq 1.4$. The bifurcation diagram for the situation when the non-smooth behaviours are included, however, shows that the that the steady-state dynamic responses are non-periodic for most values of μ_{k}. Another difference between the results in these two situation is that the limit cycle vibration appears from very small μ_{k} (0.15) when the non-smooth behaviours are included, while in the situation of excluding non-smooth behaviours, the limit cycle vibration arises from $\mu_{\mathrm{k}} = 1.4$, which is only slightly smaller than the critical friction coefficient for the instability of the equilibrium point that is 1.735 in this example, as indicated in Fig. 6.17(c). Besides, the values of index L_{s} in these two situations in Fig. 6.17(c) demonstrate that the steady-state vibration when excluding non-smooth behaviours is much stronger than that when the non-smooth behaviours are included. Based on the above observations, it is concluded that the nonlinearity of the non-smooth states of motion in the system also has a significant effect on the steady-state responses of the system. Therefore it is indispensable to incorporate all non-smooth states of motion including stick, slip and separation in order to accurately acquire the dynamic responses of the frictional systems.

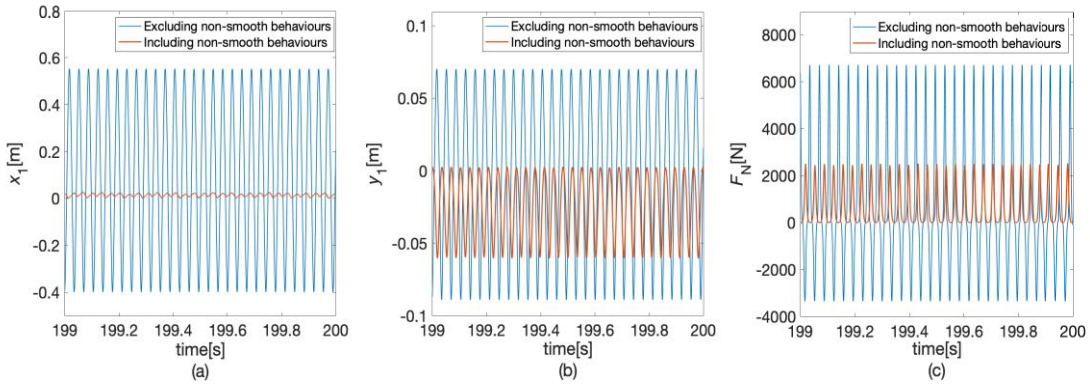

Figure 6.16 Comparisons of the system responses including and excluding the non-smooth behaviours of the 5-DoF frictional model: (a) x_1, (b) y_1 and (c) F_{N}.

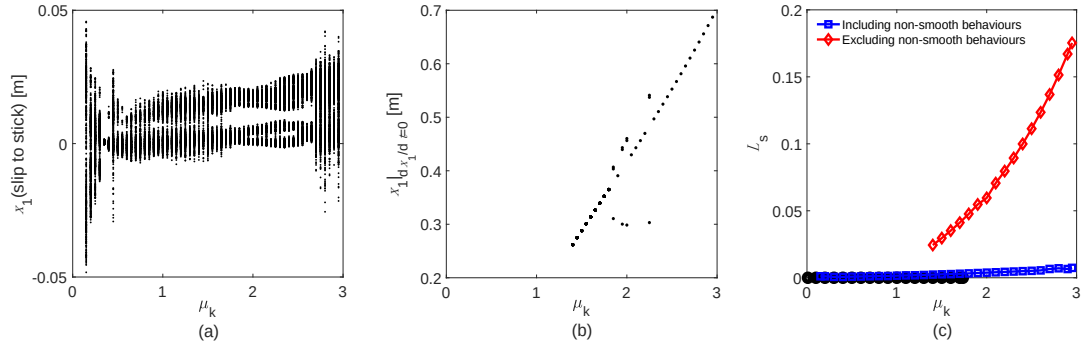

Figure 6.17 The bifurcation behaviour and index L_{s} of the steady-state responses of the 5-DoF frictional model as the function of μ_{k}: (a) the bifurcation behaviour when including non-smooth behaviours, (b) the bifurcation behaviour when excluding non-smooth behaviours and (c) index L_{s} in the two situations.

The unstable eigenfrequencies obtained from the CEA are usually regarded as the frequencies of the self-excited vibration in the brake system in industry, which may not be accurate as the nonlinearities in the brake system can cause the frequencies of the self-excited vibration to be quite different from the unstable eigenfrequencies in the linearized system. To clarify their differences, the frequencies of the steady-state responses are compared with the unstable eigenfrequencies in the linearized system in a numerical example, where the values of other parameters are the same as those in Fig. 6.17. The colour in Fig. 6.18 indicates the response amplitude and the dark marked lines exhibit the unstable eigenfrequencies in the linearized system with the variation of μ_{k}. It is observed from Fig. 6.18(a) that the frequencies of the steady-state responses in this nonlinear frictional system deviate markedly from the unstable eigenfrequencies in the linearized system. To reveal the effects of each type of nonlinearity, the comparisons are also made when a single type of nonlinearity exists

in the system and displayed in Fig. 6.18(b)(c)(d), which show that the frequencies of the steady-state responses are close to the unstable eigenfrequencies in the situation of the single geometrical nonlinearity, while in the situations of the single nonlinearity of contact stiffness and the single nonlinearity of non-smooth states of motion, there exist larger differences between the frequencies of the steady-state responses and the unstable eigenfrequencies .

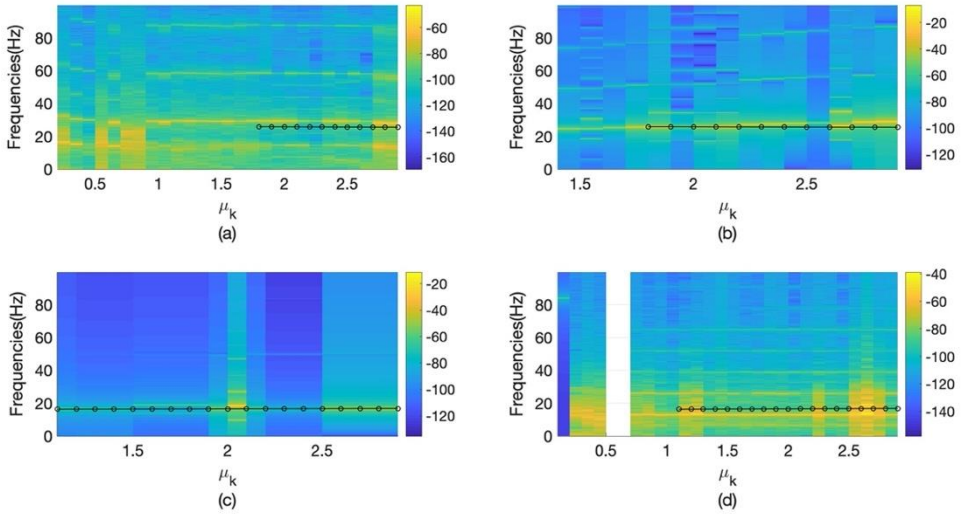

Figure 6.18 The frequencies of the steady-state responses of the system and unstable eigenfrequency of the linearized system of the 5-DoF frictional model: (a) with all three types of nonlinearities, (b) with the single nonlinearity of contact stiffness, (c) with the single geometrical nonlinearity and (d) with the single nonlinearity of non-smooth states of motion.

6.5 The effects of multiple nonlinearities on the dynamics of slider-on-disc model

The dynamics of a slider-on-disc model as shown in Fig. 6.19 with multiple types of nonlinearities is investigated. The disc is modelled as a Kirchhoff plate clamped at inner boundary and free at outer boundary. A slider, which is assumed to be a point mass, is connected to the fixture by a tangential spring k_1, an inclined spring k_3 at 45 degree to the tangential direction and dashpots c_1 and c_2 in the tangential and normal directions. Without loss of generality, the circumferential coordinate of the fixtures is set as $\theta = 0$. The contact stiffness between the slider and disc is represented by the combination of a linear spring k_2 and a nonlinear spring k_{nl}. The slider is assumed to be fixed radially at r_0 from the disc centre and pressed by a preload F into frictional

contact with the disc which is rotating at the speed Ω. The Coulomb's law of friction with the coefficient of static friction μ_s and the coefficient of kinetic friction μ_k is also employed here to describe the friction force on the interface. There are also three different types of nonlinearities in this model. The first type of nonlinearity is the nonlinear contact stiffness, the second is the non-smooth states of motion including stick, slip and separation, and the third is the geometrical nonlinearity brought about by the moving-load feature of the slider on the flexible disc.

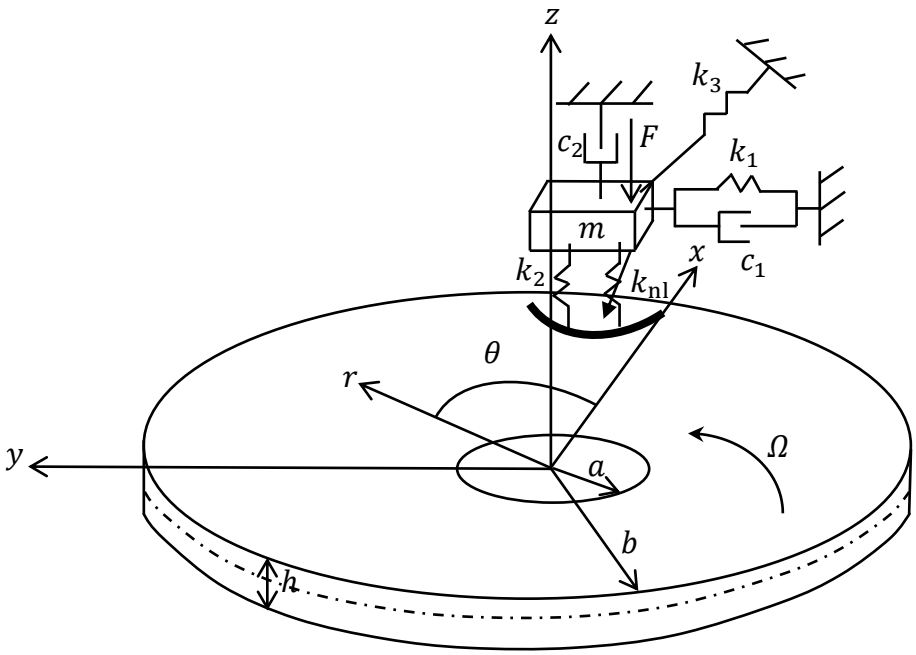

Figure 6.19 The slider-on-disc model with nonlinearities.

In this model, the vibration of the slider in the normal and tangential directions and the transverse vibration of the disc are considered. The equations of motion of the slider can be written as,

$$mr_0\ddot{\varphi} + c_1 r_0\dot{\varphi} + k_1 r_0\varphi + \frac{1}{2}k_3 r_0\varphi - \frac{1}{2}k_3 u = F_T \tag{6.21}$$

$$m\ddot{u} + c_2\dot{u} - \frac{1}{2}k_3 r_0\varphi + \frac{1}{2}k_3 u = F_N - F \tag{6.22}$$

The transverse displacement of the disc can be expressed as,

$$w(r,\theta,t) = \sum_{k=0}^{\infty}\sum_{l=0}^{\infty} R_{kl}(r)[\cos(l\theta)\cdot C_{kl}(t) + \sin(l\theta)\cdot D_{kl}(t)] \tag{6.23}$$

where k and l denote the numbers of nodal circles and nodal diameters respectively, $C_{kl}(t)$, $D_{kl}(t)$ are modal coordinates, $R_{kl}(r)$ is a combination of Bessel functions

satisfying the inner and outer boundary conditions of the nonrotating disc and orthogonality conditions. The equation of transverse motion of the disc under the action of the slider is obtained as,

$$\rho h\left(\frac{\partial^2 w}{\partial t^2}+2\Omega\frac{\partial^2 w}{\partial\theta\partial t}+\Omega^2\frac{\partial^2 w}{\partial\theta^2}\right)+d^*\nabla^4\dot{w}+D^*\nabla^4 w=\frac{1}{r}\Big\{-F_{\mathrm{N}}\delta(r-r_0)\delta(\theta-\varphi)+\frac{\partial}{r\partial\theta}\left[\frac{h}{2}F_{\mathrm{T}}\delta(\theta-\varphi)\right]\delta(r-r_0)\Big\} \tag{6.24}$$

where ρ is the density of material, $D^*=\frac{Eh^3}{12(1-\nu^2)}$ is the bending rigidity, E and ν are the Young's modulus and the Poisson's ratio of the disc material, respectively, d^* is the damping coefficient of the disc. By substituting Eq. (6.23) into Eq. (6.24), then multiplying both sides of the equation by $R_{kl}(r)\cos(l\theta)$ or $R_{kl}(r)\sin(l\theta)$ and integrating them over the whole plate surface, and by using the orthogonal conditions of modal functions as described in Section 3.3.3, the equations of transverse vibration of the disc with respect to the modal coordinates can be derived. Similar to that in the 5-DoF frictional system, the friction force F_{T} and the normal force F_{N} in the slider-on-disc system take different forms in the three distinct states of motion, i.e., slip, stick and separation.

When the slider is in contact with the disc, in the states of slip and stick, the normal force is the resultant force of the linear spring k_2 and the nonlinear spring k_{nl}, i.e.,

$$F_{\mathrm{N}}=k_2(w(r_0,\varphi,t)-u)+k_{\mathrm{nl}}(w(r_0,\varphi,t)-u)^3 \tag{6.25}$$

The friction force takes different forms in the states of slip and stick. In the state of slip, the friction force is an applied force and can be expressed as,

$$F_{\mathrm{T}}=\mathrm{sgn}(\Omega-\dot{\varphi})\mu_{\mathrm{k}}F_{\mathrm{N}} \tag{6.26}$$

The condition for the system to stay in the state of slip is,

$$\begin{cases}\dot{\varphi}\neq\Omega\\ F_{\mathrm{N}}>0\end{cases} \tag{6.27}$$

In the state of stick, the friction force is a reaction force and can be obtained from the equilibrium equation which is derived by setting $\ddot{\varphi}=0,\dot{\varphi}=\Omega$ in Eq. (6.21), i.e.,

$$F_{\mathrm{T}}=c_1r_0\Omega+k_1r_0\varphi+\frac{1}{2}k_3r_0\varphi-\frac{1}{2}k_3u \tag{6.28}$$

The condition for the system to stay in the state of stick is,

$$\begin{cases} |F_{\mathrm{T}}| \le \mu_{\mathrm{s}} F_{\mathrm{N}} \\ F_{\mathrm{N}} > 0 \end{cases} \tag{6.29}$$

While in the state of separation, the slider and the disc are not in contact, therefore $F_{\mathrm{N}} = 0$, $F_{\mathrm{T}} = 0$. The condition for the system to stay in the state of separation is,

$$w(r_0, \varphi, t) - u < 0 \tag{6.30}$$

With the formulations of F_{T} and F_{N} in each of the three states obtained, the equations of motion for each of the states are determined. It is also assumed that the perfectly plastic impact acts between the slider and the disc at the time of re-contact after separation, which causes the velocity jump for the slider and the disc at the time of re-contact. The method given in Ref. [189] is also used here to derive the velocities of the slider and the disc immediately after the re-contact. Suppose the impulse between the slider and the disc at the time of re-contact is p and based on the theorem of momentum, the velocity jump for the slider and the disc due to the impact can be obtained as,

$$\dot{C}_{kl}(t_r^+) - \dot{C}_{kl}(t_r^-) = -\frac{pR_{kl}(r_0)\cos\left(l\varphi(t_r)\right)}{M_{kl}} \tag{6.31}$$

$$\dot{D}_{kl}(t_r^+) - \dot{D}_{kl}(t_r^-) = -\frac{pR_{kl}(r_0)\sin\left(l\varphi(t_r)\right)}{M_{kl}} \tag{6.32}$$

$$\dot{u}(t_r^+) - \dot{u}(t_r^-) = \frac{p}{m} \tag{6.33}$$

in which t_r^+, t_r^- denote the instant after and before the re-contact, respectively. Combining Eq. (6.33) and Eqs. (6.31) and (6.32) gives,

$$\dot{C}_{kl}(t_r^+) - \dot{C}_{kl}(t_r^-) = -\frac{mR_{kl}(r_0)\cos\left(l\varphi(t_r)\right)\left[\dot{u}(t_r^+) - \dot{u}(t_r^-)\right]}{M_{kl}} \tag{6.34}$$

$$\dot{D}_{kl}(t_r^+) - \dot{D}_{kl}(t_r^-) = -\frac{mR_{kl}(r_0)\sin\left(l\varphi(t_r)\right)\left[\dot{u}(t_r^+) - \dot{u}(t_r^-)\right]}{M_{kl}} \tag{6.35}$$

For perfectly plastic impact, the slider has the same velocity as that of the disc at the instant t_r^+, therefore,

$$\dot{u}(t_r^+) = \left(\frac{\partial w}{\partial t} + \dot{\varphi}\frac{\partial w}{\partial \varphi}\right)_{t=t_r^+} \tag{6.36}$$

The transverse displacement of the disc and the tangential motion of the slider are unchanged by the normal impact, namely, the following equations are satisfied,

$$\begin{gathered} C_{kl}(t_r^+) = C_{kl}(t_r^-) = C_{kl}(t_r), D_{kl}(t_r^+) = D_{kl}(t_r^-) = D_{kl}(t_r), \\ \varphi(t_r^+) = \varphi(t_r^-) = \varphi(t_r), \dot{\varphi}(t_r^+) = \dot{\varphi}(t_r^-) = \dot{\varphi}(t_r) \end{gathered} \tag{6.37}$$

By substituting Eq. (6.36) into Eqs. (6.34) and (6.35) and utilizing Eq. (6.37), the normal velocity of the slider and the modal velocities of the disc after the impact can be derived as,

$$\dot{C}_{kl}(t_r^+) = \dot{C}_{kl}(t_r^-) - \frac{mR_{kl}(r_0)\cos(l\varphi(t_r))}{M_{kl}} \left\{ \frac{\sum_{r=0}^{\infty}\sum_{s=0}^{\infty} R_{rs}(r_0)\left[\cos(s\varphi(t_r))\dot{C}_{rs}(t_r^-)+\sin(s\varphi(t_r))\dot{D}_{rs}(t_r^-)+\frac{mR_{rs}(r_0)}{M_{rs}}\dot{u}(t_r^-)-\dot{\varphi}(t_r)s\sin(s\varphi(t_r))C_{rs}(t_r)+\dot{\varphi}(t_r)s\cos(s\varphi(t_r))D_{rs}(t_r)\right]}{1+\sum_{r=0}^{\infty}\sum_{s=0}^{\infty}\frac{mR_{rs}^2(r_0)}{M_{rs}}} - \dot{u}(t_r^-) \right\} \tag{6.38}$$

$$\dot{D}_{kl}(t_r^+) = \dot{D}_{kl}(t_r^-) - \frac{mR_{kl}(r_0)\sin(l\varphi(t_r))}{M_{kl}} \left\{ \frac{\sum_{r=0}^{\infty}\sum_{s=0}^{\infty} R_{rs}(r_0)\left[\cos(s\varphi(t_r))\dot{C}_{rs}(t_r^-)+\sin(s\varphi(t_r))\dot{D}_{rs}(t_r^-)+\frac{mR_{rs}(r_0)}{M_{rs}}\dot{u}(t_r^-)-\dot{\varphi}(t_r)s\sin(s\varphi(t_r))C_{rs}(t_r)+\dot{\varphi}(t_r)s\cos(s\varphi(t_r))D_{rs}(t_r)\right]}{1+\sum_{r=0}^{\infty}\sum_{s=0}^{\infty}\frac{mR_{rs}^2(r_0)}{M_{rs}}} - \dot{u}(t_r^-) \right\} \tag{6.39}$$

$$\dot{u}(t_r^+) = \frac{\sum_{r=0}^{\infty}\sum_{s=0}^{\infty} R_{rs}(r_0)\left[\cos(s\varphi(t_r))\dot{C}_{rs}(t_r^-)+\sin(s\varphi(t_r))\dot{D}_{rs}(t_r^-)+\frac{mR_{rs}(r_0)}{M_{rs}}\dot{u}(t_r^-)-\dot{\varphi}(t_r)s\sin(s\varphi(t_r))C_{rs}(t_r)+\dot{\varphi}(t_r)s\cos(s\varphi(t_r))D_{rs}(t_r)\right]}{1+\sum_{r=0}^{\infty}\sum_{s=0}^{\infty}\frac{mR_{rs}^2(r_0)}{M_{rs}}} \tag{6.40}$$

6.5.1 Linear stability analysis of the slider-on-disc model

In the state of slip, the equations of motion of the slider and disc are as follows,

$$mr_0\ddot{\varphi} + c_1 r_0\dot{\varphi} + k_1 r_0\varphi + \frac{1}{2}k_3 r_0\varphi - \frac{1}{2}k_3 u = \mathrm{sgn}(\Omega - \dot{\varphi})\mu_\mathrm{k} F_\mathrm{N} \tag{6.41a}$$

$$m\ddot{u} + c_2\dot{u} - \frac{1}{2}k_3 r_0\varphi + \frac{1}{2}k_3 u = F_\mathrm{N} - F \tag{6.41b}$$

$$M_{kl}\ddot{C}_{kl} + 2\xi\omega_{kl}M_{kl}\dot{C}_{kl} + 2lM_{kl}\Omega\dot{D}_{kl} + (\omega_{kl}^2 M_{kl} - l^2 M_{kl}\Omega^2)C_{kl} = \left[-R_{kl}(r_0)\cos(l\varphi) - \frac{h}{2r_0}\mu_\mathrm{k} l R_{kl}(r_0)\sin(l\varphi)\right]F_\mathrm{N} \tag{6.41c}$$

$$M_{kl}\ddot{D}_{kl} + 2\xi\omega_{kl}M_{kl}\dot{D}_{kl} - 2lM_{kl}\Omega\dot{C}_{kl} + (\omega_{kl}^2 M_{kl} - l^2 M_{kl}\Omega^2)D_{kl} = \left[-R_{kl}(r_0)\sin(l\varphi) + \frac{h}{2r_0}\mu_\mathrm{k} R_{kl}(r_0)\cos(l\varphi)\right]F_\mathrm{N} \tag{6.41d}$$

where,

$$F_\mathrm{N} = k_2\left(\sum_{k=0}^{\infty}\sum_{l=0}^{\infty}\left[R_{kl}(r_0)\left(\cos(l\varphi)\cdot C_{kl}(t) + \sin(l\varphi)\cdot D_{kl}(t)\right)\right] - u\right) + k_\mathrm{nl}\left(\sum_{k=0}^{\infty}\sum_{l=0}^{\infty}\left[R_{kl}(r_0)\left(\cos(l\varphi)\cdot C_{kl}(t) + \sin(l\varphi)\cdot D_{kl}(t)\right)\right] - u\right)^3$$

By setting all the terms involving velocity and acceleration in Eq. (6.41) to be zero, the algebraic nonlinear equations to determine the equilibrium point of the system are obtained and ca be solved numerically using *fsolve* in MATLAB. Then the nonlinear Eq. (6.41) is linearized around the equilibrium point and a linearized system is derived. By calculating the eigenvalues of linearized system, the stability of the system at the equilibrium point is identified.

The values of basic system parameters are listed in Table 6.2. To avoid excessive computations, only the first seven disc modes are included in the transverse vibration of the disc, which are found to be adequate in terms of the convergence of the results. The first seven natural frequencies of the disc are 1492, 1517, 1517, 1824, 1824, 2774 and 2774 rad/s.

Table 6.2 The values of basic system parameters of the slider-on-disc model

a	b	r_0	ρ	E	h	ν	Ω
0.044 m	0.12 m	0.1 m	7200 kg/m^3	150 GPa	0.002 m	0.211	10rad/s
m	k_1	k_2	k_3	c_1	c_2	ξ	
1 kg	10^5N/m	$5\cdot10^4$N	$6\cdot10^4$N/m	0.1 N · s/	0.1 N · s/	10^{-4}	

Firstly, the effects of nonlinear contact stiffness k_{nl} on the linear stability of the system are investigated. Figs. 6.20 and 6.21 depict respectively the real parts (growth rates) and imaginary parts (frequencies) of the complex eigenvalues of the linearized system as a function of μ_{k} with different values of k_{nl} when $F = 10^4$N. It is observed from Fig. 6.20 that four modes (mode 1, mode 4, mode 5 and mode 7) become unstable with the increase of μ_{k}, namely, the real parts of eigenvalues become positive. The value of the friction coefficient at which the real part of an eigenvalue turns positive can be called the critical friction coefficient for the instability of the corresponding mode. The results in Fig. 6.20 show that a larger nonlinear contact stiffness k_{nl} leads to a smaller critical friction coefficient for the instability of mode 1 and mode 4, while the critical friction coefficients for the instability of mode 5 and mode 7 are nearly unchanged with the variation of k_{nl}. Besides, the results in Fig. 6.21 demonstrate that the nonlinear contact stiffness has notable effect on the frequencies of some modes (mode 1, 2, 5, 7, 9) but little effect on the frequencies of other modes (mode 3, 4, 6, 8).

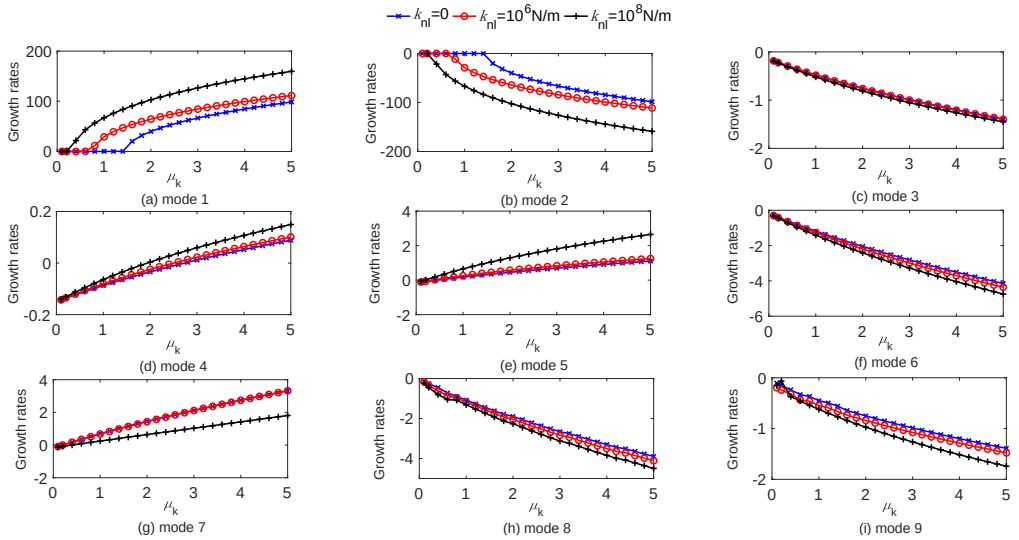

Figure 6.20 The real parts of the complex eigenvalues of the linearized system of the slider-on-disc model as a function of μ_{k} with different values of k_{nl}.

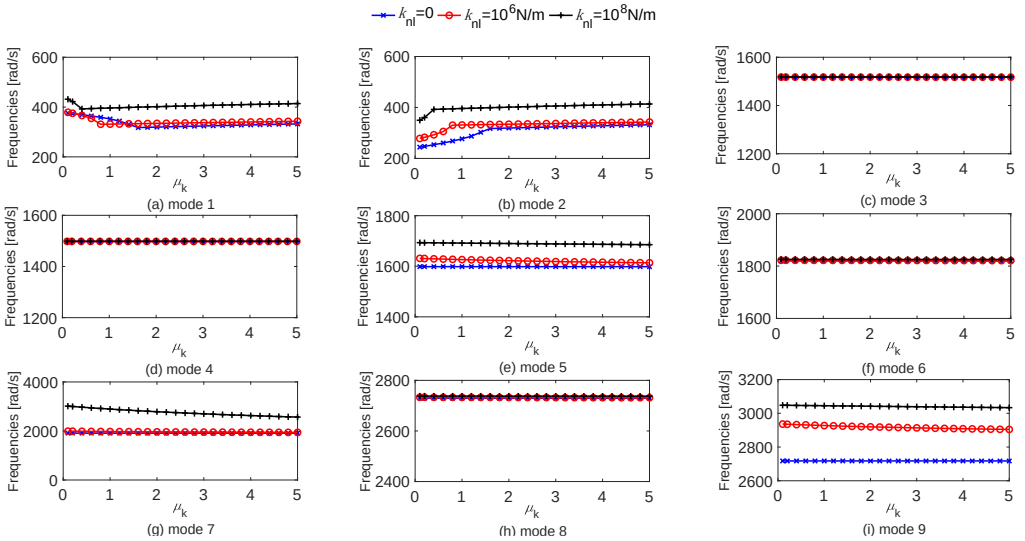

Figure 6. 21 The imaginary parts of the complex eigenvalues of the linearized system of the slider-on-disc model as a function of μ_{k} with different values of k_{nl}.

Secondly the effects of the geometrical nonlinearity (GN) on the linear stability of the system are investigated. The geometrical nonlinearity in the system originate from the coupling of tangential motion of the slider and transverse motion of the disc, i.e., the coupling of $\varphi(t)$ and modal coordinates $C_{kl}(t)$, $D_{kl}(t)$. To reveal its effect on the stability of the system, the linear stability analysis for the system when the disc is assumed to be rigid, i.e., without the geometrical nonlinearity, is conducted. For the system without the geometrical nonlinearity, only the tangential and normal motion of the slider are considered and the mode-coupling instability will happen, as exhibited in Fig. 6.22. It is seen from the figure that the critical friction coefficient for the

instability when $k_{\mathrm{nl}} = 10^6\mathrm{N/m}$ is less than that when $k_{\mathrm{nl}} = 0$, but the critical friction coefficient for the instability when $k_{\mathrm{nl}} = 10^8\mathrm{N/m}$ is greater than that when $k_{\mathrm{nl}} = 0$. The comparisons between Fig. 6.20 and Fig. 6.22 (b) indicate the discrepancies between the critical friction coefficients for the instability with and without the geometrical nonlinearity. For the system with the geometrical nonlinearity, the critical friction coefficient at which one of the modes becomes unstable is obviously smaller than the critical friction coefficient for the system without the geometrical nonlinearity. In Fig. 6.23, the critical friction coefficients for the system with and without the geometrical nonlinearity as functions of the preload are given. When $k_{\mathrm{nl}} = 0$, the critical friction coefficient for the system without the geometrical nonlinearity is constant with the variation of preload and quite greater than that for the system with the geometrical nonlinearity; when $k_{\mathrm{nl}} = 10^6\mathrm{N/m}$, the critical friction coefficient with the geometrical nonlinearity is also smaller than without, but the two quantities get close to each other as the preload increases between $1000\mathrm{N}$ and $15000\mathrm{N}$; when $k_{\mathrm{nl}} = 10^8\mathrm{N/m}$, the critical friction coefficient for the system without the geometrical nonlinearity firstly decreases and then increases with the increase of preload, and is much larger than that for the system with the geometrical nonlinearity except when $F = 1000\mathrm{N}$ and $2000\mathrm{N}$. From these results, it is reasonable to conclude that the geometrical nonlinearity promotes the occurrence of dynamic instability. Besides, the results shown in Fig. 6.23 demonstrate that the nonlinear contact stiffness has more significant effect on the critical friction coefficient for the system without the geometrical nonlinearity than on the critical friction coefficient for the system with the geometrical nonlinearity.

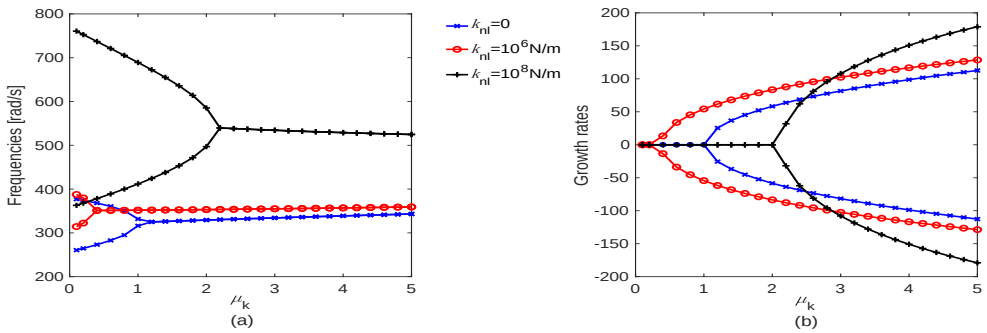

Figure 6.22 Stability analysis of the slider-on-disc model without the geometrical nonlinearity as a function of μ_{k} with different values of k_{nl}: (a) frequencies and (b) growth rates.

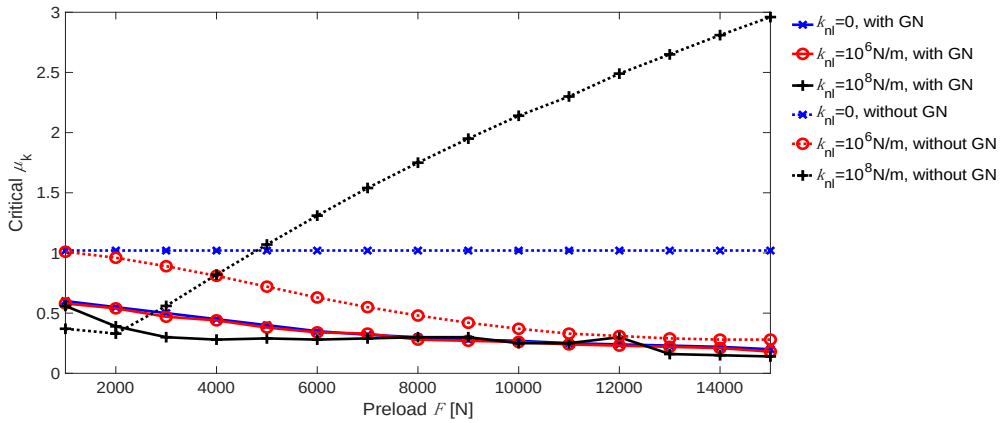

Figure 6.23 The critical friction coefficients for the slider-on-disc model with and without the geometrical nonlinearity (GN) as functions of the preload.

Thirdly, the nonlinearity with respect to the non-smooth states of motion has no effect on the linear stability of the system because the system is in the state of slip in the vicinity of the equilibrium point.

6.5.2 Nonlinear steady-state responses of the slider-on-disc model

The nonlinear steady-state responses of the slider-on-disc system are investigated by means of the transient dynamic analysis and the effects of different types of nonlinearities on the steady-state responses of the system are examined. The values of the basic system parameters are identical with those in Table 6.2.

Firstly, the time responses of the system under two values of μ_k $(0.3, 2.2)$ with $\mu_s = 3$, $k_{nl} = 10^6 \mathrm{N/m}$ and $F = 1000\mathrm{N}$ are obtained and plotted in Fig. 6.24 and Fig. 6.25, respectively. For either value of μ_k , the system responses from two different initial conditions, i.e., one near the equilibrium point and the other far from the equilibrium point, are exhibited. When $\mu_k = 0.3$, the two initial conditions lead to different steady-state responses. The dynamic responses from the initial condition near the equilibrium point approach the equilibrium point while the dynamic responses from the initial condition far from the equilibrium approach a non-periodic oscillation, which indicates the coexistence of two stable solutions in the system. When $\mu_k = 2.2$, however, the dynamic responses from both initial conditions approach the same quasi-periodic oscillation, indicating there is only one stable quasi-periodic solution for the steady-state responses of the system.

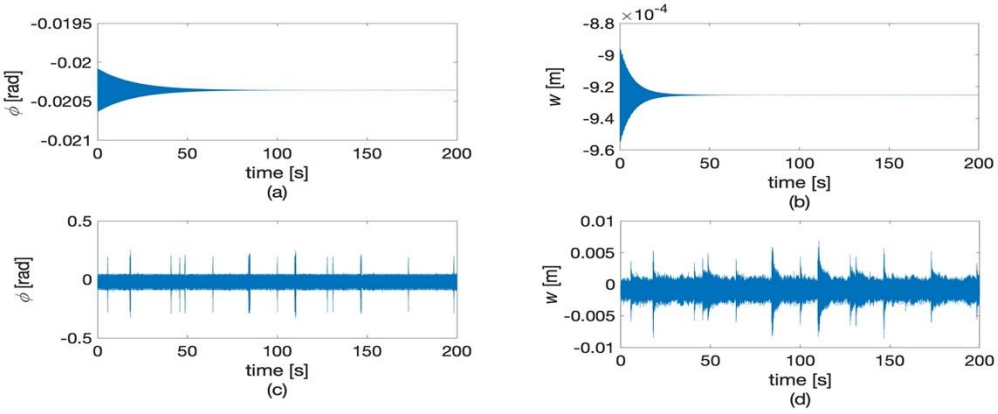

Figure 6.24 The time histories of the tangential motion of the slider and the transverse displacement of a specific point $(r = r_0, \theta = 1)$ on the disc under $\mu_k = 0.3$ with $\mu_s = 3$, $k_{nl} = 10^6 \mathrm{N/m}$ and $F = 1000\mathrm{N}$ from two initial conditions: (a)(b) near the equilibrium point and (c)(d) far from the equilibrium point.

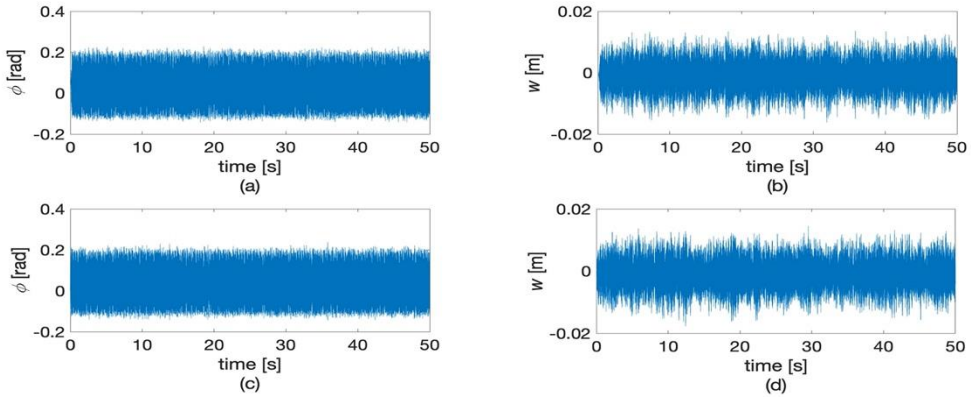

Figure 6.25 The time histories of the tangential motion of the slider and the transverse displacement of a specific point $(r = r_0, \theta = 1)$ on the disc under $\mu_k = 2.2$ with $\mu_s = 3$, $k_{nl} = 10^6 \mathrm{N/m}$ and $F = 1000\mathrm{N}$ from two initial conditions: (a)(b) near the equilibrium point and (c)(d) far from the equilibrium point.

Similarly, an index is defined to measure the intensity of steady-state vibration of the slider in the system, which is,

$$L_s = \frac{\int_T [(\varphi - \varphi_e)^2 + (u - u_e)^2] \mathrm{d}t}{T} \tag{6.42}$$

where φ_e, u_e are the values of φ and u at the equilibrium point, T represents a time period in the steady state. In Fig. 6.26, the values of L_s as μ_k varies between 0.1 and 2.95 are exhibited. It is observed from the figure that the system has a single stable equilibrium point when $0.4 < \mu_k \leq 0.9$ and a single stable oscillation (with finite amplitude) when $\mu_k > 0.9$ for the steady-state responses, while two stable solutions

(the equilibrium point and the oscillation with finite amplitude) coexist when $0.1 \leq \mu_{\mathrm{k}} \leq 0.4$. Fig. 6.27 depicts the periodicity of the steady-state responses when $0.05 \leq \mu_{\mathrm{k}} \leq 2.95$ by showing the values of φ at the transition points from slip to stick. The figure indicates that the system has periodic steady-state responses when $0.1 \leq \mu_{\mathrm{k}} \leq 0.2$, and non-periodic steady-state responses for other values of μ_{k} except $0.4 < \mu_{\mathrm{k}} \leq 0.9$ at which the system is stationary at the equilibrium point in the steady state.

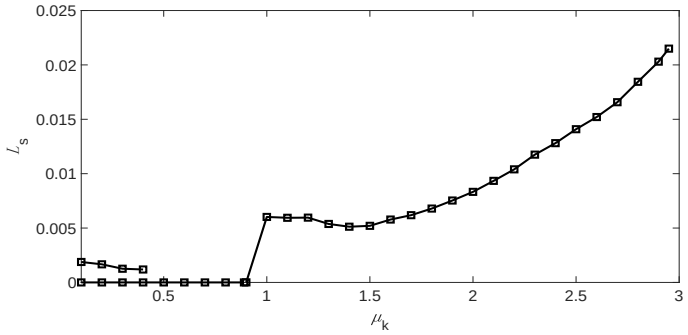

Figure 6.26 Index L_{s} as a function of μ_{k} of the slider-on-disc model.

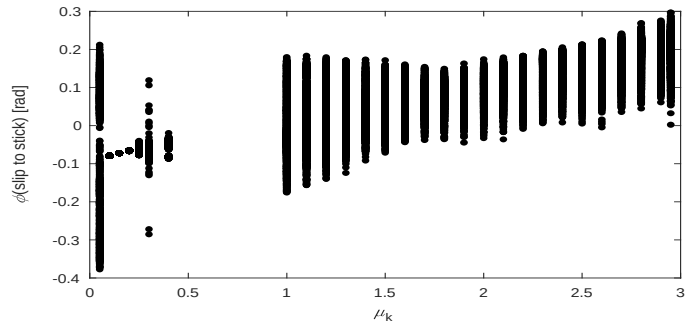

Figure 6.27 The bifurcation behaviour of the steady-state response of the slider-on-disc model dependent on μ_{k}.

Next the effects of each type of nonlinearity on the steady-state response of the slider-on-disc system are revealed. Firstly, the effects of the nonlinear contact stiffness are examined. In Fig. 6.28, the bifurcation behaviours of the steady-state response dependent on μ_{k} when $k_{\mathrm{nl}} = 0$ and $k_{\mathrm{nl}} = 10^8 \mathrm{N/m}$ are exhibited. By comparing the results in Fig. 6.28 with those in Fig. 6.27, it is observed that the bifurcation behaviours of the system response under the three different values of k_{nl} are generally similar. One difference exists that while some small values of μ_{k} corresponds to periodic oscillation under $k_{\mathrm{nl}} = 0$ and $k_{\mathrm{nl}} = 10^6 \mathrm{N/m}$, there is no value of μ_{k} corresponding to periodic response under $k_{\mathrm{nl}} = 10^8 \mathrm{N/m}$. Overall, the bifurcation behaviours under the

three different values of k_{nl} demonstrate that the nonlinear contacts stiffness has little effect on the periodicity of steady-state response of the system. Subsequently the values of L_{s} as the function of μ_{k} with the three different values of k_{nl} are shown in Fig. 6.29. It is seen that the values of L_{s} under $k_{\mathrm{nl}} = 0$ and $k_{\mathrm{nl}} = 10^6\mathrm{N/m}$ are nearly identical at every value of μ_{k} except $\mu_{\mathrm{k}} = 0.2$, while the values of L_{s} under $k_{\mathrm{nl}} = 10^8\mathrm{N/m}$ are greater than those under $k_{\mathrm{nl}} = 0$ and $k_{\mathrm{nl}} = 10^6\mathrm{N/m}$ for $\mu_{\mathrm{k}} \geq 1.2$, which indicates stronger steady-state vibration when $k_{\mathrm{nl}} = 10^8\mathrm{N/m}$ than those when $k_{\mathrm{nl}} = 0$ and $k_{\mathrm{nl}} = 10^6\mathrm{N/m}$. Besides, it is shown in Fig. 6.29 that at $0.4 < \mu_{\mathrm{k}} < 1$ under $k_{\mathrm{nl}} = 0$ and $k_{\mathrm{nl}} = 10^6\mathrm{N/m}$ and at $0.3 < \mu_{\mathrm{k}} < 0.6$ under $k_{\mathrm{nl}} = 10^8\mathrm{N/m}$, there is no vibration in the steady state, i.e., a single stable equilibrium point exists in the system.

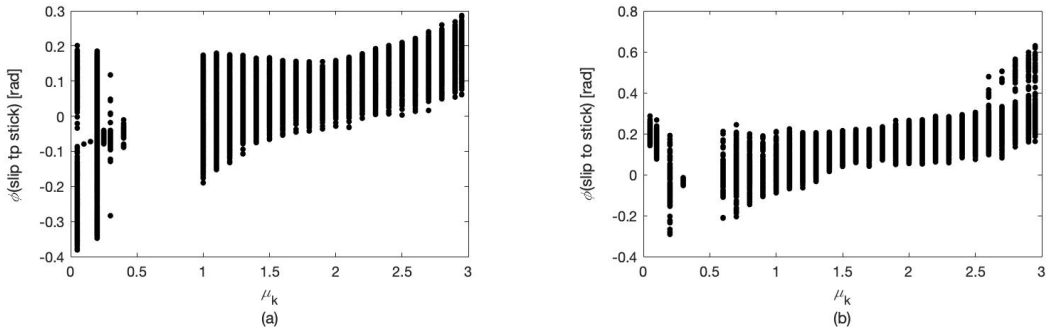

Figure 6.28 The bifurcation behaviours of the steady-state response of the slider-on-disc model dependent on μ_{k} with different values of k_{nl}: (a) $k_{\mathrm{nl}} = 0$ and (b) $k_{\mathrm{nl}} = 10^8\mathrm{N/m}$.

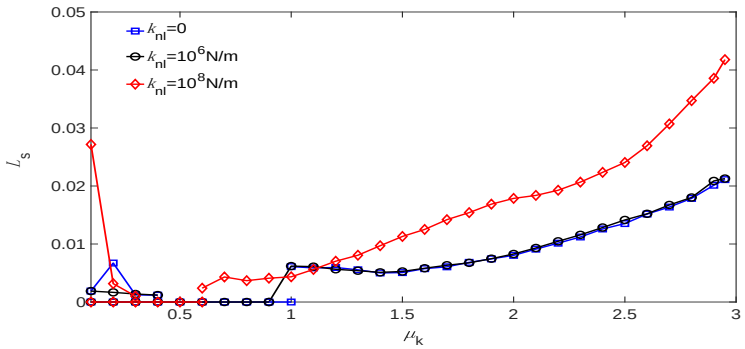

Figure 6.29 Index L_{s} as the function of μ_{k} of the slider-on-disc model with different values of k_{nl}.

Secondly, the effects of the geometrical nonlinearity on the steady-state response of the slider-on-disc system are investigated. To reveal the effects of the geometrical nonlinearity, the steady-state responses of the system without the geometrical

nonlinearity are obtained and compared with the results of the original system with the geometrical nonlinearity. In Fig. 6.30, the bifurcation behaviours of the steady-state response when $0.05 \leq \mu_{\mathrm{k}} \leq 2.95$ for the system without the geometrical nonlinearity are plotted. It is observed from the figure that there are small values of μ_{k} $(0.1 \leq \mu_{\mathrm{k}} < 0.2)$ corresponding to periodic oscillation under $k_{\mathrm{nl}} = 0$ and $k_{\mathrm{nl}} = 10^6\mathrm{N/m}$, while no value of μ_{k} corresponds to periodic response under $k_{\mathrm{nl}} = 10^8\mathrm{N/m}$. The comparison between the bifurcation behaviours with and without the geometrical nonlinearity indicates that the geometrical nonlinearity has little effect on the periodicity of steady-state response of the system. In Fig. 6.31, the values of index L_{s} as the function of μ_{k} for the system without the geometrical nonlinearity are presented. The comparison between Fig. 6.31 and Fig. 6.29 highlight two significant differences between the values of L_{s} with and without the geometrical nonlinearity. Firstly, the values of L_{s} for the system with the geometrical nonlinearity are greater than those for the system without the geometrical nonlinearity at $\mu_{\mathrm{k}} > 1$ under each of the three values of k_{nl}, which indicates stronger steady-state response for the system with the geometrical nonlinearity than that for the system without the geometrical nonlinearity. Secondly, the values of L_{s} at $\mu_{\mathrm{k}} \geq 0.8$ under $k_{\mathrm{nl}} = 10^8\mathrm{N/m}$ are smaller than or nearly equal to those under $k_{\mathrm{nl}} = 0$ and $k_{\mathrm{nl}} = 10^6\mathrm{N/m}$ at for the system without the geometrical nonlinearity, which is quite different from the scenario of the system with the geometrical nonlinearity. These two differences embody the significant effect of the geometrical nonlinearity on the values of L_{s}, i.e., the intensity of steady-state response of the slider. However, one similarity between the results of L_{s} with and without the geometrical nonlinearity is also observed, that is, the similar trend of L_{s} with the variation of μ_{k} under each value of k_{nl}.

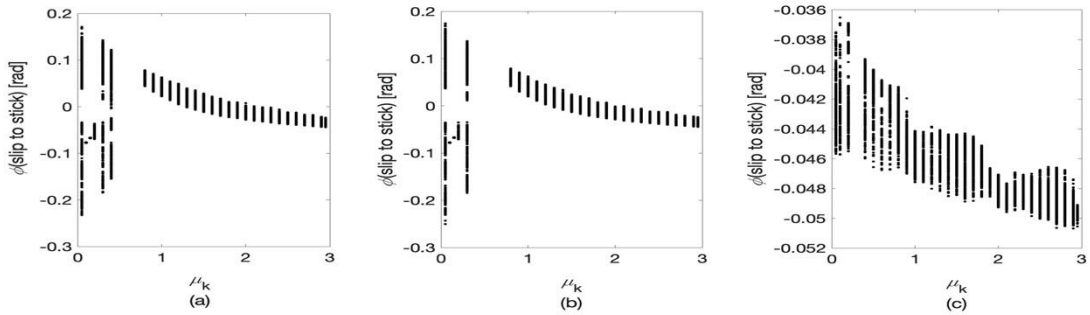

Figure 6.30 The bifurcation behaviours of the steady-state response for the slider-on-disc model without the geometrical nonlinearity: (a)$k_{\mathrm{nl}} = 0$, (b) $k_{\mathrm{nl}} = 10^6\mathrm{N/m}$ and (c) $k_{\mathrm{nl}} = 10^8\mathrm{N/m}$.

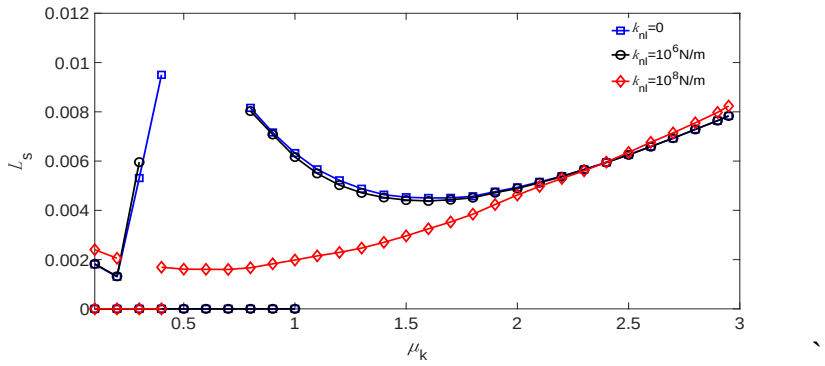

Figure 6.31 Index L_s as the function of μ_k for the slider-on-disc model without the geometrical nonlinearity.

Thirdly, the effects of the non-smooth states of motion on the steady-state response of the slider-on-disc are studied. To reveal the effects of the non-smooth states of motion including stick/slip and contact/separation on the steady-state responses of the system, the dynamic responses of the system with the following three different kinds of assumptions about the states of motion are calculated and compared with those of the original system. The first kind of assumption is that there exists the single state of unidirectional relative sliding in the vibration; the second is that there exist two distinct states of motion that are unidirectional relative sliding and separation in the vibration; the third is that there exist three possible states of motion in the vibration which are sliding, reverse-sliding and separation. In other word, the states of stick and separation are neglected in the first kind of assumption, while in the second and third kind of assumptions, the state of stick is neglected. It is found by computations that the amplitudes of dynamic responses will grow to infinity for μ_k greater than a certain value when the first kind of assumption is implemented, therefore it is not feasible to acquire the bifurcation behaviour and intensity of the steady-state response. Nevertheless, the range of μ_k at which the self-excited vibration exists in the steady state can be obtained. The numerical results demonstrate that the self-excited vibration exists in the steady state at $\mu_k \geq 0.6$ for each value of k_{nl} (0, 10^6N/m, 10^8N/m), while at $\mu_k < 0.6$ the system is stationary at the equilibrium point in the steady state. This scenario is different from that of the original system in which the self-excited vibration also exists in the steady state at small values of μ_k, e.g. $\mu_k \leq 0.4$.

The steady-state responses of the system with other two kinds of assumptions are next obtained. The bifurcation behaviours of the steady-state response for the system with

the second kind of assumption about the states of motion are displayed in Fig. 6.32, which shows the values of φ when $\dot{\varphi} = 0$. The self-excited vibration exists in the steady state at $\mu_k \geq 0.6$ for each value of k_{nl} (0, 10^6N/m, 10^8N/m). It is found that for each of the three values of k_{nl}, the system has non-periodic steady-state response at any values of μ_k ($\mu_k \geq 0.6$). The values of index L_s as the function of μ_k for the system with the second kind of assumption about the states of motion are given in Fig. 6.33. Roughly speaking, the values of L_s grows with the increase of μ_k, indicating stronger steady-state vibration at larger μ_k. And the comparison between the results in Fig. 6.33 and the results in Fig. 6.29 manifests that the values of L_s for the system with the second kind of assumption about the states of motion are much larger than those of the original system, namely, there exists stronger steady-state vibration for the system with the second kind of assumption than that of the original system.

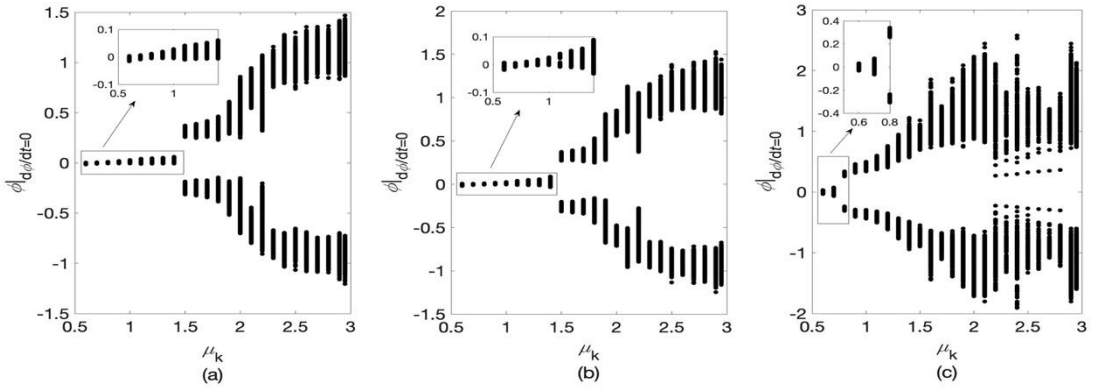

Figure 6.32 The bifurcation behaviours of the steady-state response for the slider-on-disc model with the second kind of assumption about the states of motion: (a)$k_{nl} = 0$, (b) $k_{nl} = 10^6$N/m and (c) $k_{nl} = 10^8$N/m.

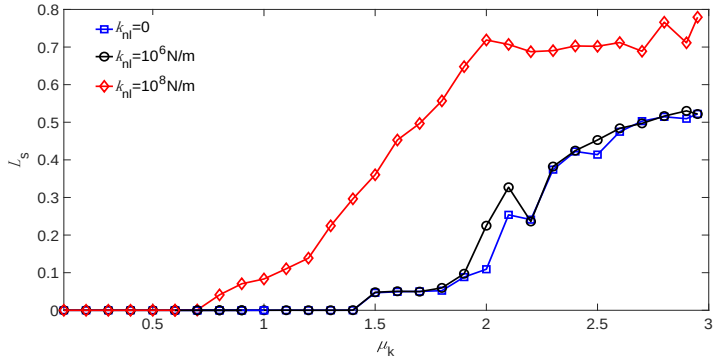

Figure 6.33 Index L_s as the function of μ_k for the slider-on-disc model with the second kind of assumption about the states of motion.

The bifurcation behaviours of the steady-state response for the system with the third kind of assumption about the states of motion are displayed in Fig. 6.34. The self-excited vibration exists in the steady state at $\mu_{\mathrm{k}} \geq 0.6$ for each value of k_{nl} (0, $10^6\mathrm{N/m}$, $10^8\mathrm{N/m}$). It is found that the system has periodic steady-state response at some values of μ_{k} under each value of k_{nl}, e.g. at $1.1 < \mu_{\mathrm{k}} < 1.5$ under $k_{\mathrm{nl}} = 0$ and $k_{\mathrm{nl}} = 10^6\mathrm{N/m}$, at $0.6 \leq \mu_{\mathrm{k}} < 1$ under $k_{\mathrm{nl}} = 10^8\mathrm{N/m}$. The steady-state responses at other values of μ_{k} are non-periodic. The values of index L_{s} as the function of μ_{k} for the system with the third kind of assumption about the states of motion are given in Fig. 6.35. The comparison of the results in Fig. 6.35 with the results in Fig. 6.29 also manifests much greater values of L_{s} with this kind of assumption than those of the original system.

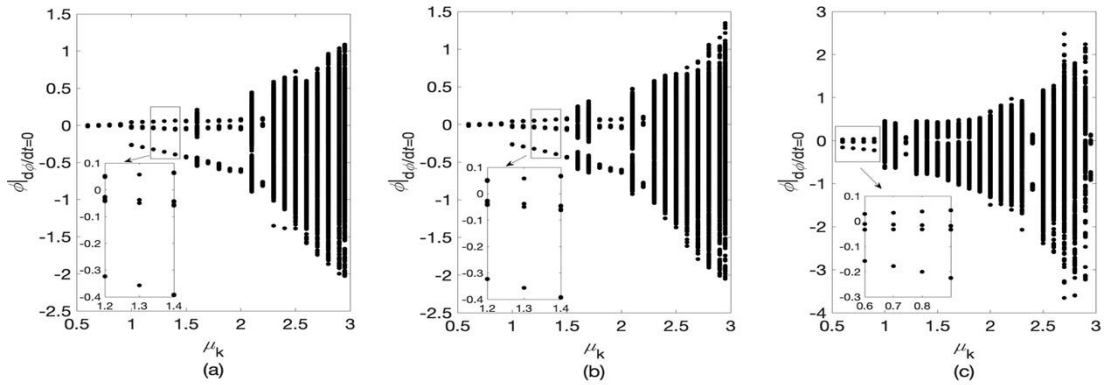

Figure 6.34 The bifurcation behaviours of the steady-state response for the slider-on-disc model with the third kind of assumption about the states of motion: (a)$k_{\mathrm{nl}} = 0$, (b) $k_{\mathrm{nl}} = 10^6\mathrm{N/m}$ and (c) $k_{\mathrm{nl}} = 10^8\mathrm{N/m}$.

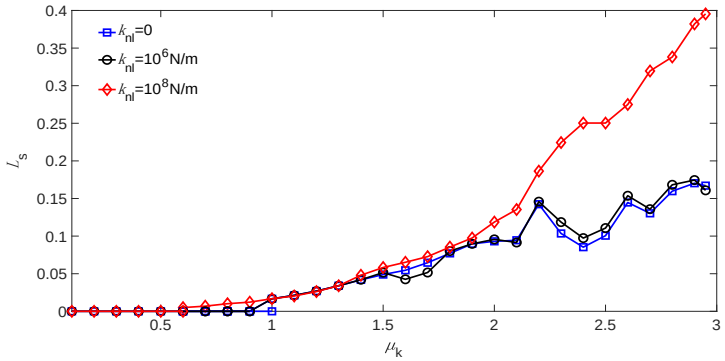

Figure 6.35 Index L_{s} as the function of μ_{k} for the slider-on-disc mode with the third kind of assumption about the states of motion.

Overall, it can be concluded from the above observations that the nonlinearity of the non-smooth states of motion has significant effects on the steady-state responses of the slider-on-disc system, especially on the intensity of vibration which is reflected by the values of index L_s.

6.6. Conclusions

In this chapter, the dynamics of a novel 5-DoF mass-on-belt frictional model with three different types of nonlinearities is investigated. The first type of nonlinearity is the nonlinear contact stiffness, the second is the non-smooth states of motion including stick, slip and separation, and the third is the geometrical nonlinearity caused by the moving-load feature of the mass on the rigid belt. Both the linear stability of the system and the nonlinear steady-state responses are studied. The effects of each type of nonlinearity on the system dynamics are revealed. Besides, a similar study is carried out on a continuous slider-on-disc model. Based on the observations from the numerical study, the following conclusions are reached,

1. The mode-coupling instability arises in the 5-DoF frictional system with the increase of the coefficient of kinetic friction μ_k. The critical friction coefficient for the instability decreases with the increase of the preload.
2. The nonlinearity of contact stiffness and the geometrical nonlinearity have significant effects on the linear stability of the 5-DoF frictional system. The increase of nonlinear contact stiffness leads to the decrease of critical friction coefficient for the instability. The presence of geometrical nonlinearity contributes to the decrease of critical friction coefficient for the instability and increases the complexity of the instability in the system.
3. There is coexistence of two stable solutions, i.e., the equilibrium point and the limit cycle vibration, in both the 5-DoF frictional system and the slider-on-disc system in a certain range of μ_k, and the linear stability analysis fails to detect the occurrence of self-excited vibration when the system is bi-stable, which can only be found out by the transient dynamic analysis. Besides, the bifurcation behaviours of the steady-state responses of the systems with the variation of μ_k are found.
4. Each of the three different types of nonlinearities has significant effects on the steady-state responses of the 5-DoF frictional system in terms of both the

periodicity and the intensity of vibration, which are demonstrated in the numerical study.

5. Frequencies of the steady-state responses in the 5-DoF frictional system deviate markedly from the unstable eigenfrequencies of the linearized system and each type of nonlinearity has different effects on the deviation of vibration frequencies from the unstable eigenfrequencies.

6. Multiple modes become unstable with the increase of μ_k in the slider-on-disc system. The nonlinearity of contact stiffness has distinct effects on the instabilities of different modes. For some modes, the increase of nonlinear contact stiffness leads to the decrease of critical friction coefficient for the instability, while the critical friction coefficients for some modes are nearly unchanged with the variation of nonlinear contact stiffness. The geometrical nonlinearity promotes the occurrence of dynamic instability in the slider-on-disc system.

7. The nonlinear contact stiffness and the geometrical nonlinearity have significant effect on the intensity of steady-state response but little effect on the periodicity of steady-state response in the slider-on-disc system, while the nonlinearity of the non-smooth states of motion has significant effect on both the intensity and the periodicity of steady-state response in the slider-on-disc system.

Chapter 7

Friction induced vibration of a pin-on-disc system considering non-uniform friction interface

In this chapter, a new pin-on-disc system with an L-mechanism is proposed and the friction induced dynamics of the system is studied. The Coulomb's law of friction with static friction coefficient μ_s and kinetic friction coefficient μ_k is utilized to model the friction force between the pin and disc. The stick-slip motion of the pin in the circumferential direction of the spinning disc is analysed, while the normal force between them is adjusted by the vibration of an L-shaped component which is induced by the pin's motion. It is found that the variable normal force contributes to the occurrence of bifurcation behaviours of system responses. Besides, it is observed that the system is bi-stable at low disc speed and high normal preload when $\mu_s > \mu_k$, i.e., there is coexistence of a stable pure sliding solution and a stable stick-slip limit cycle for the pin. The non-uniform friction interface in which a sector of the disc surface possesses a different set of friction property from that on the rest of the disc surface is then introduced and the corresponding friction induced dynamics of the system is investigated. It is found that with appropriate friction coefficients on the sector and an appropriate span angle of the sector, the range of disc speed and normal preload at which the stick-slip vibration exists will be greatly diminished in comparison with the original uniform friction interface.

7.1 Introduction

Stick-slip phenomenon occurring in engineering or in daily life is a typical kind of vibration caused by friction, in which the dynamical systems experience non-smooth transitions between the two states (slip and stick) at zero relative velocity during operation. The vibration instability in numerous mechanical systems results from the friction induced stick-slip vibration, e.g., the sound of string music instruments [212], the squeaking joints of robots [213], the stick-slip oscillation of drill-strings [12], the noise of windscreen wipers [7] and the low-frequency automobile brake noise called creep groan [10], etc. As introduced in the literature review, there have been a number of published studies on the stick-slip vibration. For example, Popp et al. [20] investigated stick-slip vibration of discrete and continuous models and observed the rich bifurcation and chaotic behaviour for the models with the governing equations which can be expressed as three- or higher-dimension first-order ordinary differential equations; Hetzler [31] studied the effect of non-smooth Coulomb friction on a simple oscillator on a belt exhibiting self-excited vibration due to negative damping in the case of negative friction force-relative velocity slope; Papangelo [33] investigated the subcritical bifurcation of a slider-on-belt system which experienced friction induced vibration in the case of a weakening-strengthening friction law, and the results showed there was a range of parameter values where two stable solutions coexisted, i.e., a stable sliding equilibrium and a stable stick-slip limit cycle. Although only two distinct states are involved in stick-slip oscillations, very complicated dynamic behaviours can still arise and the dynamic responses vary among the mechanical systems with stick-slip vibration.

The stick-slip vibration can adversely affect the performance of machines. For example, the stick-slip vibration in automobile brake systems causes low-frequency brake noise such as creep groan which may cause discomfort to passengers and impact the reputations of automobile brands. To help suppress the adverse stick-slip vibration in mechanical systems, some researchers conducted theoretical or/and experimental studies. In Ref. [214], an approach for the robust suppression of stick-slip oscillations in oil drill-strings was presented. In Ref. [215], the approach of normal load modulation was put forward to stabilize the frictional system against stick-slip oscillations. Jang et al. [216] examined creep groan propensity of different friction

materials. Fuadi et al. [217] studied the fundamental mechanism of creep groan generation of an experimental caliper-slider model. Both works showed that the creep groan could be successfully avoided by using friction materials with small difference between coefficients of static and kinetic friction. Zhao et al. [195] integrated piezoceramic actuators into a disc brake system to provide harmonic high-frequency vibrations to reduce the difference between coefficients of static and kinetic friction so as to eliminate the stick-slip limit cycle vibration of the system.

However, there is no universal solution for the suppression of stick-slip vibration in mechanical systems yet. To gain more insights into this problem, a new pin-on-disc system with an L-mechanism to adjust the normal force is proposed and the friction induced stick-slip vibration of the system is investigated. Especially, the friction induced dynamics with a non-uniform friction interface on the disc, i.e., a sector of the disc surface possesses a different set of friction property from that on the rest of the disc surface, is studied.

7.2 Model description and dynamic equations

A new pin-on-disc arrangement with an L-mechanism to adjust the normal force during vibration is proposed, as shown in Fig. 7.1. Such a mechanism was also employed in a mass-on-moving-belt model in Ref. [104]. The pin, fixed on a vertical plate protruding from the leading end of a hollow cylinder which can rotate around the central axis, is pressed against the spinning disc by a preload N_0. The resultant friction force leads to the rotation of the cylinder and attached structures, which is constrained by linear spring k_1 at the end of a horizontal arm protruding from the cylinder. Linear spring k_3, which connects a vertical arm protruding from the trailing end of the cylinder with one side of an L-shaped component, brings it into rotation around the pivot as the cylinder rotates. The other side of the L-shaped component is connected to the back of the plate on which the pin is fixed by linear spring k_2, therefore the normal force between the pin and disc is changed with the rotation of the L-shaped component.

The dynamic equations of the system are next derived. The angular displacements of the cylinder and the L-shaped component, which are denoted by φ and θ respectively, are considered. The kinetic energy of the system can be written as,

$$T = \frac{1}{2}J_c\dot{\varphi}^2 + \frac{1}{2}J_L\dot{\theta}^2 \tag{7.1}$$

where J_c, J_L are the rotational inertia of the cylinder and the L-shape structure, respectively. The potential energy of the system is the sum of the elastic potential energy of springs k_1, k_2 and k_3, i.e.,

$$U = \frac{1}{2}k_1\Delta l_1^2 + \frac{1}{2}k_2\Delta l_2^2 + \frac{1}{2}k_3\Delta l_3^2 \tag{7.2}$$

where Δl_i $(i = 1,2,3)$ represent the amount of deformation of spring k_i.

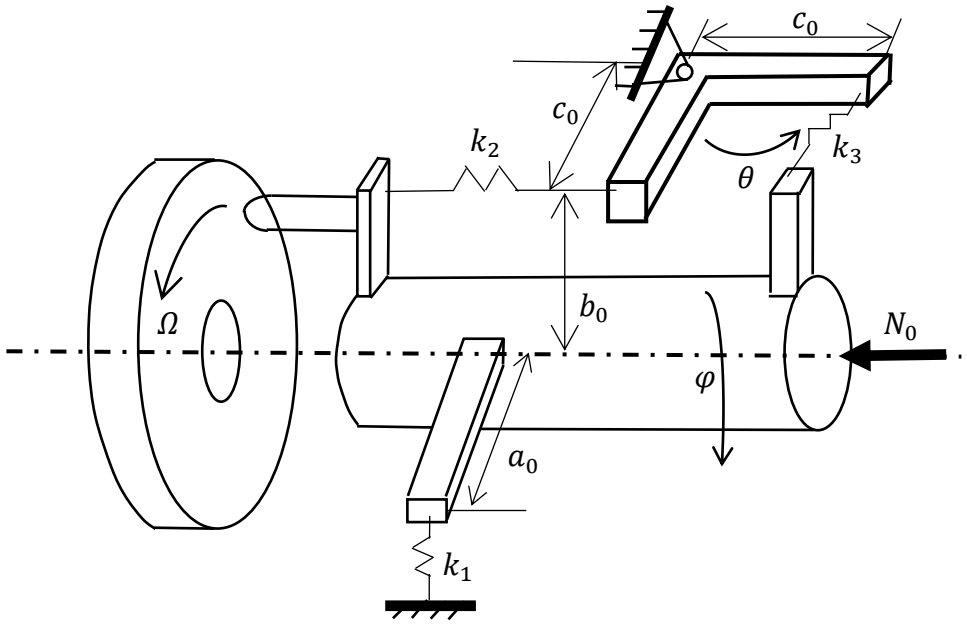

Figure 7.1 A new pin-on-disc setup.

Denoting the distance between the fixed point of spring k_1 on the horizontal arm and the central axis as a_0, the distance between the fixed point of spring k_2 at the back of the vertical plate and the central axis as b_0, both the distances between the fixed points of spring k_2 and k_3 on the L-shape structure and the pivot as c_0, the amount of deformation of springs can be expressed as,

$$\Delta l_1 = \sqrt{(l_1 - a_0\sin\varphi)^2 + a_0^2(1-\cos\varphi)^2} - l_1 \tag{7.3}$$

$$\Delta l_2 = \sqrt{[c_0(1-\cos\theta) + b_0\sin\varphi]^2 + b_0^2(1-\cos\varphi)^2 + (l_2 + c_0\sin\theta)^2} - l_2 \tag{7.4}$$

$$\Delta l_3 = \sqrt{(l_3 + c_0\sin\theta + b_0\sin\varphi)^2 + b_0^2(1-\cos\varphi)^2 + c_0^2(1-\cos\theta)^2} - l_3 \tag{7.5}$$

where l_i $(i = 1,2,3)$ is the free length of spring k_i. By expanding the above expressions into the Taylor series with respect to φ and θ and neglecting the third and

higher order terms, which can be done as the magnitudes of φ and θ are assumed to be small, it is derived that,

$$\Delta l_1 = -a_0\varphi \tag{7.6}$$

$$\Delta l_2 = c_0\theta + \frac{b_0^2}{2l_2}\varphi^2 \tag{7.7}$$

$$\Delta l_3 = c_0\theta + b_0\varphi \tag{7.8}$$

The virtual work of external forces include the work done by the friction force and by the rotational damping forces, i.e.,

$$\delta W = -c_1\dot{\varphi}\delta\varphi - c_2\dot{\theta}\delta\theta + fb_0\delta\varphi = (-c_1\dot{\varphi} + fb_0)\delta\varphi - c_2\dot{\theta}\delta\theta \tag{7.9}$$

where c_1, c_2 are the damping coefficients, f is the friction force between the pin and disc. By substituting Eqs. (7.1)-(7.2), (7.6)-(7.9) into the Lagrange's equations,

$$\frac{\mathrm{d}}{\mathrm{d}t}\frac{\partial(T-U)}{\partial\dot{\varphi}} - \frac{\partial(T-U)}{\partial\varphi} = Q_1 \tag{7.10}$$

$$\frac{\mathrm{d}}{\mathrm{d}t}\frac{\partial(T-U)}{\partial\dot{\theta}} - \frac{\partial(T-U)}{\partial\theta} = Q_2 \tag{7.11}$$

where the generalized forces $Q_1 = -c_1\dot{\varphi} + fb_0$, $Q_2 = -c_2\dot{\theta}$, the equations of motion of the system can be obtained as,

$$J_{\mathrm{c}}\ddot{\varphi} + c_1\dot{\varphi} + (k_1a_0^2 + k_3b_0^2)\varphi + k_2\frac{b_0^2\varphi}{l_2}\left(c_0\theta + \frac{b_0^2\varphi^2}{2l_2}\right) + k_3b_0c_0\theta = fb_0 \tag{7.12}$$

$$J_{\mathrm{L}}\ddot{\theta} + c_2\dot{\theta} + k_3c_0(c_0\theta + b_0\varphi) + k_2c_0\left(c_0\theta + \frac{b_0^2\varphi^2}{2l_2}\right) = 0 \tag{7.13}$$

As the Coulomb's friction law is utilized, the friction force during relative sliding can be expressed as,

$$f = \mathrm{sgn}(\Omega - \dot{\varphi})\mu_{\mathrm{k}}N \tag{7.14}$$

where μ_{k} is the coefficient of kinetic friction. The friction force during sticking is obtained by the dynamic equation Eq. (7.12), i.e.,

$$f = \frac{1}{b_0}\left[c_1\Omega + (k_1a_0^2 + k_3b_0^2)\varphi + k_2\frac{b_0^2\varphi}{l_2}\left(c_0\theta + \frac{b_0^2\varphi^2}{2l_2}\right) + k_3b_0c_0\theta\right] \tag{7.15}$$

And the condition for the system to stay in the state of stick is,

$$|f| \le \mu_{\mathrm{s}}N \tag{7.16}$$

in which μ_s is the coefficient of static friction. The normal force N is the sum of the preload N_0 and the component of the force of the spring k_2 in the normal direction, i.e.,

$$N = N_0 + k_2\Delta l_2 \frac{-l_2 - c_0\sin\theta}{l_2+\Delta l_2} \approx N_0 - k_2\Delta l_2 \tag{7.17}$$

7.3 Numerical study of system dynamics under the uniform friction interface

The stick-slip vibration of the system in the situation of uniform friction interface is firstly investigated. The values of basic system parameters used in the numerical simulation are listed in Table 7.1.

Table 7.1 The values of basic system parameters

J_c	J_L	k_1	k_2	k_3	c_1	c_2
$12\cdot10^{-4}$kg·m^2	$5\cdot10^{-4}$kg·m^2	1500N/m	1000N/m	1000N/m	0.001N·m·s	0.001N·m·s
a_0	b_0	c_0	l_1	l_2	l_3	
0.1m	0.1m	0.1m	0.1m	0.1m	0.1m	

It is assumed that the coefficients of friction between the pin and the disc surface are uniform with μ_s=0.4 and μ_k=0.23. In Fig. 7.2 and 7.3, the dynamic responses of the system when the disc speed $\Omega = 2\text{rad/s}$ and the preload $N_0 = 30\text{N}$ in two different sets of initial conditions are shown. It is seen that the system responses may go into a limit cycle which corresponds to periodic stick-slip oscillation for the pin, or an equilibrium point which corresponds to steady sliding for the pin, depending on the initial conditions. This indicates the coexistence of two stable solutions in the system for the above combination of Ω and N_0. Moreover, the dynamic responses of the system when $\Omega = 8\text{rad/s}$, $N_0 = 30\text{N}$ and $\Omega = 2\text{rad/s}$, $N_0 = 8\text{N}$ in different initial conditions are exhibited in Fig. 7.4 and 7.5, respectively. It is seen that different initial conditions approach the same solution, i.e., the equilibrium point, indicating there is one stable solution which is the equilibrium point in the system for these two parameter combinations. From the above observations, it is concluded that the parameter domain of (Ω, N_0) can be divided into two different regions, where one region contains the parameter combinations at which only one stable solution (the steady sliding equilibrium) exists in the system, and the other contains the parameter combinations

at which two stable solutions coexist in the system, including the steady sliding equilibrium and the stick-slip limit cycle.

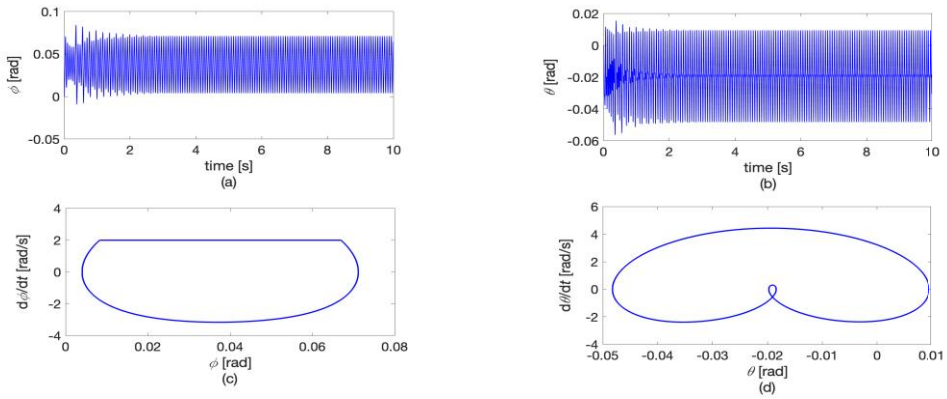

Figure 7.2 Time histories and phase plots of dynamic responses under $\Omega = 2\text{rad/s}$, $N_0 = 30\text{N}$ with $\varphi(0) = \theta(0) = \dot{\theta}(0) = 0$, $\dot{\varphi}(0) = 2\text{rad/s}$.

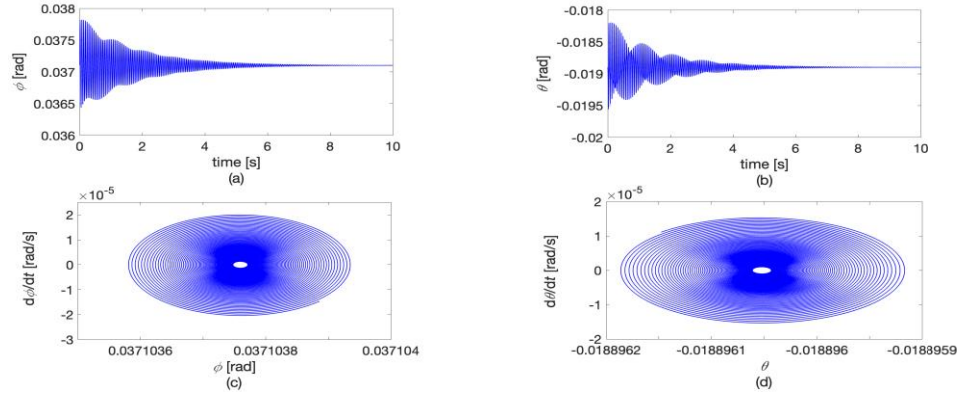

Figure 7.3 Time histories and phase plots of dynamic responses under $\Omega = 2\text{rad/s}$, $N_0 = 30\text{N}$ with $\varphi(0) = 0.037\text{rad}$, $\theta(0) = -0.019\text{rad}$, $\dot{\varphi}(0) = 0.1\text{rad/s}$, $\dot{\theta}(0) = 0$

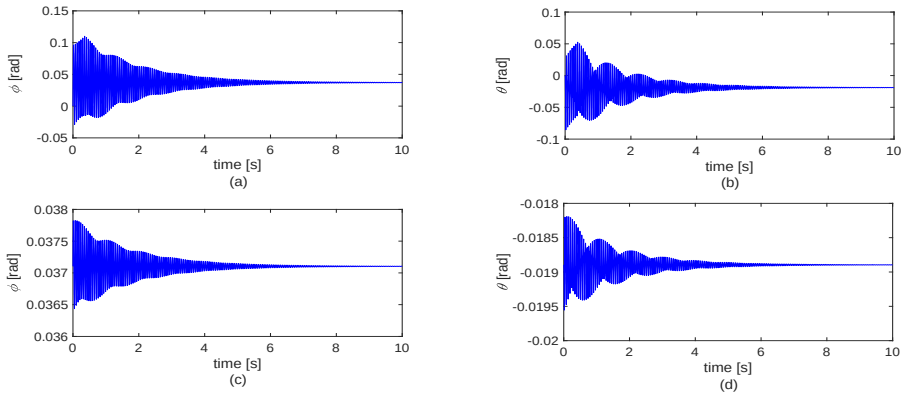

Figure 7.4 Time histories and phase plots of dynamic responses under $\Omega = 8\text{rad/s}$ and $N_0 = 30\text{N}$ with: (a) (b) $\varphi(0) = \theta(0) = \dot{\theta}(0) = 0$, $\dot{\varphi}(0) = 8\text{rad/s}$; (c) (d) $\varphi(0) = 0.037\text{rad}$, $\theta(0) = -0.019\text{rad}$, $\dot{\varphi}(0) = 0.1\text{rad/s}$, $\dot{\theta}(0) = 0$.

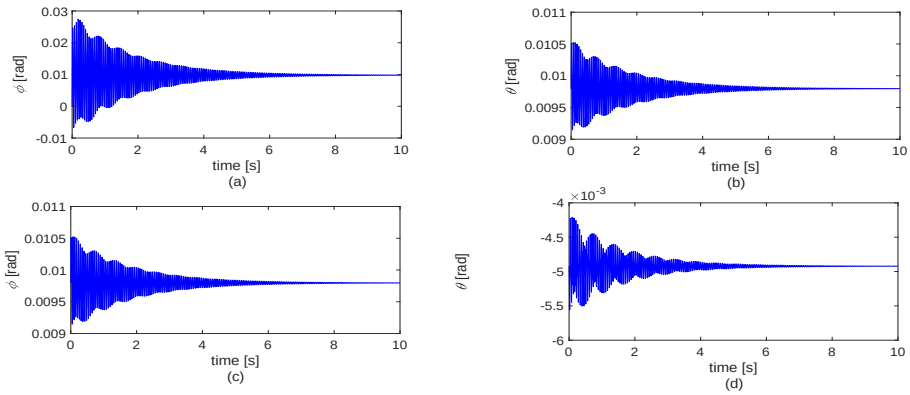

Figure 7.5 Time histories and phase plots of dynamic responses under $\Omega = 2\text{rad/s}$ and $N_0 = 8\text{N}$ with: (a) (b) $\varphi(0) = \theta(0) = \dot{\theta}(0) = 0$, $\dot{\varphi}(0) = 2\text{rad/s}$; (c) (d) $\varphi(0) = 0.0098\text{rad}$, $\theta(0) = -0.0049\text{rad}$, $\dot{\varphi}(0) = 0.1\text{rad/s}$, $\dot{\theta}(0) = 0$.

Next the ranges of parameters where the two stable solutions coexist or only one stable equilibrium exists are determined by extensive numerical simulation. The result is displayed in Fig. 7.6, in which region A represents the parameter combinations where only one stable solution exists, i.e., the steady sliding equilibrium, while region B represents the parameter combinations where two stable solutions including a stick-slip limit cycle coexist.

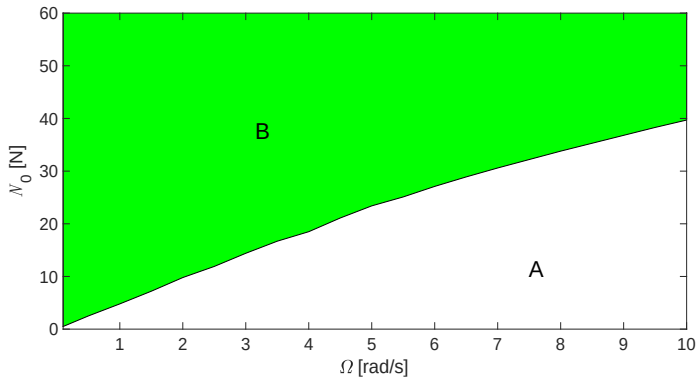

Figure 7.6 Ranges of parameters where two stable solutions coexist and only one stable equilibrium exists.

From the above analysis, the stick-slip vibration will occur when the parameter combinations lie within region B. Next the bifurcation behaviours of the stick-slip vibration with the variations of parameters are investigated. The bifurcations of the values of φ at the transition points from stick to slip with the variations of Ω and N_0 are displayed in Figs. 7.7 and 7.8, respectively. It is observed from the figures that the

system has non-periodic stick-slip response when the disc speed is low or the preload is large, which is due to the variable normal force during vibration.

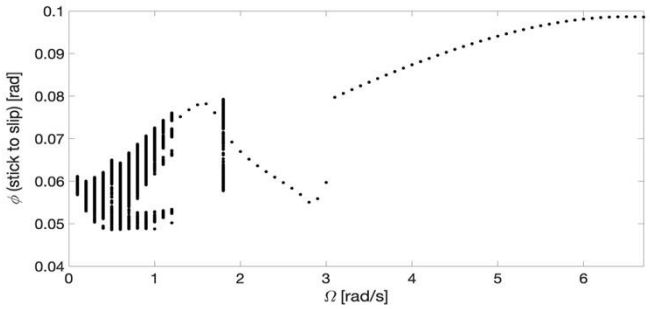

Figure 7.7 The bifurcation behaviour of the stick-slip response of the system dependent on the disc speed when $N_0 = 30\text{N}$.

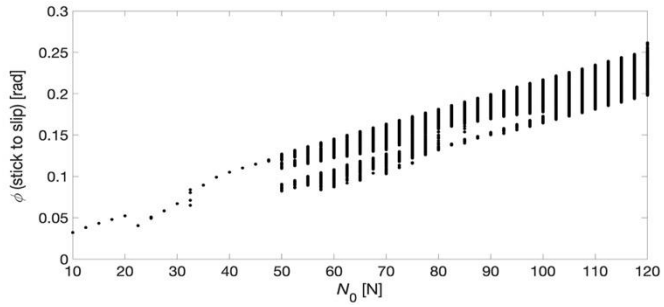

Figure 7.8 The bifurcation behaviour of the stick-slip response of the system dependent on the preload when $\Omega = 2\text{rad/s}$.

Besides, the bifurcation behaviours of the stick-slip response of the system when $c_1 = c_2 = 0$ and $c_1 = c_2 = 0.01\text{N·m·s}$ are shown in Figs. 7.9 and 7.10, respectively. The results demonstrate that the bifurcation behaviour of the system response exists in the situation of small or no structural damping. When the structural damping is sufficiently large, however, the system response does not bifurcate.

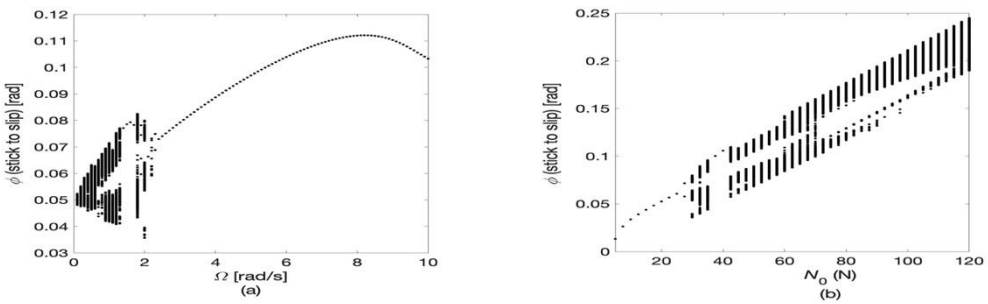

Figure 7.9 The bifurcation behaviour of the stick-slip response of the undamped system dependent on: (a) the disc speed and (b) the preload.

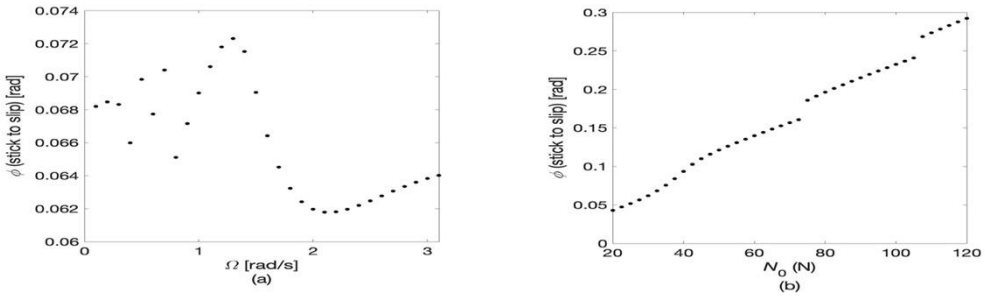

Figure 7.10 The bifurcation behaviour of the stick-slip response of the system with $c_1 = c_2 = 0.01\text{N·m·s}$ dependent on: (a) the disc speed and (b) the preload.

7.4 Numerical study of system dynamics under the non-uniform friction interface

In this section, the system dynamics under the non-uniform friction interface, i.e., a sector (the span angle is denoted by β) of the disc surface possesses a different set of friction property from that in the rest of the disc as shown in Fig. 7.11(b), is studied.

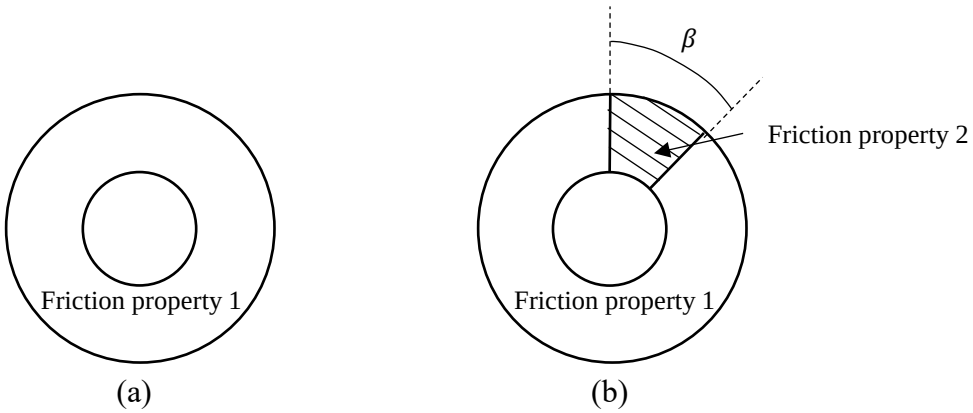

Figure 7.11 The configurations of disc surfaces: (a) uniform friction interface (b) non-uniform friction interface.

Suppose the friction property 1 is the same as that in Section 7.3 and the friction property 2 is represented by μ_s=0.3 and μ_k=0.2. The dynamic responses of the system under the non-uniform friction interface with $\beta = 15^\circ$ when $\Omega = 4\text{rad/s}$, $N_0 = 30\text{N}$ are calculated and shown in Fig. 7.12 (a)-(c). And extensive simulations from different initial conditions are carried out, all of which approach the same steady-state response as that depicted in the figure. Therefore, there is only one stable solution of the steady-state response in which no stick-slip vibration appears. It is seen from Fig. 7.12 (d)-(f) this single stable solution consists of dynamic response in two stages. When the pin is

on the small sector with the friction property 2, the dynamic response decays; When the pin is on the rest of the disc surface with the friction property 1, the dynamic response also decays to approach the steady sliding equilibrium. Moreover, one of the two stable solutions of the system under the uniform friction interface with the friction property 1 for the above combination of (Ω, N_0), i.e., the stick-slip limit cycle vibration, is exhibited, which, as seen in the figure, has much larger amplitudes than those under the non-uniform friction interface. It is thus demonstrated that for this combination of (Ω, N_0), only a single stable solution corresponding to no existence of stick-slip vibration exists under the above non-uniform friction interface, while two stable solutions including a stick-slip limit cycle coexist under the uniform friction interface with the friction property 1.

Next the ranges of parameters (Ω, N_0) concerning whether stick-slip vibration happens or not in the system in this non-uniform configuration are depicted in Fig. 7.13. In this figure, the area in green represents the parameter combinations at which the stick-slip vibration exists, and the dynamic responses at one parameter combination in this area are shown in Fig. 7.14, where two solutions, one with stick-slip vibration and one with pure slip, are possible depending on the initial conditions. The remaining area in the domain represents the parameter combinations at which the stick-slip vibration does not occur from any set of initial condition, and the dynamic responses at parameter combinations in this area are exemplified as that in Fig. 7.12. The solid blue curve and the dashed red curve in Fig. 7.13 are the boundaries between the parameter range where the stick-slip vibration exists and the parameter range where no stick-slip appears in the situation of uniform friction interface with the friction property 1 and the friction property 2, respectively. It is seen that the parameter range corresponding to the existence of stick-slip vibration under the non-uniform friction interface is diminished significantly than that under the uniform friction interface with the friction property 1, and even smaller than that under the uniform friction interface with the friction property 2.

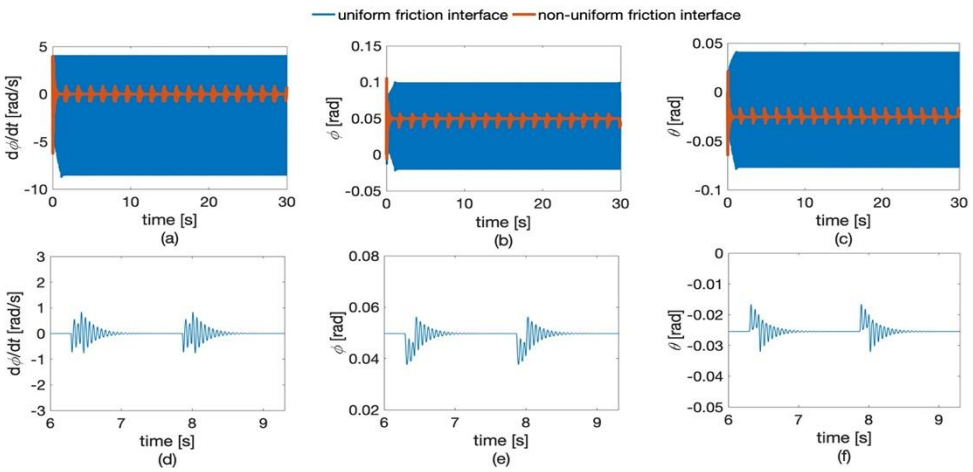

Figure 7.12 The dynamic responses under the non-uniform friction interface with $\beta = 15^{\circ}$ and comparisons with the responses under the uniform friction interface when $\Omega = 4\text{rad/s}$, $N_0 = 30\text{N}$ (a-c) and the zoom-in plot of dynamic responses under the non-uniform friction interface during $t = [6, 9.3]\text{s}$ (d-f).

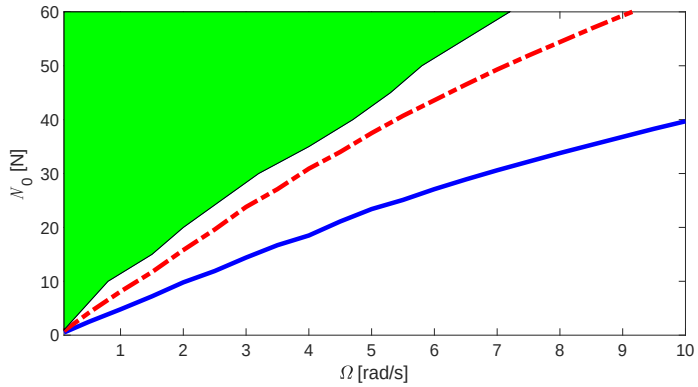

Figure 7.13 Ranges of parameters (Ω, N_0) as to whether the stick-slip vibration happens or not in the system.

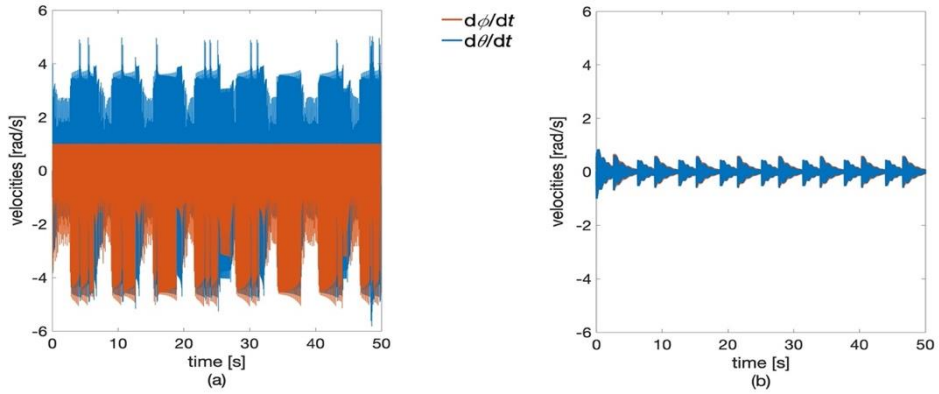

Figure 7.14 The two solutions of dynamic response under the non-uniform friction interface when $\Omega = 1\text{rad/s}$, $N_0 = 30\text{N}$: (a) with stick-slip vibration and (b) with pure slip.

The effect of the span angle of the sector β on the system dynamics is then investigated. In Fig. 7.15, the ranges of (Ω, N_0) as to whether the stick-slip vibration happens or not in the system for different values of β are illustrated, where the three curves with different colours and markers are the boundaries between the parameter range where the stick-slip vibration exists and the parameter range where no stick-slip appears in the situation of non-uniform friction interface with $\beta = 5^\circ, 15^\circ, 90^\circ$, respectively. It is observed from the figure that under the non-uniform interface with $\beta = 5^\circ$, the parameter range where the stick-slip vibration exists is not significantly reduced compared with that under the uniform interface with the friction property 1, while under the non-uniform interface with $\beta = 15^\circ$ and $\beta = 90^\circ$, the parameter range where the stick-slip vibration exists is greatly diminished than that under the uniform friction property 1.

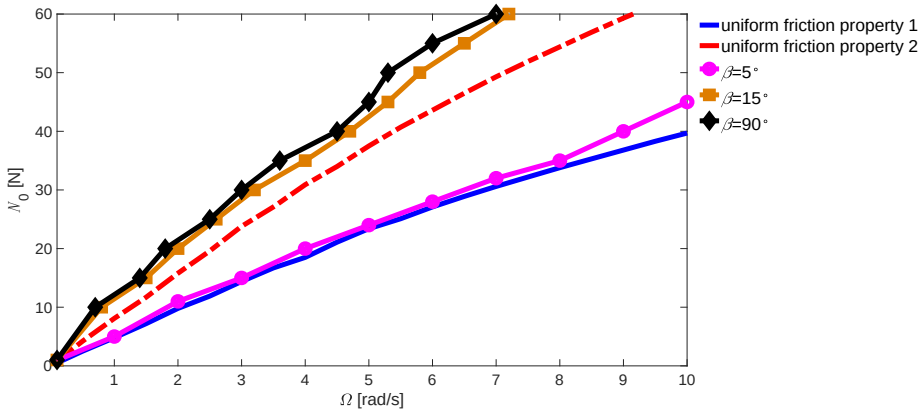

Figure 7.15 Ranges of parameters (Ω, N_0) as to whether the stick-slip vibration happens or not under the non-uniform friction interface with different β.

Moreover, the system dynamics under the non-uniform friction interface in the case of $c_1 = c_2 = 0.01\text{N·m·s}$ (the values of other system parameter are the same as those in Table 7.1) is considered. In Fig. 7.16, the boundaries between the parameter range where the stick-slip vibration exists and the parameter range where no stick-slip appears under the non-uniform friction interface with $\beta = 5^\circ, 90^\circ, 180^\circ$ and under the uniform friction interface with the friction property 1 and the friction property 2 are displayed. It is observed from the figure that the non-uniform friction interface with only $\beta = 5^\circ$ is effective in diminishing the parameter range corresponding to the existence of stick-slip vibration considerably in this case.

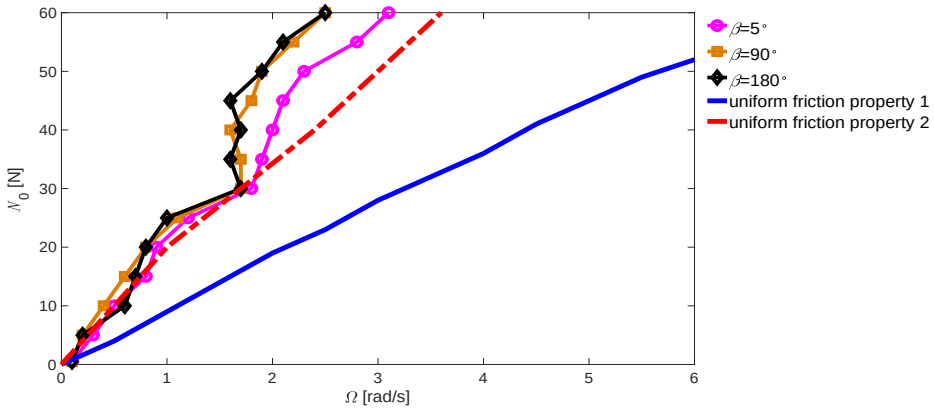

Figure 7.16 Ranges of parameters (Ω, N_0) as to whether the stick-slip vibration happens or not under the non-uniform friction interface with different β when $c_1 = c_2 = 0.01\text{N·m·s}$.

It is crucial to choose an appropriate friction property 2 on the sector to achieve the aim of diminishing the parameter range corresponding to the existence of stick-slip vibration in the system than the original uniform friction property 1. The effective friction property 2 is supposed to correspond to smaller parameter range where the stick-slip vibration exists than the friction property 1, when under the uniform friction interface. By further numerical simulations, the effective coefficients of static and kinetic friction of the friction property 2 besides the combination used in the above examples are identified and shown to be the combinations inside the marked closed curve in Fig. 7.17. Different combinations of friction coefficients in the 'effective' region can reduce the parameter range corresponding to the existence of stick-slip vibration to different extents. An extreme case is when both friction coefficients of the friction property 2 are equal to the coefficient of kinetic friction of the friction property 1, i.e. μ_s=μ_k =0.23, in which there is no stick-slip vibration appearing in the whole domain of (Ω, N_0).

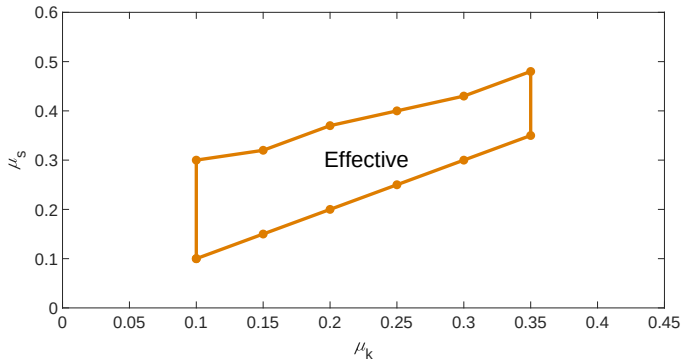

Figure 7.17 Effective coefficients of static and kinetic friction of the friction property 2 on the sector.

The examples in this section demonstrate that only a small sector of disc surface, rather than the whole disc surface, needs to be modified in the friction property in order to achieve the aim of diminishing the parameter range where the stick-slip vibration exists. There is a point worth noting that the modification of disc surface is solely in the consideration of reducing the possibility of occurrence of stick-slip vibration in the system, while other considerations are needed if applying the non-uniform friction interface to real machines, e.g., the braking capacity should be re-evaluated if the surface of a brake rotor is modified into the non-uniform friction interface.

7.5 Conclusions

A new pin-on-disc system with an L-mechanism is proposed and the friction induced dynamics of the system with uniform and non-uniform friction interface is studied in this chapter. The Coulomb's law of friction with static friction coefficient μ_s and kinetic friction coefficient μ_k is employed to model the friction force. The following conclusions can be obtained based on the numerical results,

1. For the uniform friction interface, the system is bi-stable at low disc speed and high normal preload when $\mu_s > \mu_k$, i.e., a stable pure sliding solution and a stable stick-slip solution coexist.
2. The variable normal force during vibration contributes to the occurrence of bifurcation behaviours of system responses in the case of small or no structural damping.
3. A sector of disc surface with a different friction property can be used to diminish the area of disc speeds and normal loads where the stick-slip limit cycle vibration exists in the system, thereby reducing the possibility of occurrence of friction induced stick-slip vibration. However, the friction property on the sector and the span angle of the sector need to be appropriately chosen.

Chapter 8

Conclusions and outlook

8.1 Conclusions

Friction induced vibration is widespread in mechanical systems. Because of the universality and significance of this problem, friction induced vibration attracted great research interest and abundant studies have been carried out. However, this problem is not fully resolved yet due to its immense complexity, and more research needs to be done. In this PhD project, the friction induced vibration is theoretically studied on discrete and continuous mechanical models that aim to enhance the understanding about the causes, the dynamic behaviours and the suppression of the friction induced vibration in mechanical systems. The research in this project is done in four main aspects. Firstly the friction induced vibration of a mass slider on an elastic disc spinning at time-varying speeds is investigated; secondly the suppression of friction induced vibration in multi-degree-of-freedom systems using tangential harmonic excitation is studied; Thirdly the friction induced vibration considering multiple types of nonlinearities on a five-degree-of-freedom lumped model and a slider-on-disc model is explored. Finally the friction induced stick-slip vibration of a new slider-on-disc system with an L-mechanism to adjust the normal force, especially with non-uniform friction interface, is studied. The important conclusions drawn from the research work in this project are as follows,

1. The time-varying spinning speeds of disc cause distinct dynamic behaviours of the system from that under the constant disc speed and two types of differences are found. Firstly, for the system with the parameter combinations corresponding to the stable

sliding equilibrium in the situation of constant speed, the vibration will decay with time and ceases eventually. While in the situation of time-varying disc speed, the system vibration decays with time in the early stage but grows in the later stage. This kind of time-varying characteristic of friction induced vibration results from the negative-slope friction force-relative velocity relationship in the situation of decelerating disc and the speed-dependent instability caused by the moving load in the situation of accelerating disc. Secondly, the time-varying disc speed increases the non-stationary characteristics of the system dynamics as opposed to the constant disc speed, especially the in-plane motion of the mass slider, which means there are more shifts of frequency spectra of the dynamic responses throughout the process in the situation of time-varying disc speed than that in the situation of constant speed.

2. A theoretical study for the suppression of friction induced vibration by application of a tangential harmonic excitation is carried out. It is observed that the friction induced vibration of the frictional systems can be suppressed with the tangential harmonic excitation when the amplitude and frequency of the excitation are in certain ranges. The analytical method to determine the effective ranges of the amplitude and frequency of the excitation for the suppression of friction induced vibration is established. Besides, as a verification of the analytical results, a great amount of computational effort is also made to simulate the time responses of systems with various combinations of amplitude and frequency of the excitation to obtain the effective parameter ranges. The results by the two approaches are in good agreement when the ratio between the excitation frequency and the reference frequency (associated with a natural frequency of the systems and in the same order as it) is sufficiently large.

3. There exist multiple types of nonlinearities in the friction-induced-vibration problems of mechanical systems. Two mechanical models, which are a discrete 5-DoF frictional model and a continuous slider-on-disc model, are considered, with three distinct types of nonlinearities in both models. The first type of nonlinearity is the nonlinear contact stiffness, the second is the non-smooth states of motion including stick, slip and separation, and the third is the geometrical nonlinearity caused by the moving-load feature of the mass slider on the rigid belt or the disc. The effects of each type of nonlinearity on the linear stability and steady-state responses of the two models are revealed.

In terms of the 5-DoF frictional model, it is found that the mode-coupling instability arises with the increase of the coefficient of kinetic friction μ_{k}. The critical friction coefficient for the instability decreases with the increase of nonlinear contact stiffness and the presence of geometrical nonlinearity contributes to the decrease of critical friction coefficient for the instability in the 5-DoF frictional system, which indicate that both the nonlinear contact stiffness and the geometrical nonlinearity are destabilizing factor for the frictional system. Besides, each of the three different types of nonlinearities has significant effects on the steady-state responses of the frictional system in terms of both the periodicity and the intensity of vibration, which are demonstrated in the numerical study. Frequencies of the steady-state responses deviate markedly from the unstable eigenfrequencies of the linearized system and each type of nonlinearity contributes differently to the deviation of vibration frequencies from the unstable eigenfrequencies.

As for the slider-on-disc model, it is found that multiple modes become unstable with the increase of μ_{k} . The nonlinearity of contact stiffness has distinct effects on the instabilities of different modes. For some modes, the critical friction coefficient for the instability decreases with the increase of nonlinear contact stiffness, while the critical friction coefficients for some modes are nearly unchanged with the variation of nonlinear contact stiffness. The geometrical nonlinearity is generally a contributing factor for the dynamic instability in the slider-on-disc system. As for the steady-state responses of the system, the nonlinear contact stiffness and the geometrical nonlinearity have a significant effect on the intensity of steady-state response but a small effect on the periodicity of steady-state response, while the nonlinearity of the non-smooth states of motion has a significant effect on both the intensity and the periodicity of steady-state response.

4. In the newly proposed pin-on-disc system with Coulomb's law of friction, the system is bi-stable at low disc speeds and high normal preloads when $\mu_{\mathrm{s}} > \mu_{\mathrm{k}}$, i.e., a stable pure sliding solution and a stable stick-slip solution coexist. And the variable normal force during vibration contributes to the occurrence of bifurcation behaviours of system responses in the case of small or no structural damping. Moreover, the system dynamics under the non-uniform friction interface, i.e., a sector of disc surface possesses a different set of friction property from that on the rest of the disc surface, is studied. It is found that with appropriate friction coefficients on the sector and an

appropriate span angle of the sector, the range of disc speed and normal preload at which the stick-slip vibration exists will be greatly diminished in comparison with the original uniform friction interface. Therefore a potential approach to suppress the friction induced stick-slip vibration is provided.

8.2 Outlook

The research work in the following aspects can possibly be conducted in the future,

1. In Chapter 7 the friction induced stick-slip vibration of a new pin-on-disc system, especially with a non-uniform friction interface where a sector of disc possesses a different set of friction coefficients, is studied. It is theoretically demonstrated that with appropriate friction coefficients on the sector, the range of disc speed and normal preload at which the stick-slip limit cycle exists will be greatly diminished even if the angle of the sector is very small. Therefore a theoretically effective approach to suppress the friction induced stick-slip vibration in mechanical systems is put forward. Next the effectiveness of this approach in practice can be investigated by laboratory experiments.

2. Because of the discontinuous friction force and unilateral contact, the friction induced dynamics is non-smooth. Another issue associated with the analysis of friction induced vibration is the dispersions of design parameters which can be related to the manufacturing process, operating conditions, wear, etc. Hence it will be very useful to incorporate uncertainty in the research of friction induced vibration. However, the relationship between the dynamic responses and the input parameters in the problem of friction induced vibration is highly nonlinear due to the non-smooth behaviours. Therefore, the analysis of dynamic behaviours in frictional systems involving uncertain parameters, especially the prediction of the dispersion of steady-state non-smooth responses, is a research topic of importance and challenge and can be studied in the future.

3. The friction induced vibration in real mechanical systems is a complex engineering problem that can be influenced by multiple factors, e.g., the loading condition, the surface topography, the material property, etc. Although a series of physical experiments have been conducted to study the effects of specific factors by other researchers, the theoretical studies that incorporate these influential factors in the

friction induced vibration are still in shortage. Because real mechanical systems usually consist of complex continuous structures, the theoretical modelling and computation becomes more difficult when taking into account more factors, and therefore new methods to improve the computational efficiency need to be worked out.

References

[1] A. Akay, Acoustics of friction. *The Journal of the Acoustical Society of America* 111(4) (2002) 1525-1548.

[2] K. Popp, N. Hinrichs, M. Oestreich, Dynamical behaviour of a friction oscillator with simultaneous self and external excitation. *Sadhana* 20(2-4) (1995) 627-654.

[3] N.M. Kinkaid, O.M. O'Reilly, P. Papadopoulos, Automotive disc brake squeal. *Journal of Sound and Vibration* 267(1) (2003) 105-166.

[4] A. Elmaian, F. Gautier, C. Pezerat, J.M. Duffal, How can automotive friction-induced noises be related to physical mechanisms? *Applied Acoustics* 76 (2014) 391-401.

[5] R.A. Ibrahim, Friction-induced vibration, chatter, squeal, and chaos—part II: dynamics and modelling. *Applied Mechanics Reviews* 47 (1994) 227-253.

[6] R.A. Ibrahim, Friction-induced vibration, chatter, squeal, and chaos—part I: mechanics of contact and friction. *Applied Mechanics Reviews* 47 (1994) 209-226.

[7] A. Koenen, A. Sanon, Tribological and vibroacoustic behavior of a contact between rubber and glass (application to wiper blade). *Tribology International* 40(10-12) (2007) 1484-1491.

[8] A. Crowther, N. Zhang, D.K. Liu, J.K. Jeyakumaran, Analysis and simulation of clutch engagement judder and stick-slip in automotive powertrain systems. *Proceedings of the Institution of Mechanical Engineers, Part D: Journal of Automobile Engineering* 218(12) (2004) 1427-1466.

[9] F. Pfeiffer, M. Hajek, Stick-slip motion of turbine blade dampers. *Philosophical Transactions of the Royal Society of London. Series A: Physical and Engineering Sciences* 338(1651) (1992) 503-517.

[10] J. Brecht, W. Hoffrichter, A. Dohle, Mechanisms of brake creep groan. *SAE Technical Paper* 973026 (1997).

[11] J.Y. Peng, X.B. Chen, Modelling of piezoelectric-driven stick–slip actuators. *IEEE/ASME Transactions on Mechatronics* 16(2) (2010) 394-399.

[12] R.I. Leine, D.H. Van Campen, W.J.G. Keultjes, Stick-slip whirl interaction in drillstring dynamics. *Journal of Vibration and Acoustics* 124(2) (2002) 209-220.

[13] F.F. Real, A. Batou, T.G. Ritto, C. Desceliers, R.R. Aguiar, Hysteretic bit/rock interaction model to analyze the torsional dynamics of a drill string. *Mechanical Systems and Signal Processing* 111 (2018) 222 - 233.

[14] F.F. Real, A. Batou, T.G. Ritto, C. Desceliers, Stochastic modeling for hysteretic bit–rock interaction of a drill string under torsional vibrations. *Journal of Vibration and Control* 25(10) (2019) 1663-1672.

[15] W.F. Brace, Laboratory studies of stick-slip and their application to earthquakes. *Tectonophysics* 14(3-4) (1972) 189-200.

[16] T.L. Johnson, C.H. Scholz, Dynamic properties of stick-slip friction of rock. *Journal of Geophysical Research* 81(5) (1976) 881-888.

[17] J.D. Byerlee, W.F. Brace, Stick slip, stable sliding, and earthquakes-effect of rock type, pressure, strain rate, and stiffness. *Journal of Geophysical Research* 73(18) (1968) 6031-6037.

[18] B. Feeny, A.S. Guran, N. Hinrichs, K. Popp, A historical review on dry friction and stick-slip phenomena. *Applied Mechanics Reviews* 51(5) (1998) 321-341.

[19] K. Popp, N. Hinrichs, M. Oestreich, Analysis of a self excited friction oscillator with external excitation. *Dynamics With Friction: Modeling, Analysis And Experiment: (Part I)* (1996) 1-35.

[20] K. Popp, P. Stelter, Stick–slip vibrations and chaos. *Philosophical Transactions: Physical Sciences and Engineering* 332(1624) (1990) 89-105.

[21] U. Galvanetto, Some discontinuous bifurcations in a two-block stick-slip system. *Journal of Sound and Vibration* 248(4) (2001) 653-669.

[22] R.I. Leine, D.H. van Campen, Bifurcation phenomena in non-smooth dynamical systems. *European Journal of Mechanics - A/Solids* 25(4) (2006) 595-616.

[23] H. Dankowicz, A.B. Nordmark, On the origin and bifurcations of stick-slip oscillations. *Physica D: Nonlinear Phenomena* 136(3) (2000) 280-302.

[24] C. Gao, D. Kuhlmann-Wilsdorf, D.D. Makel, The dynamic analysis of stick-slip motion. *Wear* 173(1) (1994) 1-12.

[25] C.A. Brockley, P.L. Ko, Quasi-harmonic friction-induced vibration. *Journal of Lubrication Technology* 92(4) (1970) 550-556.

[26] J.R. Anderson, A.A. Ferri, Behavior of a single-degree-of-freedom system with a generalized friction law. *Journal of Sound and Vibration* 140(2) (1990) 287-304.

[27] B.R. Pontes, V.A.D. Oliveira, J.M. Balthazar, On friction-driven vibrations in a mass block–belt–motor system with a limited power supply. *Journal of Sound and Vibration* 234(4) (2000) 713-723.

[28] N.M. Kinkaid, O.M. O'Reilly, P. Papadopoulos, On the transient dynamics of a multi-degree-of-freedom friction oscillator: a new mechanism for disc brake noise. *Journal of Sound and Vibration* 287(4-5) (2005) 901-917.

[29] J. Behrendt, C. Weiss, N.P. Hoffmann, A numerical study on stick–slip motion of a brake pad in steady sliding. *Journal of Sound and Vibration* 330(4) (2011) 636-651.

[30] B.L. Van de Vrande, D.H. Van Campen, A. De Kraker, An approximate analysis of dry-friction-induced stick–slip vibrations by a smoothing procedure. *Nonlinear Dynamics* 19(2) (1999) 159-171.

[31] H. Hetzler, On the effect of nonsmooth Coulomb friction on Hopf bifurcations in a 1-DoF oscillator with self-excitation due to negative damping. *Nonlinear Dynamics* 69(1-2) (2012) 601-614.

[32] D. Tonazzi, F. Massi, L. Baillet, A. Culla, M. Di Bartolomeo, Y. Berthier, Experimental and numerical analysis of frictional contact scenarios: from macro stick–slip to continuous sliding. *Meccanica.* 50(3) (2015) 649-664.

[33] A. Papangelo, M. Ciavarella, N. Hoffmann, Subcritical bifurcation in a self-excited single-degree-of-freedom system with velocity weakening–strengthening friction law: analytical results and comparison with experiments. *Nonlinear Dynamics* 90(3) (2017) 2037-2046.

[34] J.J. Thomsen, A. Fidlin, Analytical approximations for stick–slip vibration amplitudes. *International Journal of Non-Linear Mechanics* 38(3) (2003) 389-403.

[35] F. Van De Velde, P. De Baets, Mathematical approach of the influencing factors on stick-slip induced by decelerative motion. *Wear* 201(1-2) (1996) 80-93.

[36] P. Vielsack, Stick–slip instability of decelerative sliding. *International Journal of Non-linear Mechanics* 36(2) (2001) 237-247.

[37] R.T. Spurr, A theory of brake squeal. *Proceedings of the Institution of Mechanical Engineers: Automobile Division* 15(1) (1961) 33-52.

[38] R.P. Jarvis, B. Mills, Vibrations induced by dry friction. *Proceedings of the Institution of Mechanical Engineers* 178(1) (1963) 847-857.

[39] S.W.E. Earles, C.K. Lee, Instabilities arising from the frictional interaction of a pin-disk system resulting in noise generation. *Journal of Engineering for Industry* 98 (1) (1976) 81-86.

[40] J.J. Sinou, F. Thouverez, L. Jezequel, Analysis of friction and instability by the centre manifold theory for a non-linear sprag-slip model. *Journal of Sound and Vibration* 265(3) (2003) 527-559.

[41] M. Painlevé, Sur les Lois du Frottement de Glissement. *Comptes Rendus de l'Academie des Science* 121 (1895) 112-115.

[42] R.I. Leine, B. Brogliato, H. Nijmeijer, Periodic motion and bifurcations induced by the Painlevé paradox. *European Journal of Mechanics-A/Solids* 21(5) (2002) 869-896.

[43] N. Hoffmann, L. Gaul, A sufficient criterion for the onset of sprag-slip oscillations. *Archive of Applied Mechanics* 73(9-10) (2004) 650-660.

[44] H. Keitzel, N. Hoffmann, Influence of the contact model on the onset of sprag-slip. *PAMM: Proceedings in Applied Mathematics and Mechanics* 6 (2006) 311-312.

[45] J. Kang, C.M. Krousgrill, The onset of friction-induced vibration and spragging. *Journal of Sound and Vibration* 329(17) (2010) 3537-3549.

[46] H.R. Mills, Brake squeak. Research report nos.9000 B (1938) 9162 B. *Institution of Automobile Engineers* (1939).

[47] R.A.C. Fosberry, Z. Holubecki, Disc brake squeal: Its mechanism and suppression. *Lindley: Motor Industry Research Association* (1961).

[48] D. Sinclair, N. Manville, Frictional vibrations. *Journal of Applied Mechanics, Transactions of the ASME* 22 (1955) 13-207.

[49] J.T. Oden, J.A.C. Martins, Models and computational methods for dynamic friction phenomena. *Computer Methods in Applied Mechanics and Engineering* 52(1) (1985) 527-634.

[50] Y. Yuan, A study of the effects of negative friction-speed slope on brake squeal. *Proceedings of the ASME Design Engineering Technical Conference, Boston* (1995).

[51] G.X. Chen, Z.R. Zhou, Correlation of a negative friction–velocity slope with squeal generation under reciprocating sliding conditions. *Wear* 255(1–6) (2003) 376-384.

[52] H. Ouyang, J.E. Mottershead, M.P. Cartmell, M.I. Friswell, Friction-induced parametric resonances in discs: Effect of a negative friction-velocity relationship. *Journal of Sound and Vibration* 209(2) (1998) 251-263.

[53] M. Eriksson, S. Jacobson, Friction behaviour and squeal generation of disc brakes at low speeds. *Proceedings of the Institution of Mechanical Engineers, Part D: Journal of Automobile Engineering* 215(12) (2001) 1245-1256.

[54] M.R. North, Disc brake squeal. *Proceedings of the Institution of the Automotive Mechanical Engineers* 1 (1976) 169-176.

[55] N. Hoffmann, M. Fischer, R. Allgaier, L. Gaul, A minimal model for studying properties of the mode-coupling type instability in friction induced oscillations. *Mechanics Research Communications* 29(4) (2002) 197-205.

[56] N. Hoffmann, L. Gaul, Effects of damping on mode-coupling instability in friction induced oscillations. *ZAMM-Journal of Applied Mathematics and Mechanics* 83(8) (2003) 524-534.

[57] J. Kang, C.M. Krousgrill, F. Sadeghi, Dynamic instability of a thin circular plate with friction interface and its application to disc brake squeal. *Journal of Sound and Vibration* 316(1-5) (2008) 164-179.

[58] U. von Wagner, D. Hochlenert, P. Hagedorn, Minimal models for disk brake squeal. *Journal of Sound and Vibration* 302(3) (2007) 527-539.

[59] G. Fritz, J.J. Sinou, J.M. Duffal, L. Jézéquel, Investigation of the relationship between damping and mode-coupling patterns in case of brake squeal. *Journal of Sound and Vibration* 307(3-5) (2007) 591-609.

[60] F. Chevillot, J.J. Sinou, N. Hardouin, Nonlinear transient vibrations and coexistences of multi-instabilities induced by friction in an aircraft braking system. *Journal of Sound and Vibration* 328(4-5) (2009) 555-574.

[61] F. Chen, J. Chern, J. Swayze, Modal coupling and its effect on brake squeal (No. 2002-01-0922). *SAE Technical Paper* (2002).

[62] J.J. Sinou, L. Jézéquel, Mode coupling instability in friction-induced vibrations and its dependency on system parameters including damping. *European Journal of Mechanics-A/Solids* 26(1) (2007) 106-122.

[63] J. Huang, C.M. Krousgrill, A.K. Bajaj, Modelling of automotive drum brakes for squeal and parameter sensitivity analysis. *Journal of Sound and Vibration* 289(1-2) (2006) 245-263.

[64] J. Hulten, Drum break squeal-a self-exciting mechanism with constant friction. *Proceedings of the SAE Truck and Bus Meeting, SAE Paper* 932965 (1993).

[65] S.N. Chan, J.E. Mottershead, M.P. Cartmell, Parametric resonances at subcritical speeds in discs with rotating frictional loads. *Proceedings of the Institution of Mechanical Engineers, Part C: Journal of Mechanical Engineering Science* 208(6) (1994) 417-425.

[66] D. Hochlenert, G. Spelsberg-Korspeter, P. Hagedorn, Friction induced vibrations in moving continua and their application to brake squeal. *Journal of Applied Mechanics* 74(3) (2007) 542-549.

[67] H. Ouyang, J.E. Mottershead, Dynamic instability of an elastic disk under the action of a rotating friction couple. *Journal of Applied Mechanics* 71(6) (2004) 753-758.

[68] G.X. Chen, Q.Y. Liu, X.S. Jin, Z.R. Zhou, Stability analysis of a squealing vibration model with time delay. *Journal of Sound and Vibration* 311(1-2) (2008) 516-536.

[69] M. Graf, G.P. Ostermeyer, Friction-induced vibration and dynamic friction laws: instability at positive friction–velocity-characteristic. *Tribology International* 92 (2015) 255-258.

[70] G. Amontons, De la resistance cause'e dans les machines. *Mémoires de l'Academie Royale des Sciences.* (1699) 206-226.

[71] C.A. Coulomb, Théorie des machines simples, en ayant égard au frottement de leurs parties, et à la roideur des cordages. *Mémoire de Mathématique et de Physique, Paris, France* (1785).

[72] R. Stribeck, Die wesentlichen eigenschaften der gleit-und rollenlager. *Zeitschrift des Vereines Deutscher Ingenieure* 46 (1902) 1341-1348.

[73] L.C. Bo, D. Pavelescu, The friction-speed relation and its influence on the critical velocity of stick-slip motion. *Wear* 82 (1982) 277-289.

[74] S. Andersson, A. Söderberg, S. Björklund, Friction models for sliding dry, boundary and mixed lubricated contacts. *Tribology International* 40 (2007) 580-587.

[75] L. Chen, G. Xi, Stability and response of a self-amplified braking system under velocity-dependent actuation force. *Nonlinear Dynamics* 78(4) (2014) 2459-2477.

[76] A. Stefański, J. Wojewoda, M. Wiercigroch, T. Kapitaniak, Chaos caused by non-reversible dry friction. *Chaos, Solitons & Fractals* 16(5) (2003) 661-664.

[77] J. Wojewoda, A. Stefański, M. Wiercigroch, T. Kapitaniak, Hysteretic effects of dry friction: modelling and experimental studies. *Philosophical Transactions of the Royal Society A: Mathematical, Physical and Engineering Sciences* 366(1866) (2008) 747-765.

[78] D. Karnopp, Computer simulation of stick-slip friction in mechanical dynamic systems. *Journal of Dynamic Systems, Measurement, and Control* 107 (1985) 100-103.

[79] R.I. Leine, D.H. van Campen, A. De Kraker, L. Van Den Steen, Stick-slip vibrations induced by alternate friction models. *Nonlinear Dynamics* 16 (1998) 41-54.

[80] J.A.C. Ambrósio, Impact of rigid and flexible multibody systems: deformation description and contact model. *Virtual Nonlinear Multibody Systems* 103 (2003) 57-81.

[81] J. Awrejcewicz, D. Grzelczyk, Y. Pyryev, A novel dry friction modeling and its impact on differential equations computation and Lyapunov exponents estimation. *Journal of Vibroengineering* 10 (2008) 475-482.

[82] P.R. Dahl, A solid friction model. *Technical Report, The Aerospace Corporation, El Segundo, California* (1968).

[83] P.R. Dahl, Solid friction damping in mechanical vibrations. *AIAA Journal* 14 (1976) 1675-1682.

[84] D.A. Haessig Jr, B. Friedland, On the modeling and simulation of friction. *Journal of Dynamic Systems, Measurement, and Control* 113(3) (1991) 354-362.

[85] C.C. De Wit, H. Olsson, K.J. Astrom, P. Lischinsky, A new model for control of systems with friction. *IEEE Transactions on Automatic Control* 40(3) (1995) 419-425.

[86] K. Johanastrom, C.C. De Wit, Revisiting the LuGre friction model. *IEEE Control Systems Magazine* 28(6) (2008) 101-114.

[87] T. Piatkowski, Dahl and LuGre dynamic friction models-The analysis of selected properties. *Mechanism and Machine Theory* 73 (2014) 91-100.

[88] B. Friedland, S. Mentzelopoulou, On estimation of dynamic friction. *Proceedings of 32nd IEEE Conference on Decision and Control* (1993) 1919-1924.

[89] P. Dupont, V. Hayward, B. Armstrong, F. Altpeter, Single state elastoplastic friction models. *IEEE Transactions on Automatic Control* 47(5) (2002) 787-792.

[90] J. Swevers, F. Al-Bender, C.G. Ganseman, T. Projogo, An integrated friction model structure with improved presliding behavior for accurate friction compensation. *IEEE Transactions on Automatic Control* 45(4) (2000) 675-686.

[91] Y. Gonthier, J. McPhee, C. Lange, J.C. Piedboeuf, A regularized contact model with asymmetric damping and dwell-time dependent friction. *Multibody System Dynamics* 11(3) (2004) 209-233.

[92] J. Liang, S. Fillmore, O. Ma, An extended bristle friction force model with experimental validation. *Mechanism and Machine Theory* 56 (2012) 123-137.

[93] Y. Li, Z.C. Feng, Bifurcation and chaos in friction-induced vibration. *Communications in Nonlinear Science and Numerical Simulation* 9(6) (2004) 633-647.

[94] D. Pikunov, A. Stefanski, Numerical analysis of the friction-induced oscillator of Duffing's type with modified LuGre friction model. *Journal of Sound and Vibration* 440 (2019) 23-33.

[95] M.N.A. Emira, Friction-induced oscillations of a slider: Parametric study of some system parameters. *Journal of Sound and Vibration* 300(3-5) (2007) 916-931.

[96] U. Andreaus, P. Casini, Friction oscillator excited by moving base and colliding with a rigid or deformable obstacle. *International Journal of Non-Linear Mechanics* 37(1) (2002) 117-133.

[97] Z. Li, H. Ouyang, Z. Guan. Nonlinear friction-induced vibration of a slider–belt system. *Journal of Vibration and Acoustics* 138(4) (2016) 041006.

[98] Z. Zhang, S. Oberst, J.C. Lai, On the potential of uncertainty analysis for prediction of brake squeal propensity. *Journal of Sound and Vibration* 377 (2016) 123-132.

[99] U. Andreaus, P. Casini, Dynamics of friction oscillators excited by a moving base and/or driving force. *Journal of Sound and Vibration* 245(4) (2001) 685-699.

[100] K. Shin, M.J. Brennan, J.E. Oh, C.J. Harris, Analysis of disc brake noise using a two-degree-of-freedom model. *Journal of Sound and Vibration* 254(5) (2002) 837-848.

[101] A.C. Luo, S. Thapa, Periodic motions in a simplified brake system with a periodic excitation. *Communications in Nonlinear Science and Numerical Simulation* 14(5) (2009) 2389-2414.

[102] C. Duan, R. Singh, Influence of harmonically varying normal load on steady-state behavior of a 2dof torsional system with dry friction. *Journal of Sound and Vibration* 294(3) (2006) 503-528.

[103] S. Kruse, M. Tiedemann, B. Zeumer, P. Reuss, H. Hetzler, N. Hoffmann, The influence of joints on friction induced vibration in brake squeal. *Journal of Sound and Vibration* 340 (2015) 239-252.

[104] V. Pilipchuk, P. Olejnik, J. Awrejcewicz, Transient friction-induced vibrations in a 2-DOF model of brakes. *Journal of Sound and Vibration* 344 (2015) 297-312.

[105] J. Brunetti, F. Massi, Y. Berthier, A new instability index for unstable mode selection in squeal prediction by complex eigenvalue analysis. *Journal of Sound and Vibration* 377 (2016) 106-122.

[106] A.R. Crowther, R. Singh, Identification and quantification of stick-slip induced brake groan events using experimental and analytical investigations. *Noise Control Engineering Journal* 56(4) (2008) 235-255.

[107] Z. Li, Q. Cao, A. Léger, The complicated bifurcation of an archetypal self-excited SD oscillator with dry friction. *Nonlinear Dynamics* 89(1) (2017) 91-106.

[108] D. Wei, J. Song, Y. Nan, W. Zhu, Analysis of the stick-slip vibration of a new brake pad with double-layer structure in automobile brake system. *Mechanical Systems and Signal Processing* 118 (2019) 305-316.

[109] J. Slavič, M.D. Bryant, M. Boltežar, A new approach to roughness-induced vibrations on a slider. *Journal of Sound and Vibration* 306(3-5) (2007) 732-750.

[110] V. Magnier, J.F. Brunel, P. Dufrénoy, Impact of contact stiffness heterogeneities on friction-induced vibration. *International Journal of Solids and Structures* 51(9) (2014) 1662-1669.

[111] H. Hetzler, D. Schwarzer, W. Seemann, Analytical investigation of steady-state stability and Hopf-bifurcations occurring in sliding friction oscillators with application to low-frequency disc brake noise. *Communications in Nonlinear Science and Numerical Simulation* 12(1) (2007) 83-99.

[112] W.J. Kim, N.C. Perkins, Harmonic balance/Galerkin method for non-smooth dynamic systems. *Journal of Sound and Vibration* 261(2) (2003) 213-224.

[113] J. Giné, On the determination of the limit cycles using the harmonic balance method. *Journal of Mathematical Physics* 54(10) (2013) 103510.

[114] S. Yang, S. Guo, Two-stop-two-slip motions of a dry friction oscillator. *Science China Technological Sciences* 53(3) (2010) 623-632.

[115] M. Oestreich, N. Hinrichs, K. Popp, Bifurcation and stability analysis for a non-smooth friction oscillator. *Archive of Applied Mechanics* 66(5) (1996) 301-314.

[116] S. Divenyi, M.A. Savi, M. Wiercigroch, E. Pavlovskaia, Drill-string vibration analysis using non-smooth dynamics approach. *Nonlinear Dynamics* 70(2) (2012) 1017-1035.

[117] A. Nobari, H. Ouyang, P. Bannister, Statistics of complex eigenvalues in friction-induced vibration. *Journal of Sound and Vibration* 338 (2015) 169-183.

[118] L. Nechak, J.J. Sinou, Hybrid surrogate model for the prediction of uncertain friction-induced instabilities. *Journal of Sound and Vibration* 396 (2017) 122-143.

[119] L. Nechak, S. Berger, E. Aubry, Non-intrusive generalized polynomial chaos for the robust stability analysis of uncertain nonlinear dynamic friction systems. *Journal of Sound and Vibration* 332(5) (2013) 1204-1215.

[120] J. Flint, J. Hulten, Lining-deformation-induced modal coupling as squeal generator in a distributed parameter disc brake model. *Journal of Sound and Vibration* 254(1) (2002) 1-21.

[121] A. Meziane, L. Baillet, B. Laulagnet, Experimental and numerical investigation of friction-induced vibration of a beam-on-beam in contact with friction. *Applied Acoustics* 71(9) (2010) 843-853.

[122] H.I. Won, J. Chung, Numerical analysis for the stick-slip vibration of a transversely moving beam in contact with a frictional wall. *Journal of Sound and Vibration* 419 (2018) 42-62.

[123] R.A. Ibrahim, R.J. Somnay, Nonlinear dynamic analysis of an elastic beam isolator sliding on frictional supports. *Journal of Sound and Vibration* 308(3-5) (2007) 737-757.

[124] D. Tonazzi, F. Massi, A. Culla, L. Baillet, A. Fregolent, Y. Berthier, Instability scenarios between elastic media under frictional contact. *Mechanical Systems and Signal Processing* 40(2) (2013) 754-766.

[125] C.M. Jung, B.F. Feeny, Friction-induced vibration in periodic linear elastic media. *Journal of Sound and Vibration* 252(5) (2002) 945-954.

[126] A. Loyer, J.J. Sinou, O. Chiello, X. Lorang, Study of nonlinear behaviors and modal reductions for friction destabilized systems. Application to an elastic layer. *Journal of Sound and Vibration* 331(5) (2012) 1011-1041.

[127] H. Ouyang, J.E. Mottershead, M.P. Cartmell, D.J. Brookfield, Friction-induced vibration of an elastic slider on a vibrating disc. *International Journal of Mechanical Sciences* 41(3) (1999) 325-336.

[128] I.Y. Shen, Response of a stationary, damped, circular plate under a rotating slider bearing system. *Journal of Vibration and Acoustics* 115(1) (1993) 65-69.

[129] G. Spelsberg-Korspeter, D. Hochlenert, O.N. Kirillov, P. Hagedorn, In-and out-of-plane vibrations of a rotating plate with frictional contact: investigations on squeal phenomena. *Journal of Applied Mechanics* 76(4) (2009) 041006.

[130] Q. Cao, H. Ouyang, M.I. Friswell, J.E. Mottershead, Linear eigenvalue analysis of the disc-brake squeal problem. *International Journal for Numerical Methods in Engineering* 61(9) (2004) 1546-1563.

[131] Y. Dai, T.C. Lim, Suppression of brake squeal noise applying finite element brake and pad model enhanced by spectral-based assurance criteria. *Applied Acoustics* 69(3) (2008) 196-214.

[132] J. Kang, Squeal analysis of gyroscopic disc brake system based on finite element method. *International Journal of Mechanical Sciences* 51(4) (2009) 284-294.

[133] J. Kang, Automotive brake squeal analysis with rotating finite elements of asymmetric disc in time. *Journal of Sound and Vibration* 393 (2017) 388-400.

[134] J. Kang, Finite element modelling for the investigation of in-plane modes and damping shims in disc brake squeal. *Journal of Sound and Vibration* 331(9) (2012) 2190-2202.

[135] P. Blaschke, M. Tan, A. Wang, On the analysis of brake squeal propensity using finite element method (No. 2000-01-2765). *SAE Technical Paper* (2000).

[136] J. Wei, Y. Sun, S. Wang, P. Zhou, Research on brake squeal based on abaqus. *Machinery Design & Manufacture* 2016(6) (2016) 151-154 (in Chinese).

[137] G. Liles, Analysis of disc brake squeal using finite element methods. *SAE Technical Paper* 891150 (1989).

[138] A. Meziane, S. D'Errico, L. Baillet, B. Laulagnet, Instabilities generated by friction in a pad-disc system during the braking process. *Tribology International* 40(7) (2007) 1127-1136.

[139] M. Matsuzaki, T. Izumihara, Brake noise caused by longitudinal vibration of the disc rotor (No. 930804). *SAE Technical Paper* (1993).

[140] J.G. Tseng, J.A. Wickert, Nonconservative stability of a friction loaded disk. *Journal of Vibration and Acoustics* 120(4) (1998) 922-929.

[141] H.Q. Do, F. Massa, T. Tison, B. Lallemand, A global strategy for the stability analysis of friction induced vibration problem with parameter variations. *Mechanical Systems and Signal Processing* 84 (2017) 346-364.

[142] J.J. Sinou, Transient non-linear dynamic analysis of automotive disc brake squeal-on the need to consider both stability and non-linear analysis. *Mechanics Research Communications* 37(1) (2010) 96-105.

[143] K. Soobbarayen, J.J. Sinou, S. Besset, Numerical study of friction-induced instability and acoustic radiation-effect of ramp loading on the squeal propensity for a simplified brake model. *Journal of Sound and Vibration* 333(21) (2014) 5475-5493.

[144] N. Coudeyras, J.J. Sinou, S. Nacivet, A new treatment for predicting the self-excited vibrations of nonlinear systems with frictional interfaces: The constrained harmonic balance method, with application to disc brake squeal. *Journal of Sound and Vibration* 319(3-5) (2009) 1175-1199.

[145] D. Brizard, O. Chiello, J.J. Sinou, X. Lorang, Performances of some reduced bases for the stability analysis of a disc/pads system in sliding contact. *Journal of Sound and Vibration* 330(4) (2011) 703-720.

[146] S. Besset, J.J. Sinou, Modal reduction of brake squeal systems using complex interface modes. *Mechanical Systems and Signal Processing* 85 (2017) 896-911.

[147] O. Fazio, S. Nacivet, Reduction strategy for a brake system with local frictional non-linearities–Application for the prediction of unstable vibration modes. *Applied Acoustics* 91 (2015) 12-24.

[148] Vermot Des Roches G, Frequency and time simulation of squeal instabilities. Application to the design of industrial automotive brakes. *Ecole Centrale Paris Doctoral Dissertation* (2011).

[149] Z. Li, X. Wang, Q. Zhang, Z. Guan, J. Mo, H. Ouyang, Model reduction for friction-induced vibration of multi-degree-of-freedom systems and experimental validation. *International Journal of Mechanical Sciences* 145 (2018) 106-119.

[150] W.D. Iwan, K.J. Stahl, The response of an elastic disk with a moving mass system. *Journal of Applied Mechanics* 40(2) (1973) 445-451.

[151] W.D. Iwan, T.L. Moeller, The stability of a spinning elastic disk with a transverse load system. *Journal of Applied Mechanics* 43(3) (1976) 485-490.

[152] S.G. Hutton, S. Chonan, B.F. Lehmann, Dynamic response of a guided circular saw. *Journal of Sound and Vibration* 112(3) (1987) 527-539.

[153] K. Ono, J.S. Chen, D.B. Bogy, Stability analysis for the head-disk interface in a flexible disk drive. *Journal of Applied Mechanics* 58(4) (1991) 1005-1014.

[154] J.S. Chen, D.B. Bogy, Mathematical structure of modal interactions in a spinning disk-stationary load system. *Journal of Applied Mechanics* 59(2) (1992) 390-397.

[155] T.H. Young, C.Y. Lin, Stability of a spinning disk under a stationary oscillating unit. *Journal of Sound and Vibration* 298(1-2) (2006) 307-318.

[156] H. Ouyang, Stationary and non-stationary vibration of atomising discs. *Journal of Sound and Vibration* 308(3-5) (2007) 699-708.

[157] H. Ouyang, Moving-load dynamic problems: A tutorial (with a brief overview). *Mechanical Systems and Signal Processing* 25(6) (2011) 2039-2060.

[158] D. Lee, A.M. Waas, Stability analysis of a rotating multi-layer annular plate with a stationary frictional follower load. *International Journal of Mechanical Sciences* 39(10) (1997) 1117-1138.

[159] Y.C. Pei, L. He, F.J. He, The transverse runout of a rotating flexible disc under stationary sliders. *Proceedings of the Institution of Mechanical Engineers, Part C: Journal of Mechanical Engineering Science* 223(6) (2009) 1319-1326.

[160] L. Zhang, J. Wu, D. Meng, Transient analysis of a flexible pin-on-disk system and its application to the research into time-varying squeal. *Journal of Vibration and Acoustics* 140(1) (2018) 011006.

[161] J. Kang, C.M. Krousgrill, F. Sadeghi, Wave pattern motion and stick–slip limit cycle oscillation of a disc brake. *Journal of Sound and Vibration* 325(3) (2009) 552-564.

[162] J. Kang, Moving mode shape function approach for spinning disk and asymmetric disc brake squeal. *Journal of Sound and Vibration* 424 (2018) 48-63.

[163] Z. Li, H. Ouyang, Z. Guan, Friction-induced vibration of an elastic disc and a moving slider with separation and reattachment. *Nonlinear Dynamics* 87(2) (2017) 1045-1067.

[164] X. Sui, Q. Ding, Instability and stochastic analyses of a pad-on-disc frictional system in moving interactions. *Nonlinear Dynamics* 93(3) (2018) 1619-1634.

[165] D. Hochlenert, Nonlinear stability analysis of a disk brake model. *Nonlinear Dynamics* 58(1-2) (2009) 63-73.

[166] T. Butlin, J. Woodhouse, Friction-induced vibration: Model development and comparison with large-scale experimental tests. *Journal of Sound and Vibration* 332(21) (2013) 5302-5321.

[167] T. Butlin, J. Woodhouse, Friction-induced vibration: Quantifying sensitivity and uncertainty. *Journal of Sound and Vibration* 329(5) (2010) 509-526.

[168] P. Duffour, J. Woodhouse, Instability of systems with a frictional point contact—Part 3: Experimental tests. *Journal of Sound and Vibration* 304(1-2) (2007) 186-200.

[169] P.D. Neis, P. De Baets, W. Ost, Y.P. Delgado, M. Loccufier, F. Al-Bender, N.F. Ferreira, F.J. Lorini, Investigation of the dynamic response in a dry friction process using a rotating stick–slip tester. *Wear* 271(9-10) (2011) 2640-2650.

[170] C. Ferrer, F. Salas, M. Pascual, J. Orozco, Discrete acoustic emission waves during stick–slip friction between steel samples. *Tribology International* 43(1-2) (2010) 1-6.

[171] O. Giannini, A. Akay, F. Massi, Experimental analysis of brake squeal noise on a laboratory brake setup. *Journal of Sound and Vibration* 292(1-2) (2006) 1-20.

[172] F. Massi, O. Giannini, L. Baillet, Brake squeal as dynamic instability: an experimental investigation. *The Journal of the Acoustical Society of America* 120(3) (2006) 1388-1398.

[173] N. Gräbner, M. Tiedemann, U. Von Wagner, N. Hoffmann, Nonlinearities in friction brake NVH-experimental and numerical studies (No. 2014-01-2511). *SAE Technical Paper* (2014).

[174] G.X. Chen, Z.R. Zhou, Experimental observation of the initiation process of friction-induced vibration under reciprocating sliding conditions. *Wear* 259(1-6) (2005) 277-281.

[175] N. Mihajlovic, A.A. Van Veggel, N. Van de Wouw, H. Nijmeijer, Analysis of friction-induced limit cycling in an experimental drill-string system. *Journal of Dynamic Systems, Measurement, and Control* 126(4) (2004) 709-720.

[176] M. Nishiwaki, H. Harada, H. Okamura, T. Ikeuchi, Study on disc brake squeal. *S.A.E. Technical Paper* 890864 (1989).

[177] S. Oberst, J.C.S. Lai, Statistical analysis of brake squeal noise. *Journal of Sound and Vibration* 330 (2011) 2978-2994.

[178] A.R. AbuBakar, H. Ouyang, Wear prediction of friction material and brake squeal using the finite element method. *Wear* 264(11-12) (2008) 1069-1076.

[179] M. Triches Jr, S.N.Y. Gerges, R. Jordan, Reduction of squeal noise from disc brake systems using constrained layer damping. *Journal of the Brazilian Society of Mechanical Sciences and Engineering* 26(3) (2004) 340-348.

[180] A.Y. Wang, J.L. Mo, X.C. Wang, M.H. Zhu, Z.R. Zhou, Effect of surface roughness on friction-induced noise: exploring the generation of squeal at sliding friction interface. *Wear* 402 (2018) 80-90.

[181] X. Quan, J. Mo, B. Huang, B. Tang, H. Ouyang, Z. Zhou, Influence of the Friction Block Shape and Installation Angle of High-Speed Train Brakes on Brake Noise. *Journal of Tribology* 142(3) (2020) 031701.

[182] D.W. Wang, J.L. Mo, M.Q. Liu, J.X. Li, H. Ouyang, M.H. Zhu, Z.R. Zhou, Improving tribological behaviours and noise performance of railway disc brake by grooved surface texturing. *Wear* 376 (2017) 1586-1600.

[183] H. Kanki, K. Adachi, T. Takahashi, N. Nozaki, Y. Asano, An Experimental Investigation of Brake Squeal Suppression of Air Brake Systems for Electric Passenger Trains Using Oil Damper. *ASME International Mechanical Engineering Congress and Exposition* (2006) 53-59.

[184] J.J. Sinou, A. Loyer, O. Chiello, G. Mogenier, X. Lorang, F. Cocheteux, S. Bellaj, A global strategy based on experiments and simulations for squeal prediction on industrial railway brakes. *Journal of Sound and Vibration* 332(20) (2013) 5068-5085.

[185] S.S. Rao, Vibration of continuous systems (Vol. 464). *New York: Wiley* (2007).

[186] H. Pollard, M. Tenenbaum, Ordinary differential equations. *New York: Harper & Row* (1964).

[187] D. McFarland, B.L. Smith, Analysis of plates. *New York: Spartan Books* (1972).

[188] J. Chung, J.E. Oh, H.H. Yoo, Non-linear vibration of a flexible spinning disc with angular acceleration. *Journal of Sound and Vibration* 231(2) (2000) 375-391.

[189] D. Stancioiu, H. Ouyang, J.E. Mottershead, Vibration of a beam excited by a moving oscillator considering separation and reattachment. *Journal of Sound and Vibration* 310(4-5) (2008) 1128-1140.

[190] L. Hammerström, S. Jacobson, Surface modification of brake discs to reduce squeal problems. *Wear* 261(1) (2006) 53-57.

[191] D.W. Wang, J.L. Mo, X.H. Ge, H. Ouyang, Z.R. Zhou, Disc surface modifications for enhanced performance against friction noise. *Applied Surface Science* 382 (2016) 101-110.

[192] K. Nakano, C. Tadokoro, N. Kado, Yawing angular misalignment provides positive damping to suppress frictional vibration: basic applicability to disc brake systems. *SAE International Journal of Passenger Cars-Mechanical Systems* 6(2013-01-2069) (2013) 1493-1498.

[193] K.A. Cunefare, A.J. Graf, Experimental active control of automotive disc brake rotor squeal using dither. *Journal of Sound and Vibration* 250(4) (2002) 579-590.

[194] B.F. Feeny, F.C. Moon, Quenching stick-slip chaos with dither. *Journal of Sound and Vibration* 237 (2000) 173-180.

[195] X. Zhao, N. Gräbner, U. von Wagner, Avoiding creep groan: Investigation on active suppression of stick-slip limit cycle vibrations in an automotive disk brake via piezoceramic actuators. *Journal of Sound and Vibration* 441 (2019) 174-186.

[196] A. Fidlin, Nonlinear oscillations in mechanical engineering. *Springer Science & Business Media* (2005).

[197] J.J. Thomsen, Using fast vibrations to quench friction-induced oscillations. *Journal of Sound and Vibration* 228(5) (1999) 1079-1102.

[198] F. Marques, P. Flores, J.P. Claro, H.M. Lankarani, A survey and comparison of several friction force models for dynamic analysis of multibody mechanical systems. *Nonlinear Dynamics* 86(3) (2016) 1407-1443.

[199] J. Ma, V. Rokhlin, S. Wandzura, Generalized Gaussian quadrature rules for systems of arbitrary functions. *SIAM Journal on Numerical Analysis* 33(3) (1996) 971-996.

[200] J. Kang, C.M. Krousgrill, F. Sadeghi, Comprehensive stability analysis of disc brake vibrations including gyroscopic, negative friction slope and mode-coupling mechanisms. *Journal of Sound and Vibration* 324(1-2) (2009) 387-407.

[201] H. Ouyang, J.E. Mottershead, A bounded region of disc-brake vibration instability. *Journal of Vibration and Acoustics* 123(4) (2001) 543-545.

[202] J. Kang, C.M. Krousgrill, F. Sadeghi, Analytical formulation of mode-coupling instability in disc-pad coupled system. *International Journal of Mechanical Sciences* 51(1) (2009) 52-63.

[203] P. Liu, H. Zheng, C. Cai, Y.Y. Wang, C. Lu, K.H. Ang, G.R. Liu, Analysis of disc brake squeal using the complex eigenvalue method. *Applied Acoustics* 68(6) (2007) 603-615.

[204] H. Ouyang, Q. Cao, J.E. Mottershead, T. Treyde, Vibration and squeal of a disc brake: modelling and experimental results. *Proceedings of the Institution of Mechanical Engineers, Part D: Journal of Automobile Engineering* 217(10) (2003) 867-875.

[205] F. Massi, L. Baillet, O. Giannini, A. Sestieri, Brake squeal: linear and nonlinear numerical approaches. *Mechanical System and Signal Processing* 21(6) (2007) 2374-2393.

[206] S. Oberst, J.C.S. Lai, S. Marburg, Guidelines for numerical vibration and acoustic analysis of disc brake squeal using simple models of brake systems. *Journal of Sound and Vibration* 332(9) (2013) 2284-2299.

[207] Z. Zhang, S. Oberst, J.C.S. Lai, A non-linear friction work formulation for the analysis of self-excited vibrations. *Journal of Sound and Vibration* 443 (2019) 328-340.

[208] J. Brunetti, F. Massi, W. D'Ambrogio, Y. Berthier, Dynamic and energy analysis of frictional contact instabilities on a lumped system. *Meccanica* 50(3) (2015) 633-647.

[209] J.J. Sinou, O. Chiello, L. Charroyer, Non Smooth Contact Dynamics Approach for Mechanical Systems Subjected to Friction-Induced Vibration. *Lubricants* 7(7) (2019) 59.

[210] A. Niknam, K. Farhang, Friction-induced vibration due to mode-coupling and intermittent contact loss. *Journal of Vibration and Acoustics* 141(2) (2019) 021012.

[211] D. Wei, J. Ruan, W. Zhu, Z. Kang, Properties of stability, bifurcation, and chaos of the tangential motion disk brake. *Journal of Sound and Vibration* 375 (2016) 353-365.

[212] L. Cremer, D.E. Hall, The physics of the violin. *American Journal of Physics* 54 (1986) 285.

[213] L. Cai, G. Songag, Joint stick-slip friction compensation of robot manipulators by using smooth robust controllers. *Journal of Robotic Systems* 11(6) (1994) 451-470.

[214] H. Puebla, J. Alvarez-Ramirez, Suppression of stick-slip in drillstrings: A control approach based on modeling error compensation. *Journal of Sound and Vibration* 310(4-5) (2008) 881-901.

[215] A. Cochard, L. Bureau, T. Baumberger, Stabilization of frictional sliding by normal load modulation. *Journal of Applied Mechanics* 70(2) (2003) 220-226.

[216] H. Jang, J.S. Lee, J.W. Fash, Compositional effects of the brake friction material on creep groan phenomena. *Wear* 251(1) (2001) 1477-1483.

[217] Z. Fuadi, S. Maegawa, K. Nakano, K. Adachi, Map of low-frequency stick-slip of a creep groan. *Proceedings of the Institution of Mechanical Engineers, Part J: Journal of Engineering Tribology* 224(12) (2010) 1235-1246.